MODELING AND ANALYSIS OF WAX DEPOSITION FROM MULTIPHASE FLOW IN FIELD-SCALE CRUDE OIL PIPELINE TRANSPORT SYSTEMS

FRANCIS OKETCH OCHIENG

DOCTOR OF PHILOSOPHY
(Applied Mathematics)

JOMO KENYATTA UNIVERSITY
OF
AGRICULTURE AND TECHNOLOGY

2024

Modeling and Analysis of Wax Deposition from Multiphase Flow in Field-Scale Crude Oil Pipeline Transport Systems

Francis Oketch Ochieng

A Thesis Submitted in Partial Fulfillment of the Requirements for the Degree of Doctor of Philosophy in Applied Mathematics of the Jomo Kenyatta University of Agriculture and Technology

2024

DECLARATION

This thesis is my original work and has not been presented for a degree in any other university.

Signature:..... Date:.....

Francis Oketch Ochieng

This thesis has been submitted for examination with our approval as university supervisors.

Signature:..... Date:.....

Prof. Mathew N. Kinyanjui, PhD
JKUAT, Kenya

Signature:..... Date:.....

Prof. Jeconia O. Abonyo, PhD
JKUAT, Kenya

Signature:..... Date:.....

Dr. Phineas R. Kiogora, PhD
JKUAT, Kenya

DEDICATION

This thesis is dedicated to my parents, Mr. Meshack Ochieng and Mrs. Jane Ochieng, my lovely wife Daniela, my son Dylan, and my siblings. Thank you for your encouragement, support, love, care, inspiration, endurance, and prayers throughout my academic life. You will forever remain my reasons for living.

ACKNOWLEDGEMENT

First and foremost, I wish to thank the Almighty God for the gift of life, love, and protection throughout my postgraduate program at Jomo Kenyatta University of Agriculture and Technology (JKUAT). Secondly, I am obliged to my supervisors, Prof. Mathew N. Kinyanjui, Prof. Jeconia O. Abonyo, and Dr. Phineas R. Kiogora, for their insightful, constructive, and valuable comments and guidance throughout the development of this thesis. I also wish to acknowledge the many authors of books and articles and the new generation of contributors to electronic media (the World Wide Web) who have provided me with additional insight and ideas to facilitate the successful completion of this research study. I am also very much grateful to my colleagues from the department of Pure and Applied Mathematics (PAM) for making my stay in the department very pleasant and memorable. Lastly, I wish to recognize my parents, wife, and siblings for offering me the most needed social and spiritual support for making this thesis a success.

TABLE OF CONTENTS

LIST OF TABLES

LIST OF FIGURES

LIST OF APPENDICES

ABBREVIATIONS AND ACRONYMS

AB	Adams-Bashforth
API	American Petroleum Institute
BVP	Boundary Value Problem
CN	Crank-Nicolson
CSF	Continuum Surface Force
FDM	Finite Difference Method
IVP	Initial Value Problem
MATLAB	Matrix Laboratory
ODE	Ordinary Differential Equation
PDE	Partial Differential Equation
PPE	Pressure Poisson Equation
PSP	Pseudo-Single Phase
VOF	Volume of Fluid
WAT	Wax Appearance Temperature

NOMENCLATURE

Roman Symbols

Symbol	Meaning
A	Area of the porous material, [m^2]
C	Total concentration of wax in crude oil, [kg/m^3]
$\bar{C}$	Dimensionless total concentration of wax
C_a	Concentration of aggregated wax crystals, [kg/m^3]
C_d	Concentration of dissolved wax in crude oil (solubility of wax), [kg/m^3]
C_n	Concentration of non-aggregated wax crystals, [kg/m^3]
C_p	Concentration of precipitated (crystallized) wax, [kg/m^3]
C_∞	Equilibrium concentration of wax in the bulk of the fluid, [kg/m^3]
C_{wall}	Concentration of wax at the pipeline wall, [kg/m^3]
$(Cp)_{gel}$	Specific heat capacity of gel at constant pressure, [J/(kg·K)]
$(Cp)_{oil}$	Specific heat capacity of waxy crude oil at constant pressure, [J/(kg·K)]
$(Cp)_{water}$	Specific heat capacity of water-in-oil emulsions at constant pressure, [J/(kg·K)]
$(Cp)_f$	Average heat capacity of the fluid phase at constant pressure, [J/(kg·K)]
$(Cp)_{mix}$	Average heat capacity of the mixture fluid at constant pressure, [J/(kg·K)]
C_f	Skin-friction coefficient
d_{water}	Diameter of water-in-oil emulsion, [m]
$\bar{d}$	Dimensionless diameter of water-in-oil emulsion
D_d	Molecular diffusivity of wax in crude oil, [m^2/s]
D_p	Shear dispersion coefficient, [m]
D_e	Effective diffusion coefficient of wax inside the gel layer, [m^2/s]

Roman Symbols

Symbol	Meaning
$\vec{F}$	Force per unit mass, [N/kg]
$\vec{F}_{\text{Darcy}}$	Body force due to Darcy's law, [N/m^3]
g	Acceleration due to gravity, [m/s^2]
h_{r}	Convective heat transfer coefficient, [W/(m^2·K)]
J_{wall}	Wall mass flux, [kg/(m^2·s)]
$\vec{J}_{\text{d}}$	Mass flux of dissolved wax, [kg/(m^2·s)]
$\vec{J}_{\text{p}}$	Mass flux of precipitated wax, [kg/(m^2·s)]
$\vec{J}_{\text{tot}}$	Total mass flux of wax, [kg/(m^2·s)]
K	Curvature of the oil-gel interface, [1/m]
K_1	Smooth positive function of temperature, [1/s]
K_2	Smooth positive function of temperature, [1/Pa]
k_{m}	Convective mass transfer coefficient, [m/s]
k_{gel}	Effective thermal conductivity of deposited layer, [W/m·K]
k_{oil}	Thermal conductivity of waxy crude oil, [W/(m·K)]
k_{water}	Thermal conductivity of water-in-oil emulsions, [W/(m·K)]
k_{f}	Average thermal conductivity of fluid phase, [W/(m·K)]
k_{mix}	Average thermal conductivity of mixture fluid, [W/(m·K)]
$\hat{\mathbf{k}}$	Unit vector in the axial direction
MW_{oil}	Molecular weight of waxy crude oil,[lb/lb-mol]
$\vec{n}$	Outward-drawn vector normal to the oil-gel interface
$\hat{\mathbf{n}}$	Outward-drawn unit vector normal to the oil-gel interface
p	Pressure field, [Pa]

Roman Symbols

Symbol	Meaning
p^*	Pressure shift, [Pa]
p_∞	Hydrostatic pressure, [Pa]
P	Dimensionless pressure field
Q	Volumetric flow rate of the mixture fluid, [m^3/s]
q_{h}	Heat source, [$W/m^3 \cdot K$]
q_{wall}	Wall heat flux, [W/m^2]
r	Radial distance from pipe center, [m]
$\bar{r}$	Dimensionless radial distance from pipe center
$\hat{\mathbf{r}}$	Unit vector in the radial direction
R	Inner radius of clean pipe, [m]
R_{eff}	Effective radius for oil flow, [m]
$\bar{R}_{\text{eff}}$	Dimensionless effective radius for oil flow
S_{a}	Rate of production of aggregated wax crystals, [kg $m^{-3}s^{-1}$]
S_{c}	Concentration source term, [kg/m^3]
S_{d}	Rate of production of dissolved wax, [kg $m^{-3}s^{-1}$]
S_{e}	Energy source term, [J]
S_{f}	Shift factor
S_{n}	Rate of production of non-aggregated wax crystals, [kg $m^{-3}s^{-1}$]
S_{p}	Rate of production of precipitated wax, [kg $m^{-3}s^{-1}$]
t	Time, [s]
$\bar{t}$	Dimensionless time
T	Absolute temperature of the mixture fluid, [K]

Roman Symbols

Symbol	Meaning
T_∞	Temperature of the mixture fluid at the free-stream, [K]
T_{int}	Fluid temperature at the oil-gel interface, [K]
T_{wall}	Fluid temperature at the inner pipeline wall, [K]
T_{WAT}	Wax appearance temperature, [K]
U_∞	Average velocity of the mixture fluid at the free-stream, [m/s]
u_r	Radial velocity, [m/s]
u	Dimensionless radial velocity
u_z	Axial velocity, [m/s]
v	Dimensionless axial velocity
$\vec{V}$	Velocity vector of the mixture fluid, [m/s]
x	Weight fraction of solid wax in the gel layer
z	Axial distance from pipe inlet, [m]
$\bar{z}$	Dimensionless axial distance from pipe inlet

Greek Symbols

Symbol	Meaning
α_{avg}	Average aspect ratio of the wax crystals
α_{m}	Aggregation degree
β_C	Coefficient of volume expansion due to concentration gradient, [m^3/kg]
β_T	Coefficient of volume expansion due to temperature gradient, [1/K]
δ	Thickness of gel layer, [m]
γ	Correlation coefficient
γ_{n}	Shear rate, [1/s]
κ	Intrinsic permeability of the gel layer, [m^2]
λ	Time dependent length scale, [m]
μ_{gel}	Dynamic viscosity of the deposit layer, [Nsm^{-2}]
μ_{oil}	Dynamic viscosity of waxy crude oil, [Nsm^{-2}]
μ_{water}	Dynamic viscosity of water-in-oil emulsions, [Nsm^{-2}]
μ_{f}	Dynamic viscosity of the fluid phase, [Nsm^{-2}]
μ_{mix}	Dynamic viscosity of the mixture fluid, [Nsm^{-2}]
μ_{T}	Turbulent viscosity, [Nsm^{-2}]
ν	Kinematic viscosity, [m^2/s]
$\vec{\omega}$	Dimensionless vorticity vector
ω	Dimensionless tangential vorticity
Φ	Porosity of the deposit layer (liquid fraction of the gel layer)
ϕ	Dimensionless concentration of the non-aggregated wax
φ	Angle of inclination of the pipeline to the horizontal

Greek Symbols

Symbol	Meaning
ϕ_{gel}	Volume fraction of gel layer
ϕ_{oil}	Volume fraction of waxy crude oil
ϕ_{water}	Volume fraction of water-in-oil emulsions
Ψ	Viscous dissipation function, [N/m^{2}s]
ψ	Stream function
ρ_{gel}	Density of the solid wax deposit, [kg/m^3]
ρ_{oil}	Density of waxy crude oil, [kg/m^3]
ρ_{water}	Density of water-in-oil emulsions, [kg/m^3]
ρ_f	Average density of the fluid phase, [kg/m^3]
ρ_{mix}	Average density of the mixture fluid, [kg/m^3]
ρ_∞	Mixture fluid density at edge of boundary layer, [kg/m^3]
σ	Surface tension coefficient, [N/m]
$\vec{\tau}$	Viscous stress tensor, [N/m^2]
τ_0	Yield stress, [N/m^2]
τ_{wall}	Wall shear stress, [N/m^2]
θ	Angular distance from pipe center, [m]
Θ	Dimensionless temperature
ε	Computational constant
ε_{tol}	Absolute error tolerance, [$\varepsilon_{tol} = 10^{-13}$]
ξ	Dimensionless unsteadiness parameter

Dimensionless Numbers

Symbol	Meaning
Da	Darcy number
Ec	Eckert number
$\mathrm{Gr_C}$	Mass Grashof number
$\mathrm{Gr_T}$	Thermal Grashof number
Nu	Nusselt number
Nu_z	Local Nusselt number
Pe	Peclet number
Pr	Prandtl number
Re	Reynolds number
Sc	Schmidt number
Sh	Sherwood number
Sh_z	Local Sherwood number
St	Stanton number
We	Weber number

ABSTRACT

The formation of solid wax crystals that interlock and form a gel-like layer on the inner wall of the pipeline greatly influences the transportation of waxy crude oil through pipeline systems. The deposited layer grows continuously and hardens during oil transportation. This phenomenon reduces the effective internal diameter of the pipeline and the flow rate. In extreme cases, the deposited layer may block the crude oil pipeline leading to permanent pipeline shutdown and loss of capital investment. In this study, wax deposition from multiphase flow in field-scale crude oil pipeline transport systems has been investigated numerically. The novelty of this work is to develop a mathematical model that incorporates water-in-oil emulsions, wax precipitation kinetics, molecular diffusion, and shear dispersion to enable accurate predictions of both the wax deposit growth rate and aging of the deposit. The coupled nonlinear partial differential equations governing the flow are discretized in time by a second-order semi-implicit time discretization scheme, which is based on the Adams-Bashforth and Crank-Nicolson methods that completely decouple the computation of the governing equations. The resulting temporal numerical schemes are discretized in space by the bivariate spectral collocation method, which is based on Chebyshev-Gauss-Lobatto grid points. The resulting numerical schemes are simulated in MATLAB® software to obtain the profiles of the flow variables. The simulation results are presented in graphical and tabular forms and also discussed. The model's predictive capabilities are evaluated by investigating the impact of various flow parameters on the flow variables, wall shear stress, and heat and mass fluxes. The key findings reveal that wax deposition is significantly influenced by the intricate interplay of flow conditions, wax precipitation kinetics, and heat and mass transfer phenomena. Notably, increasing Reynolds number from 2.2361 to 3.1361 leads to at most 2.5% increase in wax deposition, while increasing mass Grashof number from 5 to 11 results in at most 2.0% reduction in wax accumulation. Moreover, increasing Weber number from 1.0 to 2.5 tend to mitigate wax deposition by at most 7.0%. In addition, the deposit thickness steadily increases during the initial phases of wax deposition, after which it reaches a steady-state value of 0.2 and maintains that value over time. A deposition model to predict the wax deposit growth and aging is proposed in this study. The research findings can help in making informed decisions on the planning of pigging operations, thermal insulation, and other remediation techniques to be applied in controlling wax deposition in field-scale crude oil pipeline systems.

CHAPTER ONE

INTRODUCTION

In this chapter, a background of the study is presented in Section 1.1, and the key terms that are used in this study are defined and explained in Section 1.2. The statement of the problem, justification, objectives, and scope of this study are presented in Sections 1.3, 1.5, 1.4, and 1.6 respectively.

1.1 Background Information

Pipeline is currently the most efficient means for transporting fluids such as crude oil. The relative efficiency of crude oil pipeline depends on two fundamental requirements. The first requirement is that the pipeline should continue to operate without any interruption once it is commissioned, while the second requirement is that optimum discharge must be obtained with the least capital investment and the lowest operating costs. Crude oil pipelines are designed and constructed based on the above two fundamental considerations. Nevertheless, the capital investment and operating costs are often very high, especially for large diameter and long-distance crude oil transport pipelines.

The increasing demand for energy has made the exploration of oil in Africa to extend from onshore to offshore fields and to greater depths, such as the Lokichar oil fields in Kenya where crude oil gets transported through long pipelines in the range of 20-60 km from the reservoir to inland facilities. The long-distance for oil transportation means that the time is adequate for oil to cool to temperatures below the wax appearance temperature, usually between 10°C and 30°C. The deposition of solid wax crystals on the inner wall of crude oil pipelines has become a major concern in the oil industry because it slows down pipeline operation, leading to reduced flow rate and increased operational costs. Low temperature is the main factor affecting the wax precipitation and deposition process, which means that pipelines in relatively cold places are especially vulnerable to wax deposition. Addressing the problem of wax deposition at an early stage of a pipeline design and construction may reduce the operating and maintenance costs of the pipeline system.

Various wax mitigation methods are used to control wax formation and deposition, such as mechanical techniques (e.g., pigging), heating of the pipeline and use of chemical

inhibitors. Heating of the pipeline is not economical in the case of offshore oil exploration. Excessive usage of additive chemicals can damage the ecosystem in case of accidental release of chemicals to the environment. The pigging operation cannot efficiently be applied without a prior knowledge of the deposit thickness. In particular, pigs usually get stuck inside the crude oil pipeline due to thick and hard deposits making the situation worse. In the worst case, production must be stopped in order to replace the plugged portion of the pipeline, which is estimated to cost about 40,000,000 dollars per incident (Huang *et al.*, 2011). Due to the limitations of the available wax mitigation methods and the persistent challenge of wax deposition, many oil companies are still searching for a better solution to the wax deposition.

Multiphase flows such as water-oil or gas-oil two-phase flows and water-gas-oil three-phase flows are prominent in oil field operations. Water-oil two-phase flows continue to gain interests from the upstream oil industry since the water content of the ore increases significantly with the increase in extraction time. The mixing of co-existent water and crude oil by turbulence eddies promotes the formation of water-in-oil emulsions. This study is on advancing the understanding of wax deposition in the presence of water-in-oil emulsions and developing a mathematical model for wax deposition that incorporates the co-existent water to enable accurate predictions of both the wax-deposit growth rate and aging (or hardening) of the deposit layer.

1.2 Definition of Terms

The key terms that are used in this study are defined and explained in this section.

1.2.1 Multiphase Flow

Phase refers to the solid, liquid, or vapour state of matter. Thus, multiphase flow is any fluid flow consisting of more than one phase or component. Each of the phases has a separately defined volume fraction (the sum of which is unity) and velocity field.

1.2.2 Waxy Crude Oils

Crude oil is a complex mixture of hydrocarbons such as paraffins, naphthenes, asphaltenes, resins and aromatics, and other organic compounds which contain sulphur, oxygen, nickel, iron and copper. Wax refers to the long-chain high-molecular weight paraffins having between 18 to 65 carbon atoms. Thus, wax is the paraffin component of the crude oil. The

chemical reactivity of alkanes is poor due to the strong carbon to carbon (C-C) bonds and carbon to hydrogen (C-H) bonds. Hence, waxy crude oil is non-reactive.

1.2.3 The API Gravity of Crude Oils

The American Petroleum Institute (API) gravity is a scale used to grade crude oils, calibrated in degrees API (i.e., °API). Thus, crude oils are classified into three categories based on their API gravity: heavy crude oils are those whose API gravity is less than $22.1°$API, intermediate crude oils are those whose API gravity ranges between $22.1°$API and $31.5°$API (inclusive), light crude oils are those whose API gravity is greater than $31.5°$API. In this study, a heavy waxy crude oil with an API gravity of 18^oAPI is considered.

1.2.4 Wax Appearance Temperature

Wax appearance temperature (WAT) refers to the temperature at which the first wax crystals start to form in the crude oil in a cooling process, usually between 10°C and 30°C. The WAT is also called the cloud point temperature while the temperature at which crystals begin to aggregate is usually called the pour point temperature. The pour point temperature is typically $10-15$°C lower than the WAT (Fusi, 2003).

1.2.5 Wax Crystallization

Wax crystallization (or wax precipitation) refers to the process of separation of the solid phase from a homogeneous solution. The separated solid phase appears as wax crystals. Wax crystallization consists of two stages, i.e., nucleation and growth. When the temperature of the crude oil approaches the WAT during the cooling process, the kinetic energy of the wax molecules reduces due to the temperature reduction hence hindering the motion of the wax molecules. This leads to continuous reduction and strengthening of the bond between the wax molecules, forming crystal nuclei (or clusters). As the nucleation process continues, the wax molecules get tangled and hence increase the size of the nuclei up to a certain critical volume after which the nuclei become stable, giving rise to crystal growth.

1.2.6 Wax Aggregation

When the temperature of crude oil is slightly below the WAT, an equilibrium is established between the dissolved wax and crystallized (or precipitated) wax. As the temperature continues to fall, more wax crystals are formed drastically and hence forming more complex structures known as *agglomerates*. As a result of the aggregation process, the liquid oil is entrapped in a wax network, turning the oil into a highly viscous gel-like material.

Aggregation is the cause of most serious complications in processing waxy crude oils. Many companies have developed various techniques to inhibit the formation of aggregates. For instance, a slow stirring of the fluid (mechanical technique), the use of reheating stations (thermal technique), and the use of specific additives (chemical modulation).

1.2.7 Wax Deposition

Wax deposition refers to the formation of a layer of separate solid phase (called the gel layer) and the eventual growth of this layer on a surface in contact with the crude oil. Wax deposits can be formed from an already precipitated solid wax crystals or from dissolved wax molecules. Wax deposition in the pipe can only occur when the temperature of the inner wall of the pipeline falls below the WAT.

The existence of a radial concentration gradient of wax molecules causes a radial movement of wax molecules from the bulk of the fluid towards the wall, which precipitate to form solid wax crystals. The wax deposits interlock to form a pseudo-porous three-dimensional network structure of wax crystals called the gel, which contains a large fraction of oil trapped within it. Wax deposition is more severe in subsea pipelines, where the water temperature usually drop to about 5^{o}C. The incipient gel grows continuously and hardens with time in a process known as aging of the gel.

1.2.8 Wax Deposition Mechanisms

The main mechanisms responsible for wax deposition during transportation of waxy crude oil in pipelines are molecular diffusion, shear dispersion, Brownian diffusion, and gravity settling Azevedo & Teixeira (2003).

1.2.8.1 Molecular Diffusion

Molecular diffusion refers to the movement of dissolved wax molecules towards the wall of crude oil pipeline due to the existence of a radial concentration gradient of dissolved wax molecules in the waxy crude oil, induced by the radial temperature gradient inside the oil pipeline.

1.2.8.2 Shear Dispersion

Shear dispersion is a mechanism tied to the shearing of the precipitated wax particles towards the wall, induced by the existence of a radial velocity gradient.

1.2.8.3 Brownian Diffusion

Brownian diffusion refers to the movement of precipitated wax particles towards the wall due to a radial concentration gradient of the precipitated wax particles. The diffusion of the precipitated wax particles is caused by Brownian motion.

1.2.8.4 Gravity Settling

Gravity settling refers to the settling of the precipitated wax particles towards the bottom of the crude oil pipeline, due to the earth's gravity. This is because the wax crystals are denser than the surrounding liquid oil.

1.2.9 Wax Mitigation Methods

Wax mitigation (or wax remediation or dewaxing) refers to the technique applied to control wax precipitation and deposition. The mitigation methods used to control wax deposition are mechanical, thermal and chemical methods (Huang, 2011).

1.2.9.1 Mechanical Removal

Mechanical removal technique involves sending pigs in the crude oil pipeline periodically, a process commonly known as pigging operation. A pig refers to any device that moves freely through the pipeline for the purpose of inspecting or cleaning it by scraping off the wax deposit. The motion of the pig is driven by the flow field. The pig is analogous to a free moving piston. The pigging operation cannot efficiently be applied without a

proper wax deposition prediction. This study aims to accurately predict optimal pigging-frequency to improve the pigging operations.

1.2.9.2 Thermal Technique

Thermal technique involves insulating or heating the crude oil pipeline to keep the flowing crude oil temperature above the wax appearance temperature (WAT). Usually steam is used for heating the waxy crude oil to make it easier to extract. This technique is not economical in the case of offshore oil exploration.

1.2.9.3 Chemical Modulation

Chemical modulation involves injecting chemical wax inhibitors in the flowing crude oil to alter wax crystallization or crystal growth. However, excessive usage of additive chemicals can damage the ecosystem in case of accidental release of chemicals to the environment. The inhibitors may also result in corrosion of the pipeline inner wall and hence not economical.

1.2.10 Water-in-oil Emulsions

Water-in-oil emulsions refer to the highly stable water droplets formed in waxy crude oil during extraction and transportation. In this case, the water-in-oil emulsions is the dispersed phase that is distributed into the continuous oil phase. The formation of the high stable water-in-oil emulsions is one of the negative factors in extracting and processing of oil, their preparation and transportation, as well as liquidation/recycling of oil-sludge barns. The use of conventional techniques such as heating to destroy the emulsions yields no positive results.

1.2.11 Newtonian and Non-Newtonian Fluids

Newtonian fluids are fluids whose dynamic viscosity is a constant while non-Newtonian fluids are fluids whose dynamic viscosity is a variable. Waxy crude oil behaves as a Newtonian fluid at temperatures above the WAT and a non-Newtonian fluid at temperatures below the WAT (Ramirez-Jaramillo *et al.*, 2004).

1.2.12 Laminar and Turbulent Flows

Laminar flow refers to fluid flow in which the paths followed by the fluid particles do not cross each other (i.e., layers of the fluid slip smoothly over each other). Turbulent flow refers to a chaotic flow, and is characterized by velocity fluctuations since the fluid particles move in a zigzag manner.

1.2.13 Body Forces and Surface Forces

Body forces are forces which act on the volumetric mass of the fluid element from a distance without physical contact. These forces are expressed as force per unit volume of the fluid element (Nm^{-3}). The most common body forces are the gravitational force and electromagnetic force. Surface forces are forces which are exerted on the surface of the fluid element by the surrounding through direct contact. These forces are expressed as force per unit surface area of the fluid element (Nm^{-2}). The most common surface forces are pressure and shear stresses.

1.2.14 Steady and Unsteady Flows

Unsteady flow refers to a flow in which the flow variables (e.g., velocity, temperature, concentration) depend on time. On the other hand, a steady flow means that flow variables are independent of time.

1.2.15 Free Stream

Free stream (or bulk of the fluid) refers to the region in the fluid where the effect of viscous forces, heat flux and solute flux on the flow are negligible. The velocity, temperature and species concentration are often uniform in the free stream.

1.2.16 Boundary Layer

Boundary layer refers to a thin region in the fluid adjacent to the solid-fluid interface where velocity, temperature and/or concentration gradients normal to the interface are significant. In this layer, the viscous forces dominate over the inertial forces. There are three types of boundary layer, namely; velocity, thermal, and concentration boundary layers.

1.2.16.1 Velocity Boundary Layer

The velocity boundary layer develops when there exists a velocity gradient of the fluid particles between the solid-fluid interface and the free stream. The thickness of the velocity boundary layer is defined as the perpendicular distance measured from the solid-fluid interface to a point in the fluid where the fluid velocity is 99% of the free-stream velocity.

1.2.16.2 Thermal Boundary Layer

Thermal boundary layer is associated with heat transfer, and develops when there is a difference in temperature of the fluid particles between the solid-fluid interface and the free stream. The thickness of the thermal boundary layer is defined as the perpendicular distance measured from the solid-fluid interface to a point in the fluid where the temperature difference between the fluid and solid-fluid interface is 99% of the temperature difference between the free stream fluid and the solid-fluid interface.

1.2.16.3 Concentration Boundary Layer

Concentration boundary layer is associated with mass transfer and develops when there is a difference in concentration of a species between the solid-fluid interface and the free-stream. The thickness of the concentration boundary layer is defined as the perpendicular distance measured from the solid-fluid interface to a point in the fluid where the difference in concentration between the fluid and the solid-fluid interface is 99% of the difference in concentration between the free stream fluid and the solid-fluid interface.

1.2.17 No-slip Boundary Condition

No-slip boundary condition means that the fluid layer in contact with the solid surface sticks to the surface and moves with it at the same velocity of the solid surface. In particular, the fluid and solid have equal velocities at their interface. In this study, it is assumed that there is no-slip of fluid particles at the solid-liquid boundary.

1.2.18 Natural Convection Flow

Natural convection is a type of fluid flow in which the motion of the fluid is initiated by buoyancy forces which arise due to variation of density of the fluid. The density variation

is as a result of the existence of temperature or concentration gradients in the fluid. In the study of natural convection flows, the condition of the fluid particle that is far away from the boundary layer is indicated by the subscript ∞, which means that this is the value at a distance where the effect of the boundary layer is not felt.

1.2.19 Heat Transfer

Heat transfer refers to the transport of thermal energy which occurs due to existence of temperature gradient in the fluid. There are three modes of heat transfer: conduction, convection, and radiation.

1.2.19.1 Conduction

Conduction is the mode of heat transfer that occurs when a temperature gradient exists in a stationary medium, e.g., heat transfer through the wall of pipeline when crude oil is flowing. In oil pipeline transport systems, the high energy molecules of liquid oil collide with lower energy molecules resulting in heat transfer from high temperature regions to low temperature regions.

1.2.19.2 Convection

Convection is the mode of heat transfer which takes place as a result of bulk motion and mixing of macroscopic elements of warmer and cooler regions of a fluid. In crude oil pipeline transport systems, convective heat transfer involves exchange of thermal energy between the inner wall of the pipeline and liquid oil.

1.2.19.3 Radiation

Radiation is the mode of heat transfer which occurs due to the propagation of electromagnetic waves in a vacuum.

1.2.20 Mass Transfer

Mass transfer refers to the transport of molecules of a species which occurs due to the difference in concentration of the species in a mixture fluid. The basic mechanisms for mass transfer in crude oil pipeline transport systems are diffusion and convection of the wax molecules.

1.2.21 Porous Medium

A porous medium refers to a medium with fine pores which are uniformly distributed throughout the medium and through which fluid (liquid) can flow freely and continuously. The gel layer formed in crude oil pipelines is a porous medium. Some liquid oil usually seep through the gel layer. The pores which allow fluid to pass through are known as effective pores of a porous medium. The effective pores contribute to the porosity of the medium, which is defined as the fraction of the whole volume of the material which is occupied by the pores. The seepage of fluids through a porous medium is governed by Darcy's law, which is presented in detail in Chapter 3.

1.2.22 Viscous Dissipation

Viscous dissipation refers to the conversion of the kinetic energy of the flow into internal energy of the fluid (or heat) by work that is done against the viscous fluid stresses. Thus, viscous dissipation heats up the fluid as the flow progresses.

1.3 Statement of the Problem

Companies dealing with waxy crude oil are dedicated to ensuring an economically feasible flow of oil in the pipeline transport systems by pumping about 80,000 barrels of oil per day from the reservoir to inland facilities. Optimum pipeline design and construction is one aspect of achieving an economically feasible flow of oil.

However, the transportation of waxy crude oil through pipeline is greatly influenced by the formation of solid wax deposits, whose evolution depend on the cooling rate and on the quantity of wax molecules in the crude oil. The wax deposits interlock and form a gel-like layer which grows continuously and hardens during oil transportation hence reducing the effective inside diameter of the pipeline. In extreme cases, the wax deposit may block the pipeline leading to loss of production and capital investment. Furthermore, about 90% of water is usually extracted together with oil and flow together as water-oil two-phase flow in crude oil pipelines. The water-in-oil emulsions usually collect under the crevices causing pitting corrosion in the crude oil pipelines. The existing wax deposition models do not take into consideration the co-existent water and hence are unsuitable to be applied in field-scale oil pipeline transport systems since they cannot give accurate predictions of the rate of wax deposit growth and aging. Overestimation of the wax-deposit growth rate, due to inaccurate wax deposition model, results in very high pigging-frequency which

is costly and leads to production downtime. Consequently, underestimation of the wax-deposit growth rate results in very low pigging-frequency which means that the time is adequate for the wax deposits to thicken and harden hence impossible to remove during subsequent pigging operations.

In response to these problems, the current study aspires to develop a mathematical model and simulator that incorporates all the salient features of wax deposition (e.g., water-in-oil emulsions) to accurately predict the rates of deposit growth and aging. The implementation of a pigging operation usually happens when the deposit thickness reaches a threshold of about 7 millimeters. From an economic perspective, an accurate prediction of the time it takes for the wax deposits to grow to the threshold thickness is essential for the design of pigging operations to achieve optimum pigging-frequency and minimize operational costs. This study is therefore on modeling and analysis of wax deposition from multiphase flow in field-scale crude oil pipeline transport systems.

1.4 Objectives of the Study

1.4.1 General Objective

To model mathematically and analyze the wax deposition from multiphase flow in field-scale crude oil pipeline transport systems.

1.4.2 Specific Objectives

The specific objectives of this study are to:

1. Develop a mathematical model for water-oil two-phase flow in field-scale crude oil pipeline transport systems.
2. Determine the profiles of the flow variables such as velocity, temperature and species concentration on multiphase flow in field-scale crude oil pipeline transport systems.
3. Determine the effects of varying the various flow parameters on the flow variables for multiphase flow in field-scale crude oil pipeline transport systems.
4. Compute the skin-friction coefficient and the rates of heat and mass transfer in multiphase flow in field-scale crude oil pipeline transport systems.

5. Predict the rates of wax deposition on the inner wall of crude oil pipeline and aging of the wax-oil gel layer.

1.5 Significance of the Study

The knowledge of wax deposition and aging rates in field-scale crude oil pipelines helps in proper scheduling of pipeline maintenance to improve oil recovery and processing operations in the oil industry. This is achieved by accurately predicting the rates of wax deposit growth and aging; and suggesting ways to minimize the rate of wax deposition. Accurate prediction is essential for the design of pigging operations to achieve optimum pigging-frequency and minimize operational costs. Furthermore, the implementation of a proper pigging program helps in maintaining the optimum efficiency of the pipeline and hence safeguarding both the environment and assets of the oil companies.

1.6 Scope of the Study

The present study is confined to a two-dimensional flow of waxy crude oil in pipeline transport systems. The study focuses on mathematical modeling and simulation of wax deposition in fluid (water-oil) and deposit two-phase flow. In the fluid phase, the water-in-oil emulsions is dispersed in the continuous oil phase. In particular, the study focuses on accurate prediction of the amount of wax deposits in crude oil pipeline transport systems, i.e., predicting the rates of growth and aging of the wax deposits. Thus the detection of the location of the wax deposits, which is the focus of Remote Sensing, is beyond the scope of the present study.

1.7 Thesis Structure

The rest of this thesis is organized as follows. In Chapter 2, a review of existing studies which are relevant to this study is presented. In Chapter 3, the formulation of the flow problem, the modeling of wax concentration and deposition mechanisms, the equations governing the flow of waxy crude oil in pipeline transport systems, and the numerical methods used to solve the resulting model equations are presented. In Chapter 4, the results obtained from this study, a discussion of the results, and validation of the results by comparing the study results with experimental wax deposition data from the reviewed literature are presented. In Chapter 5, the conclusions drawn from this study and recommendations for improving the operations in the oil industry and for future research

work are presented. Finally, the publications of part of this study, the MATLAB codes used to generate the results and other materials which are relevant to this study are included in the appendix.

CHAPTER TWO

LITERATURE REVIEW

2.1 Introduction

This chapter reviews studies on wax deposition in multiphase flow during crude oil transportation through field-scale pipelines. It focuses on the findings relevant to wax deposition and its impact on waxy crude oil flow.

2.2 Literature Review

There are various theoretical and experimental studies in understanding the formation and deposition of wax in crude oil pipelines, and modeling the phenomenon. For example, Singh *et al.* (2000) investigated the formation and aging of the gel layer in crude oil pipelines through a series of laboratory flow loop experiments. They developed a mathematical model to predict the growth rate of the wax deposit and the increasing wax content within the gel layer over time. The model considered the scenario of externally cooled pipeline walls. The study identified a "counter-diffusion phenomenon" as the mechanism responsible for gel layer aging. This phenomenon refers to the opposing diffusion processes between the oil and the deposited wax. Additionally, they found that the aging rate of the gel layer is influenced by both the oil flow rate and the temperature of the pipeline's inner wall. However, the model has a limitation that restricts its applicability to real-world scenarios: the assumption of a quasi-steady state for all rate processes. This assumption implies that a stable temperature profile can be rapidly established due to a relatively fast heat transfer rate compared to the slow growth rate of the deposit. This is unrealistic because time plays a crucial role in any fluid flow situation. Real-world pipelines experience dynamic changes, and a quasi-steady state may not be achievable.

Kok *et al.* (2000) developed a mathematical model for estimating wax deposition in crude oil pipeline systems. This model combined analytical and numerical approaches and was applied to the Kirkuk-Ceyhan crude oil pipeline system. The study predicted a wax deposit thickness of approximately 0.34 mm after one year of operation, along with a gradual temperature decline from 303 K to 295 K along the pipeline length. The model

incorporated molecular diffusion, shear dispersion, and Brownian diffusion as mechanisms for wax deposition. However, the study neglected the potential influence of thermal diffusion. An additional limitation is the assumption of constant pressure throughout the pipeline. In real-world crude oil transportation systems, pressure typically varies along the pipeline length.

Fusi (2003) investigated the unsteady flow of waxy crude oil within a laboratory test loop, considering shear dispersion and molecular diffusion as deposition mechanisms. The analysis focused on non-isothermal conditions and used the radial coordinate of the pipe as the sole spatial variable. To simplify the problem, the researchers applied a quasi-stationary approximation to the governing equations. The study's findings suggested that slow cooling of the pipe wall is necessary for continued pipeline operation. It even proposed a strategy for selecting the cooling rate to ensure a specific time window where the formed rigid core wouldn't obstruct oil flow. However, the study has a significant limitation: the assumption of one-dimensional flow. In reality, flow variables depend on at least two spatial variables. This limitation restricts the applicability of the results to field-scale oil pipeline transportation systems.

Nazar *et al.* (2005) conducted an experimental study to investigate the variation in wax deposition for a mixture of toluene and waxy oil. They further developed a comprehensive mathematical model applicable to laminar flow conditions. The study considered two key mechanisms influencing wax deposition: molecular diffusion of wax and the sloughing effect caused by hydrodynamic forces acting on the deposited wax. The findings of the study indicated that the model exhibited excellent predictive capabilities for laminar flow. However, the study neglected frictional heating and heat generation associated with the oil phase transition from liquid oil to solid wax crystals. Incorporating these factors might improve the model's accuracy.

Banki *et al.* (2008) investigated the mathematical formulation and numerical modeling of wax deposition in crude oil pipelines for laminar flow conditions using the enthalpy-porosity approach. This approach employs an enthalpy formulation to approximate convective flow within the gel layer, utilizing a fixed-grid method that eliminates the need to explicitly determine the oil/gel interface location. The study considered both molecular diffusion and thermal diffusion, incorporating appropriate diffusion coefficients. The findings of the study indicated that the design of multiphase flow systems often relies heavily on empiricism, meaning that pressure drop and temperature profiles are predicted using established empirical or semi-empirical correlations. However, a limitation of the study is the lack of a detailed explanation

regarding the temperature interval determination for the porous medium.

Huang *et al.* (2011) developed a mathematical model for wax deposition in subsea oil pipelines. This model aimed to predict both the wax deposit growth rate and the increasing wax fraction within the gel layer, considering both laminar and turbulent flow conditions. The researchers employed the backward Euler finite difference method (FDM) to solve the resulting steady-state heat and mass transfer equations. The study investigated the effects of wax molecule precipitation within the bulk oil on wax deposition. The study found that this precipitation acts as a competing phenomenon, reducing wax deposition by decreasing the availability of dissolved wax molecules that can potentially deposit on the pipeline's inner wall. However, the assumption of a quasi-steady state is inaccurate. Time is a crucial factor in any fluid flow scenario, and a more dynamic approach might be necessary for real-world applications. Also, while the finite difference method was used in the study, its discretization process is computationally expensive. This may limit the efficiency of the developed model for complex wax deposition modeling.

Stubsjøen (2013) investigated analytical and numerical modeling of paraffin wax deposition in pipelines. The resulting model equations were solved numerically using the finite difference method based on the forward Euler scheme. The study examined the influence of wax deposit on the thermal conditions within the pipeline. The study found that the temperature at the oil/deposit interface increased with increasing wax deposit thickness. However, the study assumed that there is no thermal energy generation in the fluid. In reality, there is usually dissipation of kinetic energy from the fluid's velocity field into internal energy (heat) during crude oil transportation. The forward Euler scheme is an explicit scheme, making it less efficient for initial-boundary value problems like this one. It requires more computational effort for the numerical solution to converge to the exact solution. The assumption of Newtonian crude oil is inaccurate. Crude oil behaves as a Newtonian fluid above the wax solubility limit but transitions to non-Newtonian behavior at lower temperatures. The study also assumed the absence of water droplets in the crude oil and limited the model to one-dimensional flow.

Skjæraasen *et al.* (2014) investigated the restart behavior of subsea pipelines transporting waxy crude oil using advanced computational pressure wave modeling. The governing equations were discretized on a cylindrical grid and solved numerically using the finite difference Euler scheme. The study developed a rheology model and a simulation algorithm to track the pressure wave propagation during the initial restart of flow. The findings of the study indicated that accurate implementation of the simulation algorithm could ensure successful restart of pipelines containing gelled oil with physical wax gels.

However, the study had limitations. It focused solely on gel breakdown induced by deformation, and the finite difference Euler scheme, while used here, is not computationally efficient for wax deposition modeling due to the inherent need for high grid resolution, leading to intensive calculations.

Fatkhullina *et al.* (2015) investigated the mathematical modeling of a water-in-oil emulsion droplet's behavior under unsteady flow conditions during microwave irradiation. The study focused on the effects of microwave electromagnetic radiation on a single water-in-oil droplet. The researchers employed the Volume of Fluid (VOF) method to capture the unsteady dynamics of the free interface separating the water and oil phases throughout the flow domain. The model equations were solved numerically using a combination of the Tri-diagonal Matrix Algorithm (TDMA) and the Semi-Implicit Method for Pressure Linked Equations (SIMPLE) algorithm. The study's findings revealed that applying microwave electromagnetic radiation to the flow of waxy crude oil is an efficient method for destroying water-in-oil emulsions.

Zhang *et al.* (2018) developed a wax deposition model to predict the temperature field and location of wax deposition within a wellbore system using a heat-fluid coupling process centered on the borehole axis. The resulting heat-fluid coupled equations were solved numerically using the finite element method. The study reported that as the fluid production intensity and moisture content increased, the temperature decreased from the bottom upwards at a very slow rate. However, the model neglected the reduction in heat transfer caused by gel layer formation. This assumption is inaccurate because a significant amount of heat energy is typically lost from the liquid oil during the formation and deposition of solid wax crystals. This lost heat is then absorbed by the gel layer.

Ying *et al.* (2019) investigated the heat transfer analysis during oil phase change in an overhead pipeline shutdown. The study reported challenges in tracking the oil/gel interface as wax molecules precipitate out of the liquid oil, making it difficult to model natural convective heat transfer at this interface. The assumption of liquid crude oil being a Newtonian fluid throughout the process is inaccurate. Crude oil exhibits Newtonian behavior above the wax solubility limit in liquid oil, but transitions to non-Newtonian behavior at lower temperatures. Finally, the assumption that the flowing fluid is a single pure substance is unrealistic. Water is typically produced alongside crude oil during extraction, and its presence needs to be considered for accurate heat transfer analysis.

Magnini & Matar (2019) investigated wax deposition in crude oil-deposit two-phase flow within a pipeline using interface-resolved numerical simulations. The study assumed that molecular diffusion was the sole mechanism driving wax deposition and that water-in-oil emulsions had a negligible effect. To capture the unsteady dynamics of the free oil-deposit interface, the study employed the Volume of Fluid (VOF) method. The model equations were solved numerically using the finite volume method and simulations were conducted using ANSYS FLUENT software. The results revealed that the deposit pattern could manifest as either a uniform axisymmetric film coating the pipe wall or a completely stratified layer, depending on the relative influence of gravitational forces. Additionally, the study reported that the amount of deposit relative to the pipe volume decreased with increasing oil flow rate and pipe diameter.

Mouketou & Kolesnikov (2019) investigated the modeling and simulation of multiphase flow applicable to oil and gas industry processes. The study performed numerical simulations under steady-state conditions using CFD software. The study neglected the effects of temperature change and the volume fraction of sand particles. The results revealed that erosion primarily occurs near the bend's exit and also on the side walls of the downstream straight pipeline. This sidewall erosion was attributed to the influence of secondary flows caused by centrifugal forces. The erosion rate decreased with increasing crude oil viscosity.

Sun *et al.* (2020) conducted an experimental and theoretical study of wax deposition behavior on a heat-insulated waxy crude oil pipeline in Northeast China. The study investigated how flow rate and ambient temperature affect the thickness and wax content of the deposition layer. The model equations were solved numerically using the Euler method. The study aimed to predict wax deposition thickness in a heat-insulated crude oil pipeline across different seasons and operating times. This prediction is expected to provide a scientific basis for determining the pipeline's wax removal cycle. The predicted results indicated that the thickness of the wax deposition layer initially increases and then decreases along the pipeline.

Jiang *et al.* (2020) conducted a numerical study for removing wax deposition by thermal washing for the waxy crude oil pipeline. The study adopted the enthalpy-porosity and volume of fluid (VOF) methods to simulate the melting process of wax in the crude oil pipeline. The model equations were solved numerically using finite difference method and simulated in FLUENT, a commercial CFD program. The results obtained from the study revealed that the wax crystals melt quickly before the liquid fraction reaches 80%, while the remaining 20% melts very slowly. Increasing the water temperature and flow

rate can accelerate the melting process.

Waheed & Megahed (2022) investigated the effects of melting heat transfer on a two-dimensional flow of a micropolar fluid over a horizontal plate with heat generation/absorption in a slip flow regime. The study assumed steady flow conditions. The governing boundary layer equations for this physical problem were reduced to a system of non-linear ordinary differential equations. These model equations were then solved numerically using the Chebyshev spectral method. The results showed that velocity increased with increasing material parameter, local Eckert number, and melting parameter. Conversely, velocity decreased with increasing slip parameter and heat generation (or absorption) parameter. Temperature increased with increasing material parameter but decreased with increasing slip parameter, heat generation (or absorption) parameter, local Eckert number, melting parameter, and thermal conductivity parameter.

Shi *et al.* (2023) experimentally investigated the treatment of paraffin deposition behavior in gas-condensate wells using chemical inhibitors. The study employed the crude oil dynamic paraffin deposition rate tester to study the preventive effects of paraffin dispersants and paraffin crystal modifiers. The results revealed significant phase change behavior in gas-condensate wells, with the gas phase being the dominant form. Additionally, paraffin deposition was found to be concentrated in the 1000-1500 meter region. A paraffin deposition identification chart was established based on these findings. The maximum deposition rate reached 15.50 mm/year under temperature and pressure conditions of 45°C and 70 MPa. Furthermore, paraffin crystal modifiers exhibited a significantly greater preventive effect compared to paraffin dispersants. At the optimal concentrations (0.25-0.50 wt%), these modifiers achieved paraffin prevention rates of 85-95%. The dissolving paraffin rate reached 0.0169 g/min, resulting in an approximate 40% decrease in the paraffin appearance temperature and a significant alteration of paraffin crystal morphology.

From the above previous modeling studies on the flow of waxy crude oil in pipeline systems, most of the focus has been put on single-phase flow of crude oil in pipelines but significant problems may also occur in multiphase flow. Thus, existing studies have not fully addressed the needs of oil producers since these models have not incorporated the co-existent water during crude oil extraction. The identified research gaps prevent the direct application of existing wax deposition models to field-scale crude oil pipeline transport systems. The present study, therefore, is an attempt to come up with a more comprehensive study that takes into consideration the effects of water-in-oil emulsions, surface tension, porosity of the gel layer, internal heat generation/absorption, viscous

dissipation, precipitation kinetics of wax, molecular diffusion and shear dispersion on the growth and aging of the gel layer. From an economic perspective, an accurate prediction of the rate of wax deposition is essential for the design of pigging operations to achieve optimum pigging-frequency and minimize operational costs.

The next chapter presents the mathematical formulation of the problem, and includes the governing equations, assumptions, the non-dimensionalization process, and solution methods for the final model equations.

CHAPTER THREE

METHODOLOGY

This chapter presents the mathematical modeling of wax deposition in multiphase flow for field-scale crude oil pipeline transport systems, along with the numerical solution of the model equations.

3.1 Formulation of the Problem

Unsteady two-dimensional flow of waxy crude oil together with some water droplets in a model pipeline of circular cross-section with a semi-infinite length and inner radius R is considered, as shown in Figure 3.1. The pipeline is elevated at an angle φ to the horizontal. A cylindrical coordinate system (r, θ, z) is chosen such that r denotes the radial distance from the pipe centerline, θ denotes the tangential direction, and z denotes the stream-wise coordinate or the axial direction. At time $t = 0$, waxy crude oil of uniform temperature T_∞ is injected at the pipeline inlet. The pipeline inner wall is considered smooth, rigid and impermeable and is maintained at a uniform temperature T_{wall}. The temperature T_{wall} may either be less than or greater than the free-stream (or ambient) temperature T_∞. The simultaneous action of two wax deposition mechanisms, i.e., shear dispersion and molecular diffusion, is considered.

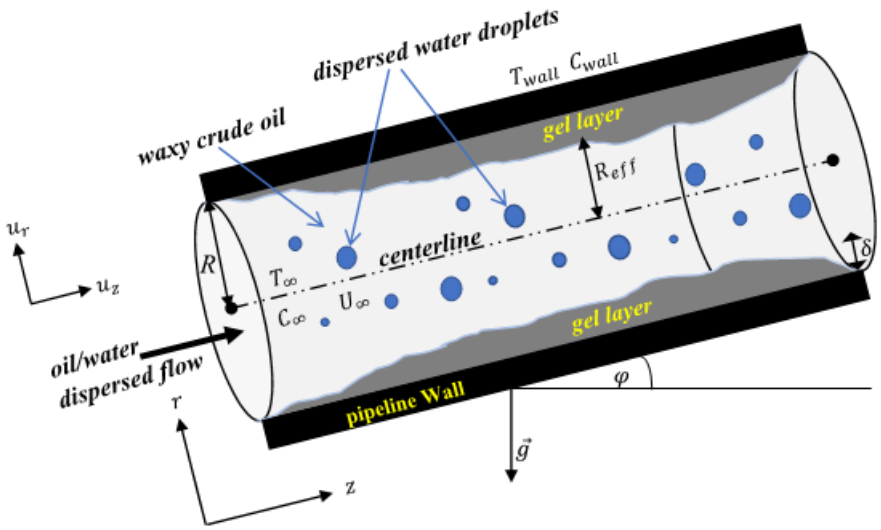

Figure 3.1: Computational Domain for a Model Crude Oil Pipeline (Banki *et al.*, 2008).

The elevation of the pipeline is necessary to avoid bends on the pipeline, which may result in flow through corners and hence causing back-flow of crude oil. The fluid phase and the solid phase are divided by a sharp interface with normal vector $\vec{n}$. The fluid system is described in terms of three pseudo-components, i.e., oil, wax and emulsions.

3.2 Assumptions

The following assumptions are made to model the flow problem presented above.

1. The flow is axisymmetric, meaning that the flow variables/properties do not depend on θ and that there is no tangential velocity component.
2. There is no gas in the crude oil pipeline system since the present study is confined to water-oil two-phase flow.
3. The fluid is considered as a continuous primary phase, whereas solid wax crystals is the discrete secondary phase. Furthermore, the dispersed water droplets flow at the same velocity as the continuous oil phase.
4. Thermophysical properties in each phase are constants. However, the variation of the density of the mixture fluid with temperature and species concentration is considered in the body force term only; and is assumed to vary linearly so that the usual Boussinesq's approximation is applicable in the boundary layer flow.
5. Molecular diffusion and shear dispersion are the only mechanisms responsible for wax deposition and that the thickness of the deposit layer is uniform.
6. There is no slip of fluid particles at the solid-liquid boundary.
7. The flow is non-relativistic, meaning that the velocity of waxy crude oil is much less than the speed of light.

3.3 Volume of Fluid Model

The crude oil, water-in-oil emulsions and the gel layer are three immiscible phases separated by an interface. This study employs an interface-tracking technique called the volume of fluid (VOF) model to capture the dynamics of the interface separating the phases, throughout the flow domain. In the VOF model, the fraction of the volume occupied by each phase in the entire domain of the study is determined at any location

and time (Safaei *et al.*, 2016). Thus, the sum of the volume fractions for all the phases is equal to unity (or one). The VOF method is appropriate since the complex interface shapes can be tracked from a simple volume fraction transport equation, without the convergence problems associated with moving grids. This makes it suitable for simulating fluid flows with phase-change. Thus, a single set of mixture momentum and energy equations is solved throughout the domain, and the resulting velocity, pressure and temperature fields are shared among the phases.

The fluid model adopted makes use of three variables to define the volume fraction of each phase within the flow domain. The fraction of the volume occupied by crude oil, water-in-oil emulsions and gel layer in the computational domain of the pipeline are denoted by ϕ_{oil}, ϕ_{water} and ϕ_{gel}, respectively. Thus,

$$\phi_{\text{oil}} + \phi_{\text{water}} + \phi_{\text{gel}} = 1 \tag{3.1}$$

Accordingly, the case when $\phi_{\text{oil}} = 1$ represents a pipeline filled with the crude oil only. Similarly, $\phi_{\text{water}} = 1$ represents a pipeline filled with water only and $\phi_{\text{gel}} = 1$ represents a pipeline filled with the wax-oil gel only (i.e., a blocked pipeline). The volume fraction of each phase takes values in the interval $[0, 1]$. Note that the volume fraction of water-in-oil emulsions remains constant throughout the computational domain of the pipeline.

3.4 Thermophysical Properties of the Mixture Fluid

This study employs the Pseudo-Single Phase (PSP) approach where the crude oil-water-gel three-phase mixture is treated as a single mixture fluid whose physical properties are computed by averaging the corresponding physical properties of the oil, water and gel, weighted by the corresponding volume fractions, as presented in (Ahmadi Nadooshan & Shirani, 2008; Zheng *et al.*, 2017; Yang *et al.*, 2019; Magnini & Matar, 2019). Thus, if the volume fractions of water and gel are being tracked, then the average density, average dynamic viscosity, and the average coefficients of volume expansion of the mixture fluid in each computational cell are given by the volume-based averaging method as:

$$\rho_{\text{f}} = (1 - \phi_{\text{water}})\, \rho_{\text{oil}} + \phi_{\text{water}} \rho_{\text{water}} \tag{3.2a}$$

$$\rho_{\text{mix}} = (1 - \phi_{\text{gel}})\, \rho_{\text{f}} + \phi_{\text{gel}} \rho_{\text{gel}}. \tag{3.2b}$$

$$\mu_{\text{f}} = (1 - \phi_{\text{water}})\, \mu_{\text{oil}} + \phi_{\text{water}} \mu_{\text{water}}. \tag{3.2c}$$

$$\mu_{\text{mix}} = (1 - \phi_{\text{gel}})\, \mu_{\text{f}} + \phi_{\text{gel}} \mu_{\text{gel}}. \tag{3.2d}$$

$$(\beta_{\mathrm{T}})_{\mathrm{f}} = (1-\phi_{\mathrm{water}})\,(\beta_{\mathrm{T}})_{\mathrm{oil}} + \phi_{\mathrm{water}}\,(\beta_{\mathrm{T}})_{\mathrm{water}}\,. \tag{3.2e}$$

$$(\beta_{\mathrm{T}})_{\mathrm{mix}} = (1-\phi_{\mathrm{gel}})\,(\beta_{\mathrm{T}})_{\mathrm{f}} + \phi_{\mathrm{gel}}\,(\beta_{\mathrm{T}})_{\mathrm{gel}}\,. \tag{3.2f}$$

$$(\beta_{\mathrm{C}})_{\mathrm{f}} = (1-\phi_{\mathrm{water}})\,(\beta_{\mathrm{C}})_{\mathrm{oil}} + \phi_{\mathrm{water}}\,(\beta_{\mathrm{C}})_{\mathrm{water}}\,. \tag{3.2g}$$

$$(\beta_{\mathrm{C}})_{\mathrm{mix}} = (1-\phi_{\mathrm{gel}})\,(\beta_{\mathrm{C}})_{\mathrm{f}} + \phi_{\mathrm{gel}}\,(\beta_{\mathrm{C}})_{\mathrm{gel}}\,. \tag{3.2h}$$

The average heat capacity of the mixture fluid at constant pressure is given by the weight-based averaging method as:

$$(Cp)_{\mathrm{f}} = \frac{(1-\phi_{\mathrm{water}})\,\rho_{\mathrm{oil}}\,(Cp)_{\mathrm{oil}} + \phi_{\mathrm{water}}\rho_{\mathrm{water}}\,(Cp)_{\mathrm{water}}}{\rho_{\mathrm{f}}}. \tag{3.3}$$

$$(Cp)_{\mathrm{mix}} = \frac{(1-\phi_{\mathrm{gel}})\,\rho_{\mathrm{f}}\,(Cp)_{\mathrm{f}} + \phi_{\mathrm{gel}}\rho_{\mathrm{gel}}\,(Cp)_{\mathrm{gel}}}{\rho_{\mathrm{mix}}}. \tag{3.4}$$

The average thermal conductivity of the mixture fluid is given by the Maxwell–Garnett correlation (Ogbuanu & Roy, 2022) as:

$$k_{\mathrm{f}} = \left[\frac{k_{\mathrm{water}} + 2k_{\mathrm{oil}} + 2\phi_{\mathrm{water}}\,(k_{\mathrm{water}} - k_{\mathrm{oil}})}{k_{\mathrm{water}} + 2k_{\mathrm{oil}} - \phi_{\mathrm{water}}\,(k_{\mathrm{water}} - k_{\mathrm{oil}})}\right] k_{\mathrm{oil}} \tag{3.5}$$

$$k_{\mathrm{mix}} = \left[\frac{k_{\mathrm{gel}} + 2k_{\mathrm{f}} + 2\phi_{\mathrm{gel}}\,(k_{\mathrm{gel}} - k_{\mathrm{f}})}{k_{\mathrm{gel}} + 2k_{\mathrm{f}} - \phi_{\mathrm{gel}}\,(k_{\mathrm{gel}} - k_{\mathrm{f}})}\right] k_{\mathrm{f}}. \tag{3.6}$$

The subscript f represents the fluid phase, i.e., crude oil and water-in-oil emulsions. Zheng *et al.* (2017) concluded that the pseudo-single phase approach is suitable for field scale simulations.

3.5 Modeling the Wax Concentration

Crude oil is a mixture of several hydrocarbon components and hence tracking the concentration of each single component is not practical as the flow evolves within the pipeline. Therefore, this study adopts a pragmatic fluid model in which wax exists in two different forms, i.e., dissolved wax and crystallized wax (or precipitated wax). Since the mass concentration of wax (or the amount of wax) which remains soluble (C_{d}) in the liquid phase must be equal to the total wax concentration (C) minus the amount of wax that has precipitated (C_{p}), the total mass concentration of wax in the crude oil at any location (r, z) and time t is given by

$$C(r,z,t) = C_{\mathrm{d}}(r,z,t) + C_{\mathrm{p}}(r,z,t). \tag{3.7}$$

Suppose that the precipitated wax (C_{p}) exists in two different forms, i.e., aggregated or deposited wax (C_{a}) and non-aggregated wax (C_{n}). Thus, the mass concentration of the non-aggregated wax crystals is given by

$$C_{\mathrm{n}}(r,z,t) = C_{\mathrm{p}}(r,z,t) - C_{\mathrm{a}}(r,z,t). \tag{3.8}$$

At temperatures above the WAT, the total wax concentration is given by $C(r,z,t) = C_{\mathrm{d}}(r,z,t)$ since this is a case of unsaturated solution. This study focuses on complete saturation, i.e., it is supposed that the dissolved wax concentration (C_{d}) is the one of saturation at all locations in the domain, which depends only on temperature, i.e.,

$$C_{\mathrm{d}} = C_{\mathrm{d}}(T(r,z,t)). \tag{3.9}$$

In order to describe the crystalline (or precipitate) component of wax in the crude oil, this study considers a dimensionless parameter α_{m} known as the aggregation degree of wax, which is defined in (Fusi, 2003) as the ratio of the concentration of aggregated wax to the concentration of precipitated wax, i.e.,

$$\alpha_{\mathrm{m}}(r,z,t) = \frac{C_{\mathrm{a}}(r,z,t)}{C_{\mathrm{p}}(r,z,t)}. \tag{3.10}$$

Thus, α_{m} takes values in the interval $[0,1]$. It plays a crucial role in determining the specific rheology of the fluid. Eliminating C_{a} between Equations (3.8) and (3.10) yields:

$$C_{\mathrm{n}} = (1-\alpha_{\mathrm{m}})\, C_{\mathrm{p}}. \tag{3.11}$$

Eliminating C_{p} between Equations (3.7) and (3.11) yields the relation:

$$C_{\mathrm{n}} = [1-\alpha_{\mathrm{m}}]\,(C - C_{\mathrm{d}})\,. \tag{3.12}$$

Equation (3.12) is used to calculate the concentration of non-aggregated wax crystals (C_{n}) in the crude oil pipeline once C, C_{d} and α_{m} are known from the numerical simulations.

3.6 Wax Deposition Mechanisms

The wax deposition mechanisms considered in this study are molecular diffusion and shear dispersion. Molecular diffusion involves dissolved wax while shear dispersion involves non-aggregated wax crystals. The mathematical models of wax deposition mechanisms via molecular diffusion and shear dispersion are presented in detail in Subsection 3.6.1 and Subsection 3.6.2, respectively.

3.6.1 Molecular Diffusion

Molecular diffusion is a deposition process due to the presence of a concentration gradient of the dissolved wax, which is induced by the temperature gradient. The process is governed by Fick's first law, which states that the mass flux of a diffusing species (or solute) goes from the region of high concentration to the region of low concentration with a magnitude that is proportional to the concentration gradient of the diffusing species. In this case, the constant of proportionality is called the diffusivity. Suppose that Fick's law of diffusion holds and other sources of diffusion such as the thermal diffusion (Soret effect or thermophoresis) are negligible. The mass flux of the dissolved wax due to molecular diffusion is given by

$$\vec{J}_{\mathrm{d}} = -D_{\mathrm{d}} \left(\vec{\nabla} C_{\mathrm{d}} \right), \tag{3.13}$$

where the negative sign on the right-hand side of Equation (3.13) means that the diffusing species moves from the region of high concentration to the region of low concentration. Since the radial concentration gradient of the dissolved wax is not readily available, the chain rule of differentiation is used in Equation (3.13) to express $\vec{\nabla} C_{\mathrm{d}}$ as a product of the change in concentration of the dissolved wax with respect to temperature and the temperature gradient. Thus, Equation (3.13) becomes

$$\vec{J}_{\mathrm{d}} = -D_{\mathrm{d}} \left(\frac{dC_{\mathrm{d}}}{dT} \vec{\nabla} T \right). \tag{3.14}$$

Equation (3.14) is known as the Fick’s diffusion equation. It expresses the rate at which the dissolved wax is transported to the pipeline wall per unit surface. In cylindrical coordinates, Equation (3.14) becomes

$$\vec{J}_{\mathrm{d}} = -D_{\mathrm{d}} \frac{dC_{\mathrm{d}}}{dT} \left(\frac{\partial T}{\partial r} \hat{\mathbf{r}} + \frac{\partial T}{\partial z} \hat{\mathbf{k}} \right). \tag{3.15}$$

Equation (3.15) is the equation governing the deposition of wax in the pipeline via molecular diffusion mechanism.

3.6.2 Shear Dispersion

Shear dispersion is a deposition process due to the "shearing" of the fluid particles, i.e., some wax crystals tend to migrate towards the wall of the crude oil pipeline because of the presence of a radial velocity gradient. The mass flux of precipitated wax due to shear

dispersion is given by

$$\vec{J}_{\mathrm{p}} = -\left[L_1(|\gamma_{\mathrm{n}}|)C_{\mathrm{a}} + L_2(|\gamma_{\mathrm{n}}|)C_{\mathrm{n}}\right]\vec{n}, \tag{3.16}$$

where L_1 and L_2 are non-negative functions of the shear rate γ_{n} (evaluated for the surface element with normal vector $\vec{n}$). In this study, it is assumed that the flux $\vec{J}_{\mathrm{p}}$ of the precipitated wax crystals is proportional to the concentration C_{n} of the non-aggregated wax and to the radial velocity gradient $\partial u_z/\partial r$ only. Thus, setting $L_1 = 0$, $L_2 = D_{\mathrm{p}}\left(\partial u_z/\partial r\right)$ and $\vec{n} = \hat{\mathbf{r}}$ in (3.16), yields the cylindrical coordinates form of $\vec{J}_{\mathrm{p}}$ as:

$$\vec{J}_{\mathrm{p}} = -D_{\mathrm{p}}C_{\mathrm{n}}\frac{\partial u_z}{\partial r}\hat{\mathbf{r}}. \tag{3.17}$$

Equation (3.17) is the equation governing the deposition of wax in the pipeline via shear dispersion mechanism.

3.7 Governing Equations

The flow of waxy crude oil in pipeline transport systems can be described mathematically by the equations of conservation of mass, conservation of linear momentum, conservation of energy, and evolution of the diffusing species. The governing equations are presented in their general forms in Subsection 3.7.1 and the specific contributions to the general governing equations are presented in detail in Subsection 3.7.2.

3.7.1 General Governing Equations

This subsection presents the general forms of the equations governing the wax deposition from multiphase flow in crude oil pipeline transport systems.

3.7.1.1 Equation of Continuity

The continuity equation is derived from the principle of conservation of mass which states that under normal conditions mass can neither be created nor destroyed. The general form of the continuity equation, in vector notation, is given by

$$\frac{\partial \rho_{\mathrm{mix}}}{\partial t} + \vec{\nabla}\cdot\left(\rho_{\mathrm{mix}}\vec{V}\right) = 0. \tag{3.18}$$

Equation (3.18) is essential in determining whether the fluid flow is possible or not. Fluid flow is possible if the continuity equation is satisfied.

3.7.1.2 Equation of Conservation of Linear Momentum

The equation of motion is derived from Newton's second law of linear motion, which states that the rate of change in momentum of a body is equal to the resultant external force acting on the body and takes place in the direction of the force. The momentum of a body is defined as the product of its mass and velocity. The general equation of motion for an incompressible fluid flow, in vector notation, is given by

$$\rho_{\text{mix}} \left[\frac{\partial \vec{V}}{\partial t} + \vec{V} \cdot \left(\vec{\nabla} \vec{V} \right) \right] = -\vec{\nabla} p + \vec{\nabla} \cdot \vec{\tau} + \rho_{\text{mix}} \vec{F}. \tag{3.19}$$

The term $\frac{\partial \vec{V}}{\partial t}$ is the temporal acceleration, $\vec{V} \cdot \left(\vec{\nabla} \vec{V} \right)$ is the convective acceleration, $\vec{\nabla} p$ is the pressure gradient, $\vec{\nabla} \cdot \vec{\tau}$ denotes the viscous forces, and $\rho_{\text{mix}} \vec{F}$ represents body forces, such as gravitational force, Lorentz force, and so on, that are driving the motion of the fluid.

3.7.1.3 Equation of Energy

The energy equation is derived from the first law of thermodynamics, which states that the amount of heat added to a system is equal to the change in internal energy and the work done. The general equation of energy for an incompressible fluid flow, in vector notation, is given by:

$$\rho_{\text{mix}} \left(Cp \right)_{\text{mix}} \left[\frac{\partial T}{\partial t} + \vec{V} \cdot \left(\vec{\nabla} T \right) \right] = \vec{\nabla} \cdot \left(k_{\text{mix}} \vec{\nabla} T \right) + S_{\text{e}}, \tag{3.20}$$

where $\rho_{\text{mix}} \left(Cp \right)_{\text{mix}}$ is the volumetric heat capacity, $\vec{V} \cdot \left(\vec{\nabla} T \right)$ is the heat flux due to convection, $\vec{\nabla} \cdot \left(k_{\text{mix}} \vec{\nabla} T \right)$ is the heat flux due to conduction and S_{e} represents the energy source term such as thermal radiation and the internal heating of the fluid due to viscous dissipation. Viscous dissipation represents the heat generated due to viscous stresses within the fluid. The dissipation function has negligible values except for large velocity gradients at supersonic speeds.

3.7.1.4 Equation of Species Concentration

Precipitation of wax molecules and formation of the gel layer on the inner wall of crude oil pipeline creates a radial concentration gradient of the dissolved wax in the liquid oil, which results in a net radial diffusive flux of wax molecules. In general, the radial diffusion of

wax molecules is governed by the mass transfer boundary layer equation:

$$\frac{\partial C}{\partial t} + \vec{V} \cdot \left(\vec{\nabla} C\right) = \vec{\nabla} \cdot \left(D_{\mathrm{d}} \vec{\nabla} C\right) + S_{\mathrm{c}}, \tag{3.21}$$

where C is the total concentration of dissolved wax in the oil phase, $\vec{V} \cdot \left(\vec{\nabla} C\right)$ is the mass flux due to convection, $\vec{\nabla} \cdot \left(D_{\mathrm{d}} \vec{\nabla} C\right)$ is the mass flux due to diffusion of the species and S_{c} represents the concentration source term due to chemical reaction or other generation of the species such as Brownian diffusion, shear dispersion, and Thermophiresis (or the Soret effect).

3.7.1.5 Volume Fraction Equation

The tracking of the interface(s) between the phases is accomplished by the solution of a continuity equation for the volume fraction of one (or more) of the phases. For the i^{th} phase, the volume fraction equation takes the general form:

$$\frac{\partial \phi_{\mathrm{i}}}{\partial t} + \vec{\nabla} \cdot \left(\phi_{\mathrm{i}} \vec{V}\right) = \frac{S_{\phi_{\mathrm{i}}}}{\rho_{\mathrm{i}}}. \tag{3.22}$$

By default, the source term on the right-hand side of Equation (3.22) is zero, but a constant or user-defined mass source can be specified for each phase. The volume fraction equation is not solved for the primary phase (i.e., the oil phase). However, the volume fraction of the primary phase is computed based on the constraint (3.1).

3.7.2 Specific Governing Equations

The specific equations governing the wax deposition from multiphase flow in crude oil pipeline transport systems are obtained by adding suitable source terms to the general governing equations. The resulting equations are then converted to cylindrical coordinates and the assumptions made are imposed on the equations.

3.7.2.1 Equation of Continuity

Imposing the assumption of mixture incompressibility (i.e., ρ_{mix} is assumed constant), the continuity Equation (3.18) reduces to the simpler form

$$\vec{\nabla} \cdot \vec{V} = 0. \tag{3.23}$$

In cylindrical coordinates, Equation (3.23) becomes

$$\frac{1}{r}\frac{\partial}{\partial r}\left(ru_r\right)+\frac{1}{r}\frac{\partial u_\theta}{\partial \theta}+\frac{\partial u_z}{\partial z}=0. \tag{3.24}$$

Since the flow is assumed to be axisymmetric, the velocity field takes the form $\vec{V} = u_r\hat{\mathbf{r}} + u_z\hat{\mathbf{k}}$. Therefore, Equation (3.24) reduces to the simpler form

$$\frac{1}{r}\frac{\partial}{\partial r}\left(ru_r\right)+\frac{\partial u_z}{\partial z}=0. \tag{3.25}$$

Multiplying Equation (3.25) through by r yields

$$\frac{\partial\left(ru_r\right)}{\partial r}+\frac{\partial\left(ru_z\right)}{\partial z}=0. \tag{3.26}$$

Equation (3.26) is the specific equation of continuity, in cylindrical coordinate system, for water-oil two-phase flow in crude oil transportation pipeline.

3.7.2.2 Equation of Conservation of Linear Momentum

In this study, the Darcy-type source term (or porous viscous term), the buoyancy force, and the surface tension force are added to the right-hand side of the momentum Equation (3.19) and the resulting equation is converted to cylindrical coordinates.

3.7.2.2.1 Darcy's Law

Darcy's law describes the flow of fluid through a porous material such as the gel-layer, driven by pressure gradient. The law states that the volumetric flow rate (Q) of a fluid through a porous material is directly proportional to both the cross-sectional area (A) of the porous material and the pressure gradient ($\vec{\nabla}p$) and inversely proportional to the dynamic viscosity (μ_{mix}) of the fluid, i.e.,

$$Q \propto \frac{A}{\mu_{\text{mix}}}\vec{\nabla}p. \tag{3.27}$$

Introducing the constant of proportionality (κ) to the Darcy's law (3.27), yields the following mathematical expression for the Darcy's law:

$$Q = -\frac{\kappa A}{\mu_{\text{mix}}}\vec{\nabla}p. \tag{3.28}$$

The negative sign in Equation (3.28) is necessary since fluid flow occurs from a region of high pressure to a region of low pressure (i.e., in a direction opposite the direction of

increasing pressure gradient). Substituting the expression for the volumetric flow rate $Q = A\vec{V}$ into the Darcy's equation (3.28) yields

$$\vec{V} = -\frac{\kappa}{\mu_{\text{mix}}}\vec{\nabla}p. \tag{3.29}$$

Making $\vec{\nabla}p$ the subject in the Darcy's Equation (3.29), yields

$$\vec{\nabla}p = -\frac{\mu_{\text{mix}}}{\kappa}\vec{V}. \tag{3.30}$$

Equation (3.31) means that the momentum equation strikes a balance between viscous forces and the pressure gradient in the porous medium. Note that the Darcy's law given by Equation (3.31) only applies to slow viscous flows through a porous material but does not apply to high velocity flows through a porous material. Therefore, the body force ($\vec{F}_{\text{Darcy}}$) due to Darcy's law is given by

$$\vec{F}_{\text{Darcy}} = -\frac{\mu_{\text{mix}}}{\kappa}\vec{V}. \tag{3.31}$$

Since the gel layer is a porous material, the Darcy-type source term given by Equation (3.31) should be added to the right-hand side of the momentum Equation (3.19) in order to describe the deceleration of the flow through the gel layer.

3.7.2.2.2 Surface Tension Force

Surface tension force exists at the interface between any two fluids if at least one of the fluids is a liquid, due to the adhesive forces between molecules of the two fluids. Since the present study deals with flow with more than one phase, the surface tension at the interface of the continuous oil phase and the gel layer should be accounted for in the momentum equation. The oil-gel interface behaves in a manner similar to a thinly stretched membrane. This study adopts the continuum surface force (CSF) model, proposed by Brackbill *et al.* (1992), which formulates the surface tension force at the oil-gel interface into an equivalent body force given as:

$$\vec{F}_{\text{surface}} = \sigma K \vec{\nabla}\phi_{\text{oil}}. \tag{3.32}$$

The direction and magnitude of body force due to surface tension are determined by the curvature (K) of the oil-gel interface. The interface curvature in the CSF model given by Equation (3.32) is calculated by the following formula:

$$K = -\left(\vec{\nabla}\cdot\hat{\mathbf{n}}\right), \tag{3.33}$$

where $\hat{\mathbf{n}} = \vec{\nabla}\phi_{\text{oil}} / \left|\vec{\nabla}\phi_{\text{oil}}\right|$ is an outward unit normal vector to the oil-gel interface. The basic idea of the CSF model is to regard the oil-gel interface as a transition region with a finite thickness, instead of a zero-thickness membrane. The surface tension effect is interpreted as a continuous body force spread across the transition region, which acts as a source term in the momentum equation. The CSF model allows us to treat the dynamic boundary condition at the interface implicitly.

The volumetric surface tension force given by Equation (3.32) is added to the momentum equation to model the effect of surface tension. With the CSF model, the location of the oil-gel interface is no longer explicitly required in the analysis, since it is already captured in the momentum equation (Wu *et al.*, 1998).

3.7.2.2.3 Boussinesq's Approximation

The flow of waxy crude oil is naturally established due to the existence of temperature and concentration gradients in the fluid. The density of the mixture fluid depends on temperature and species concentration, written mathematically as

$$\rho_{\text{mix}} = \rho_{\text{mix}}(T, C) \tag{3.34}$$

The variation of density with temperature and species concentration is responsible for numerous natural phenomena such as heat and mass transfer by natural convection. The density variation gives rise to buoyancy forces that drive the motion of the fluid. The Boussinesq's approximation, therefore, states that the variation of the density of a fluid is neglected everywhere in the flow field except in the buoyancy terms. Expanding the density function given by Equation (3.34) in Taylor's series about the reference temperature T_∞ and the reference concentration C_∞ yields

$$\begin{aligned}\rho_{\text{mix}} = \rho_\infty + \left(\frac{\partial \rho_{\text{mix}}}{\partial T}\right)_P (T - T_\infty) + \left(\frac{\partial \rho_{\text{mix}}}{\partial C}\right)_P (C - C_\infty) + \frac{1}{2!}\Bigg[\left(\frac{\partial^2 \rho_{\text{mix}}}{\partial T^2}\right)_P (T - T_\infty)^2 \\ + 2\left(\frac{\partial^2 \rho_{\text{mix}}}{\partial T \partial C}\right)_P (T - T_\infty)(C - C_\infty) + \left(\frac{\partial^2 \rho_{\text{mix}}}{\partial C^2}\right)_P (C - C_\infty)^2\Bigg] + \cdots,\end{aligned} \tag{3.35}$$

where $\rho_\infty = \rho_{\text{mix}}(T_\infty, C_\infty)$ and P is the reference point (T_∞, C_∞) about which the density function is expanded. If the temperature gradient $(T - T_\infty)$ and the concentration gradient $(C - C_\infty)$ are very small such that the terms of order ≥ 2 can be neglected, then Equation (3.35) reduces to the simpler form

$$\rho_{\text{mix}} \approx \rho_\infty + \left(\frac{\partial \rho_{\text{mix}}}{\partial T}\right)_P (T - T_\infty) + \left(\frac{\partial \rho_{\text{mix}}}{\partial C}\right)_P (C - C_\infty). \tag{3.36}$$

The coefficient of volume expansion $(\beta_{\mathrm{T}})_{\mathrm{mix}}$ due to changes in temperature of the mixture fluid is defined in Cengel & Cimbala (2010) and Bergman *et al.* (2017) as:

$$(\beta_{\mathrm{T}})_{\mathrm{mix}} = \frac{1}{V}\left(\frac{\partial V}{\partial T}\right)_P = -\frac{1}{\rho_{\mathrm{mix}}}\left(\frac{\partial \rho_{\mathrm{mix}}}{\partial T}\right)_P, \tag{3.37}$$

where V is the specific volume (or volume per unit mass, i.e., $V = 1/\rho_{\mathrm{mix}}$). A large value of $(\beta_{\mathrm{T}})_{\mathrm{mix}}$ for a fluid means a large change in density with temperature. Similarly, the coefficient of volume expansion $(\beta_{\mathrm{C}})_{\mathrm{mix}}$ due to changes in species concentration is defined as

$$(\beta_{\mathrm{C}})_{\mathrm{mix}} = \frac{1}{V}\left(\frac{\partial V}{\partial C}\right)_P = -\frac{1}{\rho_{\mathrm{mix}}}\left(\frac{\partial \rho_{\mathrm{mix}}}{\partial C}\right)_P. \tag{3.38}$$

Substituting Equations (3.37) and (3.38) into Equation (3.36) and rearranging yields

$$(\rho_\infty - \rho_{\mathrm{mix}}) \approx \rho_{\mathrm{mix}}\,(\beta_{\mathrm{T}})_{\mathrm{mix}}\,(T - T_\infty) + \rho_{\mathrm{mix}}\,(\beta_{\mathrm{C}})_{\mathrm{mix}}\,(C - C_\infty). \tag{3.39}$$

Equation (3.39) is known as the Boussinesq's approximation and it shows that in solving natural convection problems, the equations of momentum, energy and species concentration are coupled, necessitating a simultaneous solution of the governing equations.

3.7.2.2.4 Stress Tensor

The stress tensor ($\vec{\tau}$) in Equation (3.19) is given in Moukalled *et al.* (2016) as:

$$\vec{\tau} = \mu_{\mathrm{mix}}\left[\vec{\nabla}\vec{V} + \left(\vec{\nabla}\vec{V}\right)^{\mathrm{T}}\right] + \lambda \mathbf{I}\left(\vec{\nabla}\cdot\vec{V}\right), \tag{3.40}$$

where $\lambda = -(2/3)\mu_{\mathrm{mix}}$ is the bulk viscosity coefficient, the superscript T denotes the transpose, and $\mathbf{I}$ is the unit (or identity) tensor of size (3×3) defined as.

$$\mathbf{I} = \begin{pmatrix} 1 & 0 & 0 \\ 0 & 1 & 0 \\ 0 & 0 & 1 \end{pmatrix} \tag{3.41}$$

The stress tensor represents six shear stresses (i.e., stresses acting in the tangential direction to the flow field) and three normal stresses (i.e., compressive or tensile stresses perpendicular to the direction of the flow). The expanded form of the stress tensor in

three-dimensional cylindrical coordinate system is given in Ochieng *et al.* (2018) as:

$$\begin{pmatrix} \tau_{rr} & \tau_{r\theta} & \tau_{rz} \\ \tau_{\theta r} & \tau_{\theta\theta} & \tau_{\theta z} \\ \tau_{zr} & \tau_{z\theta} & \tau_{zz} \end{pmatrix} = \mu_{\text{mix}} \begin{pmatrix} 2\dfrac{\partial u_r}{\partial r} - \dfrac{2}{3}\vec{\nabla}\cdot\vec{V} & \dfrac{1}{r}\dfrac{\partial u_r}{\partial \theta} + \dfrac{\partial u_\theta}{\partial r} - \dfrac{u_\theta}{r} & \dfrac{\partial u_z}{\partial r} + \dfrac{\partial u_r}{\partial z} \\ \dfrac{1}{r}\dfrac{\partial u_r}{\partial \theta} + \dfrac{\partial u_\theta}{\partial r} - \dfrac{u_\theta}{r} & 2\Big(\dfrac{1}{r}\dfrac{\partial u_\theta}{\partial \theta} + \dfrac{u_r}{r}\Big) - \dfrac{2}{3}\vec{\nabla}\cdot\vec{V} & \dfrac{\partial u_\theta}{\partial z} + \dfrac{1}{r}\dfrac{\partial u_z}{\partial \theta} \\ \dfrac{\partial u_z}{\partial r} + \dfrac{\partial u_r}{\partial z} & \dfrac{\partial u_\theta}{\partial z} + \dfrac{1}{r}\dfrac{\partial u_z}{\partial \theta} & 2\dfrac{\partial u_z}{\partial z} - \dfrac{2}{3}\vec{\nabla}\cdot\vec{V} \end{pmatrix} \tag{3.42}$$

Equation (3.42) gives the relation between the stress components and the velocity field and is called the Stokes relations. Imposing the assumptions that the mixture fluid is incompressible (i.e., $\vec{\nabla}\cdot\vec{V} = 0$) and that the flow is axisymmetric, the stress matrix given by Equation (3.42) reduces to the simpler form:

$$\begin{pmatrix} \tau_{rr} & \tau_{r\theta} & \tau_{rz} \\ \tau_{\theta r} & \tau_{\theta\theta} & \tau_{\theta z} \\ \tau_{zr} & \tau_{z\theta} & \tau_{zz} \end{pmatrix} = \mu_{\text{mix}} \begin{pmatrix} 2\dfrac{\partial u_r}{\partial r} & 0 & \dfrac{\partial u_z}{\partial r} + \dfrac{\partial u_r}{\partial z} \\ 0 & 2\dfrac{u_r}{r} & 0 \\ \dfrac{\partial u_z}{\partial r} + \dfrac{\partial u_r}{\partial z} & 0 & 2\dfrac{\partial u_z}{\partial z} \end{pmatrix} \tag{3.43}$$

Despite the fact that the rheology of crude oils below the WAT has been extensively studied by many authors and several constitutive equations to describe their non-Newtonian behaviour have been proposed (e.g. Casson and Herschel-Bulkley models), these constitutive equations cannot be applied in the present study where the crude oil, water-in-oil emulsions and the gel-like deposit are modeled as distinct phases and specific values of the deposit viscosity (μ_{gel}) are needed.

3.7.2.2.5 Momentum Equation in Cylindrical Coordinates

Adding the Darcy-type source term ($\vec{F}_{\text{Darcy}}$) given by Equation (3.31), the buoyancy force ($-\rho_{\text{mix}}\vec{g}$), and the volumetric surface tension force ($\vec{F}_{\text{surface}}$) given by Equation (3.32) to the right-hand side of the momentum Equation (3.19) yields

$$\rho_{\text{mix}}\left[\frac{\partial \vec{V}}{\partial t} + \vec{V}\cdot\left(\vec{\nabla}\vec{V}\right)\right] = -\vec{\nabla}p + \vec{\nabla}\cdot\vec{\tau} - \frac{\mu_{\text{mix}}}{\kappa}\vec{V} - \rho_{\text{mix}}\vec{g} + \sigma K\vec{\nabla}\phi_{\text{oil}}. \tag{3.44}$$

The Boussinesq's approximation to the momentum Equation (3.44) is obtained as follows. Evaluating the momentum Equation (3.44) at the edge of the boundary layer where $\rho_{\text{mix}} \to \rho_\infty$, $p \to p_\infty$, $\vec{V} \to U_\infty$, $\kappa \to \infty$ (fluid phase) and $K \to 0$, yields the equation for

hydrostatic balance as:

$$-\vec{\nabla}p_{\infty} = \rho_{\infty}\vec{g}. \tag{3.45}$$

The pressure shift (p^*) is given in Currie (2016) as:

$$p^* = p - p_{\infty} \tag{3.46}$$

where the constant p_{∞} is the hydrostatic pressure. Making p the subject in Equation (3.46) yields

$$p = p^* + p_{\infty} \tag{3.47}$$

Substituting Equation (3.47) into the momentum Equation (3.44) and expanding the pressure term, yields

$$\rho_{\text{mix}}\left[\frac{\partial\vec{V}}{\partial t} + \vec{V}\cdot\left(\vec{\nabla}\vec{V}\right)\right] = -\vec{\nabla}p^* - \vec{\nabla}p_{\infty} + \vec{\nabla}\cdot\vec{\tau} - \frac{\mu_{\text{mix}}}{\kappa}\vec{V} - \rho_{\text{mix}}\vec{g} + \sigma K\vec{\nabla}\phi_{\text{oil}} \tag{3.48}$$

Substituting Equation (3.45) into the momentum Equation (3.48), rearranging the terms on the right-hand side and dropping the star ($*$), yields

$$\rho_{\text{mix}}\left[\frac{\partial\vec{V}}{\partial t} + \vec{V}\cdot\left(\vec{\nabla}\vec{V}\right)\right] = -\vec{\nabla}p - \frac{\mu_{\text{mix}}}{\kappa}\vec{V} + \vec{\nabla}\cdot\vec{\tau} + \left(\rho_{\infty} - \rho_{\text{mix}}\right)\vec{g} + \sigma K\vec{\nabla}\phi_{\text{oil}} \tag{3.49}$$

Substituting the Boussinesq's approximation for the density gradient $(\rho_{\infty} - \rho_{\text{mix}})$ given by Equation (3.39) into the momentum Equation (3.49), yields

$$\rho_{\text{mix}}\left[\frac{\partial\vec{V}}{\partial t} + \vec{V}\cdot\left(\vec{\nabla}\vec{V}\right)\right] = -\vec{\nabla}p - \frac{\mu_{\text{mix}}}{\kappa}\vec{V} + \vec{\nabla}\cdot\vec{\tau} + \rho_{\text{mix}}\vec{g}\left(\beta_{\text{T}}\right)_{\text{mix}}\left(T - T_{\infty}\right) + \rho_{\text{mix}}\vec{g}\left(\beta_{\text{C}}\right)_{\text{mix}}\left(C - C_{\infty}\right) + \sigma K\vec{\nabla}\phi_{\text{oil}}, \tag{3.50}$$

where $K = -\vec{\nabla}\cdot\left(\vec{\nabla}\phi_{\text{oil}}/\left|\vec{\nabla}\phi_{\text{oil}}\right|\right)$ is the curvature of the oil-gel interface. The terms $\rho_{\text{mix}}\vec{g}\left(\beta_{\text{T}}\right)_{\text{mix}}\left(T - T_{\infty}\right)$ and $\rho_{\text{mix}}\vec{g}\left(\beta_{\text{C}}\right)_{\text{mix}}\left(C - C_{\infty}\right)$ are the buoyancy forces that arise from the thermal and mass diffusion, respectively. In three-dimensional cylindrical coordinates, the stress tensor ($\vec{\tau}$) is written in component form as

$$\vec{\tau} = \left(\tau_{rr}, \tau_{r\theta}, \tau_{rz}\right)\hat{\mathbf{r}} + \left(\tau_{\theta r}, \tau_{\theta\theta}, \tau_{\theta z}\right)\hat{\mathbf{\Theta}} + \left(\tau_{zr}, \tau_{z\theta}, \tau_{zz}\right)\hat{\mathbf{k}} \tag{3.51}$$

Thus utilizing Equation (3.51), the stress form of the momentum Equation (3.50) in three-dimensional cylindrical coordinates is written in component form (Salih, 2011; Ochieng

et al., 2018) as:

$$r \text{ momentum:} \quad \rho_{\text{mix}}\left[\frac{\partial u_r}{\partial t}+u_r\frac{\partial u_r}{\partial r}+\frac{u_\theta}{r}\left(\frac{\partial u_r}{\partial \theta}-u_\theta\right)+u_z\frac{\partial u_r}{\partial z}\right]=-\frac{\partial p}{\partial r}-\frac{\mu_{\text{mix}}}{\kappa}u_r$$
$$+\frac{1}{r}\frac{\partial}{\partial r}\left(r\tau_{rr}\right)+\frac{1}{r}\frac{\partial}{\partial \theta}\left(\tau_{\theta r}\right)+\frac{\partial}{\partial z}\left(\tau_{zr}\right)-\frac{\tau_{\theta\theta}}{r}+\sigma K\frac{\partial \phi_{\text{oil}}}{\partial r}$$
$$+\rho_{\text{mix}}g_r\beta(T-T_\infty)+\rho_{\text{mix}}g_r\left(\beta_{\text{C}}\right)_{\text{mix}}\left(C-C_\infty\right) \tag{3.52a}$$

$$\theta \text{ momentum:} \quad \rho_{\text{mix}}\left[\frac{\partial u_\theta}{\partial t}+u_r\frac{\partial u_\theta}{\partial r}+\frac{u_\theta}{r}\left(\frac{\partial u_\theta}{\partial \theta}+u_r\right)+u_z\frac{\partial u_\theta}{\partial z}\right]=-\frac{1}{r}\frac{\partial p}{\partial \theta}-\frac{\mu_{\text{mix}}}{\kappa}u_\theta$$
$$+\frac{1}{r}\frac{\partial}{\partial r}\left(r\tau_{r\theta}\right)+\frac{1}{r}\frac{\partial}{\partial \theta}\left(\tau_{\theta\theta}\right)+\frac{\partial}{\partial z}\left(\tau_{z\theta}\right)+\frac{\tau_{\theta r}}{r}+\frac{\sigma K}{r}\frac{\partial \phi_{\text{oil}}}{\partial \theta}$$
$$+\rho_{\text{mix}}g_\theta\beta(T-T_\infty)+\rho_{\text{mix}}g_\theta\left(\beta_{\text{C}}\right)_{\text{mix}}\left(C-C_\infty\right) \tag{3.52b}$$

$$z \text{ momentum:} \quad \rho_{\text{mix}}\left[\frac{\partial u_z}{\partial t}+u_r\frac{\partial u_z}{\partial r}+\frac{u_\theta}{r}\frac{\partial u_z}{\partial \theta}+u_z\frac{\partial u_z}{\partial z}\right]=-\frac{\partial p}{\partial z}-\frac{\mu_{\text{mix}}}{\kappa}u_z$$
$$+\frac{1}{r}\frac{\partial}{\partial r}(r\tau_{rz})+\frac{1}{r}\frac{\partial}{\partial \theta}\left(\tau_{\theta z}\right)+\frac{\partial}{\partial z}\left(\tau_{zz}\right)+\sigma K\frac{\partial \phi_{\text{oil}}}{\partial z}$$
$$+\rho_{\text{mix}}g_z\beta(T-T_\infty)+\rho_{\text{mix}}g_z\left(\beta_{\text{C}}\right)_{\text{mix}}\left(C-C_\infty\right) \tag{3.52c}$$

where

$$K=-\left[\frac{1}{r}\frac{\partial}{\partial r}\left(\frac{r}{B}\frac{\partial \phi_{\text{oil}}}{\partial r}\right)+\frac{1}{r}\frac{\partial}{\partial \theta}\left(\frac{1}{rB}\frac{\partial \phi_{\text{oil}}}{\partial \theta}\right)+\frac{\partial}{\partial z}\left(\frac{1}{B}\frac{\partial \phi_{\text{oil}}}{\partial z}\right)\right] \tag{3.53}$$

and

$$B=\left|\vec{\nabla}\phi_{\text{oil}}\right|=\sqrt{\left(\frac{\partial \phi_{\text{oil}}}{\partial r}\right)^2+\frac{1}{r^2}\left(\frac{\partial \phi_{\text{oil}}}{\partial \theta}\right)^2+\left(\frac{\partial \phi_{\text{oil}}}{\partial z}\right)^2}. \tag{3.54}$$

Since the flow is axisymmetric, the momentum Equations (3.52a)−(3.52c) reduce to the simpler forms

$$r \text{ momentum: } \rho_{\text{mix}}\left[\frac{\partial u_r}{\partial t}+u_r\frac{\partial u_r}{\partial r}+u_z\frac{\partial u_r}{\partial z}\right]=-\frac{\partial p}{\partial r}-\frac{\mu_{\text{mix}}}{\kappa}u_r+\frac{1}{r}\frac{\partial}{\partial r}\left(r\tau_{rr}\right)+\frac{\partial}{\partial z}\left(\tau_{zr}\right)-\frac{\tau_{\theta\theta}}{r}$$
$$+\rho_{\text{mix}}g_r\left(\beta_{\text{T}}\right)_{\text{mix}}\left(T-T_\infty\right)+\rho_{\text{mix}}g_r\left(\beta_{\text{C}}\right)_{\text{mix}}\left(C-C_\infty\right)+\sigma K\frac{\partial \phi_{\text{oil}}}{\partial r}. \tag{3.55}$$
$$z \text{ momentum: } \rho_{\text{mix}}\left[\frac{\partial u_z}{\partial t}+u_r\frac{\partial u_z}{\partial r}+u_z\frac{\partial u_z}{\partial z}\right]=-\frac{\partial p}{\partial z}-\frac{\mu_{\text{mix}}}{\kappa}u_z+\frac{1}{r}\frac{\partial}{\partial r}\left(r\tau_{rz}\right)+\frac{\partial}{\partial z}\left(\tau_{zz}\right)$$
$$+\rho_{\text{mix}}g_z\left(\beta_{\text{T}}\right)_{\text{mix}}\left(T-T_\infty\right)+\rho_{\text{mix}}g_z\left(\beta_{\text{C}}\right)_{\text{mix}}\left(C-C_\infty\right)+\sigma K\frac{\partial \phi_{\text{oil}}}{\partial z}. \tag{3.56}$$

Similarly, Equations (3.53) and (3.54), respectively, reduce to the simpler forms

$$K=-\left[\frac{1}{r}\frac{\partial}{\partial r}\left(\frac{r}{B}\frac{\partial \phi_{\text{oil}}}{\partial r}\right)+\frac{\partial}{\partial z}\left(\frac{1}{B}\frac{\partial \phi_{\text{oil}}}{\partial z}\right)\right] \tag{3.57}$$

and

$$B = \sqrt{\left(\frac{\partial \phi_{\text{oil}}}{\partial r}\right)^2 + \left(\frac{\partial \phi_{\text{oil}}}{\partial z}\right)^2}. \tag{3.58}$$

Since the pipeline is inclined at an elevation φ to the horizontal, the components of the gravitational acceleration $\vec{g}$ are given as $g_r = g\cos(\varphi)$ and $g_z = g\sin(\varphi)$. Using the expressions for the shear stresses given by Equation (3.43) in Equations (3.55) and (3.56) yields

$$\frac{1}{r}\frac{\partial}{\partial r}\left(r\tau_{rr}\right) = \frac{1}{r}\frac{\partial}{\partial r}\left(2\mu_{\text{mix}} r \frac{\partial u_r}{\partial r}\right) = 2\mu_{\text{mix}}\frac{1}{r}\frac{\partial}{\partial r}\left(r\frac{\partial u_r}{\partial r}\right) = 2\mu_{\text{mix}}\left(\frac{\partial^2 u_r}{\partial r^2} + \frac{1}{r}\frac{\partial u_r}{\partial r}\right) \tag{3.59a}$$

$$\frac{\partial}{\partial z}\left(\tau_{zr}\right) = \frac{\partial}{\partial z}\left(\mu_{\text{mix}}\left(\frac{\partial u_z}{\partial r} + \frac{\partial u_r}{\partial z}\right)\right) = \mu_{\text{mix}}\left(\frac{\partial^2 u_z}{\partial r \partial z} + \frac{\partial^2 u_r}{\partial z^2}\right) \tag{3.59b}$$

$$\frac{\tau_{\theta\theta}}{r} = 2\mu_{\text{mix}}\frac{u_r}{r^2} \tag{3.59c}$$

$$\begin{aligned}
\frac{1}{r}\frac{\partial}{\partial r}(r\tau_{rz}) &= \frac{1}{r}\frac{\partial}{\partial r}\left(r\mu_{\text{mix}}\left(\frac{\partial u_z}{\partial r} + \frac{\partial u_r}{\partial z}\right)\right) = \frac{\mu_{\text{mix}}}{r}\frac{\partial}{\partial r}\left(r\frac{\partial u_z}{\partial r} + r\frac{\partial u_r}{\partial z}\right) \\
&= \frac{\mu_{\text{mix}}}{r}\left(r\frac{\partial^2 u_z}{\partial r^2} + \frac{\partial u_z}{\partial r} + r\frac{\partial^2 u_r}{\partial r \partial z} + \frac{\partial u_r}{\partial z}\right) \\
&= \mu_{\text{mix}}\left(\frac{\partial^2 u_z}{\partial r^2} + \frac{1}{r}\frac{\partial u_z}{\partial r} + \frac{\partial^2 u_r}{\partial r \partial z} + \frac{1}{r}\frac{\partial u_r}{\partial z}\right)
\end{aligned} \tag{3.59d}$$

$$\frac{\partial}{\partial z}\left(\tau_{zz}\right) = \frac{\partial}{\partial z}\left(2\mu_{\text{mix}}\frac{\partial u_z}{\partial z}\right) = 2\mu_{\text{mix}}\frac{\partial}{\partial z}\left(\frac{\partial u_z}{\partial z}\right) = 2\mu_{\text{mix}}\frac{\partial^2 u_z}{\partial z^2} \tag{3.59e}$$

Expanding the curvature (K) by computing the derivatives involved yields

$$\begin{aligned}
K &= -\left[\frac{1}{r}\frac{\partial}{\partial r}\left(\frac{r}{B}\frac{\partial \phi_{\text{oil}}}{\partial r}\right) + \frac{\partial}{\partial z}\left(\frac{1}{B}\frac{\partial \phi_{\text{oil}}}{\partial z}\right)\right] \\
&= \frac{1}{B^3}\left[\left(\frac{\partial \phi_{\text{oil}}}{\partial r}\right)^2\frac{\partial^2 \phi_{\text{oil}}}{\partial r^2} + 2\frac{\partial \phi_{\text{oil}}}{\partial r}\frac{\partial \phi_{\text{oil}}}{\partial z}\frac{\partial^2 \phi_{\text{oil}}}{\partial r \partial z} + \left(\frac{\partial \phi_{\text{oil}}}{\partial z}\right)^2\frac{\partial^2 \phi_{\text{oil}}}{\partial z^2}\right] \\
&\quad -\frac{1}{B}\left(\frac{\partial^2 \phi_{\text{oil}}}{\partial r^2} + \frac{1}{r}\frac{\partial \phi_{\text{oil}}}{\partial r} + \frac{\partial^2 \phi_{\text{oil}}}{\partial z^2}\right) \\
&= -\frac{1}{B^3}\left[\left(\frac{\partial \phi_{\text{oil}}}{\partial r}\right)^2\left(\frac{1}{r}\frac{\partial \phi_{\text{oil}}}{\partial r} + \frac{\partial^2 \phi_{\text{oil}}}{\partial z^2}\right) - 2\frac{\partial \phi_{\text{oil}}}{\partial r}\frac{\partial \phi_{\text{oil}}}{\partial z}\frac{\partial^2 \phi_{\text{oil}}}{\partial r \partial z}\right. \\
&\quad \left. + \left(\frac{\partial \phi_{\text{oil}}}{\partial z}\right)^2\left(\frac{\partial^2 \phi_{\text{oil}}}{\partial r^2} + \frac{1}{r}\frac{\partial \phi_{\text{oil}}}{\partial r}\right)\right]
\end{aligned} \tag{3.60}$$

where B is given by Equation (3.58). Substituting Equations (3.59a), (3.59b) and (3.59c) into the $r-$momentum Equation (3.55) and simplifying yields

$$r \text{ momentum:} \quad \rho_{\text{mix}}\left[\frac{\partial u_r}{\partial t}+u_r\frac{\partial u_r}{\partial r}+u_z\frac{\partial u_r}{\partial z}\right]=-\frac{\partial p}{\partial r}-\frac{\mu_{\text{mix}}}{\kappa}u_r+\sigma K\frac{\partial \phi_{\text{oil}}}{\partial r}$$
$$+\mu_{\text{mix}}\left(2\frac{\partial^2 u_r}{\partial r^2}+\frac{\partial^2 u_r}{\partial z^2}+\frac{\partial^2 u_z}{\partial r\partial z}+\frac{2}{r}\frac{\partial u_r}{\partial r}-\frac{2}{r^2}u_r\right)$$
$$+\rho_{\text{mix}}g\cos(\varphi)\left(\beta_{\text{T}}\right)_{\text{mix}}\left(T-T_\infty\right)+\rho_{\text{mix}}g\cos(\varphi)\left(\beta_{\text{C}}\right)_{\text{mix}}\left(C-C_\infty\right). \tag{3.61}$$

Substituting Equations (3.59d) and (3.59e) into the $z-$momentum Equation (3.56) and simplifying yields

$$z \text{ momentum:} \quad \rho_{\text{mix}}\left[\frac{\partial u_z}{\partial t}+u_r\frac{\partial u_z}{\partial r}+u_z\frac{\partial u_z}{\partial z}\right]=-\frac{\partial p}{\partial z}-\frac{\mu_{\text{mix}}}{\kappa}u_z+\sigma K\frac{\partial \phi_{\text{oil}}}{\partial z}$$
$$+\mu_{\text{mix}}\left(\frac{\partial^2 u_z}{\partial r^2}+2\frac{\partial^2 u_z}{\partial z^2}+\frac{\partial^2 u_r}{\partial r\partial z}+\frac{1}{r}\frac{\partial u_r}{\partial z}+\frac{1}{r}\frac{\partial u_z}{\partial r}\right)$$
$$+\rho_{\text{mix}}g\sin(\varphi)\left(\beta_{\text{T}}\right)_{\text{mix}}\left(T-T_\infty\right)+\rho_{\text{mix}}g\sin(\varphi)\left(\beta_{\text{C}}\right)_{\text{mix}}\left(C-C_\infty\right), \tag{3.62}$$

where K is given by Equation (3.60). Equations (3.61) and (3.62) are the specific equations of conservation of linear momentum, in cylindrical coordinate system, for water-oil two-phase flow in crude oil transportation pipeline. The axial velocity (u_z) is the primary velocity since the main flow is along the axial direction while the radial velocity (u_r) is the secondary velocity.

3.7.2.3 Equation of Energy

Incorporating the energetic contribution of viscous dissipation function (Ψ) and heat transfer term (q_{h}) associated with heat transfer from the oil phase to the water phase, the energy Equation (3.20) becomes.

$$\rho_{\text{mix}}\left(Cp\right)_{\text{mix}}\left[\frac{\partial T}{\partial t}+\vec{V}\cdot\left(\vec{\nabla}T\right)\right]=\vec{\nabla}\cdot\left(k_{\text{mix}}\vec{\nabla}T\right)+\Psi-q_{\text{h}}. \tag{3.63}$$

The heat transfer term (q_{h}) is given in Zheng *et al.* (2017) as:

$$q_{\text{h}}=\frac{h_{\text{r}}}{d_{\text{water}}}\left(T-T_\infty\right), \tag{3.64}$$

where h_{r} is the convective heat transfer coefficient between the oil phase and the water phase. The viscous dissipation function (Ψ) is given in Ochieng (2018) as:

$$\Psi = \left(-\frac{2}{3}\mu_{\mathrm{mix}}\vec{\nabla}\cdot\vec{V}\bar{\bar{I}} + \mu_{\mathrm{mix}}\left[\vec{\nabla}\vec{V} + \left(\vec{\nabla}\vec{V}\right)^{\mathrm{T}}\right]\right) : \vec{\nabla}\vec{V}. \tag{3.65}$$

The viscous dissipation term represents a conversion of the kinetic energy of the velocity field $\vec{V}$ to heat energy (i.e., the internal energy of the fluid). It represents a source of internal energy due to deformation work on the fluid particles. The energy Equation (3.63), in cylindrical coordinate system, for an incompressible mixture fluid with a constant thermal conductivity, reduces to the simpler form:

$$\begin{aligned}\frac{\partial T}{\partial t} + u_r\frac{\partial T}{\partial r} + \frac{u_\theta}{r}\frac{\partial T}{\partial \theta} + u_z\frac{\partial T}{\partial z} &= \alpha_{\mathrm{mix}}\left[\frac{1}{r}\frac{\partial}{\partial r}\left(r\frac{\partial T}{\partial r}\right) + \frac{1}{r}\frac{\partial}{\partial \theta}\left(\frac{1}{r}\frac{\partial T}{\partial \theta}\right) + \frac{\partial}{\partial z}\left(\frac{\partial T}{\partial z}\right)\right] \\ +2\frac{\mu_{\mathrm{mix}}}{\rho_{\mathrm{mix}}\left(Cp\right)_{\mathrm{mix}}}&\left[\left(\frac{\partial u_r}{\partial r}\right)^2 + \left(\frac{1}{r}\frac{\partial u_\theta}{\partial \theta} + \frac{u_r}{r}\right)^2 + \left(\frac{\partial u_z}{\partial z}\right)^2\right] - \frac{h_{\mathrm{r}}}{\rho_{\mathrm{mix}}\left(Cp\right)_{\mathrm{mix}} d_{\mathrm{water}}}(T - T_\infty) \\ &+\frac{\mu_{\mathrm{mix}}}{\rho_{\mathrm{mix}}\left(Cp\right)_{\mathrm{mix}}}\left[\left(\frac{1}{r}\frac{\partial u_r}{\partial \theta} + \frac{\partial u_\theta}{\partial r} - \frac{u_\theta}{r}\right)^2 + \left(\frac{\partial u_\theta}{\partial z} + \frac{1}{r}\frac{\partial u_z}{\partial \theta}\right)^2 + \left(\frac{\partial u_z}{\partial r} + \frac{\partial u_r}{\partial z}\right)^2\right],\end{aligned} \tag{3.66}$$

where $\alpha_{\mathrm{mix}} = k_{\mathrm{mix}}/\left(\rho_{\mathrm{mix}}\left(Cp\right)_{\mathrm{mix}}\right)$ is the effective thermal diffusivity of the mixture fluid. Since the flow is assumed to be axisymmetric, Equation (3.66) reduces to the simpler form:

$$\begin{aligned}\frac{\partial T}{\partial t} + u_r\frac{\partial T}{\partial r} + u_z\frac{\partial T}{\partial z} &= \alpha_{\mathrm{mix}}\left(\frac{\partial^2 T}{\partial r^2} + \frac{1}{r}\frac{\partial T}{\partial r} + \frac{\partial^2 T}{\partial z^2}\right) - \frac{h_{\mathrm{r}}}{\rho_{\mathrm{mix}}\left(Cp\right)_{\mathrm{mix}} d_{\mathrm{water}}}(T - T_\infty) \\ &+\frac{\mu_{\mathrm{mix}}}{\rho_{\mathrm{mix}}\left(Cp\right)_{\mathrm{mix}}}\left[2\left(\frac{\partial u_r}{\partial r}\right)^2 + 2\left(\frac{u_r}{r}\right)^2 + 2\left(\frac{\partial u_z}{\partial z}\right)^2 + \left(\frac{\partial u_z}{\partial r} + \frac{\partial u_r}{\partial z}\right)^2\right].\end{aligned} \tag{3.67}$$

Equation (3.67) is the specific equation of conservation of energy, in cylindrical coordinate system, for water-oil two-phase flow in crude oil transportation pipeline.

3.7.2.4 Equation of Species Concentration

In this study, the total mass flux ($\vec{J}_{\mathrm{tot}}$) of wax in the crude oil is given by the sum of the contribution of the molecular diffusion and the shear dispersion mechanisms, i.e.,

$$\vec{J}_{\mathrm{tot}} = \vec{J}_{\mathrm{d}} + \vec{J}_{\mathrm{p}}. \tag{3.68}$$

Substituting the Fick's diffusion Equation (3.15) and the shear dispersion Equation (3.17) into Equation (3.68), yields the cylindrical coordinates form of the total mass flux of wax

as:

$$\vec{J}_{\text{tot}} = -\left(D_{\text{d}}\frac{dC_{\text{d}}}{dT}\frac{\partial T}{\partial r} + D_{\text{p}}C_{\text{n}}\frac{\partial u_z}{\partial r}\right)\hat{\mathbf{r}} - D_{\text{d}}\frac{dC_{\text{d}}}{dT}\frac{\partial T}{\partial z}\hat{\mathbf{k}}. \tag{3.69}$$

In the fluid phase, the concentration of dissolved wax, C_{d}, and that of precipitated (or crystallized) wax, C_{p}, are governed by the equations:

$$\frac{\partial C_{\text{d}}}{\partial t} + \vec{V}\cdot\left(\vec{\nabla}C_{\text{d}}\right) + \vec{\nabla}\cdot\left(\vec{J}_{\text{d}}\right) = S_{\text{d}} \tag{3.70a}$$

and

$$\frac{\partial C_{\text{p}}}{\partial t} + \vec{V}\cdot\left(\vec{\nabla}C_{\text{p}}\right) + \vec{\nabla}\cdot\left(\vec{J}_{\text{p}}\right) = S_{\text{p}}, \tag{3.70b}$$

respectively. Adding Equations (3.70a) and (3.70b) and using the relation (3.7), yields

$$\frac{\partial C}{\partial t} + \vec{V}\cdot\left(\vec{\nabla}C\right) + \vec{\nabla}\cdot\left(\vec{J}_{\text{tot}}\right) = 0. \tag{3.71}$$

The right-hand side of Equation (3.71) is zero (i.e., $S_{\text{d}} + S_{\text{p}} = 0$) since no wax is added or removed from the crude oil in the control volume of the pipeline. Substituting the total mass flux given by Equation (3.69) into Equation (3.71), expressing the resulting equation in cylindrical coordinate system and rearranging yields

$$\frac{\partial C}{\partial t} + u_r\frac{\partial C}{\partial r} + u_z\frac{\partial C}{\partial z} = \frac{1}{r}\frac{\partial}{\partial r}\left(r\left(D_{\text{d}}\frac{dC_{\text{d}}}{dT}\frac{\partial T}{\partial r} + D_{\text{p}}C_{\text{n}}\frac{\partial u_z}{\partial r}\right)\right) + \frac{\partial}{\partial z}\left(D_{\text{d}}\frac{dC_{\text{d}}}{dT}\frac{\partial T}{\partial z}\right). \tag{3.72}$$

Expanding the derivatives on the right-hand side of Equation (3.72) using the product rule of differentiation and simplifying the resulting equation yields

$$\begin{aligned}\frac{\partial C}{\partial t} + u_r\frac{\partial C}{\partial r} + u_z\frac{\partial C}{\partial z} &= D_{\text{p}}\left[C_{\text{n}}\left(\frac{\partial^2 u_z}{\partial r^2} + \frac{1}{r}\frac{\partial u_z}{\partial r}\right) + \frac{\partial C_{\text{n}}}{\partial r}\frac{\partial u_z}{\partial r}\right] \\ +D_{\text{d}}\left[\frac{dC_{\text{d}}}{dT}\left(\frac{\partial^2 T}{\partial r^2} + \frac{1}{r}\frac{\partial T}{\partial r} + \frac{\partial^2 T}{\partial z^2}\right) + \frac{\partial}{\partial r}\left(\frac{dC_{\text{d}}}{dT}\right)\frac{\partial T}{\partial r} + \frac{\partial}{\partial z}\left(\frac{dC_{\text{d}}}{dT}\right)\frac{\partial T}{\partial z}\right].\end{aligned} \tag{3.73}$$

Using the chain rule of differentiation for derivatives involving C_{d}, Equation (3.73) becomes:

$$\begin{aligned}\frac{\partial C}{\partial t} + u_r\frac{\partial C}{\partial r} + u_z\frac{\partial C}{\partial z} &= D_{\text{p}}\left[C_{\text{n}}\left(\frac{\partial^2 u_z}{\partial r^2} + \frac{1}{r}\frac{\partial u_z}{\partial r}\right) + \frac{\partial C_{\text{n}}}{\partial r}\frac{\partial u_z}{\partial r}\right] \\ +D_{\text{d}}\left[\frac{dC_{\text{d}}}{dT}\left(\frac{\partial^2 T}{\partial r^2} + \frac{1}{r}\frac{\partial T}{\partial r} + \frac{\partial^2 T}{\partial z^2}\right) + \frac{d^2C_{\text{d}}}{dT^2}\left\{\left(\frac{\partial T}{\partial r}\right)^2 + \left(\frac{\partial T}{\partial z}\right)^2\right\}\right].\end{aligned} \tag{3.74}$$

Eliminating C_{n} between Equations (3.12) and (3.74), and using the chain rule of differentiation for derivatives involving C_{d} yields

$$\frac{\partial C}{\partial t}+u_r\frac{\partial C}{\partial r}+u_z\frac{\partial C}{\partial z}=D_{\mathrm{p}}\Bigg[\left(1-\alpha_{\mathrm{m}}\right)\left(C-C_{\mathrm{d}}\right)\left(\frac{\partial^2 u_z}{\partial r^2}+\frac{1}{r}\frac{\partial u_z}{\partial r}\right)$$
$$+\left\{\left(1-\alpha_{\mathrm{m}}\right)\left(\frac{\partial C}{\partial r}-\frac{dC_{\mathrm{d}}}{dT}\frac{\partial T}{\partial r}\right)-\left(C-C_{\mathrm{d}}\right)\frac{\partial \alpha_{\mathrm{m}}}{\partial r}\right\}\frac{\partial u_z}{\partial r}\Bigg]$$
$$+D_{\mathrm{d}}\left[\frac{dC_{\mathrm{d}}}{dT}\left(\frac{\partial^2 T}{\partial r^2}+\frac{1}{r}\frac{\partial T}{\partial r}+\frac{\partial^2 T}{\partial z^2}\right)+\frac{d^2C_{\mathrm{d}}}{dT^2}\left\{\left(\frac{\partial T}{\partial r}\right)^2+\left(\frac{\partial T}{\partial z}\right)^2\right\}\right]. \tag{3.75}$$

Equation (3.75) is the specific equation of total wax concentration, in cylindrical coordinate system, for water-oil two-phase flow in crude oil transportation pipeline.

3.7.2.5 Equation of Wax Precipitation Kinetics

To obtain the equation governing the precipitation kinetics of wax in crude oil pipeline, this study assumes that the material derivative (i.e., the derivative with respect to time t along the path of a fluid particle) of the aggregation degree (α_{m}) is expressed locally (Fusi, 2003) as:

$$\frac{\partial \alpha_{\mathrm{m}}}{\partial t}+\vec{V}\cdot\left(\vec{\nabla}\alpha_{\mathrm{m}}\right)=\left[1-\alpha_{\mathrm{m}}\right]K_1\left(T\right)-\alpha_{\mathrm{m}}\left|W(r,z,t)\right|K_2\left(T\right). \tag{3.76}$$

where K_1 and K_2 are positive functions of temperature, which are usually determined experimentally while $W(r,z,t)$ is the power density dissipated in the fluid by the viscous forces for an arbitrary unit volume of the pipeline and is defined in (Fusi, 2003) as:

$$W(r,z,t)=\frac{\partial u_z}{\partial r}\left(-\tau_0+\mu_{\mathrm{mix}}\frac{\partial u_z}{\partial r}\right). \tag{3.77}$$

Equation (3.76) takes into account both the spontaneous aggregation/deposition of wax crystals and the disintegration/fragmentation of the aggregated wax (or agglomerates) due to mechanical action (or thixotropy). The first term on the right-hand side of Equation (3.76) represents the tendency of wax to spontaneously aggregate while the second term represents the rate of disintegration/fragmentation of the aggregated wax (or wax deposit) due to internal friction.

Since the velocity field is assumed to take the form $\vec{V}=u_r\hat{\mathbf{r}}+u_z\hat{\mathbf{k}}$, using the expression of W given by Equation (3.77) and assuming that $\tau_0=0$, the cylindrical coordinates form

of Equation (3.76) is

$$\frac{\partial \alpha_{\mathrm{m}}}{\partial t} + u_r \frac{\partial \alpha_{\mathrm{m}}}{\partial r} + u_z \frac{\partial \alpha_{\mathrm{m}}}{\partial z} = \left[1 - \alpha_{\mathrm{m}}\right] K_1\left(T\right) - \alpha_{\mathrm{m}} \mu_{\mathrm{mix}} \left(\frac{\partial u_z}{\partial r}\right)^2 K_2\left(T\right). \quad (3.78)$$

Equation (3.78) is the specific equation governing the precipitation kinetics of wax for water-oil two-phase flow in crude oil transportation pipeline.

3.7.2.6 Equation of Conservation of Volume Fraction

In the VOF model, the conservation of the volume fraction of the oil phase is governed by the oil volume fraction transport equation given in Ahmadi Nadooshan & Shirani (2008), Yang *et al.* (2019), and Jiang *et al.* (2020) as:

$$\frac{\partial(\phi_{\mathrm{oil}}\rho_{\mathrm{oil}})}{\partial t} + \vec{V} \cdot \left[\vec{\nabla}(\phi_{\mathrm{oil}}\rho_{\mathrm{oil}})\right] = 0. \quad (3.79)$$

Imposing the assumption that the flow is axisymmetric and that the mixture fluid is incompressible, the cylindrical coordinates form of Equation (3.79) becomes

$$\frac{\partial \phi_{\mathrm{oil}}}{\partial t} + u_r \frac{\partial \phi_{\mathrm{oil}}}{\partial r} + u_z \frac{\partial \phi_{\mathrm{oil}}}{\partial z} = 0. \quad (3.80)$$

Equation (3.80) is the specific equation of conservation of oil volume fraction, in cylindrical coordinate system, for water-oil two-phase flow in crude oil transportation pipeline.

3.7.2.7 Equation of Wax Deposit Growth

The total mass concentration of wax (C) is affected by the possible growth of a deposit layer on the inner wall of the crude oil pipeline. This is because the crude oil flowing through the pipeline is always the same and a deposit on the pipeline wall implies a decrease in the total wax concentration in the fluid.

The wax molecules reaching the oil/gel interface through molecular diffusion precipitate on the interface, causing the interface to extend towards the centerline of the pipeline. Assuming that the thickness ($\delta(t)$) of the gel layer is uniform, the effective radius of the pipeline is given as

$$R_{\mathrm{eff}}(t) = R - \delta(t) \quad (3.81)$$

Suppose the control volume is taken as an arbitrary unit length portion of the pipeline.

From the principle of conservation of mass, the sum of the mass of wax in the fluid phase and the mass of wax in the gel layer must be constant at any time t. The mass balance in the control volume of the pipeline at time t is expressed mathematically in (Fasano *et al.*, 2004) as:

$$C(r,z,t)\pi R_{\text{eff}}^2(t) + \rho_{\text{gel}}\pi\left[R^2 - R_{\text{eff}}^2(t)\right] = C_\infty \pi R^2. \tag{3.82}$$

The term $C(r,z,t)\pi R_{\text{eff}}^2(t)$ is the mass of the dissolved wax in the fluid phase, $\rho_{\text{gel}}\pi\left[R^2 - R_{\text{eff}}^2(t)\right]x$ is the mass of the wax particles in the gel layer, and $C_\infty \pi R^2$ is the total mass of wax in the control volume of the pipeline at time $t \leq 0$; x being the weight fraction of wax crystals in the gel layer. Making $R_{\text{eff}}(t)$ the subject in Equation (3.82) yields.

$$R_{\text{eff}}(t) = R\left(\frac{C_\infty - \rho_{\text{gel}}}{C - \rho_{\text{gel}}}\right)^{\frac{1}{2}} \tag{3.83}$$

Eliminating $R_{\text{eff}}(t)$ between Equations (3.81) and (3.83), yields the formula for calculating the thickness of wax deposit at time t as:

$$\delta(t) = R\left[1 - \left(\frac{C_\infty - \rho_{\text{gel}}}{C - \rho_{\text{gel}}}\right)^{\frac{1}{2}}\right]. \tag{3.84}$$

The rate of deposit growth is proportional to the mass flux of dissolved wax in crude oil at the oil-gel interface (Zheng *et al.*, 2017). The present study adopts the Michigan model presented in (Gupta & Sircar, 2017) as the equation governing the rate of deposit growth.

$$\frac{d\delta}{dt} = \frac{(1 - f(x))}{x\rho_{\text{gel}}}\left(D_{\text{d}}\frac{dC_{\text{d}}}{dT}\frac{\partial T}{\partial r}\bigg|_{r=R_{\text{eff}}}\right). \tag{3.85}$$

Equation (3.85) is the specific equation governing the growth of the gel layer for water-oil two-phase flow in crude oil transportation pipeline.

3.7.2.8 Equation of Wax Deposit Aging

A concentration gradient of wax molecules exists inside the gel layer, induced by the temperature difference between the oil-gel interface and the inner wall of the pipeline. Thus, some wax molecules continue to diffuse from the oil-gel interface into the gel layer, leading to a gradual increase in the wax content inside the gel layer. The wax content or weight fraction (x) of solid wax in the gel layer is defined in Ramirez-Jaramillo *et al.*

(2004) as:

$$x = \frac{\text{mass of wax in the gel layer}}{\text{mass of wax in the gel layer } + \text{ mass of oil trapped in the gel layer}} \tag{3.86}$$

The increase in the weight fraction of wax inside the gel layer with time is called deposit aging (or hardening of the gel layer). This study adopts the Michigan model for laminar flow presented in Gupta & Sircar (2017) and Sun *et al.* (2020) as the equation governing the rate of aging of the gel layer. Incorporating the shear dispersion mechanism in the Michigan model yields.

$$\frac{dx}{dt} = \frac{2R_{\text{eff}} f(x)}{\rho_{\text{gel}} \left(R^2 - R_{\text{eff}}^2\right)} \left(D_{\text{d}} \frac{dC_{\text{d}}}{dT} \frac{\partial T}{\partial r} + D_{\text{p}} C_{\text{n}} \frac{\partial u_z}{\partial r} \right)_{r=R_{\text{eff}}} \tag{3.87}$$

The function $f(x)$ is the coefficient describing diffusion of wax molecules in the porous network (i.e., the gel layer) and is given in Gupta & Sircar (2017) and Sun *et al.* (2020) as:

$$f(x) = \frac{1-x}{\alpha_{\text{avg}}^2 x^2 - x + 1}, \tag{3.88}$$

where α_{avg} denotes the average aspect ratio of the wax crystals (or the wax crystal shape factor) and can be obtained by observing the wax crystal form of the gel layer. It is given in Sun *et al.* (2020) as:

$$\alpha_{\text{avg}} = -0.323 \ln Q + 1.684. \tag{3.89}$$

where Q is the volumetric flow rate of the mixture fluid. Eliminating C_{n} between Equations (3.12) and (3.91) yields

$$\frac{dx}{dt} = \frac{2R_{\text{eff}} f(x)}{\rho_{\text{gel}} \left(R^2 - R_{\text{eff}}^2\right)} \left(D_{\text{d}} \frac{dC_{\text{d}}}{dT} \frac{\partial T}{\partial r} + D_{\text{p}} \left(1 - \alpha_{\text{m}}\right) \left(C - C_{\text{d}}\right) \frac{\partial u_z}{\partial r} \right)_{r=R_{\text{eff}}} \tag{3.90}$$

Eliminating R_{eff} between Equations (3.81) and (3.90) and rearranging yields

$$\frac{dx}{dt} = \frac{2\left[R - \delta(t)\right]}{\delta(t)\left[2R - \delta(t)\right]} \frac{f(x)}{\rho_{\text{gel}}} \left(D_{\text{d}} \frac{dC_{\text{d}}}{dT} \frac{\partial T}{\partial r} + D_{\text{p}} \left(1 - \alpha_{\text{m}}\right) \left(C - C_{\text{d}}\right) \frac{\partial u_z}{\partial r} \right)_{r=R_{\text{eff}}} \tag{3.91}$$

Equation (3.91) is the specific equation governing the aging of the gel layer for water-oil two-phase flow in crude oil transportation pipeline.

3.7.3 Boundary and Initial Conditions

Because of the symmetry around the plane $r = 0$, the analysis of the specific governing equations in this study is limited to the upper half part of the pipeline (i.e., from the pipe centerline to the upper wall). Thus, the final set of the governing partial differential Equations (3.26), (3.61), (3.62), (3.67), (3.75), (3.78), (3.80), (3.85) and (3.91) are solved subject to the following boundary and initial conditions:

$$
\begin{cases}
\dfrac{\partial u_r}{\partial r} = 0,\ \dfrac{\partial u_z}{\partial r} = 0,\ \dfrac{\partial T}{\partial r} = 0, \\
\dfrac{\partial C}{\partial r} = 0,\ \dfrac{\partial \alpha_{\text{m}}}{\partial r} = 0,\ \dfrac{\partial \phi_{\text{oil}}}{\partial r} = 0.
& \text{at } r = 0 \quad \text{(centerline)} \\[2ex]
u_r = 0, u_z = 0, T = T_{\text{interface}}, \\
C = C_{\text{interface}},\ \alpha_{\text{m}} = 1,\ \phi_{\text{oil}} = 0.
& \text{at } r = R_{\text{eff}} \quad \text{(oil-gel interface)} \\[2ex]
u_r = 0,\ u_z = U_\infty,\ T = T_\infty,\ C = C_\infty, \\
\alpha_{\text{m}} = 0,\ \phi_{\text{oil}} = 1 - \phi_{\text{water}}.
& \text{at } z = 0 \quad \text{(pipe inlet)} \\[2ex]
\dfrac{\partial u_r}{\partial z} = 0,\ \dfrac{\partial u_z}{\partial z} = 0,\ \dfrac{\partial T}{\partial z} = 0, \\
\dfrac{\partial C}{\partial z} = 0,\ \dfrac{\partial \alpha_{\text{m}}}{\partial z} = 0,\ \dfrac{\partial \phi_{\text{oil}}}{\partial z} = 0.
& \text{as } z \to \infty \quad \text{(pipe outlet)} \\[2ex]
u_r = 0,\ u_z = U_\infty,\ T = T_\infty,\ C = C_\infty, \\
\alpha_{\text{m}} = 0,\ \phi_{\text{oil}} = 1 - \phi_{\text{water}},\ \delta = 0,\ x = 0.
& \text{at } t = 0 \quad \text{(initial conditions)}
\end{cases}
\tag{3.92}
$$

3.8 Dimensional Analysis of the Governing Equations

Dimensional analysis is a mathematical technique which considers how to determine the required set of scales for any physical model. It provides a way to compare systems having different scales. Thus, it ensures that the results obtained from the study are applicable to other geometrically similar configurations under a similar set of flow conditions. The process of dimensional analysis is based on the principle of dimensional homogeneity and it starts with selecting a suitable scale against which all dimensions in a given physical model are based. Dimensional analysis is necessary in order to identify

the dimensionless groups that govern the flow, heat and mass transfer characteristics. The dimensionless governing equations, therefore, should have solutions that are bounded in the closed interval $[0, 1]$ and they should not depend on any unit. In this study, the characteristic length is taken as the radius R of the pipe while the characteristic velocity is taken as the free-stream velocity U_∞. Therefore, the characteristic time is taken as (R/U_∞). To express the governing equations and the initial-boundary conditions in their dimensionless form, the following dimensionless variables are introduced.

$$\bar{r} = \frac{r}{R},\ \bar{z} = \frac{z}{R},\ \bar{t} = \frac{t}{R/U_\infty}. \tag{3.93a}$$

$$u = \frac{u_r}{U_\infty}, v = \frac{u_z}{U_\infty},\ P = \frac{p}{\rho_{\text{mix}} U_\infty^2},\ \Theta = \frac{T - T_{\text{wall}}}{T_\infty - T_{\text{wall}}} \tag{3.93b}$$

$$\phi = \frac{C - C_\infty}{C_{\text{wall}} - C_\infty}, \bar{C}_{\text{d}} = \frac{C_{\text{d}} - C_\infty}{C_{\text{wall}} - C_\infty}, \bar{R}_{\text{eff}} = \frac{R_{\text{eff}}}{R} \tag{3.93c}$$

$$\bar{\delta}(\bar{t}) = \frac{\delta(t)}{R}, \bar{d} = \frac{d_{\text{water}}}{R},\ \bar{K}_1 = \frac{K_1}{U_\infty/R}, \bar{K}_2 = \frac{K_2}{(\rho_{\text{mix}} R^2)/\mu_{\text{mix}}^2}. \tag{3.93d}$$

From the change of the independent variables given by Equation (3.93a), yields the following partial derivatives:

$$\frac{\partial \bar{r}}{\partial r} = \frac{1}{R}, \quad \frac{\partial \bar{r}}{\partial z} = 0, \quad \frac{\partial \bar{r}}{\partial t} = 0 \tag{3.94a}$$

$$\frac{\partial \bar{z}}{\partial r} = 0, \quad \frac{\partial \bar{z}}{\partial z} = \frac{1}{R}, \quad \frac{\partial \bar{z}}{\partial t} = 0 \tag{3.94b}$$

$$\frac{\partial \bar{t}}{\partial r} = 0, \quad \frac{\partial \bar{t}}{\partial z} = 0, \quad \frac{\partial \bar{t}}{\partial t} = \frac{U_\infty}{R} \tag{3.94c}$$

For the transformation (3.93a) to be valid, the Jacobian for the transformation should be non-zero. The Jacobian for the transformation is given by:

$$J = \frac{\partial(r,z,t)}{\partial(\bar{r},\bar{z},\bar{t})} = \begin{vmatrix} \frac{\partial r}{\partial \bar{r}} & \frac{\partial r}{\partial \bar{z}} & \frac{\partial r}{\partial \bar{t}} \\ \frac{\partial z}{\partial \bar{r}} & \frac{\partial z}{\partial \bar{z}} & \frac{\partial z}{\partial \bar{t}} \\ \frac{\partial t}{\partial \bar{r}} & \frac{\partial t}{\partial \bar{z}} & \frac{\partial t}{\partial \bar{t}} \end{vmatrix} = \begin{vmatrix} R & 0 & 0 \\ 0 & R & 0 \\ 0 & 0 & \frac{R}{U_\infty} \end{vmatrix} = \frac{R^3}{U_\infty} \tag{3.95}$$

Since $R \neq 0$ and $U_\infty \neq 0$, it implies that $J \neq 0$. Therefore, the change of the independent variables given by Equation (3.93a) is a valid transformation. Using the chain rule of differentiation and utilizing Equations (3.94a)−(3.94c), yields the following transformations for the first partial derivatives.

$$\frac{\partial}{\partial r} = \frac{\partial \bar{r}}{\partial r}\frac{\partial}{\partial \bar{r}} + \cancelto{0}{\frac{\partial \bar{z}}{\partial r}\frac{\partial}{\partial \bar{z}}} + \cancelto{0}{\frac{\partial \bar{t}}{\partial r}\frac{\partial}{\partial \bar{t}}} = \frac{1}{R}\frac{\partial}{\partial \bar{r}} \tag{3.96a}$$

$$\frac{\partial}{\partial z} = \cancelto{0}{\frac{\partial \bar{r}}{\partial z}\frac{\partial}{\partial \bar{r}}} + \frac{\partial \bar{z}}{\partial z}\frac{\partial}{\partial \bar{z}} + \cancelto{0}{\frac{\partial \bar{t}}{\partial z}\frac{\partial}{\partial \bar{t}}} = \frac{1}{R}\frac{\partial}{\partial \bar{z}} \tag{3.96b}$$

$$\frac{\partial}{\partial t} = \cancelto{0}{\frac{\partial \bar{r}}{\partial t}\frac{\partial}{\partial \bar{r}}} + \cancelto{0}{\frac{\partial \bar{z}}{\partial t}\frac{\partial}{\partial \bar{z}}} + \frac{\partial \bar{t}}{\partial t}\frac{\partial}{\partial \bar{t}} = \frac{U_\infty}{R}\frac{\partial}{\partial \bar{t}} \tag{3.96c}$$

Similarly, the transformations for the second partial derivatives involved in the specific governing equations are given as:

$$\begin{aligned} \frac{\partial^2}{\partial r^2} &= \frac{\partial}{\partial r}\left(\frac{\partial}{\partial r}\right) = \frac{\partial}{\partial r}\left(\frac{1}{R}\frac{\partial}{\partial \bar{r}}\right) \\ &= \frac{\partial \bar{r}}{\partial r}\frac{\partial}{\partial \bar{r}}\left(\frac{1}{R}\frac{\partial}{\partial \bar{r}}\right) + \cancelto{0}{\frac{\partial \bar{z}}{\partial r}\frac{\partial}{\partial \bar{z}}\left(\frac{1}{R}\frac{\partial}{\partial \bar{r}}\right)} + \cancelto{0}{\frac{\partial \bar{t}}{\partial r}\frac{\partial}{\partial \bar{t}}\left(\frac{1}{R}\frac{\partial}{\partial \bar{r}}\right)} = \frac{1}{R}\frac{\partial}{\partial \bar{r}}\left(\frac{1}{R}\frac{\partial}{\partial \bar{r}}\right) \\ &= \frac{1}{R^2}\frac{\partial^2}{\partial \bar{r}^2} \end{aligned} \tag{3.97a}$$

$$\frac{\partial^2}{\partial r \partial z} = \frac{\partial}{\partial r}\left(\frac{\partial}{\partial z}\right) = \frac{\partial}{\partial r}\left(\frac{1}{R}\frac{\partial}{\partial \bar{z}}\right)$$

$$= \frac{\partial \bar{r}}{\partial r}\frac{\partial}{\partial \bar{r}}\left(\frac{1}{R}\frac{\partial}{\partial \bar{z}}\right) + \cancelto{0}{\frac{\partial \bar{z}}{\partial r}\frac{\partial}{\partial \bar{z}}\left(\frac{1}{R}\frac{\partial}{\partial \bar{z}}\right)} + \cancelto{0}{\frac{\partial \bar{t}}{\partial r}\frac{\partial}{\partial \bar{t}}\left(\frac{1}{R}\frac{\partial}{\partial \bar{z}}\right)} = \frac{1}{R}\frac{\partial}{\partial \bar{r}}\left(\frac{1}{R}\frac{\partial}{\partial \bar{z}}\right)$$

$$= \frac{1}{R^2}\frac{\partial^2}{\partial \bar{r}\partial \bar{z}} \tag{3.97b}$$

$$\frac{\partial^2}{\partial z^2} = \frac{\partial}{\partial z}\left(\frac{\partial}{\partial z}\right) = \frac{\partial}{\partial z}\left(\frac{1}{R}\frac{\partial}{\partial \bar{z}}\right)$$

$$= \cancelto{0}{\frac{\partial \bar{r}}{\partial z}\frac{\partial}{\partial \bar{r}}\left(\frac{1}{R}\frac{\partial}{\partial \bar{z}}\right)} + \frac{\partial \bar{z}}{\partial z}\frac{\partial}{\partial \bar{z}}\left(\frac{1}{R}\frac{\partial}{\partial \bar{z}}\right) + \cancelto{0}{\frac{\partial \bar{t}}{\partial z}\frac{\partial}{\partial \bar{t}}\left(\frac{1}{R}\frac{\partial}{\partial \bar{z}}\right)} = \frac{1}{R}\frac{\partial}{\partial \bar{z}}\left(\frac{1}{R}\frac{\partial}{\partial \bar{z}}\right)$$

$$= \frac{1}{R^2}\frac{\partial^2}{\partial \bar{z}^2} \tag{3.97c}$$

Therefore, using Equations (3.96a)−(3.96b) and Equations (3.97a)−(3.97c), the derivatives involved in the specific governing equations are written in form of the dimensionless variables given by Equations (3.93a)−(3.93d) as follows.

$$\frac{\partial u_r}{\partial r} = \frac{1}{R}\frac{\partial\left(U_\infty u\right)}{\partial \bar{r}} = \frac{U_\infty}{R}\frac{\partial u}{\partial \bar{r}} \tag{3.98a}$$

$$\frac{\partial u_r}{\partial z} = \frac{1}{R}\frac{\partial\left(U_\infty u\right)}{\partial \bar{z}} = \frac{U_\infty}{R}\frac{\partial u}{\partial \bar{z}} \tag{3.98b}$$

$$\frac{\partial u_r}{\partial t} = \frac{U_\infty}{R}\frac{\partial\left(U_\infty u\right)}{\partial \bar{t}} = \frac{U_\infty^2}{R}\frac{\partial u}{\partial \bar{t}} \tag{3.98c}$$

$$\frac{\partial^2 u_r}{\partial r^2} = \frac{1}{R^2}\frac{\partial^2\left(U_\infty u\right)}{\partial \bar{r}^2} = \frac{U_\infty}{R^2}\frac{\partial^2 u}{\partial \bar{r}^2} \tag{3.98d}$$

$$\frac{\partial^2 u_r}{\partial r \partial z} = \frac{1}{R^2}\frac{\partial^2\left(U_\infty u\right)}{\partial \bar{r}\partial \bar{z}} = \frac{U_\infty}{R^2}\frac{\partial^2 u}{\partial \bar{r}\partial \bar{z}} \tag{3.98e}$$

$$\frac{\partial^2 u_r}{\partial z^2} = \frac{1}{R^2}\frac{\partial^2\left(U_\infty u\right)}{\partial \bar{z}^2} = \frac{U_\infty}{R^2}\frac{\partial^2 u}{\partial \bar{z}^2} \tag{3.98f}$$

$$\frac{\partial u_z}{\partial r} = \frac{1}{R}\frac{\partial\left(U_\infty v\right)}{\partial \bar{r}} = \frac{U_\infty}{R}\frac{\partial v}{\partial \bar{r}} \tag{3.98g}$$

$$\frac{\partial u_z}{\partial z} = \frac{1}{R}\frac{\partial \left(U_\infty v\right)}{\partial \bar{z}} = \frac{U_\infty}{R}\frac{\partial v}{\partial \bar{z}} \tag{3.98h}$$

$$\frac{\partial u_z}{\partial t} = \frac{U_\infty}{R}\frac{\partial \left(U_\infty v\right)}{\partial \bar{t}} = \frac{U_\infty^2}{R}\frac{\partial v}{\partial \bar{t}} \tag{3.98i}$$

$$\frac{\partial^2 u_z}{\partial r^2} = \frac{1}{R^2}\frac{\partial^2 \left(U_\infty v\right)}{\partial \bar{r}^2} = \frac{U_\infty}{R^2}\frac{\partial^2 v}{\partial \bar{r}^2} \tag{3.98j}$$

$$\frac{\partial^2 u_z}{\partial r \partial z} = \frac{1}{R^2}\frac{\partial^2 \left(U_\infty v\right)}{\partial \bar{r} \partial \bar{z}} = \frac{U_\infty}{R^2}\frac{\partial^2 v}{\partial \bar{r} \partial \bar{z}} \tag{3.98k}$$

$$\frac{\partial^2 u_z}{\partial z^2} = \frac{1}{R^2}\frac{\partial^2 \left(U_\infty v\right)}{\partial \bar{z}^2} = \frac{U_\infty}{R^2}\frac{\partial^2 v}{\partial \bar{z}^2} \tag{3.98l}$$

$$\frac{\partial p}{\partial r} = \frac{1}{R}\frac{\partial \left(\rho_{\text{mix}} U_\infty^2 P\right)}{\partial \bar{r}} = \frac{\rho_{\text{mix}} U_\infty^2}{R}\frac{\partial P}{\partial \bar{r}} \tag{3.98m}$$

$$\frac{\partial p}{\partial z} = \frac{1}{R}\frac{\partial \left(\rho_{\text{mix}} U_\infty^2 P\right)}{\partial \bar{z}} = \frac{\rho_{\text{mix}} U_\infty^2}{R}\frac{\partial P}{\partial \bar{z}} \tag{3.98n}$$

$$\frac{\partial T}{\partial r} = \frac{1}{R}\frac{\partial [\left(T_\infty - T_{\text{wall}}\right)\Theta + T_\infty]}{\partial \bar{r}} = \frac{\left(T_\infty - T_{\text{wall}}\right)}{R}\frac{\partial \Theta}{\partial \bar{r}} \tag{3.98o}$$

$$\frac{\partial T}{\partial z} = \frac{1}{R}\frac{\partial [\left(T_\infty - T_{\text{wall}}\right)\Theta + T_\infty]}{\partial \bar{z}} = \frac{\left(T_\infty - T_{\text{wall}}\right)}{R}\frac{\partial \Theta}{\partial \bar{z}} \tag{3.98p}$$

$$\frac{\partial T}{\partial t} = \frac{U_\infty}{R}\frac{\partial [\left(T_\infty - T_{\text{wall}}\right)\Theta + T_\infty]}{\partial \bar{t}} = \frac{U_\infty \left(T_\infty - T_{\text{wall}}\right)}{R}\frac{\partial \Theta}{\partial \bar{t}} \tag{3.98q}$$

$$\frac{\partial^2 T}{\partial r^2} = \frac{1}{R^2}\frac{\partial^2 [\left(T_\infty - T_{\text{wall}}\right)\Theta + T_\infty]}{\partial \bar{r}^2} = \frac{\left(T_\infty - T_{\text{wall}}\right)}{R^2}\frac{\partial^2 \Theta}{\partial \bar{r}^2} \tag{3.98r}$$

$$\frac{\partial^2 T}{\partial z^2} = \frac{1}{R^2}\frac{\partial^2 [\left(T_\infty - T_{\text{wall}}\right)\Theta + T_\infty]}{\partial \bar{z}^2} = \frac{\left(T_\infty - T_{\text{wall}}\right)}{R^2}\frac{\partial^2 \Theta}{\partial \bar{z}^2} \tag{3.98s}$$

$$\frac{\partial C}{\partial r} = \frac{1}{R}\frac{\partial [\left(C_{\text{wall}} - C_\infty\right)\phi + C_\infty]}{\partial \bar{r}} = \frac{\left(C_{\text{wall}} - C_\infty\right)}{R}\frac{\partial \phi}{\partial \bar{r}} \tag{3.98t}$$

$$\frac{\partial C}{\partial z} = \frac{1}{R}\frac{\partial[(C_{\text{wall}} - C_\infty)\,\phi + C_\infty]}{\partial \bar{z}} = \frac{(C_{\text{wall}} - C_\infty)}{R}\frac{\partial \phi}{\partial \bar{z}} \tag{3.98u}$$

$$\frac{\partial C}{\partial t} = \frac{U_\infty}{R}\frac{\partial[(C_{\text{wall}} - C_\infty)\,\phi + C_\infty]}{\partial \bar{t}} = \frac{U_\infty\,(C_{\text{wall}} - C_\infty)}{R}\frac{\partial \phi}{\partial \bar{t}} \tag{3.98v}$$

$$\frac{d\delta}{dt} = \frac{U_\infty}{R}\frac{d\left(R\bar{\delta}\right)}{d\bar{t}} = U_\infty \frac{d\bar{\delta}}{d\bar{t}} \tag{3.98w}$$

$$\frac{dC_{\text{d}}}{dT} = \frac{d[(C_{\text{wall}} - C_\infty)\,\bar{C}_{\text{d}} + C_\infty]}{d[(T_\infty - T_{\text{wall}})\,\Theta + T_\infty]} = \frac{(C_{\text{wall}} - C_\infty)}{(T_\infty - T_{\text{wall}})}\frac{d\bar{C}_{\text{d}}}{d\Theta} \tag{3.98x}$$

$$\frac{d^2C_{\text{d}}}{dT^2} = \frac{d^2[(C_{\text{wall}} - C_\infty)\,\bar{C}_{\text{d}} + C_\infty]}{d[(T_\infty - T_{\text{wall}})\,\Theta + T_\infty]^2} = \frac{(C_{\text{wall}} - C_\infty)}{(T_\infty - T_{\text{wall}})^2}\frac{d^2\bar{C}_{\text{d}}}{d\Theta^2} \tag{3.98y}$$

$$\bar{B} = \sqrt{\left(\frac{\partial \phi_{\text{oil}}}{\partial\,(R\bar{r})}\right)^2 + \left(\frac{\partial \phi_{\text{oil}}}{\partial\,(R\bar{z})}\right)^2} = \frac{1}{R}\sqrt{\left(\frac{\partial \phi_{\text{oil}}}{\partial \bar{r}}\right)^2 + \left(\frac{\partial \phi_{\text{oil}}}{\partial \bar{z}}\right)^2} \tag{3.99a}$$

$$\begin{aligned}\bar{K} = -\frac{1}{R^4\bar{B}^3}\Bigg[&\left(\frac{\partial \phi_{\text{oil}}}{\partial \bar{r}}\right)^2\left(\frac{1}{\bar{r}}\frac{\partial \phi_{\text{oil}}}{\partial \bar{r}} + \frac{\partial^2 \phi_{\text{oil}}}{\partial \bar{z}^2}\right) - 2\frac{\partial \phi_{\text{oil}}}{\partial \bar{r}}\frac{\partial \phi_{\text{oil}}}{\partial \bar{z}}\frac{\partial^2 \phi_{\text{oil}}}{\partial \bar{r}\partial \bar{z}} \\ &+ \left(\frac{\partial \phi_{\text{oil}}}{\partial \bar{z}}\right)^2\left(\frac{\partial^2 \phi_{\text{oil}}}{\partial \bar{r}^2} + \frac{1}{\bar{r}}\frac{\partial \phi_{\text{oil}}}{\partial \bar{r}}\right)\Bigg]\end{aligned} \tag{3.99b}$$

3.8.1 Dimensionless Governing Equations

Substituting Equations (3.93a)−(3.98h) into Equation (3.26) and simplifying, yields the dimensionless form of the continuity equation as:

$$\frac{\partial\,(R\bar{r}U_\infty u)}{\partial\,(R\bar{r})} + \frac{\partial\,(R\bar{r}U_\infty v)}{\partial\,(R\bar{z})} = 0 \quad \Rightarrow \quad \frac{\partial\,(\bar{r}u)}{\partial \bar{r}} + \frac{\partial\,(\bar{r}v)}{\partial \bar{z}} = 0. \tag{3.100}$$

Substituting Equations (3.93a)−(3.98l) into the $r-$momentum Equation (3.61) yields

$$\rho_{\text{mix}}\left[\frac{U_\infty^2}{R}\frac{\partial u}{\partial \bar{t}}+\frac{U_\infty^2}{R}u\frac{\partial u}{\partial \bar{r}}+\frac{U_\infty^2}{R}v\frac{\partial u}{\partial \bar{z}}\right]=-\frac{\rho_{\text{mix}}U_\infty^2}{R}\frac{\partial P}{\partial \bar{r}}-\frac{\mu_{\text{mix}}}{\kappa}U_\infty u+\frac{\sigma\bar{K}}{R}\frac{\partial \phi_{\text{oil}}}{\partial \bar{r}}$$
$$+\mu_{\text{mix}}\left(2\frac{U_\infty}{R^2}\frac{\partial^2 u}{\partial \bar{r}^2}+\frac{U_\infty}{R^2}\frac{\partial^2 u}{\partial \bar{z}^2}+\frac{U_\infty}{R^2}\frac{\partial^2 v}{\partial \bar{r}\partial \bar{z}}+\frac{2}{R\bar{r}}\frac{U_\infty}{R}\frac{\partial u}{\partial \bar{r}}-\frac{2}{R^2\bar{r}^2}U_\infty u\right)$$
$$+\rho_{\text{mix}}g\cos(\varphi)\left(\beta_{\text{T}}\right)_{\text{mix}}\left(T_\infty-T_{\text{wall}}\right)\Theta+\rho_{\text{mix}}g\cos(\varphi)\left(\beta_{\text{C}}\right)_{\text{mix}}\left(C_{\text{wall}}-C_\infty\right)\phi. \tag{3.101}$$

Multiplying through by $R/\rho_{\text{mix}}U_\infty^2$ and simplifying yields

$$\frac{\partial u}{\partial \bar{t}}+u\frac{\partial u}{\partial \bar{r}}+v\frac{\partial u}{\partial \bar{z}}=-\frac{\partial P}{\partial \bar{r}}-\frac{\mu_{\text{mix}}R}{\kappa\rho_{\text{mix}}U_\infty}u+\frac{\sigma\bar{K}R}{\rho_{\text{mix}}U_\infty^2R}\frac{\partial \phi_{\text{oil}}}{\partial \bar{r}}$$
$$+\frac{\mu_{\text{mix}}}{\rho_{\text{mix}}RU}\left(2\frac{\partial^2 u}{\partial \bar{r}^2}+\frac{\partial^2 u}{\partial \bar{z}^2}+\frac{\partial^2 v}{\partial \bar{r}\partial \bar{z}}+\frac{2}{\bar{r}}\frac{\partial u}{\partial \bar{r}}-\frac{2}{\bar{r}^2}u\right)$$
$$+\frac{g\cos(\varphi)R\left(\beta_{\text{T}}\right)_{\text{mix}}}{U_\infty^2}\left(T_\infty-T_{\text{wall}}\right)\Theta+\frac{g\cos(\varphi)R\left(\beta_{\text{C}}\right)_{\text{mix}}}{U_\infty^2}\left(C_{\text{wall}}-C_\infty\right)\phi. \tag{3.102}$$

Introducing the dimensionless groups, yields the dimensionless form of the $r-$momentum equation as:

$$\frac{\partial u}{\partial \bar{t}}+u\frac{\partial u}{\partial \bar{r}}+v\frac{\partial u}{\partial \bar{z}}=-\frac{\partial P}{\partial \bar{r}}+\frac{\lambda_2}{\text{Re}}\left(2\frac{\partial^2 u}{\partial \bar{r}^2}+\frac{\partial^2 u}{\partial \bar{z}^2}+\frac{\partial^2 v}{\partial \bar{r}\partial \bar{z}}+\frac{2}{\bar{r}}\frac{\partial u}{\partial \bar{r}}-\frac{2}{\bar{r}^2}u\right)$$
$$-\frac{\lambda_2}{(\text{Re}\cdot\text{Da})}u+\lambda_3\frac{\text{Gr}_{\text{T}}}{\text{Re}^2}\cos(\varphi)\Theta+\lambda_4\frac{\text{Gr}_{\text{C}}}{\text{Re}^2}\cos(\varphi)\phi+\frac{\lambda_1}{\text{We}}R\bar{K}\frac{\partial \phi_{\text{oil}}}{\partial \bar{r}}. \tag{3.103}$$

Substituting Equations (3.93a)−(3.98l) into the $z-$momentum Equation (3.62) yields

$$\rho_{\text{mix}}\left[\frac{U_\infty^2}{R}\frac{\partial v}{\partial \bar{t}}+\frac{U_\infty^2}{R}u\frac{\partial v}{\partial \bar{r}}+\frac{U_\infty^2}{R}v\frac{\partial v}{\partial \bar{z}}\right]=-\frac{\rho_{\text{mix}}U_\infty^2}{R}\frac{\partial P}{\partial \bar{z}}-\frac{\mu_{\text{mix}}}{\kappa}U_\infty v+\frac{\sigma\bar{K}}{R}\frac{\partial \phi_{\text{oil}}}{\partial \bar{z}}$$
$$+\mu_{\text{mix}}\left(\frac{U_\infty}{R^2}\frac{\partial^2 v}{\partial \bar{r}^2}+2\frac{U_\infty}{R^2}\frac{\partial^2 v}{\partial \bar{z}^2}+\frac{U_\infty}{R^2}\frac{\partial^2 u}{\partial \bar{r}\partial \bar{z}}+\frac{1}{R\bar{r}}\frac{U_\infty}{R}\frac{\partial u}{\partial \bar{z}}+\frac{1}{R\bar{r}}\frac{U_\infty}{R}\frac{\partial v}{\partial \bar{r}}\right)$$
$$+\rho_{\text{mix}}g\sin(\varphi)\left(\beta_{\text{T}}\right)_{\text{mix}}\left(T_\infty-T_{\text{wall}}\right)\Theta+\rho_{\text{mix}}g\sin(\varphi)\left(\beta_{\text{C}}\right)_{\text{mix}}\left(C_{\text{wall}}-C_\infty\right)\phi. \tag{3.104}$$

Multiplying through by $R/\rho_{\text{mix}}U_\infty^2$ and simplifying yields

$$\frac{\partial v}{\partial \bar{t}}+u\frac{\partial v}{\partial \bar{r}}+v\frac{\partial v}{\partial \bar{z}}=-\frac{\partial P}{\partial \bar{z}}-\frac{\mu_{\text{mix}}R}{\kappa\rho_{\text{mix}}U_\infty}v+\frac{\sigma\bar{K}R}{\rho_{\text{mix}}U_\infty^2R}\frac{\partial \phi_{\text{oil}}}{\partial \bar{z}}$$
$$+\frac{\mu_{\text{mix}}}{\rho_{\text{mix}}RU_\infty}\left(\frac{\partial^2 v}{\partial \bar{r}^2}+2\frac{\partial^2 v}{\partial \bar{z}^2}+\frac{\partial^2 u}{\partial \bar{r}\partial \bar{z}}+\frac{1}{\bar{r}}\frac{\partial u}{\partial \bar{z}}+\frac{1}{\bar{r}}\frac{\partial v}{\partial \bar{r}}\right)$$
$$+\frac{g\sin(\varphi)R\left(\beta_{\text{T}}\right)_{\text{mix}}}{U_\infty^2}\left(T_\infty-T_{\text{wall}}\right)\Theta+\frac{g\sin(\varphi)R\left(\beta_{\text{C}}\right)_{\text{mix}}}{U_\infty^2}\left(C_{\text{wall}}-C_\infty\right)\phi. \tag{3.105}$$

Introducing the dimensionless groups, yields the dimensionless form of the $z-$momentum equation as:

$$\frac{\partial v}{\partial \bar{t}} + u\frac{\partial v}{\partial \bar{r}} + v\frac{\partial v}{\partial \bar{z}} = -\frac{\partial P}{\partial \bar{z}} + \frac{\lambda_2}{\mathrm{Re}}\left(\frac{\partial^2 v}{\partial \bar{r}^2} + 2\frac{\partial^2 v}{\partial \bar{z}^2} + \frac{\partial^2 u}{\partial \bar{r}\partial \bar{z}} + \frac{1}{\bar{r}}\frac{\partial u}{\partial \bar{z}} + \frac{1}{\bar{r}}\frac{\partial v}{\partial \bar{r}}\right) - \frac{\lambda_2}{(\mathrm{Re}\cdot\mathrm{Da})}v + \lambda_3\frac{\mathrm{Gr_T}}{\mathrm{Re}^2}\sin(\varphi)\Theta + \lambda_4\frac{\mathrm{Gr_C}}{\mathrm{Re}^2}\sin(\varphi)\phi + \frac{\lambda_1}{\mathrm{We}}R\bar{K}\frac{\partial \phi_{\text{oil}}}{\partial \bar{z}}. \quad (3.106)$$

where $\mathrm{Da} = \dfrac{\kappa}{R^2}$ is the Darcy number, $\mathrm{Gr_T} = \dfrac{\rho_\mathrm{f}^2 g R^3 (\beta_\mathrm{T})_\mathrm{f}}{\mu_\mathrm{f}^2}(T_\infty - T_{\text{wall}})$ is the thermal Grashof number, $\mathrm{Gr_C} = \dfrac{\rho_\mathrm{f}^2 g R^3 (\beta_\mathrm{C})_\mathrm{f}}{\mu_\mathrm{f}^2}(C_{\text{wall}} - C_\infty)$ is the mass transfer Grashof number, $\mathrm{Re} = \dfrac{\rho_\mathrm{f} R U_\infty}{\mu_\mathrm{f}}$ is the Reynolds number, $\mathrm{We} = \dfrac{\rho_\mathrm{f} U_\infty^2 R}{\sigma}$ is the Weber number, and

$$\lambda_1 = \frac{\rho_\mathrm{f}}{\rho_{\text{mix}}} = \left[1 - \phi_{\text{gel}}\left(1 - \frac{\rho_{\text{gel}}}{(1-\phi_{\text{water}})\rho_{\text{oil}} + \phi_{\text{water}}\rho_{\text{water}}}\right)\right]^{-1} \quad (3.107a)$$

$$\lambda_2 = \frac{\mu_{\text{mix}}}{\mu_\mathrm{f}}\frac{\rho_\mathrm{f}}{\rho_{\text{mix}}} = \left[1 - \phi_{\text{gel}}\left(1 - \frac{\mu_{\text{gel}}}{(1-\phi_{\text{water}})\mu_{\text{oil}} + \phi_{\text{water}}\mu_{\text{water}}}\right)\right]\lambda_1. \quad (3.107b)$$

$$\lambda_3 = \frac{(\beta_\mathrm{T})_{\text{mix}}}{(\beta_\mathrm{T})_\mathrm{f}} = \left[1 - \phi_{\text{gel}}\left(1 - \frac{(\beta_\mathrm{T})_{\text{gel}}}{(1-\phi_{\text{water}})(\beta_\mathrm{T})_{\text{oil}} + \phi_{\text{water}}(\beta_\mathrm{T})_{\text{water}}}\right)\right]. \quad (3.107c)$$

$$\lambda_4 = \frac{(\beta_\mathrm{C})_{\text{mix}}}{(\beta_\mathrm{C})_\mathrm{f}} = \left[1 - \phi_{\text{gel}}\left(1 - \frac{(\beta_\mathrm{C})_{\text{gel}}}{(1-\phi_{\text{water}})(\beta_\mathrm{C})_{\text{oil}} + \phi_{\text{water}}(\beta_\mathrm{C})_{\text{water}}}\right)\right]. \quad (3.107d)$$

The expressions for the functions $\lambda_1, \lambda_2, \lambda_3$ and λ_4 are obtained from the thermophysical properties presented in Section 3.4. From Equations (3.99a) and (3.99b), it is clear that

$$R\bar{K} = -\left[\left(\frac{\partial \phi_{\text{oil}}}{\partial \bar{r}}\right)^2 + \left(\frac{\partial \phi_{\text{oil}}}{\partial \bar{z}}\right)^2\right]^{-\frac{3}{2}}\left[\left(\frac{\partial \phi_{\text{oil}}}{\partial \bar{r}}\right)^2\left(\frac{1}{\bar{r}}\frac{\partial \phi_{\text{oil}}}{\partial \bar{r}} + \frac{\partial^2 \phi_{\text{oil}}}{\partial \bar{z}^2}\right) - 2\frac{\partial \phi_{\text{oil}}}{\partial \bar{r}}\frac{\partial \phi_{\text{oil}}}{\partial \bar{z}}\frac{\partial^2 \phi_{\text{oil}}}{\partial \bar{r}\partial \bar{z}} + \left(\frac{\partial \phi_{\text{oil}}}{\partial \bar{z}}\right)^2\left(\frac{\partial^2 \phi_{\text{oil}}}{\partial \bar{r}^2} + \frac{1}{\bar{r}}\frac{\partial \phi_{\text{oil}}}{\partial \bar{r}}\right)\right]. \quad (3.108)$$

The ratio $\mathrm{Ri} = \dfrac{\mathrm{Gr_T}}{\mathrm{Re}^2}$ is called the Richardson number. Generally, the combined effects of free and forced convection must be considered when $\mathrm{Ri} \approx 1$. If the inequality $\mathrm{Ri} \ll 1$ is satisfied, free convection effects may be neglected. Consequently, if $\mathrm{Ri} \gg 1$, forced convection effects may be neglected. Substituting Equations (3.93a)$-$(3.98s) into the

energy Equation (3.66) yields

$$\begin{aligned}
&\frac{U_\infty\left(T_\infty - T_{\text{wall}}\right)}{R}\frac{\partial\Theta}{\partial\bar{t}} + \frac{U_\infty\left(T_\infty - T_{\text{wall}}\right)}{R}u\frac{\partial\Theta}{\partial\bar{r}} + \frac{U_\infty\left(T_\infty - T_{\text{wall}}\right)}{R}v\frac{\partial\Theta}{\partial\bar{z}} \\
&= \alpha_{\text{mix}}\left[\frac{\left(T_\infty - T_{\text{wall}}\right)}{R^2}\frac{\partial^2\Theta}{\partial\bar{r}^2} + \frac{1}{R\bar{r}}\frac{\left(T_\infty - T_{\text{wall}}\right)}{R}\frac{\partial\Theta}{\partial\bar{r}} + \frac{\left(T_\infty - T_{\text{wall}}\right)}{R^2}\frac{\partial^2\Theta}{\partial\bar{z}^2}\right] \\
&\quad + \frac{\mu_{\text{mix}}}{\rho_{\text{mix}}\left(Cp\right)_{\text{mix}}}\left[2\left(\frac{U_\infty}{R}\frac{\partial u}{\partial\bar{r}}\right)^2 + 2\left(\frac{U_\infty}{R}\frac{u}{\bar{r}}\right)^2 + 2\left(\frac{U_\infty}{R}\frac{\partial v}{\partial\bar{z}}\right)^2\right. \\
&\quad \left. + \left(\frac{U_\infty}{R}\frac{\partial v}{\partial\bar{r}} + \frac{U_\infty}{R}\frac{\partial u}{\partial\bar{z}}\right)^2\right] - \frac{h_{\text{r}}}{\rho_{\text{mix}}\left(Cp\right)_{\text{mix}}R\bar{d}}\left(T_\infty - T_{\text{wall}}\right)\Theta. \qquad (3.109)
\end{aligned}$$

Multiplying through by $R/U_\infty\left(T_\infty - T_{\text{wall}}\right)$ and simplifying yields

$$\begin{aligned}
&\frac{\partial\Theta}{\partial\bar{t}} + u\frac{\partial\Theta}{\partial\bar{r}} + v\frac{\partial\Theta}{\partial\bar{z}} = \frac{\alpha_{\text{mix}}}{U_\infty R}\left(\frac{\partial^2\Theta}{\partial\bar{r}^2} + \frac{1}{\bar{r}}\frac{\partial\Theta}{\partial\bar{r}} + \frac{\partial^2\Theta}{\partial\bar{z}^2}\right) - \frac{h_{\text{r}}}{\rho_{\text{mix}}U_\infty\left(Cp\right)_{\text{mix}}\bar{d}}\Theta \\
&+ \frac{\mu_{\text{mix}}U_\infty}{\rho_{\text{mix}}R\left(Cp\right)_{\text{mix}}\left(T_\infty - T_{\text{wall}}\right)}\left[2\left(\frac{\partial u}{\partial\bar{r}}\right)^2 + 2\left(\frac{u}{\bar{r}}\right)^2 + 2\left(\frac{\partial v}{\partial\bar{z}}\right)^2 + \left(\frac{\partial v}{\partial\bar{r}} + \frac{\partial u}{\partial\bar{z}}\right)^2\right]. \qquad (3.110)
\end{aligned}$$

Introducing the dimensionless groups, yields the dimensionless form of the energy equation as:

$$\begin{aligned}
&\frac{\partial\Theta}{\partial\bar{t}} + u\frac{\partial\Theta}{\partial\bar{r}} + v\frac{\partial\Theta}{\partial\bar{z}} = \frac{\lambda_5}{\text{Pe}}\left(\frac{\partial^2\Theta}{\partial\bar{r}^2} + \frac{1}{\bar{r}}\frac{\partial\Theta}{\partial\bar{r}} + \frac{\partial^2\Theta}{\partial\bar{z}^2}\right) - \text{St}\frac{\lambda_6}{\bar{d}}\Theta \\
&+ \lambda_7\frac{\text{Ec}}{\text{Re}}\left[2\left(\frac{\partial u}{\partial\bar{r}}\right)^2 + 2\left(\frac{u}{\bar{r}}\right)^2 + 2\left(\frac{\partial v}{\partial\bar{z}}\right)^2 + \left(\frac{\partial v}{\partial\bar{r}} + \frac{\partial u}{\partial\bar{z}}\right)^2\right], \qquad (3.111)
\end{aligned}$$

where $\text{Pe} = \dfrac{U_\infty R}{\alpha_{\text{f}}}$ is the Peclet number, $\text{Ec} = \dfrac{U_\infty^2}{\left(Cp\right)_{\text{f}}\left(T_\infty - T_{\text{wall}}\right)}$ is the Eckert number, $\text{Re} = \dfrac{\rho_{\text{f}}U_\infty R}{\mu_{\text{f}}}$ is the Reynolds number, $\text{St} = \dfrac{h_{\text{r}}}{\rho_{\text{f}}U_\infty\left(Cp\right)_{\text{f}}}$ is the Stanton number, and

$$\lambda_5 = \frac{\alpha_{\text{mix}}}{\alpha_{\text{f}}} = \frac{k_{\text{mix}}}{k_{\text{f}}}\frac{\rho_{\text{f}}}{\rho_{\text{mix}}}\frac{\left(Cp\right)_{\text{f}}}{\left(Cp\right)_{\text{mix}}}, \quad \lambda_6 = \frac{\rho_{\text{f}}}{\rho_{\text{mix}}}\frac{\left(Cp\right)_{\text{f}}}{\left(Cp\right)_{\text{mix}}}, \quad \lambda_7 = \frac{\mu_{\text{mix}}}{\mu_{\text{f}}}\lambda_6. \qquad (3.112)$$

The expressions for the functions λ_5, λ_6 and λ_7 are obtained from the thermophysical properties presented in Section 3.4. Substituting Equations (3.93a)−(3.98y) into the

species concentration Equation (3.75) yields

$$\begin{aligned}
&\frac{U_\infty\left(C_{\text{wall}}-C_\infty\right)}{R}\frac{\partial\phi}{\partial\bar{t}}+\frac{U_\infty\left(C_{\text{wall}}-C_\infty\right)}{R}u\frac{\partial\phi}{\partial\bar{r}}+\frac{U_\infty\left(C_{\text{wall}}-C_\infty\right)}{R}v\frac{\partial\phi}{\partial\bar{z}}\\
&\quad=D_{\text{p}}\left(1-\alpha_{\text{m}}\right)\left(C_{\text{wall}}-C_\infty\right)\left(\phi-\bar{C}_{\text{d}}\right)\left(\frac{U_\infty}{R^2}\frac{\partial^2 v}{\partial\bar{r}^2}+\frac{1}{R\bar{r}}\frac{U_\infty}{R}\frac{\partial v}{\partial\bar{r}}\right)\\
&+D_{\text{p}}\Bigg\{\left(1-\alpha_{\text{m}}\right)\left(\frac{\left(C_{\text{wall}}-C_\infty\right)}{R}\frac{\partial\phi}{\partial\bar{r}}-\frac{\left(C_{\text{wall}}-C_\infty\right)}{\left(T_\infty-T_{\text{wall}}\right)}\frac{d\bar{C}_{\text{d}}}{d\Theta}\frac{\left(T_\infty-T_{\text{wall}}\right)}{R}\frac{\partial\Theta}{\partial\bar{r}}\right)\\
&\quad-\left(C_{\text{wall}}-C_\infty\right)\left(\phi-\bar{C}_{\text{d}}\right)\frac{\partial\alpha_{\text{m}}}{\partial r}\Bigg\}\frac{U_\infty}{R}\frac{\partial v}{\partial\bar{r}}\\
&+D_{\text{d}}\frac{\left(C_{\text{wall}}-C_\infty\right)}{\left(T_\infty-T_{\text{wall}}\right)}\frac{d\bar{C}_{\text{d}}}{d\Theta}\left(\frac{\left(T_\infty-T_{\text{wall}}\right)}{R^2}\frac{\partial^2\Theta}{\partial\bar{r}^2}+\frac{1}{R\bar{r}}\frac{\left(T_\infty-T_{\text{wall}}\right)}{R}\frac{\partial\Theta}{\partial\bar{r}}+\frac{\left(T_\infty-T_{\text{wall}}\right)}{R^2}\frac{\partial^2\Theta}{\partial\bar{z}^2}\right)\\
&\quad+D_{\text{d}}\frac{\left(C_{\text{wall}}-C_\infty\right)}{\left(T_\infty-T_{\text{wall}}\right)^2}\frac{d^2\bar{C}_{\text{d}}}{d\Theta^2}\left\{\left(\frac{\left(T_\infty-T_{\text{wall}}\right)}{R}\frac{\partial\Theta}{\partial\bar{r}}\right)^2+\left(\frac{\left(T_\infty-T_{\text{wall}}\right)}{R}\frac{\partial\Theta}{\partial\bar{z}}\right)^2\right\}.
\end{aligned}\tag{3.113}$$

Multiplying through by $R/U_\infty\left(C_{\text{wall}}-C_\infty\right)$ and simplifying yields

$$\begin{aligned}
&\frac{\partial\phi}{\partial\bar{t}}+u\frac{\partial\phi}{\partial\bar{r}}+v\frac{\partial\phi}{\partial\bar{z}}=\frac{D_{\text{p}}}{R}\Bigg[\left(1-\alpha_{\text{m}}\right)\left(\phi-\bar{C}_{\text{d}}\right)\left(\frac{\partial^2 v}{\partial\bar{r}^2}+\frac{1}{\bar{r}}\frac{\partial v}{\partial\bar{r}}\right)\\
&\quad+\left\{\left(1-\alpha_{\text{m}}\right)\left(\frac{\partial\phi}{\partial\bar{r}}-\frac{d\bar{C}_{\text{d}}}{d\Theta}\frac{\partial\Theta}{\partial\bar{r}}\right)-\left(\phi-\bar{C}_{\text{d}}\right)\frac{\partial\alpha_{\text{m}}}{\partial\bar{r}}\right\}\frac{\partial v}{\partial\bar{r}}\Bigg]\\
&+\frac{D_{\text{d}}}{U_\infty R}\left[\frac{d\bar{C}_{\text{d}}}{d\Theta}\left(\frac{\partial^2\Theta}{\partial\bar{r}^2}+\frac{1}{\bar{r}}\frac{\partial\Theta}{\partial\bar{r}}+\frac{\partial^2\Theta}{\partial\bar{z}^2}\right)+\frac{d^2\bar{C}_{\text{d}}}{d\Theta^2}\left\{\left(\frac{\partial\Theta}{\partial\bar{r}}\right)^2+\left(\frac{\partial\Theta}{\partial\bar{z}}\right)^2\right\}\right].
\end{aligned}\tag{3.114}$$

Introducing the dimensionless groups and parameters, yields the dimensionless form of the species concentration equation as:

$$\begin{aligned}
&\frac{\partial\phi}{\partial\bar{t}}+u\frac{\partial\phi}{\partial\bar{r}}+v\frac{\partial\phi}{\partial\bar{z}}=\varepsilon_{\text{p}}\Bigg[\left(1-\alpha_{\text{m}}\right)\left(\phi-\bar{C}_{\text{d}}\right)\left(\frac{\partial^2 v}{\partial\bar{r}^2}+\frac{1}{\bar{r}}\frac{\partial v}{\partial\bar{r}}\right)\\
&\quad+\left\{\left(1-\alpha_{\text{m}}\right)\left(\frac{\partial\phi}{\partial\bar{r}}-\frac{d\bar{C}_{\text{d}}}{d\Theta}\frac{\partial\Theta}{\partial\bar{r}}\right)-\left(\phi-\bar{C}_{\text{d}}\right)\frac{\partial\alpha_{\text{m}}}{\partial\bar{r}}\right\}\frac{\partial v}{\partial\bar{r}}\Bigg]\\
&+\frac{1}{\text{Re}\cdot\text{Sc}}\left[\frac{d\bar{C}_{\text{d}}}{d\Theta}\left(\frac{\partial^2\Theta}{\partial\bar{r}^2}+\frac{1}{\bar{r}}\frac{\partial\Theta}{\partial\bar{r}}+\frac{\partial^2\Theta}{\partial\bar{z}^2}\right)+\frac{d^2\bar{C}_{\text{d}}}{d\Theta^2}\left\{\left(\frac{\partial\Theta}{\partial\bar{r}}\right)^2+\left(\frac{\partial\Theta}{\partial\bar{z}}\right)^2\right\}\right].
\end{aligned}\tag{3.115}$$

where $\text{Re}=\dfrac{\rho_{\text{f}}U_\infty R}{\mu_{\text{f}}}$ is the Reynolds number, $\text{Sc}=\dfrac{\mu_{\text{f}}}{\rho_{\text{f}}D_{\text{d}}}$ is the Schmidt number, $\varepsilon_{\text{p}}=D_{\text{p}}/R$ is the shear dispersion parameter. Substituting Equations (3.93a)−(3.98y) into the wax precipitation kinetics Equation (3.78) yields

$$\frac{U_\infty}{R}\frac{\partial\alpha_{\text{m}}}{\partial\bar{t}}+\frac{U_\infty}{R}u\frac{\partial\alpha_{\text{m}}}{\partial\bar{r}}+\frac{U_\infty}{R}v\frac{\partial\alpha_{\text{m}}}{\partial\bar{z}}=\left[1-\alpha_{\text{m}}\right]\frac{U_\infty}{R}\bar{K}_1\left(\Theta\right)-\alpha_{\text{m}}\mu_{\text{mix}}\left(\frac{U_\infty}{R}\frac{\partial v}{\partial\bar{r}}\right)^2\frac{\rho_{\text{mix}}R^2}{\mu_{\text{mix}}^2}\bar{K}_2\left(\Theta\right),\tag{3.116}$$

Multiplying through by R/U_∞ and simplifying yields

$$\frac{\partial \alpha_{\mathrm{m}}}{\partial \bar{t}} + u\frac{\partial \alpha_{\mathrm{m}}}{\partial \bar{r}} + v\frac{\partial \alpha_{\mathrm{m}}}{\partial \bar{z}} = \left[1-\alpha_{\mathrm{m}}\right]\bar{K}_1\left(\Theta\right) - \alpha_{\mathrm{m}}\frac{\rho_{\mathrm{mix}}U_\infty R}{\mu_{\mathrm{mix}}}\left(\frac{\partial v}{\partial \bar{r}}\right)^2 \bar{K}_2\left(\Theta\right). \quad (3.117)$$

Introducing the dimensionless groups, yields the dimensionless form of the wax precipitation kinetics equation as:

$$\frac{\partial \alpha_{\mathrm{m}}}{\partial \bar{t}} + u\frac{\partial \alpha_{\mathrm{m}}}{\partial \bar{r}} + v\frac{\partial \alpha_{\mathrm{m}}}{\partial \bar{z}} = \left[1-\alpha_{\mathrm{m}}\right]\bar{K}_1\left(\Theta\right) - \alpha_{\mathrm{m}}\frac{\mathrm{Re}}{\lambda_2}\left(\frac{\partial v}{\partial \bar{r}}\right)^2 \bar{K}_2\left(\Theta\right). \quad (3.118)$$

where $\mathrm{Re} = \dfrac{\rho_{\mathrm{f}}U_\infty R}{\mu_{\mathrm{f}}}$ is the Reynolds number and λ_2 is given by Equation (3.107b). Substituting Equations (3.93a)−(3.98y) into Equation (3.84), yields the dimensionless form of the wax deposit thickness as:

$$\bar{\delta}(\bar{t}) = 1 - \sqrt{\frac{\phi_0}{\phi+\phi_0}}. \quad (3.119)$$

where $\phi_0 = \left(C_\infty - \rho_{\mathrm{gel}}\right)/\left(C_{\mathrm{wall}} - C_\infty\right)$. Substituting Equations (3.93a)−(3.98y) into the wax deposit growth Equation (3.85) yields

$$U_\infty\frac{d\bar{\delta}}{d\bar{t}} = \frac{\left(1-f(x)\right)}{x\rho_{\mathrm{gel}}}\left(D_{\mathrm{d}}\frac{\left(C_{\mathrm{wall}}-C_\infty\right)}{\left(T_\infty - T_{\mathrm{wall}}\right)}\frac{d\bar{C}_{\mathrm{d}}}{d\Theta}\frac{\left(T_\infty - T_{\mathrm{wall}}\right)}{R}\left.\frac{\partial\Theta}{\partial\bar{r}}\right|_{R\bar{r}=R\bar{R}_{\mathrm{eff}}}\right). \quad (3.120)$$

Multiplying through by $1/U_\infty$ and simplifying yields

$$\frac{d\bar{\delta}}{d\bar{t}} = \frac{\left(C_{\mathrm{wall}}-C_\infty\right)}{\rho_{\mathrm{gel}}}\frac{\left(1-f(x)\right)}{x}\left(\frac{D_{\mathrm{d}}}{U_\infty R}\frac{d\bar{C}_{\mathrm{d}}}{d\Theta}\left.\frac{\partial\Theta}{\partial\bar{r}}\right|_{\bar{r}=\bar{R}_{\mathrm{eff}}}\right). \quad (3.121)$$

Introducing the dimensionless groups, yields the dimensionless form of the wax deposit growth equation as:

$$\frac{d\bar{\delta}}{d\bar{t}} = \phi_1\frac{\left(1-f(x)\right)}{x}\left(\frac{1}{\mathrm{Re}\cdot\mathrm{Sc}}\frac{d\bar{C}_{\mathrm{d}}}{d\Theta}\left.\frac{\partial\Theta}{\partial\bar{r}}\right|_{\bar{r}=\bar{R}_{\mathrm{eff}}}\right), \quad (3.122)$$

where $\mathrm{Re} = \dfrac{\rho_{\mathrm{f}}U_\infty R}{\mu_{\mathrm{f}}}$ is the Reynolds number, $\mathrm{Sc} = \dfrac{\mu_{\mathrm{f}}}{\rho_{\mathrm{f}}D_{\mathrm{d}}}$ is the Schmidt number, $\bar{R}_{\mathrm{eff}} = 1-\bar{\delta}$ is the dimensionless effective pipeline radius, $\phi_1 = \left(C_{\mathrm{wall}}-C_\infty\right)/\rho_{\mathrm{gel}}$, and the function $f(x)$ is given by Equation (5.9). Substituting Equations (3.93a)−(3.98y) into the

wax deposit aging Equation (3.91) yields

$$\frac{U_\infty}{R}\frac{dx}{d\bar{t}} = \frac{2\left(R - R\bar{\delta}\right)}{R\bar{\delta}\left(2R - R\bar{\delta}\right)}\frac{f(x)}{\rho_{\text{gel}}}\left[D_{\text{d}}\frac{\left(C_{\text{wall}} - C_\infty\right)}{\left(T_\infty - T_{\text{wall}}\right)}\frac{d\bar{C}_{\text{d}}}{d\Theta}\frac{\left(T_\infty - T_{\text{wall}}\right)}{R}\frac{\partial\Theta}{\partial\bar{r}}\right.$$
$$\left. + D_{\text{p}}\left(1 - \alpha_{\text{m}}\right)\left(C_{\text{wall}} - C_\infty\right)\left(\phi - \bar{C}_{\text{d}}\right)\frac{U_\infty}{R}\frac{\partial v}{\partial\bar{r}}\right]_{R\bar{r}=R\bar{R}_{\text{eff}}} \tag{3.123}$$

Multiplying through by R/U_∞ and simplifying yields

$$\frac{dx}{d\bar{t}} = \frac{\left(C_{\text{wall}} - C_\infty\right)}{\rho_{\text{gel}}}\frac{2\left(1 - \bar{\delta}\right)f(x)}{\bar{\delta}\left(2 - \bar{\delta}\right)}\left[\frac{D_{\text{d}}}{U_\infty R}\frac{d\bar{C}_{\text{d}}}{d\Theta}\frac{\partial\Theta}{\partial\bar{r}} + \frac{D_{\text{p}}}{R}\left(1 - \alpha_{\text{m}}\right)\left(\phi - \bar{C}_{\text{d}}\right)\frac{\partial v}{\partial\bar{r}}\right]_{\bar{r}=\bar{R}_{\text{eff}}} \tag{3.124}$$

Introducing the dimensionless groups, yields the dimensionless form of the wax deposit aging equation as:

$$\frac{dx}{d\bar{t}} = \phi_1 f(x)\frac{2\left(1 - \bar{\delta}\right)}{\bar{\delta}\left(2 - \bar{\delta}\right)}\left[\frac{1}{\text{Re}\cdot\text{Sc}}\frac{d\bar{C}_{\text{d}}}{d\Theta}\frac{\partial\Theta}{\partial\bar{r}} + \varepsilon_{\text{p}}\left(1 - \alpha_{\text{m}}\right)\left(\phi - \bar{C}_{\text{d}}\right)\frac{\partial v}{\partial\bar{r}}\right]_{\bar{r}=\bar{R}_{\text{eff}}}, \tag{3.125}$$

where $\text{Re} = \dfrac{\rho_{\text{f}} U_\infty R}{\mu_{\text{f}}}$ is the Reynolds number, $\text{Sc} = \dfrac{\mu_{\text{f}}}{\rho_{\text{f}} D_{\text{d}}}$ is the Schmidt number, $\varepsilon_{\text{p}} = D_{\text{p}}/R$ is the shear dispersion parameter, $\bar{R}_{\text{eff}} = 1 - \bar{\delta}$ is the dimensionless effective pipeline radius, $\phi_1 = \left(C_{\text{wall}} - C_\infty\right)/\rho_{\text{gel}}$, and the function $f(x)$ is given by Equation (5.9). Substituting Equations (3.93a)−(3.98y) into the oil volume fraction conservation Equation (3.80) yields

$$\frac{U_\infty}{R}\frac{\partial\phi_{\text{oil}}}{\partial\bar{t}} + \frac{U_\infty}{R}u\frac{\partial\phi_{\text{oil}}}{\partial\bar{r}} + \frac{U_\infty}{R}v\frac{\partial\phi_{\text{oil}}}{\partial\bar{z}} = 0. \tag{3.126}$$

Multiplying Equation (3.126) through by R/U_∞, yields the dimensionless form of the oil volume fraction conservation equation as:

$$\frac{\partial\phi_{\text{oil}}}{\partial\bar{t}} + u\frac{\partial\phi_{\text{oil}}}{\partial\bar{r}} + v\frac{\partial\phi_{\text{oil}}}{\partial\bar{z}} = 0. \tag{3.127}$$

3.8.2 Dimensionless Boundary and Initial Conditions

Substituting Equations (3.93a)−(3.98y) into the initial-boundary conditions given by Equation (3.92), yields the dimensionless form of the initial-boundary conditions for the

governing equations as:

$$\begin{cases} \dfrac{\partial u}{\partial \bar{r}} = 0,\ \dfrac{\partial v}{\partial \bar{r}} = 0,\ \dfrac{\partial \Theta}{\partial \bar{r}} = 0,\ \dfrac{\partial \phi}{\partial \bar{r}} = 0,\ \dfrac{\partial \alpha_{\mathrm{m}}}{\partial \bar{r}} = 0,\ \dfrac{\partial \phi_{\mathrm{oil}}}{\partial \bar{r}} = 0. & \text{at } \bar{r} = 0 \\ u = 0,\ v = 0,\ \Theta = \beta_0,\ \phi = \beta_1,\ \alpha_{\mathrm{m}} = 1,\ \phi_{\mathrm{oil}} = 0. & \text{at } \bar{r} = \lambda \\ u = 0,\ v = 1,\ \Theta = 1,\ \phi = 0,\ \alpha_{\mathrm{m}} = 0,\ \phi_{\mathrm{oil}} = 1 - \phi_{\mathrm{water}}. & \text{at } \bar{z} = 0 \\ \dfrac{\partial u}{\partial \bar{z}} = 0,\ \dfrac{\partial v}{\partial \bar{z}} = 0,\ \dfrac{\partial \Theta}{\partial \bar{z}} = 0,\ \dfrac{\partial \phi}{\partial \bar{z}} = 0,\ \dfrac{\partial \alpha_{\mathrm{m}}}{\partial \bar{z}} = 0,\ \dfrac{\partial \phi_{\mathrm{oil}}}{\partial \bar{z}} = 0. & \text{as } \bar{z} \to \infty \\ u = 0,\ v = 1,\ \Theta = 1,\ \phi = 0,\ \alpha_{\mathrm{m}} = 0, \\ \quad \phi_{\mathrm{oil}} = 1 - \phi_{\mathrm{water}},\ \bar{\delta} = 0,\ x = 0. & \text{at } \bar{t} = 0 \end{cases} \tag{3.128}$$

Here, $\lambda = \dfrac{R_{\mathrm{eff}}}{R}$, $\beta_0 = \dfrac{T_{\mathrm{interface}} - T_{\mathrm{wall}}}{T_\infty - T_{\mathrm{wall}}}$, and $\beta_1 = \dfrac{C_{\mathrm{interface}} - C_\infty}{C_{\mathrm{wall}} - C_\infty}$. Note that if $\lambda = 1$, then there is no gel layer. The physical significance of the dimensionless numbers which have been obtained from the process of dimensional analysis of the governing equations in this study are discussed in Subsection 3.8.3.

3.8.3 Dimensionless Numbers

Expressing the governing equations in their dimensionless forms results in dimensionless numbers which are very useful in determining the flow characteristics of waxy crude oil in pipeline systems. The dimensionless numbers obtained in this study are discussed below.

3.8.3.1 Reynolds Number

The Reynolds number (Re) is the ratio of inertial forces to viscous forces. It is expressed as

$$\mathrm{Re} = \frac{\text{inertial forces}}{\text{viscous forces}} = \frac{\rho_{\mathrm{f}} U_\infty R}{\mu_{\mathrm{f}}}. \tag{3.129}$$

It gives the information whether the flow is inertial or viscous force dominant. It helps us to determine whether the flow is laminar or turbulent. It may be interpreted as a measure of the relative importance of convective to viscous momentum fluxes. If the momentum fluxes are in the same direction then the Reynolds number reveals the boundary layer characteristics of the flow. If the fluxes are defined such that the diffusion is in the cross

stream direction, then Re conveys the flow regime (i.e., laminar flow-$0 < \mathrm{Re} < 2000$, transitional flow-$\mathrm{Re} = 2000$, or turbulent flow-$\mathrm{Re} > 2000$). It controls the ratio of length scale to velocity boundary layer thickness in forced convection flow.

3.8.3.2 Thermal Grashof Number

The thermal Grashof number ($\mathrm{Gr_T}$) is defined as the ratio of the thermal buoyancy force to the viscous force. It is expressed as

$$\mathrm{Gr_T} = \frac{\text{thermal buoyancy forces}}{\text{viscous forces}} = \frac{\rho_\mathrm{f}^2 g \left(\beta_\mathrm{T}\right)_\mathrm{f} \Delta T R^3}{\mu_\mathrm{f}^2} \tag{3.130}$$

where $\Delta T = (T_\infty - T_{\text{wall}})$. A positive value of $\mathrm{Gr_T}$ corresponds to cooling of the pipeline wall (or heating the fluid in contact with the wall) while a negative value corresponds to heating the wall of the pipeline (or cooling of the fluid in contact with the wall). It controls the ratio of length scale to thermal boundary layer thickness in natural convection flow.

3.8.3.3 Mass Grashof Number

The mass (or solutal) Grashof number ($\mathrm{Gr_C}$) is defined as the ratio of the species buoyancy force to the viscous force. It is expressed as

$$\mathrm{Gr_C} = \frac{\text{species buoyancy forces}}{\text{viscous forces}} = \frac{\rho_\mathrm{f}^2 g \left(\beta_\mathrm{C}\right)_\mathrm{f} \Delta C R^3}{\mu_\mathrm{f}^2} \tag{3.131}$$

where $\Delta C = (C_{\text{wall}} - C_\infty)$. A positive value of $\mathrm{Gr_C}$ means that the wax molecules are diffusing towards the bulk of the fluid. It controls the ratio of length scale to concentration boundary layer thickness in natural convection flow.

3.8.3.4 Richardson Number

Richardson number (Ri) is the ratio of Grashof number to the square of the Reynolds number, i.e.,

$$\mathrm{Ri} = \frac{\mathrm{Gr}}{\mathrm{Re}^2}. \tag{3.132}$$

It is a measure of the relative strength of the natural convection and forced convection for a particular flow. The case $\mathrm{Ri} \gg 1$ means that natural convection is dominant, $\mathrm{Ri} \ll 1$ means that forced convection is dominant, and $\mathrm{Ri} = 1$ means that mixed convection is dominant.

3.8.3.5 Darcy Number

The Darcy number (Da) is the ratio of permeability (κ) of the porous medium to its cross-sectional area (commonly the square of the diameter or radius). It is expressed as

$$\mathrm{Da} = \frac{\kappa}{R^2}. \tag{3.133}$$

A decrease in κ means an increase in flow resistance. A decrease in the Da is a consequence of decreasing the permeability of the porous medium.

3.8.3.6 Eckert Number

The Eckert number (Ec) is a dimensionless number defined as the ratio of kinetic energy of the flow to the boundary layer enthalpy difference. It is expressed as

$$\mathrm{Ec} = \frac{\text{kinetic energy of flow}}{\text{enthalpy difference}} = \frac{U_\infty^2}{(Cp)_\mathrm{f}\Delta T} \tag{3.134}$$

where $\Delta T = (T_\infty - T_{\text{wall}})$ is the temperature gradient. The Eckert number represents the viscous dissipation potential in the flow. It plays an important role in high speed flows for which viscous dissipation is significant. A large positive value of Ec indicates high viscous dissipation occurring at high speed of the flow (high kinetic energy). Very small values of Eckert number (i.e., $\mathrm{Ec} \ll 1$) means that the effect of viscous dissipation term in the energy equation is negligible. A positive value of Ec implies cooling of the pipeline wall (or loss of heat from the wall to the fluid).

3.8.3.7 Prandtl Number

The Prandtl number (Pr) is defined as the ratio of momentum diffusivity ($\nu = \mu_\mathrm{f}/\rho_\mathrm{f}$) to thermal diffusivity (α_f), i.e.,

$$\mathrm{Pr} = \frac{\text{momentum diffusivity}}{\text{thermal diffusivity}} = \frac{\mu_\mathrm{f}}{\rho_\mathrm{f}\alpha_\mathrm{f}}. \tag{3.135}$$

The Prandtl number provides the information about the thickness of the velocity boundary layer relative to the thickness of the thermal boundary layer. It also gives the information about the type of fluid since it is an intrinsic property of a fluid. In particular, the Prandtl values for oils, water, mercury, and air are 50-2000, 6.90, 0.03, and 0.71, respectively.

3.8.3.8 Peclet Number

The Peclet number (Pe) is defined as the ratio of the convection rate to the diffusion rate in a fluid. It is expressed as

$$\mathrm{Pe} = \frac{\text{inertia (convection)}}{\text{Diffusion rate}} = \frac{U_\infty R}{\alpha_\mathrm{f}} \tag{3.136}$$

Pe is also the product of Re and Pr, i.e., $\mathrm{Pe} = \mathrm{Re} \cdot \mathrm{Pr}$. It is used to determine plug flow or perfect mixing.

3.8.3.9 Stanton Number

The Stanton Number (St) is the ratio of heat transferred through a fluid to the thermal capacity of the same fluid. Expressed as

$$\mathrm{St} = \frac{\text{convective heat transfer}}{\text{thermal capacity}} = \frac{h_\mathrm{r}}{\rho_\mathrm{f} U_\infty \left(Cp\right)_\mathrm{f}} \tag{3.137}$$

It characterizes the rate of heat exchange between the oil phase and the water droplets phase. St is also the ratio of Nu and the product of Re and Pr, i.e., $\mathrm{St} = \mathrm{Nu}/(\mathrm{Re} \cdot \mathrm{Pr})$.

3.8.3.10 Nusselt Number

The Nusselt number (Nu) is the ratio of the rate of convective heat transfer to the rate of conductive heat transfer within the thermal boundary layer. It is expressed as

$$\mathrm{Nu} = \frac{\text{convective heat transfer}}{\text{conductive heat transfer}} = \frac{h_\mathrm{r}}{k_\mathrm{f}/R} = \frac{h_\mathrm{r} R}{k_\mathrm{f}}. \tag{3.138}$$

It represents the dimensionless temperature gradient at the wall of the pipeline. It characterizes the rate of heat loss from the oil phase to the coolant stream (or the surrounding sea water) through the pipe wall. It provides a measure of the convective heat transfer occurring at the pipeline wall. A very small Nusselt number means that the heat transfer by conduction is dominant. The Nusselt number does not arise as a dimensionless group when writing the governing equations in non-dimensional forms; rather, it is used to report data on the convection heat transfer by calculating the heat transfer coefficient.

3.8.3.11 Schmidt Number

The Schmidt number (Sc) is the ratio of the momentum diffusivity (ν_{eff}) to mass diffusivity (D_{d}). It is expressed as

$$\mathrm{Sc} = \frac{\text{momentum diffusivity}}{\text{mass diffusivity}} = \frac{\mu_{\mathrm{f}}}{\rho_{\mathrm{f}} D_{\mathrm{d}}}. \tag{3.139}$$

The Schmidt number provides the information about the thickness of the velocity boundary layer relative to the thickness of the concentration boundary layer.

3.8.3.12 Sherwood Number

The Sherwood number (Sh) is the ratio of the rate of convective mass transfer to the rate of diffusive mass transfer within the concentration boundary layer. It is expressed as

$$\mathrm{Sh} = \frac{\text{convective mass transfer rate}}{\text{mass diffusion rate}} = \frac{k_{\mathrm{m}}}{D_{\mathrm{d}}/R} = \frac{k_{\mathrm{m}} R}{D_{\mathrm{d}}}. \tag{3.140}$$

It represents the dimensionless concentration gradient at the pipeline wall. It provides a measure of the convective mass transfer occurring at the pipeline wall. The Sherwood number does not arise as a dimensionless group when writing the governing equations in non-dimensional forms; rather, it is used to report data on convection mass transfer by calculating the mass transfer coefficient.

3.8.3.13 Weber Number

The Weber number (We) is defined as the ratio of inertial forces to the surface tension forces. It is expressed as

$$\mathrm{We} = \frac{\text{inertial forces}}{\text{surface tension forces}} = \frac{\rho_{\mathrm{f}} U_{\infty}^2 R}{\sigma} \tag{3.141}$$

The formation of water-in-oil emulsions is due to surface tension. Small values of We means that the surface tension forces are dominant and vice versa.

3.9 Pressure Poisson Formulation

Since the pressure field is desired in the present study, an extra equation is needed for determining the dimensionless pressure field (P) explicitly. In the pressure Poisson formulation of the governing equations, the continuity equation is replaced by a Pressure

Poisson Equation (PPE) and a Neumann boundary condition for the pressure. The pressure field is then obtained by solving the PPE, which is presented in Subsection 3.9.1.

3.9.1 Derivation of the Pressure Poisson Equation

The PPE is derived by cross-differentiation of the momentum equations along with the continuity equation as follows. Making $\frac{\partial P}{\partial \bar{r}}$ the subject in the dimensionless $r-$momentum Equation (3.103) yields

$$\begin{aligned}\frac{\partial P}{\partial \bar{r}} = &-\frac{\partial u}{\partial \bar{t}} - u\frac{\partial u}{\partial \bar{r}} - v\frac{\partial u}{\partial \bar{z}} + \frac{\lambda_2}{\mathrm{Re}}\left(2\frac{\partial^2 u}{\partial \bar{r}^2} + \frac{\partial^2 u}{\partial \bar{z}^2} + \frac{\partial^2 v}{\partial \bar{r}\partial \bar{z}} + \frac{2}{\bar{r}}\frac{\partial u}{\partial \bar{r}} - \frac{2}{\bar{r}^2}u\right) \\ &-\frac{\lambda_2}{(\mathrm{Re}\cdot\mathrm{Da})}u + \lambda_3\frac{\mathrm{Gr_T}}{\mathrm{Re}^2}\cos(\varphi)\Theta + \lambda_4\frac{\mathrm{Gr_C}}{\mathrm{Re}^2}\cos(\varphi)\phi + \frac{\lambda_1}{\mathrm{We}}R\bar{K}\frac{\partial \phi_{\text{oil}}}{\partial \bar{r}}. \end{aligned} \tag{3.142}$$

Differentiating Equation (3.142) partially with respect to r yields

$$\begin{aligned}\frac{\partial^2 P}{\partial \bar{r}^2} = &-\frac{\partial^2 u}{\partial \bar{r}\partial \bar{t}} - u\frac{\partial^2 u}{\partial \bar{r}^2} - \left(\frac{\partial u}{\partial \bar{r}}\right)^2 - v\frac{\partial^2 u}{\partial \bar{r}\partial \bar{z}} - \frac{\partial v}{\partial \bar{r}}\frac{\partial u}{\partial \bar{z}} - \frac{\lambda_2}{(\mathrm{Re}\cdot\mathrm{Da})}\frac{\partial u}{\partial \bar{r}} \\ &+\frac{\lambda_2}{\mathrm{Re}}\left(2\frac{\partial^3 u}{\partial \bar{r}^3} + \frac{\partial^3 u}{\partial \bar{r}\partial \bar{z}^2} + \frac{\partial^3 v}{\partial \bar{r}^2\partial \bar{z}} + \frac{2}{\bar{r}}\frac{\partial^2 u}{\partial \bar{r}^2} - \frac{4}{\bar{r}^2}\frac{\partial u}{\partial \bar{r}} + \frac{4}{\bar{r}^3}u\right) \\ &+\lambda_3\frac{\mathrm{Gr_T}}{\mathrm{Re}^2}\cos(\varphi)\frac{\partial \Theta}{\partial \bar{r}} + \lambda_4\frac{\mathrm{Gr_C}}{\mathrm{Re}^2}\cos(\varphi)\frac{\partial \phi}{\partial \bar{r}} + \frac{\lambda_1}{\mathrm{We}}R\bar{K}\frac{\partial^2 \phi_{\text{oil}}}{\partial \bar{r}^2} + \frac{\lambda_1}{\mathrm{We}}\frac{\partial (R\bar{K})}{\partial \bar{r}}\frac{\partial \phi_{\text{oil}}}{\partial \bar{r}}. \end{aligned} \tag{3.143}$$

Making $\frac{\partial P}{\partial \bar{z}}$ the subject in the dimensionless $z-$momentum Equation (3.106) yields

$$\begin{aligned}\frac{\partial P}{\partial \bar{z}} = &-\frac{\partial v}{\partial \bar{t}} - u\frac{\partial v}{\partial \bar{r}} - v\frac{\partial v}{\partial \bar{z}} + \frac{\lambda_2}{\mathrm{Re}}\left(\frac{\partial^2 v}{\partial \bar{r}^2} + 2\frac{\partial^2 v}{\partial \bar{z}^2} + \frac{\partial^2 u}{\partial \bar{r}\partial \bar{z}} + \frac{1}{\bar{r}}\frac{\partial u}{\partial \bar{z}} + \frac{1}{\bar{r}}\frac{\partial v}{\partial \bar{r}}\right) \\ &-\frac{\lambda_2}{(\mathrm{Re}\cdot\mathrm{Da})}v + \lambda_3\frac{\mathrm{Gr_T}}{\mathrm{Re}^2}\sin(\varphi)\Theta + \lambda_4\frac{\mathrm{Gr_C}}{\mathrm{Re}^2}\sin(\varphi)\phi + \frac{\lambda_1}{\mathrm{We}}R\bar{K}\frac{\partial \phi_{\text{oil}}}{\partial \bar{z}}. \end{aligned} \tag{3.144}$$

Differentiating Equation (3.144) partially with respect to z yields

$$\begin{aligned}\frac{\partial^2 P}{\partial \bar{z}^2} = &-\frac{\partial^2 v}{\partial \bar{z}\partial \bar{t}} - u\frac{\partial^2 v}{\partial \bar{r}\partial \bar{z}} - \frac{\partial u}{\partial \bar{z}}\frac{\partial v}{\partial \bar{r}} - v\frac{\partial^2 v}{\partial \bar{z}^2} - \left(\frac{\partial v}{\partial \bar{z}}\right)^2 - \frac{\lambda_2}{(\mathrm{Re}\cdot\mathrm{Da})}\frac{\partial v}{\partial \bar{z}} \\ &+\frac{\lambda_2}{\mathrm{Re}}\left(\frac{\partial^3 v}{\partial \bar{r}^2\partial \bar{z}} + 2\frac{\partial^3 v}{\partial \bar{z}^3} + \frac{\partial^3 u}{\partial \bar{r}\partial \bar{z}^2} + \frac{1}{\bar{r}}\frac{\partial^2 u}{\partial \bar{z}^2} + \frac{1}{\bar{r}}\frac{\partial^2 v}{\partial \bar{r}\partial \bar{z}}\right) \\ &+\lambda_3\frac{\mathrm{Gr_T}}{\mathrm{Re}^2}\sin(\varphi)\frac{\partial \Theta}{\partial \bar{z}} + \lambda_4\frac{\mathrm{Gr_C}}{\mathrm{Re}^2}\sin(\varphi)\frac{\partial \phi}{\partial \bar{z}} + \frac{\lambda_1}{\mathrm{We}}R\bar{K}\frac{\partial^2 \phi_{\text{oil}}}{\partial \bar{z}^2} + \frac{\lambda_1}{\mathrm{We}}\frac{\partial (R\bar{K})}{\partial \bar{z}}\frac{\partial \phi_{\text{oil}}}{\partial \bar{z}}. \end{aligned} \tag{3.145}$$

Adding equations (3.142), (3.143) and (3.145) yields

$$\begin{aligned}
\frac{\partial^2 P}{\partial \bar{r}^2}+\frac{1}{\bar{r}}\frac{\partial P}{\partial \bar{r}}+\frac{\partial^2 P}{\partial \bar{z}^2} &= -\left(\frac{\partial^2 u}{\partial \bar{r}\partial \bar{t}}+\frac{1}{\bar{r}}\frac{\partial u}{\partial \bar{t}}+\frac{\partial^2 v}{\partial \bar{z}\partial \bar{t}}\right)-u\left(\frac{\partial^2 u}{\partial \bar{r}^2}+\frac{\partial^2 v}{\partial \bar{r}\partial \bar{z}}\right)\\
&\quad -v\left(\frac{\partial^2 u}{\partial \bar{r}\partial \bar{z}}+\frac{\partial^2 v}{\partial \bar{z}^2}\right)-\frac{\partial u}{\partial \bar{r}}\left(\frac{\partial u}{\partial \bar{r}}+\frac{u}{r}\right)-\frac{\partial u}{\partial \bar{z}}\left(2\frac{\partial v}{\partial \bar{r}}+\frac{v}{\bar{r}}\right)-\left(\frac{\partial v}{\partial \bar{z}}\right)^2\\
&\quad +\frac{\lambda_2}{\mathrm{Re}}\left(2\frac{\partial^3 u}{\partial \bar{r}^3}+2\frac{\partial^3 v}{\partial \bar{r}^2\partial \bar{z}}+2\frac{\partial^3 u}{\partial \bar{r}\partial \bar{z}^2}+2\frac{\partial^3 v}{\partial \bar{z}^3}+\frac{4}{\bar{r}}\frac{\partial^2 u}{\partial \bar{r}^2}+\frac{2}{\bar{r}}\frac{\partial^2 v}{\partial \bar{r}\partial \bar{z}}+\frac{2}{\bar{r}}\frac{\partial^2 u}{\partial \bar{z}^2}\right.\\
&\quad \left.-\frac{2}{\bar{r}^2}\frac{\partial u}{\partial \bar{r}}+\frac{2}{\bar{r}^3}u\right)+\lambda_3\frac{\mathrm{Gr_T}}{\mathrm{Re}^2}\left[\cos(\varphi)\left(\frac{\partial \Theta}{\partial \bar{r}}+\frac{1}{\bar{r}}\Theta\right)+\sin(\varphi)\frac{\partial \Theta}{\partial \bar{z}}\right]\\
&\quad +\lambda_4\frac{\mathrm{Gr_C}}{\mathrm{Re}^2}\left[\cos(\varphi)\left(\frac{\partial \phi}{\partial \bar{r}}+\frac{1}{\bar{r}}\phi\right)+\sin(\varphi)\frac{\partial \phi}{\partial \bar{z}}\right]-\frac{\lambda_2}{(\mathrm{Re}\cdot\mathrm{Da})}\left(\frac{\partial u}{\partial \bar{r}}+\frac{u}{\bar{r}}+\frac{\partial v}{\partial \bar{z}}\right)\\
&\quad +\frac{\lambda_1}{\mathrm{We}}R\bar{K}\left(\frac{\partial^2 \phi_{\mathrm{oil}}}{\partial \bar{r}^2}+\frac{1}{\bar{r}}\frac{\partial \phi_{\mathrm{oil}}}{\partial \bar{r}}+\frac{\partial^2 \phi_{\mathrm{oil}}}{\partial \bar{z}^2}\right)+\frac{\lambda_1}{\mathrm{We}}\left(\frac{\partial(R\bar{K})}{\partial \bar{r}}\frac{\partial \phi_{\mathrm{oil}}}{\partial \bar{r}}+\frac{\partial(R\bar{K})}{\partial \bar{z}}\frac{\partial \phi_{\mathrm{oil}}}{\partial \bar{z}}\right). \qquad (3.146)
\end{aligned}$$

Factoring out the common derivative operators, Equation (3.146) becomes

$$\begin{aligned}
\frac{\partial^2 P}{\partial \bar{r}^2}+\frac{1}{\bar{r}}\frac{\partial P}{\partial \bar{r}}+\frac{\partial^2 P}{\partial \bar{z}^2} &= -\frac{\partial}{\partial \bar{t}}\left(\frac{\partial u}{\partial \bar{r}}+\frac{u}{\bar{r}}+\frac{\partial v}{\partial \bar{z}}\right)-u\frac{\partial}{\partial \bar{r}}\left(\frac{\partial u}{\partial \bar{r}}+\frac{\partial v}{\partial \bar{z}}\right)\\
&\quad -v\frac{\partial}{\partial \bar{z}}\left(\frac{\partial u}{\partial \bar{r}}+\frac{\partial v}{\partial \bar{z}}\right)-\frac{\partial u}{\partial \bar{r}}\left(\frac{\partial u}{\partial \bar{r}}+\frac{u}{r}\right)-\frac{\partial u}{\partial \bar{z}}\left(2\frac{\partial v}{\partial \bar{r}}+\frac{v}{\bar{r}}\right)-\left(\frac{\partial v}{\partial \bar{z}}\right)^2\\
&\quad +\frac{\lambda_2}{\mathrm{Re}}\left[2\frac{\partial^2}{\partial \bar{r}^2}\left(\frac{\partial u}{\partial \bar{r}}+\frac{\partial v}{\partial \bar{z}}\right)+2\frac{\partial^2}{\partial \bar{z}^2}\left(\frac{\partial u}{\partial \bar{r}}+\frac{\partial v}{\partial \bar{z}}\right)+\frac{2}{\bar{r}}\frac{\partial}{\partial \bar{r}}\left(\frac{\partial u}{\partial \bar{r}}+\frac{\partial v}{\partial \bar{z}}\right)+\frac{2}{\bar{r}}\frac{\partial^2 u}{\partial \bar{z}^2}\right.\\
&\quad \left.+\frac{2}{\bar{r}}\frac{\partial^2 u}{\partial \bar{r}^2}-\frac{2}{\bar{r}^2}\frac{\partial u}{\partial \bar{r}}+\frac{2}{\bar{r}^3}u\right]+\lambda_3\frac{\mathrm{Gr_T}}{\mathrm{Re}^2}\left[\cos(\varphi)\left(\frac{\partial \Theta}{\partial \bar{r}}+\frac{1}{\bar{r}}\Theta\right)+\sin(\varphi)\frac{\partial \Theta}{\partial \bar{z}}\right]\\
&\quad +\lambda_4\frac{\mathrm{Gr_C}}{\mathrm{Re}^2}\left[\cos(\varphi)\left(\frac{\partial \phi}{\partial \bar{r}}+\frac{1}{\bar{r}}\phi\right)+\sin(\varphi)\frac{\partial \phi}{\partial \bar{z}}\right]-\frac{\lambda_2}{(\mathrm{Re}\cdot\mathrm{Da})}\left(\frac{\partial u}{\partial \bar{r}}+\frac{u}{\bar{r}}+\frac{\partial v}{\partial \bar{z}}\right)\\
&\quad +\frac{\lambda_1}{\mathrm{We}}R\bar{K}\left(\frac{\partial^2 \phi_{\mathrm{oil}}}{\partial \bar{r}^2}+\frac{1}{\bar{r}}\frac{\partial \phi_{\mathrm{oil}}}{\partial \bar{r}}+\frac{\partial^2 \phi_{\mathrm{oil}}}{\partial \bar{z}^2}\right)+\frac{\lambda_1}{\mathrm{We}}\left(\frac{\partial(R\bar{K})}{\partial \bar{r}}\frac{\partial \phi_{\mathrm{oil}}}{\partial \bar{r}}+\frac{\partial(R\bar{K})}{\partial \bar{z}}\frac{\partial \phi_{\mathrm{oil}}}{\partial \bar{z}}\right). \qquad (3.147)
\end{aligned}$$

From the dimensionless continuity Equation (3.100), it is clear that

$$\frac{\partial u}{\partial \bar{r}}+\frac{u}{\bar{r}}+\frac{\partial v}{\partial \bar{z}}=0 \qquad (3.148)$$

Substituting the continuity constraint given by Equation (3.148) into Equation (3.147) yields

$$\begin{aligned}\frac{\partial^2 P}{\partial \bar{r}^2}+\frac{1}{\bar{r}}\frac{\partial P}{\partial \bar{r}}+\frac{\partial^2 P}{\partial \bar{z}^2}=&-u\frac{\partial}{\partial \bar{r}}\left(-\frac{u}{\bar{r}}\right)-v\frac{\partial}{\partial \bar{z}}\left(-\frac{u}{\bar{r}}\right)-\frac{\partial u}{\partial \bar{r}}\frac{\partial v}{\partial \bar{z}}-\frac{\partial u}{\partial \bar{z}}\left(2\frac{\partial v}{\partial \bar{r}}+\frac{v}{\bar{r}}\right)\\&-\left(\frac{\partial v}{\partial \bar{z}}\right)^2+\frac{\lambda_2}{\mathrm{Re}}\left[2\frac{\partial^2}{\partial \bar{r}^2}\left(-\frac{u}{\bar{r}}\right)+2\frac{\partial^2}{\partial \bar{z}^2}\left(-\frac{u}{\bar{r}}\right)+\frac{2}{\bar{r}}\frac{\partial}{\partial \bar{r}}\left(-\frac{u}{\bar{r}}\right)+\frac{2}{\bar{r}}\frac{\partial^2 u}{\partial \bar{z}^2}\right.\\&\left.+\frac{2}{\bar{r}}\frac{\partial^2 u}{\partial \bar{r}^2}-\frac{2}{\bar{r}^2}\frac{\partial u}{\partial \bar{r}}+\frac{2}{\bar{r}^3}u\right]+\lambda_3\frac{\mathrm{Gr_T}}{\mathrm{Re}^2}\left[\cos(\varphi)\left(\frac{\partial \Theta}{\partial \bar{r}}+\frac{1}{\bar{r}}\Theta\right)+\sin(\varphi)\frac{\partial \Theta}{\partial \bar{z}}\right]\\&+\lambda_4\frac{\mathrm{Gr_C}}{\mathrm{Re}^2}\left[\cos(\varphi)\left(\frac{\partial \phi}{\partial \bar{r}}+\frac{1}{\bar{r}}\phi\right)+\sin(\varphi)\frac{\partial \phi}{\partial \bar{z}}\right]\\&+\frac{\lambda_1}{\mathrm{We}}R\bar{K}\left(\frac{\partial^2 \phi_{\mathrm{oil}}}{\partial \bar{r}^2}+\frac{1}{\bar{r}}\frac{\partial \phi_{\mathrm{oil}}}{\partial \bar{r}}+\frac{\partial^2 \phi_{\mathrm{oil}}}{\partial \bar{z}^2}\right)+\frac{\lambda_1}{\mathrm{We}}\left(\frac{\partial (R\bar{K})}{\partial \bar{r}}\frac{\partial \phi_{\mathrm{oil}}}{\partial \bar{r}}+\frac{\partial (R\bar{K})}{\partial \bar{z}}\frac{\partial \phi_{\mathrm{oil}}}{\partial \bar{z}}\right).\end{aligned}\tag{3.149}$$

Expanding the partial derivatives involved in Equation (3.149) yields

$$\frac{\partial}{\partial \bar{r}}\left(-\frac{u}{\bar{r}}\right)=-\frac{1}{\bar{r}}\frac{\partial u}{\partial \bar{r}}+\frac{u}{\bar{r}^2}\tag{3.150a}$$

$$\frac{\partial}{\partial \bar{z}}\left(-\frac{u}{\bar{r}}\right)=-\frac{1}{\bar{r}}\frac{\partial u}{\partial \bar{z}}\tag{3.150b}$$

$$\frac{\partial^2}{\partial \bar{r}^2}\left(-\frac{u}{\bar{r}}\right)=\frac{\partial}{\partial \bar{r}}\left(-\frac{1}{\bar{r}}\frac{\partial u}{\partial \bar{r}}+\frac{u}{\bar{r}^2}\right)=-\frac{1}{\bar{r}}\frac{\partial^2 u}{\partial \bar{r}^2}+\frac{2}{\bar{r}^2}\frac{\partial u}{\partial \bar{r}}-\frac{2}{\bar{r}^3}u\tag{3.150c}$$

$$\frac{\partial^2}{\partial \bar{z}^2}\left(-\frac{u}{\bar{r}}\right)=-\frac{1}{\bar{r}}\frac{\partial^2 u}{\partial \bar{z}^2}\tag{3.150d}$$

Substituting Equations (3.150a)−(3.150d) into Equation (3.149) and simplifying using the continuity constraint given by Equation (3.148), yields

$$\begin{aligned}\frac{\partial^2 P}{\partial \bar{r}^2}+\frac{1}{\bar{r}}\frac{\partial P}{\partial \bar{r}}+\frac{\partial^2 P}{\partial \bar{z}^2}=&-\frac{2}{\bar{r}^2}u^2-2\frac{\partial u}{\partial \bar{z}}\frac{\partial v}{\partial \bar{r}}+\frac{\lambda_1}{\mathrm{We}}R\bar{K}\left(\frac{\partial^2 \phi_{\mathrm{oil}}}{\partial \bar{r}^2}+\frac{1}{\bar{r}}\frac{\partial \phi_{\mathrm{oil}}}{\partial \bar{r}}+\frac{\partial^2 \phi_{\mathrm{oil}}}{\partial \bar{z}^2}\right)\\&+\frac{\lambda_1}{\mathrm{We}}\left(\frac{\partial (R\bar{K})}{\partial \bar{r}}\frac{\partial \phi_{\mathrm{oil}}}{\partial \bar{r}}+\frac{\partial (R\bar{K})}{\partial \bar{z}}\frac{\partial \phi_{\mathrm{oil}}}{\partial \bar{z}}\right)+\lambda_3\frac{\mathrm{Gr_T}}{\mathrm{Re}^2}\left[\cos(\varphi)\left(\frac{\partial \Theta}{\partial \bar{r}}+\frac{1}{\bar{r}}\Theta\right)+\sin(\varphi)\frac{\partial \Theta}{\partial \bar{z}}\right]\\&+\lambda_4\frac{\mathrm{Gr_C}}{\mathrm{Re}^2}\left[\cos(\varphi)\left(\frac{\partial \phi}{\partial \bar{r}}+\frac{1}{\bar{r}}\phi\right)+\sin(\varphi)\frac{\partial \phi}{\partial \bar{z}}\right].\end{aligned}\tag{3.151}$$

Equation (3.151) is the dimensionless pressure Poisson equation, in cylindrical coordinate system, for water-oil two-phase flow in crude oil transportation pipeline. Poisson equation for pressure is an elliptic PDE, showing the elliptic nature of pressure in incompressible flows. It enforces the incompressibility condition for the velocity field. The term $R\bar{K}$ is

given by Equation (3.108). To solve the PPE, boundary and initial conditions for pressure are required. The boundary conditions for the pressure field are of the Neumann type and are defined from Equations (3.142) and (3.144). The boundary values of pressure are obtained by tangential momentum equation to the fluid adjacent to the wall surface (Salih, 2013). Hence, for a wall located at $r = 1$ in cylindrical coordinate system, the tangential momentum equation ($z-$momentum equation) reduces to

$$\left.\frac{\partial P}{\partial \bar{z}}\right|_{\bar{r}=1} = \frac{\lambda_2}{\mathrm{Re}}\left(\frac{\partial^2 v}{\partial \bar{r}^2} + \frac{1}{\bar{r}}\frac{\partial v}{\partial \bar{r}}\right)\Bigg|_{\bar{r}=1} + \Bigg[-\frac{\lambda_2}{(\mathrm{Re}\cdot\mathrm{Da})}v + \lambda_3\frac{\mathrm{Gr_T}}{\mathrm{Re}^2}\sin(\varphi)\Theta + \lambda_4\frac{\mathrm{Gr_C}}{\mathrm{Re}^2}\sin(\varphi)\phi + \frac{\lambda_1}{\mathrm{We}}R\bar{K}\frac{\partial \phi_{\mathrm{oil}}}{\partial \bar{z}}\Bigg]_{\bar{r}=1} \tag{3.152}$$

In general, for incompressible flow, the vector form of the PPE is given in Orszag *et al.* (1986) and Johnston & Liu (2004) as:

$$\nabla^2 p = -\vec{\nabla}\cdot\left(\vec{V}\cdot\left(\vec{\nabla}\vec{V}\right)\right) + \vec{\nabla}\cdot\vec{F} \tag{3.153}$$

and the corresponding Neumann boundary condition for the pressure field is given as:

$$\left.\frac{\partial p}{\partial \mathbf{n}}\right|_{\mathrm{wall}} = \left[\frac{\mu}{\rho}\mathbf{n}\cdot\left(\vec{\nabla}\times\left(\vec{\nabla}\times\vec{V}\right)\right) + \mathbf{n}\cdot\vec{F}\right]_{\mathrm{wall}} \tag{3.154}$$

where $\mathbf{n}$ is a unit normal along the wall and $\vec{F}$ is the body force term.

3.9.2 Final Set of Specific Equations Governing the Flow

The final set of the model equations to be solved are the dimensionless $r-$momentum Equation (3.103), the dimensionless $z-$momentum Equation (3.106), the dimensionless pressure Poisson Equation (3.151), the dimensionless energy Equation (3.111), the dimensionless species concentration Equation (3.115), the dimensionless deposit growth rate Equation (3.122), the dimensionless deposit aging rate Equation (3.125), and the dimensionless oil volume fraction Equation (3.127) subject to the dimensionless initial-boundary conditions (3.128). In summary, the mathematical model developed for the present study is a system of coupled partial differential equations (PDEs) given as:

$$\frac{\partial u}{\partial \bar{t}} + u\frac{\partial u}{\partial \bar{r}} + v\frac{\partial u}{\partial \bar{z}} + \frac{\partial P}{\partial \bar{r}} = \frac{\lambda_2}{\mathrm{Re}}\left(2\frac{\partial^2 u}{\partial \bar{r}^2} + \frac{\partial^2 u}{\partial \bar{z}^2} + \frac{\partial^2 v}{\partial \bar{r}\partial \bar{z}} + \frac{2}{\bar{r}}\frac{\partial u}{\partial \bar{r}} - \frac{2}{\bar{r}^2}u\right) - \frac{\lambda_2}{(\mathrm{Re}\cdot\mathrm{Da})}u + \lambda_3\frac{\mathrm{Gr_T}}{\mathrm{Re}^2}\cos(\varphi)\Theta + \lambda_4\frac{\mathrm{Gr_C}}{\mathrm{Re}^2}\cos(\varphi)\phi + \frac{\lambda_1}{\mathrm{We}}R\bar{K}\frac{\partial \phi_{\mathrm{oil}}}{\partial \bar{r}}. \tag{3.155a}$$

$$\frac{\partial v}{\partial \bar{t}} + u\frac{\partial v}{\partial \bar{r}} + v\frac{\partial v}{\partial \bar{z}} + \frac{\partial P}{\partial \bar{z}} = \frac{\lambda_2}{\mathrm{Re}}\left(\frac{\partial^2 v}{\partial \bar{r}^2} + 2\frac{\partial^2 v}{\partial \bar{z}^2} + \frac{\partial^2 u}{\partial \bar{r}\partial \bar{z}} + \frac{1}{\bar{r}}\frac{\partial u}{\partial \bar{z}} + \frac{1}{\bar{r}}\frac{\partial v}{\partial \bar{r}}\right)$$
$$-\frac{\lambda_2}{(\mathrm{Re}\cdot\mathrm{Da})}v + \lambda_3\frac{\mathrm{Gr_T}}{\mathrm{Re}^2}\sin(\varphi)\Theta + \lambda_4\frac{\mathrm{Gr_C}}{\mathrm{Re}^2}\sin(\varphi)\phi + \frac{\lambda_1}{\mathrm{We}}R\bar{K}\frac{\partial \phi_{\mathrm{oil}}}{\partial \bar{z}}. \tag{3.155b}$$

$$\frac{\partial^2 P}{\partial \bar{r}^2} + \frac{1}{\bar{r}}\frac{\partial P}{\partial \bar{r}} + \frac{\partial^2 P}{\partial \bar{z}^2} = -\frac{2}{\bar{r}^2}u^2 - 2\frac{\partial u}{\partial \bar{z}}\frac{\partial v}{\partial \bar{r}} + \frac{\lambda_1}{\mathrm{We}}R\bar{K}\left(\frac{\partial^2 \phi_{\mathrm{oil}}}{\partial \bar{r}^2} + \frac{1}{\bar{r}}\frac{\partial \phi_{\mathrm{oil}}}{\partial \bar{r}} + \frac{\partial^2 \phi_{\mathrm{oil}}}{\partial \bar{z}^2}\right)$$
$$+\frac{\lambda_1}{\mathrm{We}}\left(\frac{\partial(R\bar{K})}{\partial \bar{r}}\frac{\partial \phi_{\mathrm{oil}}}{\partial \bar{r}} + \frac{\partial(R\bar{K})}{\partial \bar{z}}\frac{\partial \phi_{\mathrm{oil}}}{\partial \bar{z}}\right) + \lambda_3\frac{\mathrm{Gr_T}}{\mathrm{Re}^2}\left[\cos(\varphi)\left(\frac{\partial \Theta}{\partial \bar{r}} + \frac{1}{\bar{r}}\Theta\right) + \sin(\varphi)\frac{\partial \Theta}{\partial \bar{z}}\right]$$
$$+\lambda_4\frac{\mathrm{Gr_C}}{\mathrm{Re}^2}\left[\cos(\varphi)\left(\frac{\partial \phi}{\partial \bar{r}} + \frac{1}{\bar{r}}\phi\right) + \sin(\varphi)\frac{\partial \phi}{\partial \bar{z}}\right]. \tag{3.155c}$$

$$\frac{\partial \Theta}{\partial \bar{t}} + u\frac{\partial \Theta}{\partial \bar{r}} + v\frac{\partial \Theta}{\partial \bar{z}} = \frac{\lambda_5}{\mathrm{Pe}}\left(\frac{\partial^2 \Theta}{\partial \bar{r}^2} + \frac{1}{\bar{r}}\frac{\partial \Theta}{\partial \bar{r}} + \frac{\partial^2 \Theta}{\partial \bar{z}^2}\right) - \mathrm{St}\frac{\lambda_6}{\bar{d}}\Theta$$
$$+\lambda_7\frac{\mathrm{Ec}}{\mathrm{Re}}\left[2\left(\frac{\partial u}{\partial \bar{r}}\right)^2 + 2\left(\frac{u}{\bar{r}}\right)^2 + 2\left(\frac{\partial v}{\partial \bar{z}}\right)^2 + \left(\frac{\partial v}{\partial \bar{r}} + \frac{\partial u}{\partial \bar{z}}\right)^2\right]. \tag{3.155d}$$

$$\frac{\partial \phi}{\partial \bar{t}} + u\frac{\partial \phi}{\partial \bar{r}} + v\frac{\partial \phi}{\partial \bar{z}} = \varepsilon_{\mathrm{p}}\Bigg[(1-\alpha_{\mathrm{m}})\left(\phi - \bar{C}_{\mathrm{d}}\right)\left(\frac{\partial^2 v}{\partial \bar{r}^2} + \frac{1}{\bar{r}}\frac{\partial v}{\partial \bar{r}}\right)$$
$$+\left\{(1-\alpha_{\mathrm{m}})\left(\frac{\partial \phi}{\partial \bar{r}} - \frac{d\bar{C}_{\mathrm{d}}}{d\Theta}\frac{\partial \Theta}{\partial \bar{r}}\right) - \left(\phi - \bar{C}_{\mathrm{d}}\right)\frac{\partial \alpha_{\mathrm{m}}}{\partial \bar{r}}\right\}\frac{\partial v}{\partial \bar{r}}\Bigg]$$
$$+\frac{1}{\mathrm{Re}\cdot\mathrm{Sc}}\left[\frac{d\bar{C}_{\mathrm{d}}}{d\Theta}\left(\frac{\partial^2 \Theta}{\partial \bar{r}^2} + \frac{1}{\bar{r}}\frac{\partial \Theta}{\partial \bar{r}} + \frac{\partial^2 \Theta}{\partial \bar{z}^2}\right) + \frac{d^2\bar{C}_{\mathrm{d}}}{d\Theta^2}\left\{\left(\frac{\partial \Theta}{\partial \bar{r}}\right)^2 + \left(\frac{\partial \Theta}{\partial \bar{z}}\right)^2\right\}\right]. \tag{3.155e}$$

$$\frac{\partial \alpha_{\mathrm{m}}}{\partial \bar{t}} + u\frac{\partial \alpha_{\mathrm{m}}}{\partial \bar{r}} + v\frac{\partial \alpha_{\mathrm{m}}}{\partial \bar{z}} = \left[1-\alpha_{\mathrm{m}}\right]\bar{K}_1\left(\Theta\right) - \alpha_{\mathrm{m}}\frac{\mathrm{Re}}{\lambda_2}\left(\frac{\partial v}{\partial \bar{r}}\right)^2\bar{K}_2\left(\Theta\right). \tag{3.155f}$$

$$\frac{\partial \phi_{\mathrm{oil}}}{\partial \bar{t}} + u\frac{\partial \phi_{\mathrm{oil}}}{\partial \bar{r}} + v\frac{\partial \phi_{\mathrm{oil}}}{\partial \bar{z}} = 0. \tag{3.155g}$$

$$\frac{d\bar{\delta}}{d\bar{t}} = \phi_1\frac{(1-f(x))}{x}\left(\frac{1}{\mathrm{Re}\cdot\mathrm{Sc}}\frac{d\bar{C}_{\mathrm{d}}}{d\Theta}\frac{\partial \Theta}{\partial \bar{r}}\bigg|_{\bar{r}=\bar{R}_{\mathrm{eff}}}\right) \tag{3.155h}$$

$$\frac{dx}{d\bar{t}} = \phi_1 f(x)\frac{2\left(1-\bar{\delta}\right)}{\bar{\delta}\left(2-\bar{\delta}\right)}\left[\frac{1}{\mathrm{Re}\cdot\mathrm{Sc}}\frac{d\bar{C}_{\mathrm{d}}}{d\Theta}\frac{\partial \Theta}{\partial \bar{r}} + \varepsilon_{\mathrm{p}}\left(1-\alpha_{\mathrm{m}}\right)\left(\phi - \bar{C}_{\mathrm{d}}\right)\frac{\partial v}{\partial \bar{r}}\right]_{\bar{r}=\bar{R}_{\mathrm{eff}}} \tag{3.155i}$$

where the function $R\bar{K}$ is given by Equation (3.108). The following temperature-dependent solubility equation (or thermodynamic model) for waxy crude

oil, proposed by Al-Ahmad *et al.* (1990), is adopted in this study:

$$\bar{C}_{\mathrm{d}} = \frac{1}{S_{\mathrm{f}}}\left(\frac{0.981 + 0.0677\Theta}{1 - 0.0208\Theta}\right), \tag{3.156}$$

where $S_{\mathrm{f}} = (0.0077\mathrm{MW}_{\mathrm{oil}} - 1.737)$ and $\mathrm{MW}_{\mathrm{oil}}$ denotes the molecular weight of the crude oil. The molecular weight of crude oil is estimated by the Cragoe correlation given in Cragoe (1929) as:

$$\mathrm{MW}_{\mathrm{oil}} = \frac{6084}{{}^{o}\mathrm{API} - 5.9}, \tag{3.157}$$

where ^{o}API denotes the API gravity of the crude oil. In particular, this study considers heavy crude oil whose ${}^{o}\mathrm{API} = 18$. Equations (3.155a)−(3.155g) are subject to the following boundary conditions

$$\begin{gathered} u_{\bar{r}}(0,\bar{z},\bar{t}) = 0,\ v_{\bar{r}}(0,\bar{z},\bar{t}) = 0,\ \Theta_{\bar{r}}(0,\bar{z},\bar{t}) = 0,\ \phi_{\bar{r}}(0,\bar{z},\bar{t}) = 0, \\ (\alpha_{\bar{r}})_{\mathrm{m}}(0,\bar{z},\bar{t}) = 0,\ (\phi_{\bar{r}})_{\mathrm{oil}}(0,\bar{z},\bar{t}) = 0. \end{gathered} \tag{3.158a}$$

$$\begin{gathered} u(\lambda,\bar{z},\bar{t}) = 0,\ v(\lambda,\bar{z},\bar{t}) = 0,\ \Theta(\lambda,\bar{z},\bar{t}) = \beta_0,\ \phi(\lambda,\bar{z},\bar{t}) = \beta_1 \\ \frac{\partial P}{\partial \bar{z}}(\lambda,\bar{z},\bar{t}) = \frac{\lambda_2}{\mathrm{Re}}\left[v''(\lambda,\bar{z},\bar{t}) + v'(\lambda,\bar{z},\bar{t})\right] - \frac{\lambda_2}{(\mathrm{Re}\cdot\mathrm{Da})}v(\lambda,\bar{z},\bar{t}) \\ +\lambda_3\frac{\mathrm{Gr_T}}{\mathrm{Re}^2}\sin(\varphi)\Theta(\lambda,\bar{z},\bar{t}) + \lambda_4\frac{\mathrm{Gr_C}}{\mathrm{Re}^2}\sin(\varphi)\phi(\lambda,\bar{z},\bar{t}) + \frac{\lambda_1}{\mathrm{We}}R\bar{K}(\lambda,\bar{z},\bar{t})\frac{\partial\phi_{\mathrm{oil}}}{\partial\bar{z}}(\lambda,\bar{z},\bar{t}) \end{gathered} \tag{3.158b}$$

$$\begin{gathered} u(\bar{r},0,\bar{t}) = 0,\ v(\bar{r},0,\bar{t}) = 1,\ \Theta(\bar{r},0,\bar{t}) = 1,\ \phi(\bar{r},0,\bar{t}) = 0 \\ \alpha_{\mathrm{m}}(\bar{r},0,\bar{t}) = 0,\ \phi_{\mathrm{oil}}(\bar{r},0,\bar{t}) = 1 - \phi_{\mathrm{water}} \end{gathered} \tag{3.158c}$$

$$\begin{gathered} u_{\bar{z}}(\bar{r},\infty,\bar{t}) = 0,\ v_{\bar{z}}(\bar{r},\infty,\bar{t}) = 0,\ \Theta_{\bar{z}}(\bar{r},\infty,\bar{t}) = 0,\ \phi_{\bar{z}}(\bar{r},\infty,\bar{t}) = 0, \\ (\alpha_{\bar{z}})_{\mathrm{m}}(\bar{r},\infty,\bar{t}) = 0,\ (\phi_{\bar{z}})_{\mathrm{oil}}(\bar{r},\infty,\bar{t}) = 0. \end{gathered} \tag{3.158d}$$

The initial conditions are

$$\begin{gathered} u(\bar{r},\bar{z},0) = 0,\ v(\bar{r},\bar{z},0) = 1,\ P(\bar{r},\bar{z},0) = 1,\ \Theta(\bar{r},\bar{z},0) = 1,\ \phi(\bar{r},\bar{z},0) = 0 \\ \alpha_{\mathrm{m}}(\bar{r},\bar{z},0) = 0,\ \phi_{\mathrm{oil}}(\bar{r},\bar{z},0) = 1 - \phi_{\mathrm{water}},\ \bar{\delta}(0) = 0,\ x(0) = 0 \end{gathered} \tag{3.159}$$

The determination of the skin-friction coefficient and the rates of heat and mass transfer is presented in Section 3.10.

3.10 Skin-Friction Coefficient and Rates of Heat and Mass Transfer

In this study, the physical parameters of engineering interest are the skin-friction coefficient C_f, the local Nusselt number Nu_z and the local Sherwood number Sh_z. The skin-friction coefficient relates the dynamic pressure to the shear stress at the pipeline wall. The heat transfer coefficient is a proportionality constant which relates the heat flux at the wall of the pipeline to the difference between the temperature at the wall and that in the bulk of the fluid. Similarly, the mass transfer coefficient relates the solute diffusion flux at the wall of the pipeline to the difference between the concentration at the wall and that in the bulk of the fluid. We remark that the phrase "bulk of the fluid" is also called the free-stream, i.e., the region in the fluid that is far away from the boundary layer where the effect of the viscous forces are negligible. These important parameters are defined in Ibrahim (2020) and Magagula *et al.* (2020) as:

$$C_f = \frac{\tau_{\text{wall}}}{\frac{1}{2}\rho_{\text{f}} U_\infty^2}, \quad \mathrm{Nu}_z = \frac{R q_{\text{wall}}}{k_{\text{f}}(T_{\text{wall}} - T_\infty)}, \quad \mathrm{Sh}_z = \frac{R J_{\text{wall}}}{D_{\text{d}}(C_{\text{wall}} - C_\infty)}. \tag{3.160}$$

The skin-friction coefficient, the local Nusselt number and the local Sherwood number describe the shear stress, the heat flux rate and the mass flux rate at the wall of the crude oil pipeline, respectively. Shear stress refers to the drag force on a surface per unit surface area It is given by the Newton's law of viscosity. Heat flux refers to the rate of heat transfer (or energy flow) per unit area. It is given by the Fourier's law of heat conduction which states that the conductive heat flux through a material is proportional to the temperature gradient. Mass flux refers to the rate of mass transfer per unit surface area perpendicular to the direction of the flow. It is given by the Fick's law of diffusion. The wall shear stress τ_{wall}, wall heat flux q_{wall} and wall mass flux J_{wall} are defined by

$$\tau_{\text{wall}} = \mu_{\text{f}} \left(\frac{\partial u_z}{\partial r}\right)_{r=R}, \quad q_{\text{wall}} = -k_{\text{f}} \left(\frac{\partial T}{\partial r}\right)_{r=R}, \quad J_{\text{wall}} = -D_{\text{d}} \left(\frac{\partial C}{\partial r}\right)_{r=R} \tag{3.161}$$

Using the dimensionless variables given by Equations (3.93a)−(3.93d), yields the dimensionless form of the Equations (3.161) as:

$$\tau_{\text{wall}} = \mu_{\text{f}} \left(\frac{\partial u_z}{\partial r}\right)_{r=R} = \mu_{\text{f}} \frac{U_\infty}{R} \left(\frac{\partial v}{\partial \bar{r}}\right)_{\bar{r}=1} \tag{3.162a}$$

$$q_{\text{wall}} = -k_{\text{f}} \left(\frac{\partial T}{\partial r}\right)_{r=R} = -k_{\text{f}} \frac{(T_\infty - T_{\text{wall}})}{R} \left(\frac{\partial \Theta}{\partial \bar{r}}\right)_{\bar{r}=1} \tag{3.162b}$$

$$J_{\text{wall}} = -D_{\text{d}} \left(\frac{\partial C}{\partial r} \right)_{r=R} = -D_{\text{d}} \frac{(C_{\text{wall}} - C_{\infty})}{R} \left(\frac{\partial \phi}{\partial \bar{r}} \right)_{\bar{r}=1} \tag{3.162c}$$

Substituting Equations (3.162a)−(3.162c) into Equations (3.160), yields

$$C_f = \frac{\mu_{\text{f}} \dfrac{U_{\infty}}{R}}{\frac{1}{2}\rho_{\text{f}} U_{\infty}^2} \left(\frac{\partial v}{\partial \bar{r}} \right)_{\bar{r}=1} = \frac{\mu_{\text{f}}}{\frac{1}{2}\rho_{\text{f}} U_{\infty} R} \left(\frac{\partial v}{\partial \bar{r}} \right)_{\bar{r}=1} = \frac{2}{Re} \left(\frac{\partial v}{\partial \bar{r}} \right)_{\bar{r}=1} \tag{3.163a}$$

$$\text{Nu}_z = -\frac{Rk_{\text{f}} \dfrac{(T_{\infty} - T_{\text{wall}})}{R}}{k_{\text{f}}(T_{\text{wall}} - T_{\infty})} \left(\frac{\partial \Theta}{\partial \bar{r}} \right)_{\bar{r}=1} = - \left(\frac{\partial \Theta}{\partial \bar{r}} \right)_{\bar{r}=1} \tag{3.163b}$$

$$\text{Sh}_z = -\frac{RD_{\text{d}} \dfrac{(C_{\text{wall}} - C_{\infty})}{R}}{D_{\text{d}}(C_{\text{wall}} - C_{\infty})} \left(\frac{\partial \phi}{\partial \bar{r}} \right)_{\bar{r}=1} = - \left(\frac{\partial \phi}{\partial \bar{r}} \right)_{\bar{r}=1} \tag{3.163c}$$

where $\text{Re} = (\rho_{\text{f}} U_{\infty} R)/\mu_{\text{f}}$ is the Reynolds number. Rearranging Equations (3.163a)−(3.163c) yields

$$C_f \text{Re} = 2 \left(\frac{\partial v}{\partial \bar{r}} \right)_{\bar{r}=1}, \quad \text{Nu}_z = - \left(\frac{\partial \Theta}{\partial \bar{r}} \right)_{\bar{r}=1}, \quad \text{Sh}_z = - \left(\frac{\partial \phi}{\partial \bar{r}} \right)_{\bar{r}=1}. \tag{3.164}$$

Equations (3.164) show that the skin-friction coefficient, the local Nusselt number and the local Sherwood number are proportional to the negative velocity gradient, the negative temperature gradient and the negative concentration gradient, respectively. The numerical techniques applied to the model Equations (3.155a)−(3.155g) subject to the boundary conditions (3.158a)−(3.158d) and the initial conditions (3.159) together with the skin-friction coefficient and the rates of heat and mass transfer given by Equations (3.164) are presented in Section 3.11.

3.11 Numerical Method of Solution of the Model Equations

The numerical solution of time-dependent PDEs by spectral methods requires that the discretization be done in two different ways, i.e., temporal discretization using finite difference methods and spatial discretization using spectral methods (Trefethen, 2000). The coupled system of nonlinear PDEs given by Equations (3.155a) to (3.155g) subject to the boundary conditions (3.158a)−(3.158d) and the initial conditions (3.159) is discretized by the second order semi-implicit time discretization method, as presented in

Section 3.11.1. The resulting system of linear PDEs are discretized in space by the bivariate spectral collocation method based on Chebyshev-Gauss-Lobatto points, as presented in Subsection 3.11.2.

3.11.1 Temporal Discretization Using Second-order Semi-implicit Method

The second order semi-implicit time discretization method is a direct discretization of the governing equations using second order finite differences implemented on a staggered grid with explicit time discretization of the nonlinear terms and a second order implicit time discretization of the linear terms, while at the same time decoupling the system of the governing PDEs using the Gauss-Jacobi approach. Of course, decoupling the system is necessary to save on computer memory. Moreover, the nonlinear terms are treated explicitly in time to avoid the costly solution of a nonlinear system at each time stage. In particular, the semi-implicit time discretization method combines an explicit second-order Adams-Bashforth scheme for the nonlinear terms and an implicit Crank-Nicolson scheme for the linear terms involving spatial derivatives, as presented in Subsubsection 3.11.1.1. The intermediate functions in the Adams-Bashforth scheme are then approximated by the forward Euler scheme, presented in Subsubsection 3.11.1.3. The stability, consistency and convergence of this method has been analyzed in (Johnston & Liu, 2004). In this study, the time derivatives are discretized by the forward Euler's formula and the boundary conditions are discretized implicitly in time.

3.11.1.1 Adams-Bashforth and Crank-Nicolson Schemes

The temporal discretization of the $r-$momentum Equation (3.155a) yields

$$\begin{aligned}
\frac{u^{k+1}-u^{k}}{\Delta\bar{t}}+\frac{1}{2}\left(3u^{k}\frac{\partial u^{k}}{\partial\bar{r}}-u^{k-1}\frac{\partial u^{k-1}}{\partial\bar{r}}\right)+\frac{1}{2}\left(3v^{k}\frac{\partial u^{k}}{\partial\bar{z}}-v^{k-1}\frac{\partial u^{k-1}}{\partial\bar{z}}\right)+\frac{\partial P^{k}}{\partial\bar{r}} \\
=\frac{\lambda_2}{\mathrm{Re}}\left[\frac{1}{2}\left(2\frac{\partial^2 u^{k+1}}{\partial\bar{r}^2}+2\frac{\partial^2 u^{k}}{\partial\bar{r}^2}\right)+\frac{1}{2}\left(\frac{\partial^2 u^{k+1}}{\partial\bar{z}^2}+\frac{\partial^2 u^{k}}{\partial\bar{z}^2}\right)+\frac{\partial^2 v^{k}}{\partial\bar{r}\partial\bar{z}}\right. \\
\left.+\frac{1}{2}\left(\frac{2}{\bar{r}}\frac{\partial u^{k+1}}{\partial\bar{r}}+\frac{2}{\bar{r}}\frac{\partial u^{k}}{\partial\bar{r}}\right)-\frac{1}{2}\left(\frac{2}{\bar{r}^2}u^{k+1}+\frac{2}{\bar{r}^2}u^{k}\right)\right]-\frac{\lambda_2}{(\mathrm{Re}\cdot\mathrm{Da})}\frac{1}{2}\left(u^{k+1}+u^{k}\right) \\
+\lambda_3\frac{\mathrm{Gr_T}}{\mathrm{Re}^2}\cos(\varphi)\Theta^{k}+\lambda_4\frac{\mathrm{Gr_C}}{\mathrm{Re}^2}\cos(\varphi)\phi^{k} \\
+\frac{\lambda_1}{\mathrm{We}}\frac{1}{2}\left[3\left(R\bar{K}\right)^{k}\frac{\partial(\phi_{\mathrm{oil}})^{k}}{\partial\bar{r}}-\left(R\bar{K}\right)^{k-1}\frac{\partial(\phi_{\mathrm{oil}})^{k-1}}{\partial\bar{r}}\right], \qquad (3.165)
\end{aligned}$$

where $\Delta\bar{t}$ denotes the time-step size from the current time level to the next time level, $u^{k-1}=u(\bar{r},\bar{z},\bar{t}_{k-1})$, $u^{k}=u(\bar{r},\bar{z},\bar{t}_{k})$, $u^{k+1}=u(\bar{r},\bar{z},\bar{t}_{k+1})$, etc., and $k=1,2,3,\cdots$

The functions at time level k are approximated by the forward Euler scheme, presented in Subsubsection 3.11.1.3. Rearranging Equation (3.165) by writing the terms at time level $k+1$ on the left-hand side and the terms at time level k and $k-1$ on the right-hand side, yields the time discretized $r-$momentum equation as:

$$
\begin{aligned}
-\frac{\Delta\bar{t}\lambda_2}{\mathrm{Re}}\frac{\partial^2 u^{k+1}}{\partial\bar{r}^2} - \frac{\Delta\bar{t}\lambda_2}{2\mathrm{Re}}\frac{\partial^2 u^{k+1}}{\partial\bar{z}^2} - \frac{\Delta\bar{t}\lambda_2}{\mathrm{Re}}\frac{1}{\bar{r}}\frac{\partial u^{k+1}}{\partial\bar{r}} + \left(1 + \frac{\Delta\bar{t}\lambda_2}{\mathrm{Re}}\frac{1}{\bar{r}^2} + \frac{\Delta\bar{t}\lambda_2}{2(\mathrm{Re}\cdot\mathrm{Da})}\right)u^{k+1} \\
= u^k + \Delta\bar{t}\Bigg\{ -\frac{1}{2}\left(3u^k\frac{\partial u^k}{\partial\bar{r}} - u^{k-1}\frac{\partial u^{k-1}}{\partial\bar{r}}\right) - \frac{1}{2}\left(3v^k\frac{\partial u^k}{\partial\bar{z}} - v^{k-1}\frac{\partial u^{k-1}}{\partial\bar{z}}\right) - \frac{\partial P^k}{\partial\bar{r}} \\
+\frac{\lambda_2}{\mathrm{Re}}\left(\frac{\partial^2 u^k}{\partial\bar{r}^2} + \frac{1}{2}\frac{\partial^2 u^k}{\partial\bar{z}^2} + \frac{\partial^2 v^k}{\partial\bar{r}\partial\bar{z}} + \frac{1}{\bar{r}}\frac{\partial u^k}{\partial\bar{r}} - \frac{1}{\bar{r}^2}u^k\right) - \frac{\lambda_2}{2(\mathrm{Re}\cdot\mathrm{Da})}u^k \\
+\lambda_3\frac{\mathrm{Gr_T}}{\mathrm{Re}^2}\cos(\varphi)\Theta^k + \lambda_4\frac{\mathrm{Gr_C}}{\mathrm{Re}^2}\cos(\varphi)\phi^k \\
+\frac{\lambda_1}{2\mathrm{We}}\left[3\left(R\bar{K}\right)^k\frac{\partial(\phi_{\mathrm{oil}})^k}{\partial\bar{r}} - \left(R\bar{K}\right)^{k-1}\frac{\partial(\phi_{\mathrm{oil}})^{k-1}}{\partial\bar{r}}\right]\Bigg\}
\end{aligned}
\tag{3.166}
$$

The linear iterative scheme represented by Equation (3.166) is discrete in time but continuous in space. Similarly, the temporal discretization of the $z-$momentum Equation (3.155b) yields

$$
\begin{aligned}
\frac{v^{k+1}-v^k}{\Delta\bar{t}} + \frac{1}{2}\left(3u^k\frac{\partial v^k}{\partial\bar{r}} - u^{k-1}\frac{\partial v^{k-1}}{\partial\bar{r}}\right) + \frac{1}{2}\left(3v^k\frac{\partial v^k}{\partial\bar{z}} - v^{k-1}\frac{\partial v^{k-1}}{\partial\bar{z}}\right) + \frac{\partial P^k}{\partial\bar{z}} \\
= \frac{\lambda_2}{\mathrm{Re}}\Bigg[\frac{1}{2}\left(\frac{\partial^2 v^{k+1}}{\partial\bar{r}^2} + \frac{\partial^2 v^k}{\partial\bar{r}^2}\right) + \frac{1}{2}\left(2\frac{\partial^2 v^{k+1}}{\partial\bar{z}^2} + 2\frac{\partial^2 v^k}{\partial\bar{z}^2}\right) + \frac{\partial^2 u^k}{\partial\bar{r}\partial\bar{z}} + \frac{1}{\bar{r}}\frac{\partial u^k}{\partial\bar{z}} \\
+\frac{1}{2}\left(\frac{1}{\bar{r}}\frac{\partial v^{k+1}}{\partial\bar{r}} + \frac{1}{\bar{r}}\frac{\partial v^k}{\partial\bar{r}}\right)\Bigg] - \frac{\lambda_2}{(\mathrm{Re}\cdot\mathrm{Da})}\frac{1}{2}\left(v^{k+1}+v^k\right) + \lambda_3\frac{\mathrm{Gr_T}}{\mathrm{Re}^2}\sin(\varphi)\Theta^k \\
+\lambda_4\frac{\mathrm{Gr_C}}{\mathrm{Re}^2}\sin(\varphi)\phi^k + \frac{\lambda_1}{\mathrm{We}}\frac{1}{2}\left[3(R\bar{K})^k\frac{\partial(\phi_{\mathrm{oil}})^k}{\partial\bar{z}} - (R\bar{K})^{k-1}\frac{\partial(\phi_{\mathrm{oil}})^{k-1}}{\partial\bar{z}}\right].
\end{aligned}
\tag{3.167}
$$

Rearranging Equation (3.167) by writing the terms at time level $k+1$ on the left-hand side and the terms at time level k and $k-1$ on the right-hand side, yields the time discretized

$z-$momentum equation as:

$$
\begin{aligned}
&-\frac{\Delta\bar{t}\lambda_2}{2\mathrm{Re}}\frac{\partial^2 v^{k+1}}{\partial\bar{r}^2}-\frac{\Delta\bar{t}\lambda_2}{\mathrm{Re}}\frac{\partial^2 v^{k+1}}{\partial\bar{z}^2}-\frac{\Delta\bar{t}\lambda_2}{2\mathrm{Re}}\frac{1}{\bar{r}}\frac{\partial v^{k+1}}{\partial\bar{r}}+\left(1+\frac{\Delta\bar{t}\lambda_2}{2(\mathrm{Re}\cdot\mathrm{Da})}\right)v^{k+1}\\
&=v^k+\Delta\bar{t}\Bigg\{-\frac{1}{2}\left(3u^k\frac{\partial v^k}{\partial\bar{r}}-u^{k-1}\frac{\partial v^{k-1}}{\partial\bar{r}}\right)-\frac{1}{2}\left(3v^k\frac{\partial v^k}{\partial\bar{z}}-v^{k-1}\frac{\partial v^{k-1}}{\partial\bar{z}}\right)-\frac{\partial P^k}{\partial\bar{z}}\\
&\quad+\frac{\lambda_2}{\mathrm{Re}}\left(\frac{1}{2}\frac{\partial^2 v^k}{\partial\bar{r}^2}+\frac{\partial^2 v^k}{\partial\bar{z}^2}+\frac{\partial^2 u^k}{\partial\bar{r}\partial\bar{z}}+\frac{1}{\bar{r}}\frac{\partial u^k}{\partial\bar{z}}+\frac{1}{2\bar{r}}\frac{\partial v^k}{\partial\bar{r}}\right)-\frac{\lambda_2}{2(\mathrm{Re}\cdot\mathrm{Da})}v^k\\
&+\lambda_3\frac{\mathrm{Gr_T}}{\mathrm{Re}^2}\sin(\varphi)\Theta^k+\lambda_4\frac{\mathrm{Gr_C}}{\mathrm{Re}^2}\sin(\varphi)\phi^k+\frac{\lambda_1}{2\mathrm{We}}\left[3(R\bar{K})^k\frac{\partial(\phi_{\mathrm{oil}})^k}{\partial\bar{z}}-(R\bar{K})^{k-1}\frac{\partial(\phi_{\mathrm{oil}})^{k-1}}{\partial\bar{z}}\right]\Bigg\}
\end{aligned}
\tag{3.168}
$$

The temporal discretization of the energy Equation (3.155d) yields

$$
\begin{aligned}
&\frac{\Theta^{k+1}-\Theta^k}{\Delta\bar{t}}+\frac{1}{2}\left(3u^k\frac{\partial\Theta^k}{\partial\bar{r}}-u^{k-1}\frac{\partial\Theta^{k-1}}{\partial\bar{r}}\right)+\frac{1}{2}\left(3v^k\frac{\partial\Theta^k}{\partial\bar{z}}-v^{k-1}\frac{\partial\Theta^{k-1}}{\partial\bar{z}}\right)\\
&=\frac{\lambda_5}{\mathrm{Pe}}\left[\frac{1}{2}\left(\frac{\partial^2\Theta^{k+1}}{\partial\bar{r}^2}+\frac{\partial^2\Theta^k}{\partial\bar{r}^2}\right)+\frac{1}{\bar{r}}\frac{1}{2}\left(\frac{\partial\Theta^{k+1}}{\partial\bar{r}}+\frac{\partial\Theta^k}{\partial\bar{r}}\right)+\frac{1}{2}\left(\frac{\partial^2\Theta^{k+1}}{\partial\bar{z}^2}+\frac{\partial^2\Theta^k}{\partial\bar{z}^2}\right)\right]\\
&\quad+\lambda_7\frac{\mathrm{Ec}}{\mathrm{Re}}\frac{1}{2}\Bigg\{3\left[2\left(\frac{\partial u^k}{\partial\bar{r}}\right)^2+2\left(\frac{u^k}{\bar{r}}\right)^2+2\left(\frac{\partial v^k}{\partial\bar{z}}\right)^2+\left(\frac{\partial v^k}{\partial\bar{r}}+\frac{\partial u^k}{\partial\bar{z}}\right)^2\right]\\
&\quad-\left[2\left(\frac{\partial u^{k-1}}{\partial\bar{r}}\right)^2+2\left(\frac{u^{k-1}}{\bar{r}}\right)^2+2\left(\frac{\partial v^{k-1}}{\partial\bar{z}}\right)^2+\left(\frac{\partial v^{k-1}}{\partial\bar{r}}+\frac{\partial u^{k-1}}{\partial\bar{z}}\right)^2\right]\Bigg\}\\
&\quad-\mathrm{St}\frac{\lambda_6}{\bar{d}}\frac{1}{2}\left(\Theta^{k+1}+\Theta^k\right).
\end{aligned}
\tag{3.169}
$$

Rearranging Equation (3.169) by writing the terms at time level $k+1$ on the left-hand side and the terms at time level k and $k-1$ on the right-hand side, yields the time discretized energy equation as:

$$
\begin{aligned}
&-\frac{\Delta\bar{t}\lambda_5}{2\mathrm{Pe}}\frac{\partial^2\Theta^{k+1}}{\partial\bar{r}^2}-\frac{\Delta\bar{t}\lambda_5}{2\mathrm{Pe}}\frac{1}{\bar{r}}\frac{\partial\Theta^{k+1}}{\partial\bar{r}}-\frac{\Delta\bar{t}\lambda_5}{2\mathrm{Pe}}\frac{\partial^2\Theta^{k+1}}{\partial\bar{z}^2}+\left(1+\mathrm{St}\frac{\Delta\bar{t}\lambda_6}{2\bar{d}}\right)\Theta^{k+1}\\
&=\Theta^k+\Delta\bar{t}\Bigg\{-\frac{1}{2}\left(3u^k\frac{\partial\Theta^k}{\partial\bar{r}}-u^{k-1}\frac{\partial\Theta^{k-1}}{\partial\bar{r}}\right)-\frac{1}{2}\left(3v^k\frac{\partial\Theta^k}{\partial\bar{z}}-v^{k-1}\frac{\partial\Theta^{k-1}}{\partial\bar{z}}\right)\\
&\quad+\frac{\lambda_5}{2\mathrm{Pe}}\left(\frac{\partial^2\Theta^k}{\partial\bar{r}^2}+\frac{1}{\bar{r}}\frac{\partial\Theta^k}{\partial\bar{r}}+\frac{\partial^2\Theta^k}{\partial\bar{z}^2}\right)-\mathrm{St}\frac{\lambda_6}{2\bar{d}}\Theta^k\\
&\quad+\lambda_7\frac{\mathrm{Ec}}{2\mathrm{Re}}\Bigg\{3\left[2\left(\frac{\partial u^k}{\partial\bar{r}}\right)^2+2\left(\frac{u^k}{\bar{r}}\right)^2+2\left(\frac{\partial v^k}{\partial\bar{z}}\right)^2+\left(\frac{\partial v^k}{\partial\bar{r}}+\frac{\partial u^k}{\partial\bar{z}}\right)^2\right]\\
&\quad-\left[2\left(\frac{\partial u^{k-1}}{\partial\bar{r}}\right)^2+2\left(\frac{u^{k-1}}{\bar{r}}\right)^2+2\left(\frac{\partial v^{k-1}}{\partial\bar{z}}\right)^2+\left(\frac{\partial v^{k-1}}{\partial\bar{r}}+\frac{\partial u^{k-1}}{\partial\bar{z}}\right)^2\right]\Bigg\}\Bigg\}.
\end{aligned}
\tag{3.170}
$$

The temporal discretization of the species concentration Equation (3.155e) yields

$$
\begin{aligned}
&\frac{\phi^{k+1}-\phi^{k}}{\Delta\bar{t}}+\frac{1}{2}\left(3u^{k}\frac{\partial\phi^{k}}{\partial\bar{r}}-u^{k-1}\frac{\partial\phi^{k-1}}{\partial\bar{r}}\right)+\frac{1}{2}\left(3v^{k}\frac{\partial\phi^{k}}{\partial\bar{z}}-v^{k-1}\frac{\partial\phi^{k-1}}{\partial\bar{z}}\right)\\
&\qquad=\varepsilon_{\mathrm{p}}\frac{3}{2}\Bigg[\left[1-(\alpha_{\mathrm{m}})^{k}\right]\left(\phi^{k}-\left(\bar{C}_{\mathrm{d}}\right)^{k}\right)\left(\frac{\partial^{2}v^{k}}{\partial\bar{r}^{2}}+\frac{1}{\bar{r}}\frac{\partial v^{k}}{\partial\bar{r}}\right)\\
&\qquad+\left\{\left[1-(\alpha_{\mathrm{m}})^{k}\right]\left(\frac{\partial\phi^{k}}{\partial\bar{r}}-\left(\frac{d\bar{C}_{\mathrm{d}}}{d\Theta}\right)^{k}\frac{\partial\Theta^{k}}{\partial\bar{r}}\right)-\left(\phi^{k}-\left(\bar{C}_{\mathrm{d}}\right)^{k}\right)\frac{\partial\left(\alpha_{\mathrm{m}}\right)^{k}}{\partial\bar{r}}\right\}\frac{\partial v^{k}}{\partial\bar{r}}\Bigg]\\
&\qquad-\varepsilon_{\mathrm{p}}\frac{1}{2}\Bigg[\left(1-(\alpha_{\mathrm{m}})^{k-1}\right)\left(\phi^{k-1}-\left(\bar{C}_{\mathrm{d}}\right)^{k-1}\right)\left(\frac{\partial^{2}v^{k-1}}{\partial\bar{r}^{2}}+\frac{1}{\bar{r}}\frac{\partial v^{k-1}}{\partial\bar{r}}\right)\\
&\qquad+\left\{\left(1-(\alpha_{\mathrm{m}})^{k-1}\right)\left(\frac{\partial\phi^{k-1}}{\partial\bar{r}}-\left(\frac{d\bar{C}_{\mathrm{d}}}{d\Theta}\right)^{k-1}\frac{\partial\Theta^{k-1}}{\partial\bar{r}}\right)\right.\\
&\qquad\left.-\left(\phi^{k-1}-\left(\bar{C}_{\mathrm{d}}\right)^{k-1}\right)\frac{\partial\left(\alpha_{\mathrm{m}}\right)^{k-1}}{\partial\bar{r}}\right\}\frac{\partial v^{k-1}}{\partial\bar{r}}\Bigg]\\
&+\frac{1}{\mathrm{Re}\cdot\mathrm{Sc}}\frac{3}{2}\left[\left(\frac{d\bar{C}_{\mathrm{d}}}{d\Theta}\right)^{k}\left(\frac{\partial^{2}\Theta^{k}}{\partial\bar{r}^{2}}+\frac{1}{\bar{r}}\frac{\partial\Theta^{k}}{\partial\bar{r}}+\frac{\partial^{2}\Theta^{k}}{\partial\bar{z}^{2}}\right)+\left(\frac{d^{2}\bar{C}_{\mathrm{d}}}{d\Theta^{2}}\right)^{k}\left\{\left(\frac{\partial\Theta^{k}}{\partial\bar{r}}\right)^{2}+\left(\frac{\partial\Theta^{k}}{\partial\bar{z}}\right)^{2}\right\}\right]\\
&\qquad-\frac{1}{\mathrm{Re}\cdot\mathrm{Sc}}\frac{1}{2}\Bigg[\left(\frac{d\bar{C}_{\mathrm{d}}}{d\Theta}\right)^{k-1}\left(\frac{\partial^{2}\Theta^{k-1}}{\partial\bar{r}^{2}}+\frac{1}{\bar{r}}\frac{\partial\Theta^{k-1}}{\partial\bar{r}}+\frac{\partial^{2}\Theta^{k-1}}{\partial\bar{z}^{2}}\right)\\
&\qquad+\left(\frac{d^{2}\bar{C}_{\mathrm{d}}}{d\Theta^{2}}\right)^{k-1}\left\{\left(\frac{\partial\Theta^{k-1}}{\partial\bar{r}}\right)^{2}+\left(\frac{\partial\Theta^{k-1}}{\partial\bar{z}}\right)^{2}\right\}\Bigg]
\end{aligned}
\tag{3.171}
$$

Rearranging Equation (3.171) by writing the terms at time level $k+1$ on the left-hand side and the terms at time level k and $k-1$ on the right-hand side, yields the time discretized

species concentration equation as:

$$\begin{aligned}
\phi^{k+1} = \phi^k + \Delta\bar{t}\Bigg\{ &- \frac{1}{2}\left(3u^k\frac{\partial\phi^k}{\partial\bar{r}} - u^{k-1}\frac{\partial\phi^{k-1}}{\partial\bar{r}}\right) - \frac{1}{2}\left(3v^k\frac{\partial\phi^k}{\partial\bar{z}} - v^{k-1}\frac{\partial\phi^{k-1}}{\partial\bar{z}}\right) \\
&+\frac{3\varepsilon_\mathrm{p}}{2}\Bigg[\left[1-(\alpha_\mathrm{m})^k\right]\left(\phi^k - \left(\bar{C}_\mathrm{d}\right)^k\right)\left(\frac{\partial^2 v^k}{\partial\bar{r}^2} + \frac{1}{\bar{r}}\frac{\partial v^k}{\partial\bar{r}}\right) \\
&+\left\{\left[1-(\alpha_\mathrm{m})^k\right]\left(\frac{\partial\phi^k}{\partial\bar{r}} - \left(\frac{d\bar{C}_\mathrm{d}}{d\Theta}\right)^k\frac{\partial\Theta^k}{\partial\bar{r}}\right) - \left(\phi^k - \left(\bar{C}_\mathrm{d}\right)^k\right)\frac{\partial\left(\alpha_\mathrm{m}\right)^k}{\partial\bar{r}}\right\}\frac{\partial v^k}{\partial\bar{r}}\Bigg] \\
&-\frac{\varepsilon_\mathrm{p}}{2}\Bigg[\left(1-(\alpha_\mathrm{m})^{k-1}\right)\left(\phi^{k-1} - \left(\bar{C}_\mathrm{d}\right)^{k-1}\right)\left(\frac{\partial^2 v^{k-1}}{\partial\bar{r}^2} + \frac{1}{\bar{r}}\frac{\partial v^{k-1}}{\partial\bar{r}}\right) \\
&+\Bigg\{\left(1-(\alpha_\mathrm{m})^{k-1}\right)\left(\frac{\partial\phi^{k-1}}{\partial\bar{r}} - \left(\frac{d\bar{C}_\mathrm{d}}{d\Theta}\right)^{k-1}\frac{\partial\Theta^{k-1}}{\partial\bar{r}}\right) \\
&-\left(\phi^{k-1} - \left(\bar{C}_\mathrm{d}\right)^{k-1}\right)\frac{\partial\left(\alpha_\mathrm{m}\right)^{k-1}}{\partial\bar{r}}\Bigg\}\frac{\partial v^{k-1}}{\partial\bar{r}}\Bigg] \\
&+\frac{3}{2\mathrm{Re}\cdot\mathrm{Sc}}\Bigg[\left(\frac{d\bar{C}_\mathrm{d}}{d\Theta}\right)^k\left(\frac{\partial^2\Theta^k}{\partial\bar{r}^2} + \frac{1}{\bar{r}}\frac{\partial\Theta^k}{\partial\bar{r}} + \frac{\partial^2\Theta^k}{\partial\bar{z}^2}\right) + \left(\frac{d^2\bar{C}_\mathrm{d}}{d\Theta^2}\right)^k\left\{\left(\frac{\partial\Theta^k}{\partial\bar{r}}\right)^2 + \left(\frac{\partial\Theta^k}{\partial\bar{z}}\right)^2\right\}\Bigg] \\
&-\frac{1}{2\mathrm{Re}\cdot\mathrm{Sc}}\Bigg[\left(\frac{d\bar{C}_\mathrm{d}}{d\Theta}\right)^{k-1}\left(\frac{\partial^2\Theta^{k-1}}{\partial\bar{r}^2} + \frac{1}{\bar{r}}\frac{\partial\Theta^{k-1}}{\partial\bar{r}} + \frac{\partial^2\Theta^{k-1}}{\partial\bar{z}^2}\right) \\
&+\left(\frac{d^2\bar{C}_\mathrm{d}}{d\Theta^2}\right)^{k-1}\left\{\left(\frac{\partial\Theta^{k-1}}{\partial\bar{r}}\right)^2 + \left(\frac{\partial\Theta^{k-1}}{\partial\bar{z}}\right)^2\right\}\Bigg]\Bigg\}
\end{aligned} \tag{3.172}$$

The temporal discretization of the precipitation kinetics Equation (3.155f) yields

$$\begin{aligned}
&\frac{\left(\alpha_\mathrm{m}\right)^{k+1} - \left(\alpha_\mathrm{m}\right)^k}{\Delta\bar{t}} + \frac{1}{2}\left(3u^k\frac{\partial\left(\alpha_\mathrm{m}\right)^k}{\partial\bar{r}} - u^{k-1}\frac{\partial\left(\alpha_\mathrm{m}\right)^{k-1}}{\partial\bar{r}}\right) \\
&\qquad+\frac{1}{2}\left(3v^k\frac{\partial\left(\alpha_\mathrm{m}\right)^k}{\partial\bar{z}} - v^{k-1}\frac{\partial\left(\alpha_\mathrm{m}\right)^{k-1}}{\partial\bar{z}}\right) \\
&\qquad= \frac{1}{2}\left[3\left[1-(\alpha_\mathrm{m})^k\right]\left(\bar{K}_1\right)^k - \left(1-(\alpha_\mathrm{m})^{k-1}\right)\left(\bar{K}_1\right)^{k-1}\right] \\
&-\frac{\mathrm{Re}}{\lambda_2}\frac{1}{2}\left[3\left(\alpha_\mathrm{m}\right)^k\left(\frac{\partial v^k}{\partial\bar{r}}\right)^2\left(\bar{K}_2\right)^k - \left(\alpha_\mathrm{m}\right)^{k-1}\left(\frac{\partial v^{k-1}}{\partial\bar{r}}\right)^2\left(\bar{K}_2\right)^{k-1}\right].
\end{aligned} \tag{3.173}$$

Rearranging Equation (3.173) by writing the terms at time level $k+1$ on the left-hand side and the terms at time level k and $k-1$ on the right-hand side, yields the time discretized

precipitation kinetics equation as:

$$(\alpha_{\mathrm{m}})^{k+1} = (\alpha_{\mathrm{m}})^{k} + \Delta\bar{t}\Bigg\{\frac{1}{2}\left[3\left[1-(\alpha_{\mathrm{m}})^{k}\right]\left(\bar{K}_1\right)^{k} - \left(1-(\alpha_{\mathrm{m}})^{k-1}\right)\left(\bar{K}_1\right)^{k-1}\right]$$
$$-\frac{1}{2}\left(3u^{k}\frac{\partial\,(\alpha_{\mathrm{m}})^{k}}{\partial\bar{r}} - u^{k-1}\frac{\partial\,(\alpha_{\mathrm{m}})^{k-1}}{\partial\bar{r}}\right) - \frac{1}{2}\left(3v^{k}\frac{\partial\,(\alpha_{\mathrm{m}})^{k}}{\partial\bar{z}} - v^{k-1}\frac{\partial\,(\alpha_{\mathrm{m}})^{k-1}}{\partial\bar{z}}\right)$$
$$-\frac{\mathrm{Re}}{2\lambda_2}\left[3\,(\alpha_{\mathrm{m}})^{k}\left(\frac{\partial v^{k}}{\partial\bar{r}}\right)^{2}\left(\bar{K}_2\right)^{k} - (\alpha_{\mathrm{m}})^{k-1}\left(\frac{\partial v^{k-1}}{\partial\bar{r}}\right)^{2}\left(\bar{K}_2\right)^{k-1}\right]\Bigg\} \tag{3.174}$$

The temporal discretization of the oil volume fraction Equation (3.155g) yields

$$\frac{(\phi_{\mathrm{oil}})^{k+1} - (\phi_{\mathrm{oil}})^{k}}{\Delta\bar{t}} + \frac{1}{2}\left(3u^{k}\frac{\partial(\phi_{\mathrm{oil}})^{k}}{\partial\bar{r}} - u^{k-1}\frac{\partial(\phi_{\mathrm{oil}})^{k-1}}{\partial\bar{r}}\right)$$
$$+\frac{1}{2}\left(3v^{k}\frac{\partial(\phi_{\mathrm{oil}})^{k}}{\partial\bar{z}} - v^{k-1}\frac{\partial(\phi_{\mathrm{oil}})^{k-1}}{\partial\bar{z}}\right) = 0. \tag{3.175}$$

Rearranging Equation (3.175) by writing the terms at time level $k+1$ on the left-hand side and the terms at time level k and $k-1$ on the right-hand side, yields the time discretized oil volume fraction equation as:

$$(\phi_{\mathrm{oil}})^{k+1} = (\phi_{\mathrm{oil}})^{k} + \Delta\bar{t}\Bigg\{-\frac{1}{2}\left(3u^{k}\frac{\partial(\phi_{\mathrm{oil}})^{k}}{\partial\bar{r}} - u^{k-1}\frac{\partial(\phi_{\mathrm{oil}})^{k-1}}{\partial\bar{r}}\right)$$
$$-\frac{1}{2}\left(3v^{k}\frac{\partial(\phi_{\mathrm{oil}})^{k}}{\partial\bar{z}} - v^{k-1}\frac{\partial(\phi_{\mathrm{oil}})^{k-1}}{\partial\bar{z}}\right)\Bigg\}. \tag{3.176}$$

The temporal discretization of the deposit growth rate Equation (3.155h) yields

$$\frac{\bar{\delta}^{k+1} - \bar{\delta}^{k}}{\Delta\bar{t}} = \frac{3}{2}\phi_1\frac{\left(1-f(x^{k})\right)}{x^{k}}\left(\frac{1}{\mathrm{Re}\cdot\mathrm{Sc}}\left(\frac{d\bar{C}_{\mathrm{d}}}{d\Theta}\right)^{k}\frac{\partial\Theta^{k}}{\partial\bar{r}}\bigg|_{\bar{r}=\bar{R}_{\mathrm{eff}}}\right)$$
$$-\frac{1}{2}\phi_1\frac{\left(1-f(x^{k-1})\right)}{x^{k-1}}\left(\frac{1}{\mathrm{Re}\cdot\mathrm{Sc}}\left(\frac{d\bar{C}_{\mathrm{d}}}{d\Theta}\right)^{k-1}\frac{\partial\Theta^{k-1}}{\partial\bar{r}}\bigg|_{\bar{r}=\bar{R}_{\mathrm{eff}}}\right) \tag{3.177}$$

Rearranging Equation (3.177) by writing the terms at time level $k+1$ on the left-hand side and the terms at time level k and $k-1$ on the right-hand side, yields the time discretized deposit growth rate equation as:

$$\bar{\delta}^{k+1} = \bar{\delta}^{k} + \Delta\bar{t}\Bigg\{-\frac{\phi_1}{2\mathrm{Re}\cdot\mathrm{Sc}}\Bigg[3\frac{\left[1-f(x^{k})\right]}{x^{k}}\left(\left(\frac{d\bar{C}_{\mathrm{d}}}{d\Theta}\right)^{k}\frac{\partial\Theta^{k}}{\partial\bar{r}}\bigg|_{\bar{r}=\bar{R}_{\mathrm{eff}}}\right)$$
$$-\frac{\left[1-f(x^{k-1})\right]}{x^{k-1}}\left(\left(\frac{d\bar{C}_{\mathrm{d}}}{d\Theta}\right)^{k-1}\frac{\partial\Theta^{k-1}}{\partial\bar{r}}\bigg|_{\bar{r}=\bar{R}_{\mathrm{eff}}}\right)\Bigg]\Bigg\} \tag{3.178}$$

The temporal discretization of the deposit aging rate Equation (3.155i) yields

$$\begin{aligned}\frac{x^{k+1}-x^k}{\Delta\bar{t}} = \frac{3}{2}\phi_1 f(x^k)\frac{2\left(1-\bar{\delta}^k\right)}{\bar{\delta}^k\left(2-\bar{\delta}^k\right)}\Bigg[\frac{1}{\mathrm{Re}\cdot\mathrm{Sc}}\left(\frac{d\bar{C}_\mathrm{d}}{d\Theta}\right)^k\frac{\partial\Theta^k}{\partial\bar{r}} \\ +\varepsilon_\mathrm{p}\left[1-(\alpha_\mathrm{m})^k\right]\left(\phi^k-\left(\bar{C}_\mathrm{d}\right)^k\right)\frac{\partial v^k}{\partial\bar{r}}\Bigg]_{\bar{r}=\bar{R}_\mathrm{eff}} \\ -\frac{1}{2}\phi_1 f(x^{k-1})\frac{2\left(1-\bar{\delta}^{k-1}\right)}{\bar{\delta}^{k-1}\left(2-\bar{\delta}^{k-1}\right)}\Bigg[\frac{1}{\mathrm{Re}\cdot\mathrm{Sc}}\left(\frac{d\bar{C}_\mathrm{d}}{d\Theta}\right)^{k-1}\frac{\partial\Theta^{k-1}}{\partial\bar{r}} \\ +\varepsilon_\mathrm{p}\left(1-(\alpha_\mathrm{m})^{k-1}\right)\left(\phi^{k-1}-\left(\bar{C}_\mathrm{d}\right)^{k-1}\right)\frac{\partial v^{k-1}}{\partial\bar{r}}\Bigg]_{\bar{r}=\bar{R}_\mathrm{eff}}.\end{aligned} \tag{3.179}$$

Rearranging Equation (3.179) by writing the terms at time level $k+1$ on the left-hand side and the terms at time level k and $k-1$ on the right-hand side, yields the time discretized deposit aging rate equation as:

$$\begin{aligned}x^{k+1} = x^k + \Delta\bar{t}\Bigg\{\frac{3}{2}\phi_1 f(x^k)\frac{2\left(1-\bar{\delta}^k\right)}{\bar{\delta}^k\left(2-\bar{\delta}^k\right)}\Bigg[\frac{1}{\mathrm{Re}\cdot\mathrm{Sc}}\left(\frac{d\bar{C}_\mathrm{d}}{d\Theta}\right)^k\frac{\partial\Theta^k}{\partial\bar{r}} \\ +\varepsilon_\mathrm{p}\left[1-(\alpha_\mathrm{m})^k\right]\left(\phi^k-\left(\bar{C}_\mathrm{d}\right)^k\right)\frac{\partial v^k}{\partial\bar{r}}\Bigg]_{\bar{r}=\bar{R}_\mathrm{eff}} \\ -\frac{1}{2}\phi_1 f(x^{k-1})\frac{2\left(1-\bar{\delta}^{k-1}\right)}{\bar{\delta}^{k-1}\left(2-\bar{\delta}^{k-1}\right)}\Bigg[\frac{1}{\mathrm{Re}\cdot\mathrm{Sc}}\left(\frac{d\bar{C}_\mathrm{d}}{d\Theta}\right)^{k-1}\frac{\partial\Theta^{k-1}}{\partial\bar{r}} \\ +\varepsilon_\mathrm{p}\left(1-(\alpha_\mathrm{m})^{k-1}\right)\left(\phi^{k-1}-\left(\bar{C}_\mathrm{d}\right)^{k-1}\right)\frac{\partial v^{k-1}}{\partial\bar{r}}\Bigg]_{\bar{r}=\bar{R}_\mathrm{eff}}\Bigg\}\end{aligned} \tag{3.180}$$

The functions $f(x^{k-1})$ and $f(x^k)$ are deduced from Equation (5.9) and are given as:

$$f(x^{k-1}) = \frac{1-x^{k-1}}{\alpha_\mathrm{avg}^2(x^{k-1})^2 - x^{k-1}+1} \quad \text{and} \quad f(x^k) = \frac{1-x^k}{\alpha_\mathrm{avg}^2(x^k)^2 - x^k+1} \tag{3.181}$$

The temporal discretization of the boundary conditions (3.158a)−(3.158d) yields

$$\begin{gathered}u_{\bar{r}}^{k+1}(0,\bar{z})=0,\ v_{\bar{r}}^{k+1}(0,\bar{z})=0,\ \Theta_{\bar{r}}^{k+1}(0,\bar{z})=0,\ \phi_{\bar{r}}^{k+1}(0,\bar{z})=0, \\ {\alpha_\mathrm{m}}_{\bar{r}}^{k+1}(0,\bar{z})=0,\ {\phi_\mathrm{oil}}_{\bar{r}}^{k+1}(0,\bar{z})=0.\end{gathered} \tag{3.182a}$$

$$\begin{gathered}u^{k+1}(\lambda,\bar{z})=0,\ v^{k+1}(\lambda,\bar{z})=0,\ \Theta^{k+1}(\lambda,\bar{z})=\beta_0,\ \phi^{k+1}(\lambda,\bar{z})=\beta_1, \\ (\alpha_\mathrm{m})^{k+1}(\lambda,\bar{z})=1,\ (\phi_\mathrm{oil})^{k+1}(\lambda,\bar{z})=0.\end{gathered} \tag{3.182b}$$

$$u^{k+1}(\bar{r},0)=0,\ v^{k+1}(\bar{r},0)=1,\ \Theta^{k+1}(\bar{r},0)=1,\ \phi^{k+1}(\bar{r},0)=0,\\ (\alpha_{\mathrm{m}})^{k+1}(\bar{r},0)=0,\ (\phi_{\mathrm{oil}})^{k+1}(\bar{r},0)=1-\phi_{\mathrm{water}}. \tag{3.182c}$$

$$u_{\bar{z}}^{k+1}(\bar{r},\infty)=0,\ v_{\bar{z}}^{k+1}(\bar{r},\infty)=0,\ \Theta_{\bar{z}}^{k+1}(\bar{r},\infty)=0,\ \phi_{\bar{z}}^{k+1}(\bar{r},\infty)=0,\\ \alpha_{\mathrm{m}\bar{z}}^{k+1}(\bar{r},\infty)=0,\ \phi_{\mathrm{oil}\bar{z}}^{k+1}(\bar{r},\infty)=0. \tag{3.182d}$$

where the subscripts $\bar{r}$ and $\bar{z}$ denote derivatives with respect to $\bar{r}$ and $\bar{z}$, respectively. Similarly, the temporal discretization of the initial conditions (3.159) yields

$$u^0(\bar{r},\bar{z})=0,\ v^0(\bar{r},\bar{z})=1,\ P^0(\bar{r},\bar{z})=1,\ \Theta^0(\bar{r},\bar{z})=1,\ \phi^0(\bar{r},\bar{z})=0\\ \alpha_{\mathrm{m}}^0(\bar{r},\bar{z})=0,\ \phi_{\mathrm{oil}}^0(\bar{r},\bar{z})=1-\phi_{\mathrm{water}},\ \bar{\delta}^0=0,\ x^0=0 \tag{3.183}$$

3.11.1.2 Discretization of the Pressure Poisson Equation

Once the functions $u^{k+1}, v^{k+1}, (\phi_{\mathrm{oil}})^{k+1}, \Theta^{k+1}$ and ϕ^{k+1} have been determined, the pressure Poisson Equation (3.155c) is then solved using the following time discretized PPE:

$$\begin{aligned}\frac{\partial^2 P^{k+1}}{\partial\bar{r}^2}+\frac{1}{\bar{r}}\frac{\partial P^{k+1}}{\partial\bar{r}}+\frac{\partial^2 P^{k+1}}{\partial\bar{z}^2}&=-\frac{2}{\bar{r}^2}(u^{k+1})^2-2\frac{\partial u^{k+1}}{\partial\bar{z}}\frac{\partial v^{k+1}}{\partial\bar{r}}\\ &+\frac{\lambda_1}{\mathrm{We}}(R\bar{K})^{k+1}\left(\frac{\partial^2(\phi_{\mathrm{oil}})^{k+1}}{\partial\bar{r}^2}+\frac{1}{\bar{r}}\frac{\partial(\phi_{\mathrm{oil}})^{k+1}}{\partial\bar{r}}+\frac{\partial^2(\phi_{\mathrm{oil}})^{k+1}}{\partial\bar{z}^2}\right)\\ &+\frac{\lambda_1}{\mathrm{We}}\left(\frac{\partial(R\bar{K})^{k+1}}{\partial\bar{r}}\frac{\partial(\phi_{\mathrm{oil}})^{k+1}}{\partial\bar{r}}+\frac{\partial(R\bar{K})^{k+1}}{\partial\bar{z}}\frac{\partial(\phi_{\mathrm{oil}})^{k+1}}{\partial\bar{z}}\right)\\ &+\lambda_3\frac{\mathrm{Gr_T}}{\mathrm{Re}^2}\left[\cos(\varphi)\left(\frac{\partial\Theta^{k+1}}{\partial\bar{r}}+\frac{1}{\bar{r}}\Theta^{k+1}\right)+\sin(\varphi)\frac{\partial\Theta^{k+1}}{\partial\bar{z}}\right]\\ &+\lambda_4\frac{\mathrm{Gr_C}}{\mathrm{Re}^2}\left[\cos(\varphi)\left(\frac{\partial\phi^{k+1}}{\partial\bar{r}}+\frac{1}{\bar{r}}\phi^{k+1}\right)+\sin(\varphi)\frac{\partial\phi^{k+1}}{\partial\bar{z}}\right]\end{aligned} \tag{3.184}$$

subject to the following boundary condition

$$\begin{aligned}P_{\bar{z}}^{k+1}(1,\bar{z})&=\frac{\lambda_2}{\mathrm{Re}}\left[v_{\bar{r}\bar{r}}^{k+1}(1,\bar{z})+v_{\bar{r}}^{k+1}(1,\bar{z})\right]-\frac{\lambda_2}{(\mathrm{Re}\cdot\mathrm{Da})}v^{k+1}(1,\bar{z})\\ &+\lambda_3\frac{\mathrm{Gr_T}}{\mathrm{Re}^2}\sin(\varphi)\Theta^{k+1}(1,\bar{z})+\lambda_4\frac{\mathrm{Gr_C}}{\mathrm{Re}^2}\sin(\varphi)\phi^{k+1}(1,\bar{z})+\frac{\lambda_1}{\mathrm{We}}(R\bar{K})^{k+1}(1,\bar{z})\phi_{\mathrm{oil}\bar{z}}^{k+1}(1,\bar{z})\end{aligned} \tag{3.185}$$

where the subscript $\bar{z}$ denotes derivative with respect to $\bar{z}$.

3.11.1.3 Forward Euler Schemes

The intermediate functions $u^k, v^k, P^k, \Theta^k, \phi^k, (\alpha_{\mathrm{m}})^k, (\phi_{\mathrm{oil}})^k, \bar{\delta}^k$ and x^k in the above temporal schemes are calculated using the forward Euler formula as follows. The Euler's forward scheme for the function u^k is given as:

$$u^k = u^{k-1} + \Delta\bar{t}\left(\frac{\partial u}{\partial \bar{t}}\right)^{k-1} \tag{3.186}$$

Evaluating the $r-$momentum Equation (3.155a) at time level $k-1$, making $\dfrac{\partial u^{k-1}}{\partial \bar{t}}$ the subject and substituting the result on the right-hand side into Equation (3.186) yields

$$\begin{aligned} u^k = u^{k-1} + \Delta\bar{t}\Bigg\{ & -u^{k-1}\frac{\partial u^{k-1}}{\partial \bar{r}} - v^{k-1}\frac{\partial u^{k-1}}{\partial \bar{z}} - \frac{\partial P^{k-1}}{\partial \bar{r}} - \frac{\lambda_2}{(\mathrm{Re}\cdot\mathrm{Da})}u^{k-1} \\ & + \frac{\lambda_2}{\mathrm{Re}}\left(2\frac{\partial^2 u^{k-1}}{\partial \bar{r}^2} + \frac{\partial^2 u^{k-1}}{\partial \bar{z}^2} + \frac{\partial^2 v^{k-1}}{\partial \bar{r}\partial \bar{z}} + \frac{2}{\bar{r}}\frac{\partial u^{k-1}}{\partial \bar{r}} - \frac{2}{\bar{r}^2}u^{k-1}\right) \\ & + \lambda_3\frac{\mathrm{Gr_T}}{\mathrm{Re}^2}\cos(\varphi)\Theta^{k-1} + \lambda_4\frac{\mathrm{Gr_C}}{\mathrm{Re}^2}\cos(\varphi)\phi^{k-1} + \frac{\lambda_1}{\mathrm{We}}(R\bar{K})^{k-1}\frac{\partial(\phi_{\mathrm{oil}})^{k-1}}{\partial \bar{r}}\Bigg\} \end{aligned} \tag{3.187}$$

Similarly, the Euler's forward scheme for the function v^k is given as:

$$v^k = v^{k-1} + \Delta\bar{t}\left(\frac{\partial v}{\partial \bar{t}}\right)^{k-1} \tag{3.188}$$

Evaluating the $z-$momentum Equation (3.155b) at time level $k-1$, making $\dfrac{\partial v^{k-1}}{\partial \bar{t}}$ the subject and substituting the result on the right-hand side into Equation (3.188) yields

$$\begin{aligned} v^k = v^{k-1} + \Delta\bar{t}\Bigg\{ & -u^{k-1}\frac{\partial v^{k-1}}{\partial \bar{r}} - v^{k-1}\frac{\partial v^{k-1}}{\partial \bar{z}} - \frac{\partial P^{k-1}}{\partial \bar{z}} - \frac{\lambda_2}{(\mathrm{Re}\cdot\mathrm{Da})}v^{k-1} \\ & + \frac{\lambda_2}{\mathrm{Re}}\left(\frac{\partial^2 v^{k-1}}{\partial \bar{r}^2} + 2\frac{\partial^2 v^{k-1}}{\partial \bar{z}^2} + \frac{\partial^2 u^{k-1}}{\partial \bar{r}\partial \bar{z}} + \frac{1}{\bar{r}}\frac{\partial u^{k-1}}{\partial \bar{z}} + \frac{1}{\bar{r}}\frac{\partial v^{k-1}}{\partial \bar{r}}\right) \\ & + \lambda_3\frac{\mathrm{Gr_T}}{\mathrm{Re}^2}\sin(\varphi)\Theta^{k-1} + \lambda_4\frac{\mathrm{Gr_C}}{\mathrm{Re}^2}\sin(\varphi)\phi^{k-1} + \frac{\lambda_1}{\mathrm{We}}(R\bar{K})^{k-1}\frac{\partial(\phi_{\mathrm{oil}})^{k-1}}{\partial \bar{z}}\Bigg\} \end{aligned} \tag{3.189}$$

The Euler's forward scheme for the function Θ^k is given as:

$$\Theta^k = \Theta^{k-1} + \Delta\bar{t}\left(\frac{\partial \Theta}{\partial \bar{t}}\right)^{k-1} \tag{3.190}$$

Evaluating the energy Equation (3.155d) at time level $k-1$, making $\dfrac{\partial \Theta^{k-1}}{\partial \bar{t}}$ the subject and substituting the result on the right-hand side into Equation (3.190) yields

$$\begin{aligned}\Theta^{k} = \Theta^{k-1} + \Delta\bar{t}\Bigg\{ & - u^{k-1}\frac{\partial \Theta^{k-1}}{\partial \bar{r}} - v^{k-1}\frac{\partial \Theta^{k-1}}{\partial \bar{z}} \\ & + \frac{\lambda_5}{\mathrm{Pe}}\left(\frac{\partial^2 \Theta^{k-1}}{\partial \bar{r}^2} + \frac{1}{\bar{r}}\frac{\partial \Theta^{k-1}}{\partial \bar{r}} + \frac{\partial^2 \Theta^{k-1}}{\partial \bar{z}^2}\right) - \mathrm{St}\frac{\lambda_6}{\bar{d}}\Theta^{k-1} \\ & + \lambda_7\frac{\mathrm{Ec}}{\mathrm{Re}}\left[2\left(\frac{\partial u^{k-1}}{\partial \bar{r}}\right)^2 + 2\left(\frac{u^{k-1}}{\bar{r}}\right)^2 + 2\left(\frac{\partial v^{k-1}}{\partial \bar{z}}\right)^2 + \left(\frac{\partial v^{k-1}}{\partial \bar{r}} + \frac{\partial u^{k-1}}{\partial \bar{z}}\right)^2\right]\Bigg\}\end{aligned} \tag{3.191}$$

The Euler's forward scheme for the function ϕ^k is given as:

$$\phi^{k} = \phi^{k-1} + \Delta\bar{t}\left(\frac{\partial \phi}{\partial \bar{t}}\right)^{k-1} \tag{3.192}$$

Evaluating the species concentration Equation (3.155e) at time level $k-1$, making $\dfrac{\partial \phi^{k-1}}{\partial \bar{t}}$ the subject and substituting the result on the right-hand side into Equation (3.192) yields

$$\begin{aligned}\phi^{k} = \phi^{k-1} + \Delta\bar{t}\Bigg\{ & - u^{k-1}\frac{\partial \phi^{k-1}}{\partial \bar{r}} - v^{k-1}\frac{\partial \phi^{k-1}}{\partial \bar{z}} \\ & + \varepsilon_{\mathrm{p}}\Bigg[\left[1-(\alpha_{\mathrm{m}})^{k-1}\right]\left[\phi^{k-1} - (\bar{C}_{\mathrm{d}})^{k-1}\right]\left(\frac{\partial^2 v^{k-1}}{\partial \bar{r}^2} + \frac{1}{\bar{r}}\frac{\partial v^{k-1}}{\partial \bar{r}}\right) \\ & + \Bigg\{\left[1-(\alpha_{\mathrm{m}})^{k-1}\right]\left(\frac{\partial \phi^{k-1}}{\partial \bar{r}} - \left(\frac{d\bar{C}_{\mathrm{d}}}{d\Theta}\right)^{k-1}\frac{\partial \Theta^{k-1}}{\partial \bar{r}}\right) \\ & - \left(\phi^{k-1} - (\bar{C}_{\mathrm{d}})^{k-1}\right)\frac{\partial\left(\alpha_{\mathrm{m}}\right)^{k-1}}{\partial \bar{r}}\Bigg\}\frac{\partial v^{k-1}}{\partial \bar{r}}\Bigg] \\ & + \frac{1}{\mathrm{Re}\cdot\mathrm{Sc}}\Bigg[\left(\frac{d\bar{C}_{\mathrm{d}}}{d\Theta}\right)^{k-1}\left(\frac{\partial^2 \Theta^{k-1}}{\partial \bar{r}^2} + \frac{1}{\bar{r}}\frac{\partial \Theta^{k-1}}{\partial \bar{r}} + \frac{\partial^2 \Theta^{k-1}}{\partial \bar{z}^2}\right) \\ & + \left(\frac{d^2\bar{C}_{\mathrm{d}}}{d\Theta^2}\right)^{k-1}\left\{\left(\frac{\partial \Theta^{k-1}}{\partial \bar{r}}\right)^2 + \left(\frac{\partial \Theta^{k-1}}{\partial \bar{z}}\right)^2\right\}\Bigg]\Bigg\}\end{aligned} \tag{3.193}$$

The Euler's forward scheme for the function ϕ^k is given as:

$$\left(\alpha_{\mathrm{m}}\right)^{k} = \left(\alpha_{\mathrm{m}}\right)^{k-1} + \Delta\bar{t}\left(\frac{\partial \alpha_{\mathrm{m}}}{\partial \bar{t}}\right)^{k-1} \tag{3.194}$$

Evaluating the precipitation kinetics Equation (3.155f) at time level $k-1$, making $\dfrac{\partial(\alpha_{\mathrm{m}})^{k-1}}{\partial \bar{t}}$ the subject and substituting the result on the right-hand side into Equation

(3.194) yields

$$(\alpha_{\mathrm{m}})^{k} = (\alpha_{\mathrm{m}})^{k-1} + \Delta\bar{t}\Bigg\{ - u^{k-1}\frac{\partial\,(\alpha_{\mathrm{m}})^{k-1}}{\partial\bar{r}} - v^{k-1}\frac{\partial\,(\alpha_{\mathrm{m}})^{k-1}}{\partial\bar{z}} + \Big[1-(\alpha_{\mathrm{m}})^{k-1}\Big](\bar{K}_1)^{k-1} - \frac{\mathrm{Re}}{\lambda_2}(\alpha_{\mathrm{m}})^{k-1}\left(\frac{\partial v^{k-1}}{\partial\bar{r}}\right)^{2}(\bar{K}_2)^{k-1}\Bigg\} \tag{3.195}$$

The Euler's forward scheme for the function $(\phi_{\mathrm{oil}})^{k}$ is given as:

$$(\phi_{\mathrm{oil}})^{k} = (\phi_{\mathrm{oil}})^{k-1} + \Delta\bar{t}\left(\frac{\partial\phi_{\mathrm{oil}}}{\partial\bar{t}}\right)^{k-1} \tag{3.196}$$

Evaluating the oil volume fraction Equation (3.155g) at time level $k-1$, making $\dfrac{\partial(\phi_{\mathrm{oil}})^{k-1}}{\partial\bar{t}}$ the subject and substituting the result on the right-hand side into Equation (3.196) yields

$$(\phi_{\mathrm{oil}})^{k} = (\phi_{\mathrm{oil}})^{k-1} + \Delta\bar{t}\Bigg\{ - u^{k-1}\frac{\partial\,(\phi_{\mathrm{oil}})^{k-1}}{\partial\bar{r}} - v^{k-1}\frac{\partial\,(\phi_{\mathrm{oil}})^{k-1}}{\partial\bar{z}}\Bigg\} \tag{3.197}$$

The Euler's forward scheme for the function $\bar{\delta}^{k}$ is given as:

$$\bar{\delta}^{k} = \bar{\delta}^{k-1} + \Delta\bar{t}\left(\frac{d\bar{\delta}}{d\bar{t}}\right)^{k-1} \tag{3.198}$$

Evaluating the deposit growth rate Equation (3.155h) at time level $k-1$, making $\dfrac{d\bar{\delta}^{k-1}}{d\bar{t}}$ the subject and substituting the result on the right-hand side into Equation (3.198) yields

$$\bar{\delta}^{k} = \bar{\delta}^{k-1} + \Delta\bar{t}\Bigg\{\phi_1\frac{\Big(1-f(x^{k-1})\Big)}{x^{k-1}}\left(\frac{1}{\mathrm{Re}\cdot\mathrm{Sc}}\left(\frac{d\bar{C}_{\mathrm{d}}}{d\Theta}\right)^{k-1}\frac{\partial\Theta^{k-1}}{\partial\bar{r}}\Big|_{\bar{r}=\bar{R}_{\mathrm{eff}}}\right)\Bigg\} \tag{3.199}$$

The Euler's forward scheme for the function $\bar{\delta}^{k}$ is given as:

$$x^{k} = x^{k-1} + \Delta\bar{t}\left(\frac{dx}{d\bar{t}}\right)^{k-1} \tag{3.200}$$

Evaluating the deposit aging rate Equation (3.155i) at time level $k-1$, making $\dfrac{dx^{k-1}}{d\bar{t}}$ the subject and substituting the result on the right-hand side into Equation (3.200) yields

$$x^{k} = x^{k-1} + \Delta\bar{t}\Bigg\{\phi_1 f(x^{k-1})\frac{2\left(1-\bar{\delta}^{k-1}\right)}{\bar{\delta}^{k-1}\left(2-\bar{\delta}^{k-1}\right)}\Bigg[\frac{1}{\mathrm{Re}\cdot\mathrm{Sc}}\left(\frac{d\bar{C}_{\mathrm{d}}}{d\Theta}\right)^{k-1}\frac{\partial\Theta^{k-1}}{\partial\bar{r}} + \varepsilon_{\mathrm{p}}\left(1-(\alpha_{\mathrm{m}})^{k-1}\right)\left(\phi^{k-1}-(\bar{C}_{\mathrm{d}})^{k-1}\right)\frac{\partial v^{k-1}}{\partial\bar{r}}\Bigg]_{\bar{r}=\bar{R}_{\mathrm{eff}}}\Bigg\} \tag{3.201}$$

The iterative system of linear PDEs (3.166), (3.168), (3.184), (3.170), (3.172), (3.174), (3.176) and the corresponding boundary conditions (3.231a)−(3.182d) and the initial conditions (3.231d) are discretized in space by the bivariate Chebyshev spectral collocation method, presented in Subsection 3.11.2.

3.11.2 Spatial Discretization Using Chebyshev Spectral Collocation Method

The spectral collocation method is characterized by the fact that the numerical solution is forced to satisfy the governing equations exactly at the collocation points. The bivariate Chebyshev spectral collocation method is valid in the domain $[-1,1]$ in both $\bar{r}$ and $\bar{z}$. Therefore, the physical domain on which the system of governing equations are defined should be transformed from $[a,b]\times[\alpha,\beta]$ to $[-1,1]\times[-1,1]$. In particular, the domain $\bar{r}\in[a,b]$ is transformed to the new domain $\hat{r}\in[-1,1]$ using the following linear transformation.

$$\bar{r}=\frac{1}{2}(b-a)\,\hat{r}+\frac{1}{2}(b+a) \tag{3.202}$$

Similarly, the domain $\bar{z}\in[\alpha,\beta]$ is transformed to the new domain $\hat{z}\in[-1,1]$ using the following linear transformation.

$$\bar{z}=\frac{1}{2}(\beta-\alpha)\,\hat{z}+\frac{1}{2}(\beta+\alpha)\,. \tag{3.203}$$

Here, $a=0, b=\lambda, \alpha=0$ and $\beta=L_\infty$, where L_∞ is a finite number chosen to be large enough to approximate the asymptotic behaviour at infinity. The transformations (3.202) and (3.203) will be implemented in the FDM schemes when evaluating the derivatives at the collocation points $(\bar{r}_i,\bar{z}_j)$, using the chain rule of differentiation. A detailed presentation of the bivariate spectral collocation method can be found in Motsa *et al.* (2014), Magagula *et al.* (2016), Samuel & Motsa (2019), Goqo *et al.* (2019), Magagula *et al.* (2020), and Ibrahim (2020).

The iterative system of linear PDEs (3.166), (3.168), (3.184), (3.170), (3.172), (3.174), (3.176) and the corresponding boundary conditions (3.231a)−(3.182d) and the initial conditions (3.231d) is discretised in space using the Chebyshev spectral collocation method in both the $\bar{r}$ and $\bar{z}$ direction, with Lagrange fundamentals (or Lagrange coefficients) chosen as the basis functions. The unknown solutions $u(\bar{r},\bar{z},\bar{t}_{k+1})$, $v(\bar{r},\bar{z},\bar{t}_{k+1})$, $\Theta(\bar{r},\bar{z},\bar{t}_{k+1})$, $\phi(\bar{r},\bar{z},\bar{t}_{k+1})$, $\alpha_{\text{m}}(\bar{r},\bar{z},\bar{t}_{k+1})$, and $\phi_{\text{oil}}(\bar{r},\bar{z},\bar{t}_{k+1})$, which are functions of the space variables $\bar{r}$ and $\bar{z}$ only, are respectively approximated by the

bivariate Lagrange interpolating polynomial of the forms:

$$u(\bar{r},\bar{z},\bar{t}_{k+1}) \approx \sum_{m=0}^{M}\sum_{n=0}^{N} u(\hat{r}_m,\hat{z}_n,\bar{t}_{k+1})L_m(\hat{r})L_n(\hat{z}) \tag{3.204a}$$

$$v(\bar{r},\bar{z},\bar{t}_{k+1}) \approx \sum_{m=0}^{M}\sum_{n=0}^{N} v(\hat{r}_m,\hat{z}_n,\bar{t}_{k+1})L_m(\hat{r})L_n(\hat{z}) \tag{3.204b}$$

$$\Theta(\bar{r},\bar{z},\bar{t}_{k+1}) \approx \sum_{m=0}^{M}\sum_{n=0}^{N} \Theta(\hat{r}_m,\hat{z}_n,\bar{t}_{k+1})L_m(\hat{r})L_n(\hat{z}) \tag{3.204c}$$

$$\phi(\bar{r},\bar{z},\bar{t}_{k+1}) \approx \sum_{m=0}^{M}\sum_{n=0}^{N} \phi(\hat{r}_m,\hat{z}_n,\bar{t}_{k+1})L_m(\hat{r})L_n(\hat{z}) \tag{3.204d}$$

$$\alpha_{\mathrm{m}}(\bar{r},\bar{z},\bar{t}_{k+1}) \approx \sum_{m=0}^{M}\sum_{n=0}^{N} \alpha_{\mathrm{m}}(\hat{r}_m,\hat{z}_n,\bar{t}_{k+1})L_m(\hat{r})L_n(\hat{z}) \tag{3.204e}$$

$$\phi_{\mathrm{oil}}(\bar{r},\bar{z},\bar{t}_{k+1}) \approx \sum_{m=0}^{M}\sum_{n=0}^{N} \phi_{\mathrm{oil}}(\hat{r}_m,\hat{z}_n,\bar{t}_{k+1})L_m(\hat{r})L_n(\hat{z}) \tag{3.204f}$$

where the functions $L_m(\hat{r})$ are the Lagrange cardinal polynomials defined by

$$L_m(\hat{r}) = \prod_{\substack{i=0\\ i\neq m}}^{M} \frac{(\hat{r}-\hat{r}_i)}{(\hat{r}_m-\hat{r}_i)}, \text{ with } L_m(\hat{r}_i)=\delta_{mi}=\begin{cases}1, & \text{if } i=m\\ 0, & \text{if } i\neq m\end{cases} \tag{3.205}$$

Similarly, the functions $L_n(\hat{z})$ are defined by

$$L_n(\hat{z}) = \prod_{\substack{j=0\\ j\neq n}}^{N} \frac{(\hat{z}-\hat{z}_j)}{(\hat{z}_n-\hat{z}_j)}, \text{ with } L_n(\hat{z}_j)=\delta_{nj}=\begin{cases}1, & \text{if } j=n\\ 0, & \text{if } j\neq n\end{cases} \tag{3.206}$$

In particular, the assumed solution (3.204a) interpolates the function $u(\bar{r},\bar{z},\bar{t}_{k+1})$ at the symmetrically distributed Chebyshev-Gauss-Lobatto grid points $(\hat{r}_i,\hat{z}_j)$ defined on the domain $[-1,1]\times[-1,1]$ by:

$$\hat{r}_i=\cos\left(\frac{\pi i}{M}\right) \text{ and } \hat{z}_j=\cos\left(\frac{\pi j}{N}\right);\ i=0,1,\cdots,M;\ j=0,1,\cdots,N, \tag{3.207}$$

where M and N denotes the number of collocation (or grid) points in $\bar{r}$ and $\bar{z}$ direction,

respectively. The Chebyshev-Gauss-Lobatto grid points are indexed from right to left of the domains in $\bar{r}$ and $\bar{z}$ since $\hat{r}_M = -1$, $\hat{r}_0 = 1$, $\hat{z}_N = -1$, and $\hat{z}_0 = 1$. Hence, it is taken that $\bar{r}_0 = b, \bar{r}_1, \bar{r}_2, \cdots, \bar{r}_M = a$ and $\bar{z}_0 = \beta, \bar{z}_1, \bar{z}_2, \cdots, \bar{z}_N = \alpha$ as the computational grids.

The choice of the Chebyshev-Gauss-Lobatto grid points (3.207) makes it possible to convert the continuous spatial derivatives, in both $\bar{r}$ and $\bar{z}$, to discrete matrix form at the collocation points. For example, the first partial derivative of $u(\bar{r}, \bar{z}, \bar{t}_{k+1})$ with respect to $\bar{r}$ is approximated at the collocation points $(\bar{r}_i, \bar{z}_j)$, for $j = 0, 1, 2, \cdots, N$, using the chain rule of differentiation as follows:

$$\begin{aligned}
\left.\frac{\partial u}{\partial \bar{r}}\right|_{(\bar{r}_i, \bar{z}_j)} &\approx \sum_{m=0}^{M}\sum_{n=0}^{N} u(\hat{r}_m, \hat{z}_n, \bar{t}_{k+1}) L_n(\hat{z}_j) \left(\frac{\mathrm{d}L_m(\hat{r})}{\mathrm{d}\hat{r}}\frac{\mathrm{d}\hat{r}}{\mathrm{d}\bar{r}}\right)\Bigg|_{\hat{r}=\hat{r}_i} \\
&= \sum_{m=0}^{M}\sum_{n=0}^{N} u(\hat{r}_m, \hat{z}_n, \bar{t}_{k+1}) L_n(\hat{z}_j) \left(\frac{2}{b-a}\right)\left.\frac{\mathrm{d}L_m(\hat{r})}{\mathrm{d}\hat{r}}\right|_{\hat{r}=\hat{r}_i} \\
&= \sum_{m=0}^{M} \left(\frac{2}{b-a}\right) D_{i,m} u(\hat{r}_m, \hat{z}_j, \bar{t}_{k+1}), \quad i = 0, 1, 2, \cdots, M, \\
&= \mathbf{D}\mathbf{U}_j^{(k+1)}, \text{ at } \bar{z} = \bar{z}_j \text{ and } \bar{t} = \bar{t}_{k+1},
\end{aligned} \tag{3.208}$$

where $D_{i,m} = \left.\dfrac{\mathrm{d}L_m(\hat{r})}{\mathrm{d}\hat{r}}\right|_{\hat{r}=\hat{r}_i}$, for $i, m = 0, 1, 2, \cdots, M$, are the entries of the standard first derivative Chebyshev differentiation matrix $[D_{i,m}]$ of size $(M+1)\times(M+1)$ as defined in Trefethen (2000). The matrix $\mathbf{D}$ is an $(M+1)\times(M+1)$ scaling matrix for the Chebyshev derivative matrix $[D_{i,m}]$ and is given by

$$\mathbf{D} = [2/(b-a)][D_{i,m}], \text{ for } i, m = 0, 1, 2, \cdots, M. \tag{3.209}$$

The unknown column vector $\mathbf{U}_j^{(k+1)}$ is defined as

$$\mathbf{U}_j^{(k+1)} = [u(\bar{r}_0, \bar{z}_j, \bar{t}_{k+1}), u(\bar{r}_1, \bar{z}_j, \bar{t}_{k+1}), \cdots, u(\bar{r}_M, \bar{z}_j, \bar{t}_{k+1})]^{\mathrm{T}}, \tag{3.210}$$

where the superscript T denotes matrix transpose. Similarly, the first partial derivative of $u(\bar{r}, \bar{z}, \bar{t}_{k+1})$ with respect to $\bar{z}$ is approximated at the collocation points $(\bar{r}_i, \bar{z}_j)$, for $i =$

$0, 1, 2, \cdots, M$, using the chain rule of differentiation as follows:

$$\begin{aligned}
\left.\frac{\partial u}{\partial \hat{z}}\right|_{(\bar{r}_i, \bar{z}_j)} &\approx \sum_{m=0}^{M}\sum_{n=0}^{N} u(\hat{r}_m, \hat{z}_n, \bar{t}_{k+1}) L_m(\hat{r}_i) \left(\frac{\mathrm{d}L_n(\hat{z})}{\mathrm{d}\hat{z}}\frac{\mathrm{d}\hat{z}}{\mathrm{d}\bar{z}}\right)\Bigg|_{\hat{z}=\hat{z}_j} \\
&= \sum_{m=0}^{M}\sum_{n=0}^{N} u(\hat{r}_m, \hat{z}_n, \bar{t}_{k+1}) L_m(\hat{r}_i) \left(\frac{2}{\beta-\alpha}\right)\frac{\mathrm{d}L_n(\hat{z})}{\mathrm{d}\hat{z}}\Bigg|_{\hat{z}=\hat{z}_j} \\
&= \sum_{n=0}^{N} \left(\frac{2}{\beta-\alpha}\right) d_{j,n} u(\hat{r}_i, \hat{z}_n, \bar{t}_{k+1}), \quad j = 0, 1, 2, \cdots, N, \\
&= \sum_{n=0}^{N} \mathbf{d}_{j,n} \mathbf{U}_n^{(k+1)}, \qquad (3.211)
\end{aligned}$$

where $d_{j,n} = \left.\dfrac{\mathrm{d}L_n(\hat{z})}{\mathrm{d}\hat{z}}\right|_{\hat{z}=\hat{z}_j}$, for $j, n = 0, 1, 2, \cdots, N$, are the entries of the standard first derivative Chebyshev differentiation matrix $[d_{j,n}]$ of size $(N+1)\times(N+1)$. The matrix $\mathbf{d}$ is an $(N+1)\times(N+1)$ scaling matrix for the Chebyshev derivative matrix $[d_{j,n}]$ and is given by

$$\mathbf{d} = [2/(\beta-\alpha)][d_{j,n}], \text{ for } j, n = 0, 1, 2, \cdots, N. \qquad (3.212)$$

Here, $\mathbf{d}_{j,n}$ denotes the element at the j^{th} row and the n^{th} column of the matrix $\mathbf{d}$. In general, the unknown column vector $\mathbf{U}_n^{(k+1)}$ is constructed in such a manner that for every grid point in $\bar{z}$, the grid points in $\bar{r}$ are varied. This arrangement of grid points explains the presence of the single sum in the last expression in Equation (3.211). Such a pattern will be useful when assembling the system of linear algebraic equations to obtain the coefficient matrices. Similarly, the second partial derivatives of $u(\bar{r}, \bar{z}, \bar{t}_{k+1})$ with respect to $\bar{r}$ and $\bar{z}$ are approximated at the collocation points $(\bar{r}_i, \bar{z}_j)$ using the chain rule of differentiation as follows:

$$\begin{aligned}
\left.\frac{\partial^2 u}{\partial \bar{r}^2}\right|_{(\bar{r}_i, \bar{z}_j)} &\approx \sum_{m=0}^{M}\sum_{n=0}^{N} u(\hat{r}_m, \hat{z}_n, \bar{t}_{k+1}) L_n(\hat{z}_j) \left[\frac{\mathrm{d}^2 L_m(\hat{r})}{\mathrm{d}\hat{r}^2}\left(\frac{\mathrm{d}\hat{r}}{\mathrm{d}\bar{r}}\right)^2\right]\Bigg|_{\hat{r}=\hat{r}_i} \\
&= \sum_{m=0}^{M}\sum_{n=0}^{N} u(\hat{r}_m, \hat{z}_n, \bar{t}_{k+1}) L_n(\hat{z}_j) \left(\frac{2}{b-a}\right)^2 \frac{\mathrm{d}^2 L_m(\hat{r})}{\mathrm{d}\hat{r}^2}\Bigg|_{\hat{r}=\hat{r}_i} \\
&= \sum_{m=0}^{M} \left(\frac{2}{b-a}\right)^2 D_{i,m}^2 u(\hat{r}_m, \hat{z}_j, \bar{t}_{k+1}), \quad i = 0, 1, 2, \cdots, M, \\
&= \mathbf{D}^2 \mathbf{U}_j^{(k+1)}. \qquad (3.213a)
\end{aligned}$$

$$\begin{aligned}
\frac{\partial^2 u}{\partial \bar{z}^2}\Big|_{(\bar{r}_i,\bar{z}_j)} &\approx \sum_{m=0}^{M}\sum_{n=0}^{N} u(\hat{r}_m,\hat{z}_n,\bar{t}_{k+1})L_m(\hat{r}_i)\left[\frac{\mathrm{d}^2 L_n(\hat{z})}{\mathrm{d}\hat{z}^2}\left(\frac{\mathrm{d}\hat{z}}{\mathrm{d}\bar{z}}\right)^2\right]\Bigg|_{\hat{z}=\hat{z}_j} \\
&= \sum_{m=0}^{M}\sum_{n=0}^{N} u(\hat{r}_m,\hat{z}_n,\bar{t}_{k+1})L_m(\hat{r}_i)\left(\frac{2}{\beta-\alpha}\right)^2\frac{\mathrm{d}^2 L_n(\hat{z})}{\mathrm{d}\hat{z}^2}\Bigg|_{\hat{z}=\hat{z}_j} \\
&= \sum_{n=0}^{N}\left(\frac{2}{\beta-\alpha}\right)^2 d^2_{j,n}u(\hat{r}_i,\hat{z}_n,\bar{t}_{k+1}), \quad j=0,1,2,\cdots,N \\
&= \sum_{n=0}^{N}\mathbf{d}^2_{j,n}\mathbf{U}^{(k+1)}_n. \qquad (3.213b)
\end{aligned}$$

$$\begin{aligned}
\frac{\partial^2 u}{\partial \bar{r}\partial \bar{z}}\Big|_{(\bar{r}_i,\bar{z}_j)} &\approx \sum_{m=0}^{M}\sum_{n=0}^{N} u(\hat{r}_m,\hat{z}_n,\bar{t}_{k+1})\left(\frac{\mathrm{d}L_m(\hat{r})}{\mathrm{d}\hat{r}}\frac{\mathrm{d}\hat{r}}{\mathrm{d}\bar{r}}\right)\Bigg|_{\hat{r}=\hat{r}_i}\left(\frac{\mathrm{d}L_n(\hat{z})}{\mathrm{d}\hat{z}}\frac{\mathrm{d}\hat{z}}{\mathrm{d}\bar{z}}\right)\Bigg|_{\hat{z}=\hat{z}_j} \\
&= \sum_{m=0}^{M}\sum_{n=0}^{N} u(\hat{r}_m,\hat{z}_n,\bar{t}_{k+1})\left(\frac{2}{b-a}\right)\frac{\mathrm{d}L_m(\hat{r})}{\mathrm{d}\hat{r}}\Bigg|_{\hat{r}=\hat{r}_i}\left(\frac{2}{\beta-\alpha}\right)\frac{\mathrm{d}L_n(\hat{z})}{\mathrm{d}\hat{z}}\Bigg|_{\hat{z}=\hat{z}_j} \\
&= \sum_{m=0}^{M}\sum_{n=0}^{N}\left(\frac{2}{b-a}\right)D_{i,m}\left(\frac{2}{\beta-\alpha}\right)d_{j,n}u(\hat{r}_m,\hat{z}_n,\bar{t}_{k+1}), \\
&= \sum_{n=0}^{N}\mathbf{d}_{j,n}\mathbf{D}\mathbf{U}^{(k+1)}_n. \qquad (3.213c)
\end{aligned}$$

The partial derivatives of the other dependent variables, i.e., $\nu(\bar{r},\bar{z},\bar{t}_{k+1})$, $\Theta(\bar{r},\bar{z},\bar{t}_{k+1})$, $\phi(\bar{r},\bar{z},\bar{t}_{k+1})$, $\alpha_{\mathrm{m}}(\bar{r},\bar{z},\bar{t}_{k+1})$, and $\phi_{\mathrm{oil}}(\bar{r},\bar{z},\bar{t}_{k+1})$, with respect to $\bar{r}$ and $\bar{z}$ can be transformed to discrete matrix form in a similar manner. The differentiation process illustrated above can be easily extended to higher order partial derivatives.

Substituting the respective discrete derivative matrices into the $r-$momentum Equation (3.166), yields the following system of $(M+1)\times(N+1)$ linear algebraic equations:

$$\left[\mathrm{diag}(\mathbf{a}_0)\mathbf{D}^2+\mathrm{diag}(\mathbf{a}_1)\mathbf{D}+\mathrm{diag}(\mathbf{a}_2)\mathbf{I}\right]\mathbf{U}^{(k+1)}_j+\sum_{n=0}^{N}\left[\mathbf{a}_3\mathbf{d}^2_{j,n}\mathbf{I}\right]\mathbf{U}^{(k+1)}_n=\mathbf{R}\mathbf{1}^{(k)}_j \quad (3.214)$$

where $\mathrm{diag}(\cdots)$ represents a diagonal matrix of vectors. The coefficients on the left-hand side are given by

$$\mathrm{diag}(\mathbf{a}_0)=-\frac{\Delta\bar{t}\lambda_2}{\mathrm{Re}}, \quad \mathrm{diag}(\mathbf{a}_1)=-\frac{\Delta\bar{t}\lambda_2}{\mathrm{Re}}\frac{1}{\bar{r}} \qquad (3.215a)$$

$$\mathrm{diag}(\mathbf{a}_2)=\left(1+\frac{\Delta\bar{t}\lambda_2}{\mathrm{Re}}\frac{1}{\bar{r}^2}+\frac{\Delta\bar{t}\lambda_2}{2(\mathrm{Re}\cdot\mathrm{Da})}\right), \quad \mathrm{diag}(\mathbf{a}_3)=-\frac{\Delta\bar{t}\lambda_2}{2\mathrm{Re}} \qquad (3.215b)$$

and the right-hand side vector is given by

$$\begin{aligned}\mathbf{R1}_j^{(k)} = \mathbf{U}_j^{(k)} + \Delta\bar{t}\Bigg\{ &-\frac{1}{2}\left(3\mathbf{U}_j^{(k)}\cdot\mathbf{D}\mathbf{U}_j^{(k)} - \mathbf{U}_j^{(k-1)}\cdot\mathbf{D}\mathbf{U}_j^{(k-1)}\right)\\ &-\frac{1}{2}\left(3\mathbf{V}_j^{(k)}\cdot\sum_{n=0}^{N}\mathbf{d}_{j,n}\mathbf{U}_n^{(k)} - \mathbf{V}_j^{(k-1)}\cdot\sum_{n=0}^{N}\mathbf{d}_{j,n}\mathbf{U}_n^{(k-1)}\right) - \mathbf{D}\mathbf{P}_j^{(k)}\\ &+\frac{\lambda_2}{\mathrm{Re}}\left(\mathbf{D}^2\mathbf{U}_j^{(k)} + \frac{1}{2}\sum_{n=0}^{N}\mathbf{d}_{j,n}^2\mathbf{U}_n^{(k)} + \mathbf{D}\sum_{n=0}^{N}\mathbf{d}_{j,n}\mathbf{V}_n^{(k)} + \frac{1}{\bar{r}}\mathbf{D}\mathbf{U}_j^{(k)} - \frac{1}{\bar{r}^2}\mathbf{U}_j^{(k)}\right)\\ &-\frac{\lambda_2}{2(\mathrm{Re}\cdot\mathrm{Da})}\mathbf{U}_j^{(k)} + \lambda_3\frac{\mathrm{Gr_T}}{\mathrm{Re}^2}\cos(\varphi)\mathbf{\Theta}_j^{(k)} + \lambda_4\frac{\mathrm{Gr_C}}{\mathrm{Re}^2}\cos(\varphi)\mathbf{\Phi}_j^{(k)}\\ &+\frac{\lambda_1}{2\mathrm{We}}\left[3\left(R\bar{K}\right)^k\mathbf{D}\mathbf{\Phi}_{\mathrm{oil}}{}_j^{(k)} - \left(R\bar{K}\right)^{k-1}\mathbf{D}\mathbf{\Phi}_{\mathrm{oil}}{}_j^{(k-1)}\right]\Bigg\}\end{aligned} \tag{3.216}$$

where the variable $R\bar{K}$ is defined by Equation (3.108). Similarly, the discrete form of the $z-$momentum Equation (3.168) is a system of $(M+1)\times(N+1)$ linear algebraic equations given by:

$$\left[\mathrm{diag}(\mathbf{b}_0)\mathbf{D}^2 + \mathrm{diag}(\mathbf{b}_1)\mathbf{D} + \mathrm{diag}(\mathbf{b}_2)\mathbf{I}\right]\mathbf{V}_j^{(k+1)} + \sum_{n=0}^{N}\left[\mathbf{b}_3\mathbf{d}_{j,n}^2\mathbf{I}\right]\mathbf{V}_n^{(k+1)} = \mathbf{R2}_j^{(k)} \tag{3.217}$$

The coefficients on the left-hand side are given by

$$\mathrm{diag}(\mathbf{b}_0) = -\frac{\Delta\bar{t}\lambda_2}{2\mathrm{Re}}, \quad \mathrm{diag}(\mathbf{b}_1) = -\frac{\Delta\bar{t}\lambda_2}{2\mathrm{Re}}\frac{1}{\bar{r}} \tag{3.218a}$$

$$\mathrm{diag}(\mathbf{b}_2) = \left(1 + \frac{\Delta\bar{t}\lambda_2}{2(\mathrm{Re}\cdot\mathrm{Da})}\right), \quad \mathrm{diag}(\mathbf{b}_3) = -\frac{\Delta\bar{t}\lambda_2}{\mathrm{Re}} \tag{3.218b}$$

and the right-hand side vector is given by

$$\begin{aligned}\mathbf{R2}_j^{(k)} = \mathbf{V}_j^{(k)} + \Delta\bar{t}\Bigg\{ &-\frac{1}{2}\left(3\mathbf{U}_j^{(k)}\cdot\mathbf{D}\mathbf{V}_j^{(k)} - \mathbf{U}_j^{(k-1)}\cdot\mathbf{D}\mathbf{V}_j^{(k-1)}\right)\\ &-\frac{1}{2}\left(3\mathbf{V}_j^{(k)}\cdot\sum_{n=0}^{N}\mathbf{d}_{j,n}\mathbf{V}_n^{(k)} - \mathbf{V}_j^{(k-1)}\cdot\sum_{n=0}^{N}\mathbf{d}_{j,n}\mathbf{V}_n^{(k-1)}\right) - \sum_{n=0}^{N}\mathbf{d}_{j,n}\mathbf{P}_n^{(k)}\\ &+\frac{\lambda_2}{\mathrm{Re}}\left(\frac{1}{2}\mathbf{D}^2\mathbf{V}_j^{(k)} + \sum_{n=0}^{N}\mathbf{d}_{j,n}^2\mathbf{V}_n^{(k)} + \mathbf{D}\sum_{n=0}^{N}\mathbf{d}_{j,n}\mathbf{U}_n^{(k)} + \frac{1}{\bar{r}}\sum_{n=0}^{N}\mathbf{d}_{j,n}\mathbf{U}_n^{(k)} + \frac{1}{2\bar{r}}\mathbf{D}\mathbf{V}_j^{(k)}\right)\\ &-\frac{\lambda_2}{2(\mathrm{Re}\cdot\mathrm{Da})}\mathbf{V}_j^{(k)} + \lambda_3\frac{\mathrm{Gr_T}}{\mathrm{Re}^2}\sin(\varphi)\mathbf{\Theta}_j^{(k)} + \lambda_4\frac{\mathrm{Gr_C}}{\mathrm{Re}^2}\sin(\varphi)\mathbf{\Phi}_j^{(k)}\\ &+\frac{\lambda_1}{2\mathrm{We}}\left[3(R\bar{K})^k\sum_{n=0}^{N}\mathbf{d}_{j,n}\mathbf{\Phi}_{\mathrm{oil}}{}_n^{(k)} - (R\bar{K})^{k-1}\sum_{n=0}^{N}\mathbf{d}_{j,n}\mathbf{\Phi}_{\mathrm{oil}}{}_n^{(k-1)}\right]\Bigg\}\end{aligned} \tag{3.219}$$

The discrete form of the energy Equation (3.170) is a system of $(M+1)\times(N+1)$ linear

algebraic equations given by:

$$\left[\mathrm{diag}(\mathbf{d}_0)\mathbf{D}^2 + \mathrm{diag}(\mathbf{d}_1)\mathbf{D} + \mathrm{diag}(\mathbf{d}_2)\mathbf{I}\right]\boldsymbol{\Theta}_j^{(k+1)} + \sum_{n=0}^{N}\left[\mathbf{d}_3\mathbf{d}_{j,n}^2\mathbf{I}\right]\boldsymbol{\Theta}_n^{(k+1)} = \mathbf{R4}_j^{(k)} \tag{3.220}$$

The coefficients on the left-hand side are given by

$$\mathrm{diag}(\mathbf{d}_0) = -\frac{\Delta\bar{t}\lambda_5}{2\mathrm{Pe}}, \quad \mathrm{diag}(\mathbf{d}_1) = -\frac{\Delta\bar{t}\lambda_5}{2\mathrm{Pe}}\frac{1}{\bar{r}} \tag{3.221a}$$

$$\mathrm{diag}(\mathbf{d}_2) = \left(1 + \mathrm{St}\frac{\Delta\bar{t}\lambda_6}{2\bar{d}}\right), \quad \mathrm{diag}(\mathbf{d}_3) = -\frac{\Delta\bar{t}\lambda_5}{2\mathrm{Pe}} \tag{3.221b}$$

and the right-hand side vector is given by

$$\begin{aligned}
\mathbf{R4}_j^{(k)} = \boldsymbol{\Theta}_j^{(k)} + \Delta\bar{t}\Bigg\{ & -\frac{1}{2}\left(3\mathbf{U}_j^{(k)}\cdot\mathbf{D}\boldsymbol{\Theta}_j^{(k)} - \mathbf{U}_j^{(k-1)}\cdot\mathbf{D}\boldsymbol{\Theta}_j^{(k-1)}\right) \\
& -\frac{1}{2}\left(3\mathbf{V}_j^{(k)}\cdot\sum_{n=0}^{N}\mathbf{d}_{j,n}\boldsymbol{\Theta}_n^{(k)} - \mathbf{V}_j^{(k-1)}\cdot\sum_{n=0}^{N}\mathbf{d}_{j,n}\boldsymbol{\Theta}_n^{(k-1)}\right) \\
& +\frac{\lambda_5}{2\mathrm{Pe}}\left(\mathbf{D}^2\boldsymbol{\Theta}_j^{(k)} + \frac{1}{\bar{r}}\mathbf{D}\boldsymbol{\Theta}_j^{(k)} + \sum_{n=0}^{N}\mathbf{d}_{j,n}^2\boldsymbol{\Theta}_n^{(k)}\right) - \mathrm{St}\frac{\lambda_6}{2\bar{d}}\boldsymbol{\Theta}_j^{(k)} \\
& +\lambda_7\frac{\mathrm{Ec}}{2\mathrm{Re}}\Bigg\{3\Bigg[2\left(\mathbf{D}\mathbf{U}_j^{(k)}\right)^2 + 2\left(\frac{1}{\bar{r}}\mathbf{U}_j^{(k)}\right)^2 + 2\left(\sum_{n=0}^{N}\mathbf{d}_{j,n}\mathbf{V}_n^{(k)}\right)^2 \\
& + \left(\mathbf{D}\mathbf{V}_j^{(k)} + \sum_{n=0}^{N}\mathbf{d}_{j,n}\mathbf{U}_n^{(k)}\right)^2\Bigg] - \Bigg[2\left(\mathbf{D}\mathbf{U}_j^{(k-1)}\right)^2 + 2\left(\frac{1}{\bar{r}}\mathbf{U}_j^{(k-1)}\right)^2 \\
& +2\left(\sum_{n=0}^{N}\mathbf{d}_{j,n}\mathbf{V}_n^{(k-1)}\right)^2 + \left(\mathbf{D}\mathbf{V}_j^{(k-1)} + \sum_{n=0}^{N}\mathbf{d}_{j,n}\mathbf{U}_n^{(k-1)}\right)^2\Bigg]\Bigg\}\Bigg\}
\end{aligned} \tag{3.222}$$

The discrete form of the species concentration Equation (3.172) is a system of $(M+1)\times(N+1)$ linear algebraic equations given by:

$$\mathbf{I}\boldsymbol{\Phi}_j^{(k+1)} = \mathbf{R5}_j^{(k)} \tag{3.223}$$

The right-hand side vector is given by

$$\begin{aligned}
\mathbf{R5}_j^{(k)} = \mathbf{\Phi}_j^{(k)} + \Delta\bar{t}\Bigg\{ & -\frac{1}{2}\left(3\mathbf{U}_j^{(k)} \cdot \mathbf{D\Phi}_j^{(k)} - \mathbf{U}_j^{(k-1)} \cdot \mathbf{D\Phi}_j^{(k-1)}\right) \\
& -\frac{1}{2}\left(3\mathbf{V}_j^{(k)} \cdot \sum_{n=0}^{N} \mathbf{d}_{j,n}\mathbf{\Phi}_n^{(k)} - \mathbf{V}_j^{(k-1)} \cdot \sum_{n=0}^{N} \mathbf{d}_{j,n}\mathbf{\Phi}_n^{(k-1)}\right) \\
& +\frac{3\varepsilon_{\mathrm{p}}}{2}\Bigg[\left[1-\boldsymbol{\alpha}_{\mathrm{m}_j}^{(k)}\right]\left(\mathbf{\Phi}_j^{(k)} - \mathbf{C}_{\mathrm{d}_j}^{(k)}\right)\cdot\left(\mathbf{D}^2\mathbf{V}_j^{(k)} + \frac{1}{\bar{r}}\mathbf{DV}_j^{(k)}\right) \\
& +\left\{\left[1-\boldsymbol{\alpha}_{\mathrm{m}_j}^{(k)}\right]\left(\mathbf{D\Phi}_j^{(k)} - \mathbf{C1}_{\mathrm{d}_j}^{(k)} \cdot \mathbf{D\Theta}_j^{(k)}\right) - \left(\mathbf{\Phi}_j^{(k)} - \mathbf{C}_{\mathrm{d}_j}^{(k)}\right)\cdot \mathbf{D}\boldsymbol{\alpha}_{\mathrm{m}_j}^{(k)}\right\}\cdot \mathbf{DV}_j^{(k)}\Bigg] \\
& -\frac{\varepsilon_{\mathrm{p}}}{2}\Bigg[\left[1-\boldsymbol{\alpha}_{\mathrm{m}_j}^{(k-1)}\right]\left(\mathbf{\Phi}_j^{(k-1)} - \mathbf{C}_{\mathrm{d}_j}^{(k-1)}\right)\cdot\left(\mathbf{D}^2\mathbf{V}_j^{(k-1)} + \frac{1}{\bar{r}}\mathbf{DV}_j^{(k-1)}\right) \\
& +\Bigg\{\left[1-\boldsymbol{\alpha}_{\mathrm{m}_j}^{(k-1)}\right]\left(\mathbf{D\Phi}_j^{(k-1)} - \mathbf{C1}_{\mathrm{d}_j}^{(k-1)} \cdot \mathbf{D\Theta}_j^{(k-1)}\right) \\
& -\left(\mathbf{\Phi}_j^{(k-1)} - \mathbf{C}_{\mathrm{d}_j}^{(k-1)}\right)\cdot \mathbf{D}\boldsymbol{\alpha}_{\mathrm{m}_j}^{(k-1)}\Bigg\}\cdot \mathbf{DV}_j^{(k-1)}\Bigg] \\
& +\frac{3}{2\mathrm{Re}\cdot\mathrm{Sc}}\Bigg[\mathbf{C1}_{\mathrm{d}_j}^{(k)}\cdot\left(\mathbf{D}^2\mathbf{\Theta}_j^{(k)} + \frac{1}{\bar{r}}\mathbf{D\Theta}_j^{(k)} + \sum_{n=0}^{N}\mathbf{d}_{j,n}^2\mathbf{\Theta}_n^{(k)}\right) \\
& +\mathbf{C2}_{\mathrm{d}_j}^{(k)}\cdot\left\{\left(\mathbf{D\Theta}_j^{(k)}\right)^2 + \left(\sum_{n=0}^{N}\mathbf{d}_{j,n}\mathbf{\Theta}_n^{(k)}\right)^2\right\}\Bigg] \\
& -\frac{1}{2\mathrm{Re}\cdot\mathrm{Sc}}\Bigg[\mathbf{C1}_{\mathrm{d}_j}^{(k-1)}\cdot\left(\mathbf{D}^2\mathbf{\Theta}_j^{(k-1)} + \frac{1}{\bar{r}}\mathbf{D\Theta}_j^{(k-1)} + \sum_{n=0}^{N}\mathbf{d}_{j,n}^2\mathbf{\Theta}_n^{(k-1)}\right) \\
& +\mathbf{C2}_{\mathrm{d}_j}^{(k-1)}\cdot\left\{\left(\mathbf{D\Theta}_j^{(k-1)}\right)^2 + \left(\sum_{n=0}^{N}\mathbf{d}_{j,n}\mathbf{\Theta}_n^{(k-1)}\right)^2\right\}\Bigg]\Bigg\}
\end{aligned} \tag{3.224}$$

The discrete form of the precipitation kinetics Equation (3.174) is a system of $(M+1)\times(N+1)$ linear algebraic equations given by:

$$\mathbf{I}\boldsymbol{\alpha}_{\mathrm{m}_j}^{(k+1)} = \mathbf{R6}_j^{(k)} \tag{3.225}$$

The right-hand side vector is given by

$$\begin{aligned}\mathbf{R6}_j^{(k)} = {\boldsymbol{\alpha}_{\mathrm{m}}}_j^{(k)} + \Delta\bar{t}\Bigg\{ & \frac{1}{2}\left[3\left(1-{\boldsymbol{\alpha}_{\mathrm{m}}}_j^{(k)}\right)\cdot\mathbf{K1}_j^{(k)} - \left(1-{\boldsymbol{\alpha}_{\mathrm{m}}}_j^{(k-1)}\right)\cdot\mathbf{K1}_j^{(k-1)}\right] \\ & -\frac{1}{2}\left(3\mathbf{U}_j^{(k)}\cdot\mathbf{D}{\boldsymbol{\alpha}_{\mathrm{m}}}_j^{(k)} - \mathbf{U}_j^{(k-1)}\cdot\mathbf{D}{\boldsymbol{\alpha}_{\mathrm{m}}}_j^{(k-1)}\right) \\ & -\frac{1}{2}\left(3\mathbf{V}_j^{(k)}\cdot\sum_{n=0}^{N}\mathbf{d}_{j,n}{\boldsymbol{\alpha}_{\mathrm{m}}}_n^{(k)} - \mathbf{V}_j^{(k-1)}\cdot\sum_{n=0}^{N}\mathbf{d}_{j,n}{\boldsymbol{\alpha}_{\mathrm{m}}}_n^{(k-1)}\right) \\ & -\frac{\mathrm{Re}}{2\lambda_2}\left[3{\boldsymbol{\alpha}_{\mathrm{m}}}_j^{(k)}\cdot\left(\mathbf{DV}_j^{(k)}\right)^2\cdot\mathbf{K2}_j^{(k)} - {\boldsymbol{\alpha}_{\mathrm{m}}}_j^{(k-1)}\cdot\left(\mathbf{DV}_j^{(k-1)}\right)^2\cdot\mathbf{K2}_j^{(k-1)}\right]\Bigg\} \end{aligned} \tag{3.226}$$

The discrete form of the oil volume fraction Equation (3.176) is a system of $(M+1)\times(N+1)$ linear algebraic equations given by:

$$\mathbf{I}{\boldsymbol{\Phi}_{\mathrm{oil}}}_j^{(k+1)} = \mathbf{R7}_j^{(k)} \tag{3.227}$$

The right-hand side vector is given by

$$\begin{aligned}\mathbf{R7}_j^{(k)} = {\boldsymbol{\Phi}_{\mathrm{oil}}}_j^{(k)} + \Delta\bar{t}\Bigg\{ & -\frac{1}{2}\left(3\mathbf{U}_j^{(k)}\cdot\mathbf{D}{\boldsymbol{\Phi}_{\mathrm{oil}}}_j^{(k)} - \mathbf{U}_j^{(k-1)}\cdot\mathbf{D}{\boldsymbol{\Phi}_{\mathrm{oil}}}_j^{(k-1)}\right) \\ & -\frac{1}{2}\left(3\mathbf{V}_j^{(k)}\cdot\sum_{n=0}^{N}\mathbf{d}_{j,n}{\boldsymbol{\Phi}_{\mathrm{oil}}}_j^{(k)} - \mathbf{V}_j^{(k-1)}\cdot\sum_{n=0}^{N}\mathbf{d}_{j,n}{\boldsymbol{\Phi}_{\mathrm{oil}}}_j^{(k-1)}\right)\Bigg\} \end{aligned} \tag{3.228}$$

The intermediate solutions $\mathbf{U}_j^{(k)}, \mathbf{V}_j^{(k)}, \boldsymbol{\Theta}_j^{(k)}, \boldsymbol{\Phi}U_j^{(k)}, {\boldsymbol{\alpha}_{\mathrm{m}}}_j^{(k)}$ and ${\boldsymbol{\Phi}_{\mathrm{oil}}}_j^{(k)}$ in the above systems are obtained from Equations (3.187), (3.189), (3.191), (3.193), (3.195) and (3.197), respectively, i.e.,

$$\begin{aligned}\mathbf{U}_j^{(k)} = \mathbf{U}_j^{(k-1)} + \Delta\bar{t}\Bigg\{ & -\mathbf{U}_j^{(k-1)}\cdot\mathbf{D}\mathbf{U}_j^{(k-1)} - \mathbf{V}_j^{(k-1)}\cdot\sum_{n=0}^{N}\mathbf{d}_{j,n}\mathbf{U}_n^{(k-1)} - \mathbf{D}\mathbf{P}_j^{(k-1)} - \frac{\lambda_2}{(\mathrm{Re}\cdot\mathrm{Da})}\mathbf{U}_j^{(k-1)} \\ & +\frac{\lambda_2}{\mathrm{Re}}\left(2\mathbf{D}^2\mathbf{U}_j^{(k-1)} + \sum_{n=0}^{N}\mathbf{d}_{j,n}^2\mathbf{U}_n^{(k-1)} + \mathbf{D}\sum_{n=0}^{N}\mathbf{d}_{j,n}\mathbf{V}_n^{(k-1)} + \frac{2}{\bar{r}}\mathbf{D}\mathbf{U}_j^{(k-1)} - \frac{2}{\bar{r}^2}\mathbf{U}_j^{(k-1)}\right) \\ & +\lambda_3\frac{\mathrm{Gr_T}}{\mathrm{Re}^2}\cos(\varphi)\boldsymbol{\Theta}_j^{(k-1)} + \lambda_4\frac{\mathrm{Gr_C}}{\mathrm{Re}^2}\cos(\varphi)\boldsymbol{\Phi}_j^{(k-1)} + \frac{\lambda_1}{\mathrm{We}}(R\bar{K})^{k-1}\cdot\mathbf{D}{\boldsymbol{\Phi}_{\mathrm{oil}}}_j^{(k-1)}\Bigg\} \end{aligned} \tag{3.229a}$$

$$\begin{aligned}\mathbf{V}_j^{(k)} = \mathbf{V}_j^{(k-1)} + \Delta\bar{t}\Bigg\{ & -\mathbf{U}_j^{(k-1)}\cdot\mathbf{D}\mathbf{V}_j^{(k-1)} - \mathbf{V}_j^{(k-1)}\cdot\sum_{n=0}^{N}\mathbf{d}_{j,n}\mathbf{V}_n^{(k-1)} - \sum_{n=0}^{N}\mathbf{d}_{j,n}\mathbf{P}_n^{(k-1)} - \frac{\lambda_2}{(\mathrm{Re}\cdot\mathrm{Da})}\mathbf{V}_j^{(k-1)} \\ & +\frac{\lambda_2}{\mathrm{Re}}\left(\mathbf{D}^2\mathbf{V}_j^{(k-1)} + 2\sum_{n=0}^{N}\mathbf{d}_{j,n}^2\mathbf{V}_n^{(k-1)} + \mathbf{D}\sum_{n=0}^{N}\mathbf{d}_{j,n}\mathbf{U}_n^{(k-1)} + \frac{1}{\bar{r}}\sum_{n=0}^{N}\mathbf{d}_{j,n}\mathbf{U}_n^{(k-1)} + \frac{1}{\bar{r}}\mathbf{D}\mathbf{V}_j^{(k-1)}\right) \\ & +\lambda_3\frac{\mathrm{Gr_T}}{\mathrm{Re}^2}\sin(\varphi)\boldsymbol{\Theta}_j^{(k-1)} + \lambda_4\frac{\mathrm{Gr_C}}{\mathrm{Re}^2}\sin(\varphi)\boldsymbol{\Phi}_j^{(k-1)} + \frac{\lambda_1}{\mathrm{We}}(R\bar{K})^{k-1}\cdot\sum_{n=0}^{N}\mathbf{d}_{j,n}{\boldsymbol{\Phi}_{\mathrm{oil}}}_n^{(k-1)}\Bigg\} \end{aligned} \tag{3.229b}$$

$$\boldsymbol{\Theta}_j^{(k)} = \boldsymbol{\Theta}_j^{(k-1)} + \Delta\bar{t}\Bigg\{ - \mathbf{U}_j^{(k-1)} \cdot \mathbf{D}\boldsymbol{\Theta}_j^{(k-1)} - \mathbf{V}_j^{(k-1)} \cdot \sum_{n=0}^{N} \mathbf{d}_{j,n}\boldsymbol{\Theta}_n^{(k-1)}$$
$$+\frac{\lambda_5}{\mathrm{Pe}}\left(\mathbf{D}^2\boldsymbol{\Theta}_j^{(k-1)} + \frac{1}{\bar{r}}\mathbf{D}\boldsymbol{\Theta}_j^{(k-1)} + \sum_{n=0}^{N}\mathbf{d}_{j,n}^2\boldsymbol{\Theta}_n^{(k-1)}\right) - \mathrm{St}\frac{\lambda_6}{\bar{d}}\boldsymbol{\Theta}_j^{(k-1)}$$
$$+\lambda_7\frac{\mathrm{Ec}}{\mathrm{Re}}\Bigg[2\left(\mathbf{D}\mathbf{U}_j^{(k-1)}\right)^2 + 2\left(\frac{1}{\bar{r}}\mathbf{U}_j^{(k-1)}\right)^2 + 2\left(\sum_{n=0}^{N}\mathbf{d}_{j,n}\mathbf{V}_n^{(k-1)}\right)^2$$
$$+\left(\mathbf{D}\mathbf{V}_j^{(k-1)} + \sum_{n=0}^{N}\mathbf{d}_{j,n}\mathbf{U}_n^{(k-1)}\right)^2\Bigg]\Bigg\} \tag{3.229c}$$

$$\boldsymbol{\Phi}_j^{(k)} = \boldsymbol{\Phi}_j^{(k-1)} + \Delta\bar{t}\Bigg\{ - \mathbf{U}_j^{(k-1)} \cdot \mathbf{D}\boldsymbol{\Phi}_j^{(k-1)} - \mathbf{V}_j^{(k-1)} \cdot \sum_{n=0}^{N} \mathbf{d}_{j,n}\boldsymbol{\Phi}_n^{(k-1)}$$
$$+\varepsilon_{\mathrm{p}}\Bigg[\left[1 - {\boldsymbol{\alpha}_{\mathrm{m}}}_j^{(k-1)}\right]\left[\boldsymbol{\Phi}_j^{(k-1)} - {\mathbf{C}_{\mathrm{d}}}_j^{(k-1)}\right] \cdot \left(\mathbf{D}^2\mathbf{V}_j^{(k-1)} + \frac{1}{\bar{r}}\mathbf{D}\mathbf{V}_j^{(k-1)}\right)$$
$$+\Bigg\{\left[1 - {\boldsymbol{\alpha}_{\mathrm{m}}}_j^{(k-1)}\right] \cdot \left(\mathbf{D}\boldsymbol{\Phi}_j^{(k-1)} - \mathbf{C1}_{\mathrm{d}j}^{(k-1)} \cdot \mathbf{D}\boldsymbol{\Theta}_j^{(k-1)}\right)$$
$$-\left(\boldsymbol{\Phi}_j^{(k-1)} - {\mathbf{C}_{\mathrm{d}}}_j^{(k-1)}\right) \cdot \mathbf{D}{\boldsymbol{\alpha}_{\mathrm{m}}}_j^{(k-1)}\Bigg\} \cdot \mathbf{D}\mathbf{V}_j^{(k-1)}\Bigg]$$
$$+\frac{1}{\mathrm{Re}\cdot\mathrm{Sc}}\Bigg[\mathbf{C1}_{\mathrm{d}j}^{(k-1)} \cdot \left(\mathbf{D}^2\boldsymbol{\Theta}_j^{(k-1)} + \frac{1}{\bar{r}}\mathbf{D}\boldsymbol{\Theta}_j^{(k-1)} + \sum_{n=0}^{N}\mathbf{d}_{j,n}^2\boldsymbol{\Theta}_n^{(k-1)}\right)$$
$$+\mathbf{C2}_{\mathrm{d}j}^{(k-1)} \cdot \Bigg\{\left(\mathbf{D}\boldsymbol{\Theta}_j^{(k-1)}\right)^2 + \left(\sum_{n=0}^{N}\mathbf{d}_{j,n}^2\boldsymbol{\Theta}_n^{(k-1)}\right)^2\Bigg\}\Bigg]\Bigg\} \tag{3.229d}$$

$${\boldsymbol{\alpha}_{\mathrm{m}}}_j^{(k)} = {\boldsymbol{\alpha}_{\mathrm{m}}}_j^{(k-1)} + \Delta\bar{t}\Bigg\{ - \mathbf{U}_j^{(k-1)} \cdot \mathbf{D}{\boldsymbol{\alpha}_{\mathrm{m}}}_j^{(k-1)} - \mathbf{V}_j^{(k-1)} \cdot \sum_{n=0}^{N} \mathbf{d}_{j,n}{\boldsymbol{\alpha}_{\mathrm{m}}}_n^{(k-1)}$$
$$+\left[1 - {\boldsymbol{\alpha}_{\mathrm{m}}}_j^{(k-1)}\right] \cdot \mathbf{K1}_j^{(k-1)} - \frac{\mathrm{Re}}{\lambda_2}{\boldsymbol{\alpha}_{\mathrm{m}}}_j^{(k-1)} \cdot \left(\mathbf{D}\mathbf{V}_j^{(k-1)}\right)^2 \cdot \mathbf{K2}_j^{(k-1)}\Bigg\} \tag{3.229e}$$

$${\boldsymbol{\Phi}_{\mathrm{oil}}}_j^{(k)} = {\boldsymbol{\Phi}_{\mathrm{oil}}}_j^{(k-1)} + \Delta\bar{t}\Bigg\{ - \mathbf{U}_j^{(k-1)} \cdot \mathbf{D}{\boldsymbol{\Phi}_{\mathrm{oil}}}_j^{(k-1)} - \mathbf{V}_j^{(k-1)} \cdot \sum_{n=0}^{N} \mathbf{d}_{j,n}{\boldsymbol{\Phi}_{\mathrm{oil}}}_n^{(k-1)}\Bigg\} \tag{3.229f}$$

The unknown column vectors $\mathbf{U}_j^{(k+1)}, \mathbf{V}_j^{(k+1)}, \boldsymbol{\Theta}_j^{(k+1)}, \boldsymbol{\Phi}_j^{(k+1)}, {\boldsymbol{\alpha}_{\mathrm{m}}}_j^{(k+1)}$ and ${\boldsymbol{\Phi}_{\mathrm{oil}}}_j^{(k+1)}$ are

given by:

$$\mathbf{U}_j^{(k+1)} = [u(\bar{r}_0, \bar{z}_j, \bar{t}_{k+1}), u(\bar{r}_1, \bar{z}_j, \bar{t}_{k+1}), \cdots, u(\bar{r}_M, \bar{z}_j, \bar{t}_{k+1})]^{\mathrm{T}} \tag{3.230a}$$

$$\mathbf{V}_j^{(k+1)} = [v(\bar{r}_0, \bar{z}_j, \bar{t}_{k+1}), v(\bar{r}_1, \bar{z}_j, \bar{t}_{k+1}), \cdots, v(\bar{r}_M, \bar{z}_j, \bar{t}_{k+1})]^{\mathrm{T}} \tag{3.230b}$$

$$\mathbf{\Theta}_j^{(k+1)} = [\Theta(\bar{r}_0, \bar{z}_j, \bar{t}_{k+1}), \Theta(\bar{r}_1, \bar{z}_j, \bar{t}_{k+1}), \cdots, \Theta(\bar{r}_M, \bar{z}_j, \bar{t}_{k+1})]^{\mathrm{T}} \tag{3.230c}$$

$$\mathbf{\Phi}_j^{(k+1)} = [\phi(\bar{r}_0, \bar{z}_j, \bar{t}_{k+1}), \phi(\bar{r}_1, \bar{z}_j, \bar{t}_{k+1}), \cdots, \phi(\bar{r}_M, \bar{z}_j, \bar{t}_{k+1})]^{\mathrm{T}} \tag{3.230d}$$

$$\boldsymbol{\alpha}_{\mathrm{m}}{}_j^{(k+1)} = [\alpha_{\mathrm{m}}(\bar{r}_0, \bar{z}_j, \bar{t}_{k+1}), \alpha_{\mathrm{m}}(\bar{r}_1, \bar{z}_j, \bar{t}_{k+1}), \cdots, \alpha_{\mathrm{m}}(\bar{r}_M, \bar{z}_j, \bar{t}_{k+1})]^{\mathrm{T}} \tag{3.230e}$$

$$\mathbf{\Phi}_{\mathrm{oil}}{}_j^{(k+1)} = [\phi_{\mathrm{oil}}(\bar{r}_0, \bar{z}_j, \bar{t}_{k+1}), \phi_{\mathrm{oil}}(\bar{r}_1, \bar{z}_j, \bar{t}_{k+1}), \cdots, \phi_{\mathrm{oil}}(\bar{r}_M, \bar{z}_j, \bar{t}_{k+1})]^{\mathrm{T}} \tag{3.230f}$$

The discrete form of the boundary conditions (3.231a)−(3.231c) and the initial conditions (3.231d) are given by:

$$\mathbf{D}\mathbf{U}_j^{(k+1)} = 0,\ \mathbf{D}\mathbf{V}_j^{(k+1)} = 0,\ \mathbf{D}\mathbf{\Theta}_j^{(k+1)} = 0,\ \mathbf{D}\mathbf{\Phi}_j^{(k+1)} = 0,\ \mathbf{D}\boldsymbol{\alpha}_{\mathrm{m}}{}_j^{(k+1)} = 0 \text{ at } \bar{r} = \bar{r}_0 \tag{3.231a}$$

$$\mathbf{U}_j^{(k+1)} = 0,\ \mathbf{V}_j^{(k+1)} = 0,\ \mathbf{\Theta}_j^{(k+1)} = 1,\ \mathbf{\Phi}_j^{(k+1)} = 1 \text{ at } \bar{r} = \bar{r}_M \tag{3.231b}$$

$$\begin{gathered}\mathbf{U}_0^{(k+1)} = 0,\ \mathbf{V}_0^{(k+1)} = 1,\ \mathbf{\Theta}_0^{(k+1)} = 0,\ \mathbf{\Phi}_0^{(k+1)} = 0,\ \boldsymbol{\alpha}_{\mathrm{m}}{}_0^{(k+1)} = 0 \\ \mathbf{\Phi}_{\mathrm{oil}}{}_0^{(k+1)} = 1 - \phi_{\text{water}}\end{gathered} \quad \text{at } \bar{z} = \bar{z}_0 \tag{3.231c}$$

$$\begin{gathered}\mathbf{U}_j^{(0)} = 0,\ \mathbf{V}_j^{(0)} = 0,\ \mathbf{P}_j^{(0)} = 0,\ \mathbf{\Theta}_j^{(0)} = 0,\ \mathbf{\Phi}_j^{(0)} = 0 \\ \boldsymbol{\alpha}_{\mathrm{m}}{}_j^{(0)} = 0,\ \mathbf{\Phi}_{\mathrm{oil}}{}_j^{(0)} = 1 - \phi_{\text{water}},\ \bar{\delta}^0 = 0,\ x^0 = 0\end{gathered} \quad \text{at } \bar{t} = \bar{t}_0 \tag{3.231d}$$

The linear system of algebraic Equations (3.214), (3.217), (3.220), (3.223), (3.225), (3.227) and the corresponding initial-boundary conditions given by Equation (3.231a)−(3.231d) is solved as a matrix of the general form $\mathbf{A}\mathbf{F}^{(k+1)} = \mathbf{R}^{(k)}$, where $\mathbf{F}^{(k+1)}$ and $\mathbf{R}^{(k)}$ are column vectors of size $(M+1)(N+1) \times 1$ while $\mathbf{A}$ is a square matrix of size $(M+1)(N+1) \times (M+1)(N+1)$. In particular, the system (3.214) takes the form

$$\begin{bmatrix} \mathbf{A1}_{0,0} & \mathbf{A1}_{0,1} & \cdots & \mathbf{A1}_{0,N} \\ \mathbf{A1}_{1,0} & \mathbf{A1}_{1,1} & \cdots & \mathbf{A1}_{1,N} \\ \vdots & \vdots & \ddots & \vdots \\ \mathbf{A1}_{N,0} & \mathbf{A1}_{N,1} & \cdots & \mathbf{A1}_{N,N} \end{bmatrix} \begin{bmatrix} \mathbf{U}_0^{(k+1)} \\ \mathbf{U}_1^{(k+1)} \\ \vdots \\ \mathbf{U}_N^{(k+1)} \end{bmatrix} = \begin{bmatrix} \mathbf{R1}_0^{(k)} \\ \mathbf{R1}_1^{(k)} \\ \vdots \\ \mathbf{R1}_N^{(k)} \end{bmatrix} \tag{3.232}$$

where $\mathbf{A1}_{j,n}$'s are square matrices each of size $(M+1) \times (M+1)$ given by

$$\mathbf{A1}_{j,j} = \mathrm{diag}(\mathbf{a}_0)\mathbf{D}^2 + \mathrm{diag}(\mathbf{a}_1)\mathbf{D} + \mathrm{diag}(\mathbf{a}_2)\mathbf{I} + \mathbf{a}_3\mathbf{d}_{j,j}^2\mathbf{I} \tag{3.233a}$$

$$\mathbf{A1}_{j,n} = \mathbf{a}_3\mathbf{d}_{j,n}^2\mathbf{I}, \text{ when } n \neq j. \tag{3.233b}$$

Similarly, the system (3.217) takes the form

$$\begin{bmatrix} \mathbf{A2}_{0,0} & \mathbf{A2}_{0,1} & \cdots & \mathbf{A2}_{0,N} \\ \mathbf{A2}_{1,0} & \mathbf{A2}_{1,1} & \cdots & \mathbf{A2}_{1,N} \\ \vdots & \vdots & \ddots & \vdots \\ \mathbf{A2}_{N,0} & \mathbf{A2}_{N,1} & \cdots & \mathbf{A2}_{N,N} \end{bmatrix} \begin{bmatrix} \mathbf{V}_0^{(k+1)} \\ \mathbf{V}_1^{(k+1)} \\ \vdots \\ \mathbf{V}_N^{(k+1)} \end{bmatrix} = \begin{bmatrix} \mathbf{R2}_0^{(k)} \\ \mathbf{R2}_1^{(k)} \\ \vdots \\ \mathbf{R2}_N^{(k)} \end{bmatrix} \tag{3.234}$$

where $\mathbf{A2}_{j,n}$'s are square matrices each of size $(M+1) \times (M+1)$ given by

$$\mathbf{A2}_{j,j} = \operatorname{diag}(\mathbf{b}_0)\mathbf{D}^2 + \operatorname{diag}(\mathbf{b}_1)\mathbf{D} + \operatorname{diag}(\mathbf{b}_2)\mathbf{I} + \mathbf{b}_3\mathbf{d}_{j,j}^2\mathbf{I} \tag{3.235a}$$

$$\mathbf{A2}_{j,n} = \mathbf{b}_3\mathbf{d}_{j,n}^2\mathbf{I}, \text{ when } n \neq j. \tag{3.235b}$$

The system (3.220) takes the form

$$\begin{bmatrix} \mathbf{A4}_{0,0} & \mathbf{A4}_{0,1} & \cdots & \mathbf{A4}_{0,N} \\ \mathbf{A4}_{1,0} & \mathbf{A4}_{1,1} & \cdots & \mathbf{A4}_{1,N} \\ \vdots & \vdots & \ddots & \vdots \\ \mathbf{A4}_{N,0} & \mathbf{A4}_{N,1} & \cdots & \mathbf{A4}_{N,N} \end{bmatrix} \begin{bmatrix} \mathbf{\Theta}_0^{(k+1)} \\ \mathbf{\Theta}_1^{(k+1)} \\ \vdots \\ \mathbf{\Theta}_N^{(k+1)} \end{bmatrix} = \begin{bmatrix} \mathbf{R4}_0^{(k)} \\ \mathbf{R4}_1^{(k)} \\ \vdots \\ \mathbf{R4}_N^{(k)} \end{bmatrix} \tag{3.236}$$

where $\mathbf{A4}_{j,n}$'s are square matrices each of size $(M+1) \times (M+1)$ given by

$$\mathbf{A4}_{j,j} = \operatorname{diag}(\mathbf{d}_0)\mathbf{D}^2 + \operatorname{diag}(\mathbf{d}_1)\mathbf{D} + \operatorname{diag}(\mathbf{d}_2)\mathbf{I} + \mathbf{d}_3\mathbf{d}_{j,j}^2\mathbf{I} \tag{3.237a}$$

$$\mathbf{A4}_{j,n} = \mathbf{d}_3\mathbf{d}_{j,n}^2\mathbf{I}, \text{ when } n \neq j. \tag{3.237b}$$

The system (3.223) takes the form

$$\begin{bmatrix} \mathbf{A5}_{0,0} & \mathbf{A5}_{0,1} & \cdots & \mathbf{A5}_{0,N} \\ \mathbf{A5}_{1,0} & \mathbf{A5}_{1,1} & \cdots & \mathbf{A5}_{1,N} \\ \vdots & \vdots & \ddots & \vdots \\ \mathbf{A5}_{N,0} & \mathbf{A5}_{N,1} & \cdots & \mathbf{A5}_{N,N} \end{bmatrix} \begin{bmatrix} \mathbf{\Phi}_0^{(k+1)} \\ \mathbf{\Phi}_1^{(k+1)} \\ \vdots \\ \mathbf{\Phi}_N^{(k+1)} \end{bmatrix} = \begin{bmatrix} \mathbf{R5}_0^{(k)} \\ \mathbf{R5}_1^{(k)} \\ \vdots \\ \mathbf{R5}_N^{(k)} \end{bmatrix} \tag{3.238}$$

where $\mathbf{A5}_{j,n}$'s are square matrices each of size $(M+1) \times (M+1)$ given by

$$\mathbf{A5}_{j,j} = \mathbf{I} \tag{3.239a}$$

$$\mathbf{A5}_{j,n} = \mathbf{O}, \text{ when } n \neq j. \tag{3.239b}$$

The system (3.225) takes the form

$$\begin{bmatrix} \mathbf{A6}_{0,0} & \mathbf{A6}_{0,1} & \cdots & \mathbf{A6}_{0,N} \\ \mathbf{A6}_{1,0} & \mathbf{A6}_{1,1} & \cdots & \mathbf{A6}_{1,N} \\ \vdots & \vdots & \ddots & \vdots \\ \mathbf{A6}_{N,0} & \mathbf{A6}_{N,1} & \cdots & \mathbf{A6}_{N,N} \end{bmatrix} \begin{bmatrix} \boldsymbol{\alpha}_{\mathrm{m}0}^{(k+1)} \\ \boldsymbol{\alpha}_{\mathrm{m}1}^{(k+1)} \\ \vdots \\ \boldsymbol{\alpha}_{\mathrm{m}N}^{(k+1)} \end{bmatrix} = \begin{bmatrix} \mathbf{R6}_0^{(k)} \\ \mathbf{R6}_1^{(k)} \\ \vdots \\ \mathbf{R6}_N^{(k)} \end{bmatrix} \tag{3.240}$$

where $\mathbf{A6}_{j,n}$'s are square matrices each of size $(M+1) \times (M+1)$ given by

$$\mathbf{A6}_{j,j} = \mathbf{I} \tag{3.241a}$$

$$\mathbf{A6}_{j,n} = \mathbf{O}, \text{ when } n \neq j. \tag{3.241b}$$

The system (3.227) takes the form

$$\begin{bmatrix} \mathbf{A7}_{0,0} & \mathbf{A7}_{0,1} & \cdots & \mathbf{A7}_{0,N} \\ \mathbf{A7}_{1,0} & \mathbf{A7}_{1,1} & \cdots & \mathbf{A7}_{1,N} \\ \vdots & \vdots & \ddots & \vdots \\ \mathbf{A7}_{N,0} & \mathbf{A7}_{N,1} & \cdots & \mathbf{A7}_{N,N} \end{bmatrix} \begin{bmatrix} \boldsymbol{\Phi}_{\mathrm{oil}0}^{(k+1)} \\ \boldsymbol{\Phi}_{\mathrm{oil}1}^{(k+1)} \\ \vdots \\ \boldsymbol{\Phi}_{\mathrm{oil}N}^{(k+1)} \end{bmatrix} = \begin{bmatrix} \mathbf{R7}_0^{(k)} \\ \mathbf{R7}_1^{(k)} \\ \vdots \\ \mathbf{R7}_N^{(k)} \end{bmatrix} \tag{3.242}$$

where $\mathbf{A7}_{j,n}$'s are square matrices each of size $(M+1) \times (M+1)$ given by

$$\mathbf{A7}_{j,j} = \mathbf{I} \tag{3.243a}$$

$$\mathbf{A7}_{j,n} = \mathbf{O}, \text{ when } n \neq j. \tag{3.243b}$$

The corresponding boundary conditions are imposed on the leading diagonal sub-block matrices of the coefficient matrix in the above systems, i.e., on the main diagonal of the matrices $\mathbf{A1}_{j,j}$, $\mathbf{A2}_{j,j}$, $\mathbf{A4}_{j,j}$, $\mathbf{A5}_{j,j}$, $\mathbf{A6}_{j,j}$ and $\mathbf{A7}_{j,j}$, to yield a new consistent system of linear algebraic equations with a unique solution. The solutions are then obtained by pre-multiplying the matrix equation by the inverse of $\mathbf{A}$, i.e., by $\mathbf{A}^{-1}$, to get

$$\mathbf{F}^{(k+1)} = \mathbf{A}^{-1}\mathbf{R}^{(k)}. \tag{3.244}$$

The matrix system (3.244) is solved starting from suitable initial approximations (or initial guesses). The initial conditions, in this study, are used as the initial guesses. The iteration is repeated for $k = 1, 2, 3, \cdots$, until the following condition is satisfied:

$$\left\| \mathbf{F}^{(k+1)} - \mathbf{F}^{(k)} \right\|_{\infty} < \varepsilon_{\mathrm{tol}}, \tag{3.245}$$

where ϵ_{tol} denotes the prescribed absolute error tolerance which, in this study, is taken as $\varepsilon_{\mathrm{tol}} = 10^{-13}$.

3.12 Predictions Based on Objectives Four and Five

The resulting solutions for the velocity field, temperature field and concentration are then used to determine the rates of wax deposition and deposit aging together with the skin-friction coefficient, rates of heat and mass transfer, as discussed below.

3.12.1 Determination of Rates of Wax Deposition and Deposit Aging

The rate of wax deposition is determined from Equations (3.178) and (3.199). The rate of deposit aging is determined from Equations (3.180) and (3.201).

3.12.2 Determination of Skin-friction Coefficient, Rates of Heat and Mass Transfer

The wall shear stress and the rates of heat and mass transfer are obtained by applying the Bivariate Chebyshev spectral collocation method to the Equations (3.164) in a similar manner to get the following discrete matrix forms.

$$C_f \mathrm{Re} = 2\mathbf{D}\mathbf{V}_j^{k+1},\ \mathrm{Nu}_z = -\mathbf{D}\boldsymbol{\Theta}_j^{k+1},\ \mathrm{Sh}_z = -\mathbf{D}\boldsymbol{\Phi}_j^{k+1},\ \text{at } \bar{r} = \bar{r}_M. \tag{3.246}$$

3.13 Computer Simulations

Computer simulations of the numerical schemes are done in MATLAB® software to obtain the profiles of the flow variables. The data used in the computer simulations is presented in Table 3.1 and Table 3.2. The choices of the parameter values presented in Table 3.1 are to serve as baseline cases for the purpose of generating the profiles of the flow variables. In particular, the Pr values for oils are in the range 50-2000, Re-values in the range $0 < \mathrm{Re} < 2000$ means that the flow is laminar, $\mathrm{Ec} = 1.2$ means that the kinetic energy of flow is greater than the enthalpy difference, $\mathrm{Gr_T} > 0$ corresponds to cooling of the pipeline wall (or heating the fluid in contact with the wall), etc. At each time step, all time-dependent flow variables are updated. The number of collocation points in the radial direction is taken as 19 while that in the axial direction is taken as 15.

The simulation results are presented in chapter 4 in form of graphs and tables, and discussed.

Table 3.1: Values of the Dimensionless Parameters Used in the Computer Simulation.

Parameter	Value
Eckert number, Ec	1.2
Thermal Grashof number, $\mathrm{Gr_T}$	5.0
Mass Grashof number, $\mathrm{Gr_C}$	5.0
Darcy number, Da	1.0×10^{4}
Prandtl number, Pr	50
Reynolds number, Re	$\sqrt{0.5}$
Peclet number, Pe	$50\sqrt{0.5}$
Richardson number, Ri	1
Schmidt number, Sc	1.5
Stanton number, St	1.5
Weber number, We	1.0
Elevation of pipeline, φ	$\pi/12$

Table 3.2: Physical Properties Values Used in the Computer Simulation.

Physical Property	Value	Unit
API gravity of waxy crude oil	18	^{o}API
Volumetric flow rate of waxy crude oil, Q	1	m^3/s
Shear dispersion coefficient, D_{p}	4.8×10^{-3}	m
Diameter of water droplet, $\bar{d}$	1.0×10^{-2}	m
Inner radius of the pipeline, R	0.25	m
Density of oil, ρ_{oil}	950	kg/m^3
Density of water, ρ_{water}	997.1	kg/m^3
Density of gel, ρ_{gel}	900	kg/m^3
Dynamic viscosity of oil, μ_{oil}	0.5	Ns/m^2
Dynamic viscosity of water, μ_{water}	8.9×10^{-4}	Ns/m^2
Dynamic viscosity of gel, μ_{gel}	0.82	Ns/m^2
Coefficient of thermal expansion for oil, $(\beta_{\mathrm{T}})_{\mathrm{oil}}$	0.9	m^3/kg
Coefficient of thermal expansion for water, $(\beta_{\mathrm{T}})_{\mathrm{water}}$	256.32×10^{-6}	m^3/kg
Coefficient of thermal expansion for gel, $(\beta_{\mathrm{T}})_{\mathrm{gel}}$	1.2	m^3/kg
Coefficient of mass expansion for oil, $(\beta_{\mathrm{C}})_{\mathrm{oil}}$	0.9	m^3/kg
Coefficient of mass expansion for water, $(\beta_{\mathrm{C}})_{\mathrm{water}}$	1.0	m^3/kg
Coefficient of mass expansion for gel, $(\beta_{\mathrm{C}})_{\mathrm{gel}}$	1.2	m^3/kg
Specific heat capacity of waxy crude oil, $(Cp)_{\mathrm{oil}}$	2300	J/kgK
Specific heat capacity of water-in-oil emulsions, $(Cp)_{\mathrm{water}}$	4179.6	J/kgK
Specific heat capacity of gel, $(Cp)_{\mathrm{gel}}$	2900	J/kgK
Thermal conductivity of waxy crude oil, k_{oil}	0.1	W/mK
Thermal conductivity of water-in-oil emulsions, k_{water}	0.608	W/mK
Effective thermal conductivity of gel, k_{gel}	0.25	W/mK

CHAPTER FOUR

RESULTS AND DISCUSSION

In this chapter, the effects of varying the various flow parameters such as Reynolds number, Grashof number, Eckert number, Schmidt number, and Weber number on the flow variables, including the skin-friction coefficient, rates of heat and mass transfer and deposit growth and aging rates have been presented. The effects of parametric variations are presented in Section 4.3, the skin-friction coefficient and rates of heat and mass transfer are presented in Section 4.4, the rates of deposit growth and aging are presented in Section 4.5, and the validation of the study results is presented in Section 4.6.

4.1 Profiles of the Flow Variables

This section presents three-dimensional (3D) graphs of the flow variables (i.e., radial velocity, axial velocity, fluid temperature, total wax concentration, wax precipitation kinetics, and volume fraction of crude oil) at different positions $(\bar{r}, \bar{z})$ in the pipeline, at the last time step, to provide an overview of their profiles. From the refined governing equations, namely the coupled system of nonlinear partial differential equations (PDEs) (3.155a)−(3.155g), and the associated boundary conditions (3.158a)−(3.158d) and the initial conditions (3.159), the following 3D surface plots were obtained from computer simulations. The interpretation of the 3D surface plots involves the overall shape of the surface, presence of peaks and/or valleys on the surface, relationship between the independent variables, and colour gradient and how it corresponds to the values of the variable.

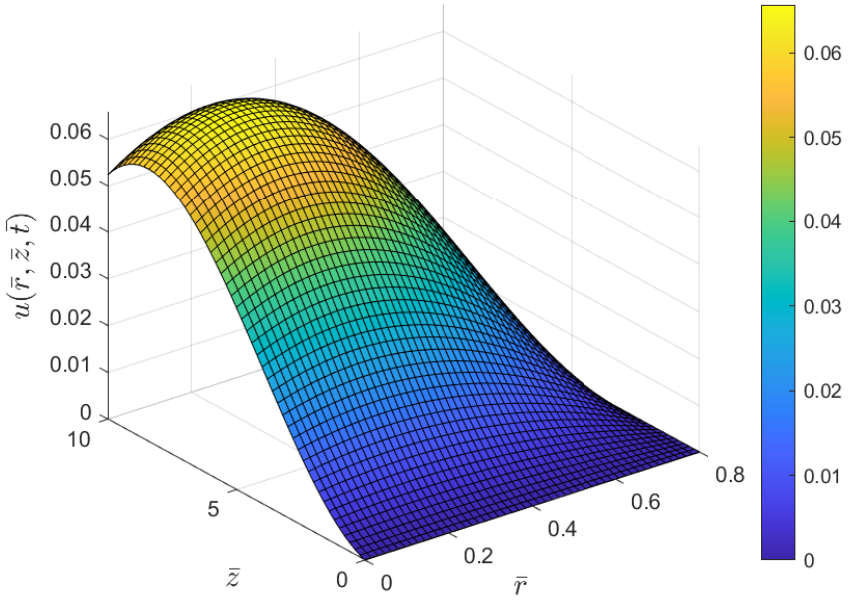

Figure 4.1: A 3D Graph of Radial Velocity Profiles Plotted Against Both Radial and Axial Distances in Waxy Crude Oil Flow Through Pipelines.

Figure 4.1 shows a three-dimensional surface plot of the radial velocity (u) plotted against radial distance ($\bar{r}$) and axial distance ($\bar{z}$). It is observed that the radial velocity distribution of waxy crude oil within the pipe exhibits a saddle-shaped pattern, indicating that the radial velocity of the waxy crude oil varies significantly across the pipe's radial and axial directions. As the radial distance increases from the pipe's center, the radial velocity decreases, approaching zero near the walls. This suggests that the flow of the oil is primarily concentrated at the center of the pipe. Along the axial direction, the radial velocity initially increases, reaching a maximum value at a certain point, implying that the flow of the oil is accelerated as it moves along the pipe due to the pressure gradient. Beyond the peak velocity point, the radial velocity decreases, suggesting that the flow is gradually decelerated due to frictional forces at the pipe walls. The peak represents the point of maximum radial velocity and flow concentration.

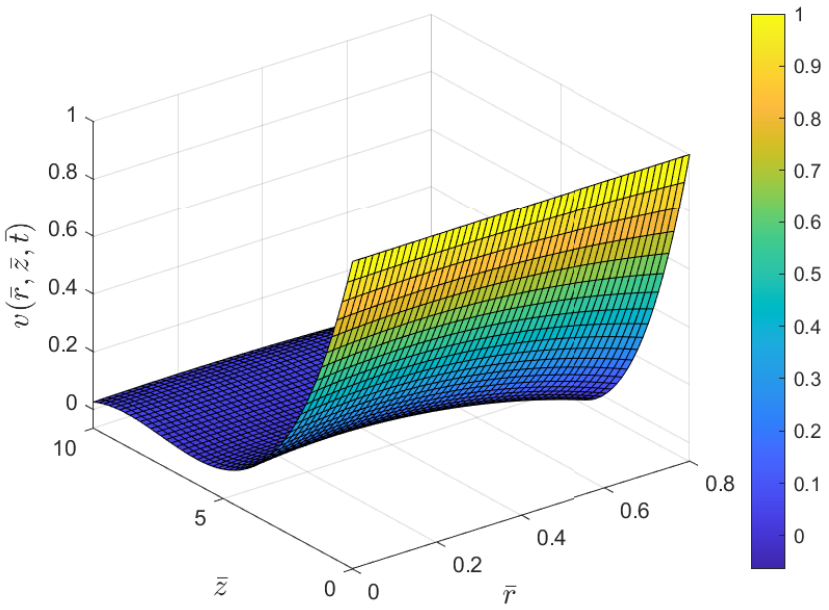

Figure 4.2: A 3D Graph of Axial Velocity Profiles Plotted Against Both Radial and Axial Distances in Waxy Crude Oil Flow Through Pipelines.

Figure 4.2 shows a three-dimensional surface plot of the axial velocity (v) plotted against radial distance ($\bar{r}$) and axial distance ($\bar{z}$). It is observed that the axial/streamwise velocity distribution of the waxy crude oil in the pipeline exhibits a dome-shaped pattern, with a distinct valley at the center of the pipe and the axial velocity decreases gradually towards the pipe walls. This suggests that the flow of the oil is primarily concentrated at the center of the pipe. Along the axial direction, the axial velocity remains relatively constant, implying that the flow velocity does not vary significantly with the distance from the pipe inlet. The valley represents the point of minimum axial velocity, indicating the region where the oil flow is least concentrated and slowest.

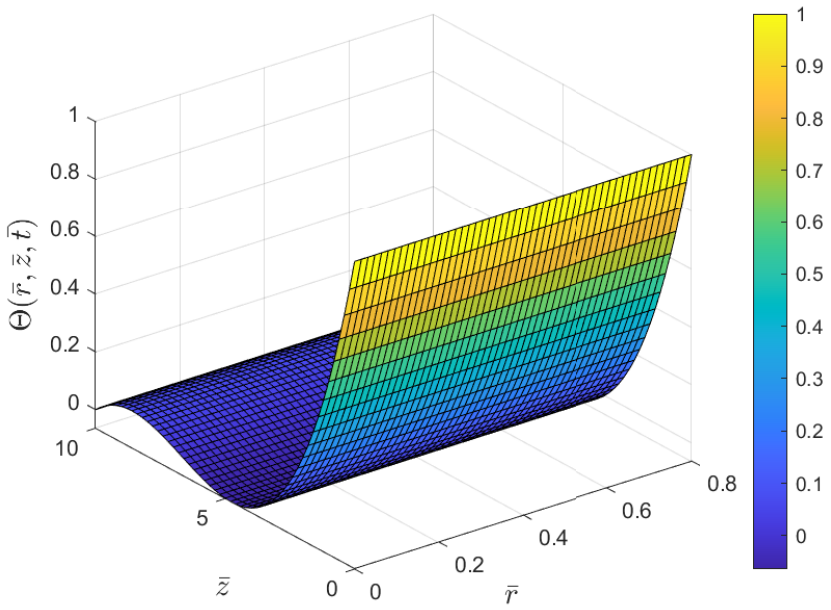

Figure 4.3: A 3D Graph of Temperature Profiles Plotted Against Both Radial and Axial Distances in Waxy Crude Oil Flow Through Pipelines.

Figure 4.3 shows a three-dimensional surface plot of the temperature (Θ) plotted against radial distance ($\bar{r}$) and axial distance ($\bar{z}$). It is observed that the temperature distribution in the pipeline exhibits a smooth and curved surface, indicating a relatively uniform temperature profile. The temperature increases with increasing radial distance from the pipe center, suggesting that heat transfer from the surrounding environment significantly influences the temperature distribution. Additionally, the temperature tends to increase along the pipe length, implying that the oil flow also contributes to the temperature distribution. The absence of distinct peaks or valleys further supports the observation of a smooth and continuous temperature distribution. The temperature variation along the radial distance is more pronounced than along the axial distance, suggesting that heat transfer from the surrounding environment plays a more significant role in determining the temperature profile than the oil flow. Moreover, the temperature is higher near the pipe walls and at the top of the pipe. This is due to the direct contact of the pipe walls with the surrounding environment, which is typically at a higher temperature than the waxy crude oil. Additionally, the oil at the top of the pipe is closer to the heat source, which is typically located at the upstream end of the pipeline. The uniform temperature distribution suggests that the heat transfer mechanisms, including conduction from the pipe walls and convective flow of the oil, are effective in maintaining a relatively constant temperature throughout the pipeline. This is crucial for preventing the solidification of wax crystals, which can obstruct the flow of oil and lead to pipeline

failures.

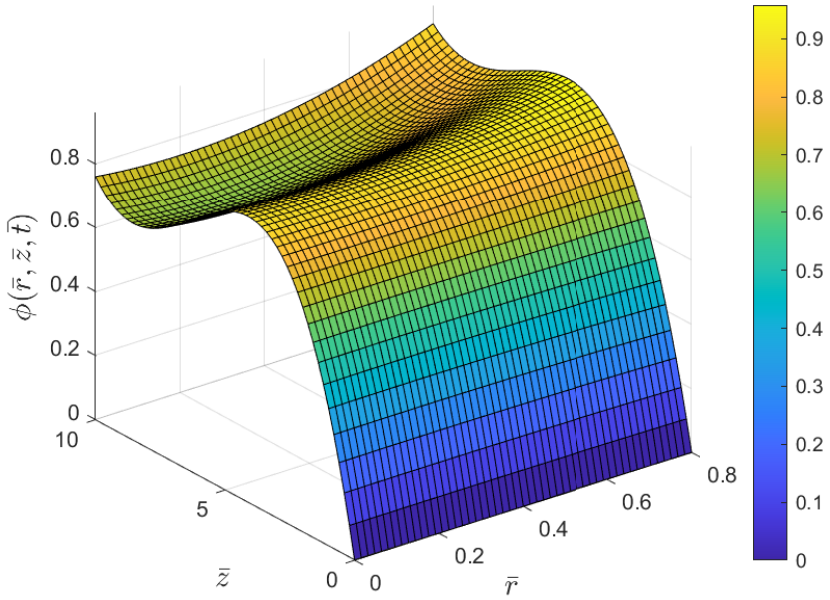

Figure 4.4: A 3D Graph of Total Wax Concentration Profiles Plotted Against Both Radial and Axial Distances in Waxy Crude Oil Flow Through Pipelines.

Figure 4.4 shows a three-dimensional surface plot of the total wax concentration (ϕ) plotted against radial distance ($\bar{r}$) and axial distance ($\bar{z}$). It is observed that the total concentration of waxy components exhibits a ridge-shaped pattern, indicating a non-uniform distribution within the pipe. The total concentration of waxy components in the crude oil pipeline decreases with increasing radial distance from the pipe's center, suggesting that waxy components tend to accumulate towards the center of the pipe, possibly due to lower shear forces in that region. Along the axial direction, the concentration initially increases, reaching a peak value at a specific axial location, and then gradually decreases towards the downstream end of the pipeline. This suggests that the waxy components tend to concentrate in a particular region along the pipe's length, possibly due to factors such as changes in flow conditions or the presence of nucleation sites. This peak represents the point of maximum concentration, indicating the region where the waxy components are most abundant. Thus, the total concentration of waxy components exhibits a strong dependence on both radial distance and axial position. The non-uniform distribution could lead to the formation of wax deposits, which can obstruct the flow of oil and cause pipeline failures.

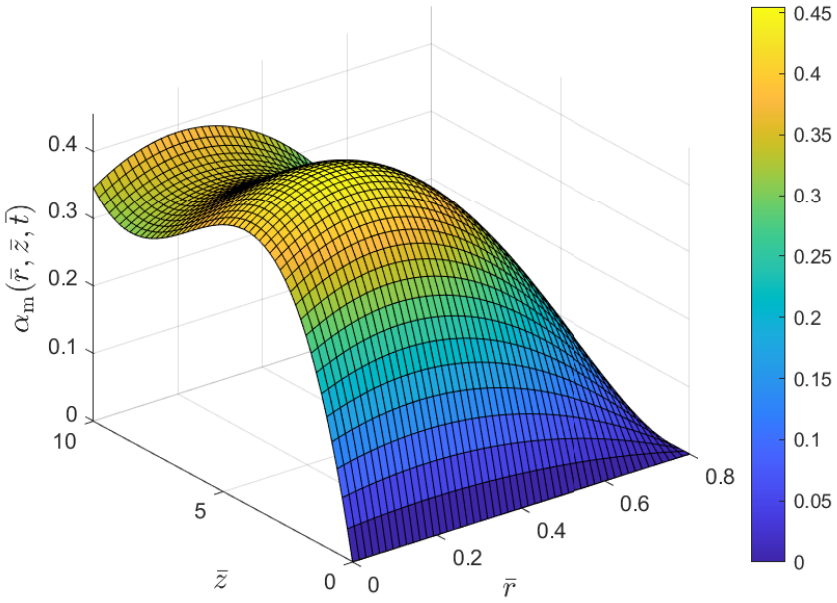

Figure 4.5: A 3D Graph of Wax Aggregation Degree Profiles Plotted Against Both Radial and Axial Distances in Waxy Crude Oil Flow Through Pipelines.

Figure 4.5 shows a three-dimensional surface plot of the wax aggregation degree (α_m) plotted against radial distance ($\bar{r}$) and axial distance ($\bar{z}$). It is observed that the aggregation degree of wax crystals in the gel layer exhibits a relatively flat and slightly curved surface, indicating a relatively uniform distribution for the aggregation of wax crystals throughout the pipe. However, there is a slight increase in the aggregation degree of wax crystals from the center of the pipe toward the pipe walls, implying that the aggregation of wax crystals is slightly more pronounced near the pipe walls due to the lower shear forces near the pipe walls, which may promote the formation of larger wax crystal clusters. Also, the aggregation degree of wax crystals in the gel layer shows a slight increase from the upstream end of the pipeline toward the downstream end, possibly due to the gradual release of waxy components from the oil phase and the formation of nucleation sites along the pipe's length. Overall, the aggregation degree of wax crystals shows a weak dependence on radial distance and a slightly stronger dependence on axial position. This suggests that the aggregation process is relatively consistent throughout the pipe, with localized areas of higher aggregation near the pipe walls and toward the downstream end of the pipeline.

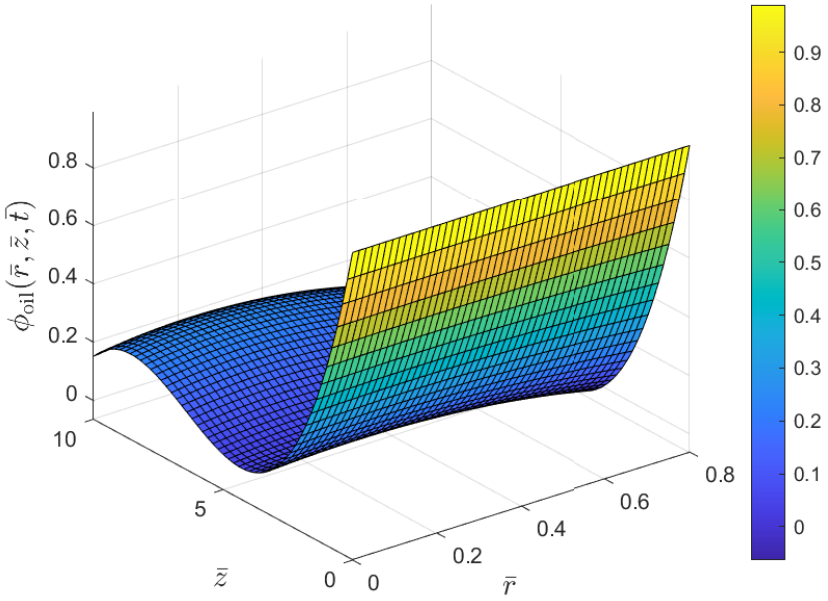

Figure 4.6: A 3D Graph of Oil Volume Fraction Profiles Plotted Against Both Radial and Axial Distances in Waxy Crude Oil Flow Through Pipelines.

Figure 4.6 shows a three-dimensional surface plot of the oil volume fraction (ϕ_{oil}) plotted against radial distance ($\bar{r}$) and axial distance ($\bar{z}$). It is observed that the volume fraction of crude oil exhibits a relatively smooth and slightly curved surface, indicating a relatively uniform distribution throughout the pipe. The oil volume fraction decreases toward the pipe walls and along the axial direction of the pipe, suggesting that there is a slight increase in the proportion of wax deposits and other non-oil components in these regions. The gradual decrease in crude oil volume fraction from the center of the pipe toward the walls implies that wax deposits and other non-oil components tend to accumulate more toward the pipe walls, possibly due to slower flow velocities near the pipe walls. The slight decrease in crude oil volume fraction from the upstream end of the pipeline toward the downstream end suggests that the accumulation of wax deposits and other non-oil components tends to increase with increasing flow distance, possibly due to the gradual release of waxy components from the oil phase and the formation of nucleation sites along the pipe's length. The oil volume fraction shows a weak dependence on radial distance and a slightly stronger dependence on axial position. The relatively uniform distribution in the volume fraction indicates a consistent distribution of crude oil and non-oil components throughout the pipe, while the gradual decreases in volume fraction of crude oil toward the pipe walls and along the axial direction suggest that wax deposits and other non-oil components tend to accumulate in these regions. This accumulation could lead to the formation of blockages and flow restrictions, which

can disrupt the operation of the pipeline.

4.2 Temporal Evolution of the Flow Variables

In this section, the flow variables are plotted against time to analyze their temporal evolution. The results are presented in the form of graphs, which are carefully examined and discussed.

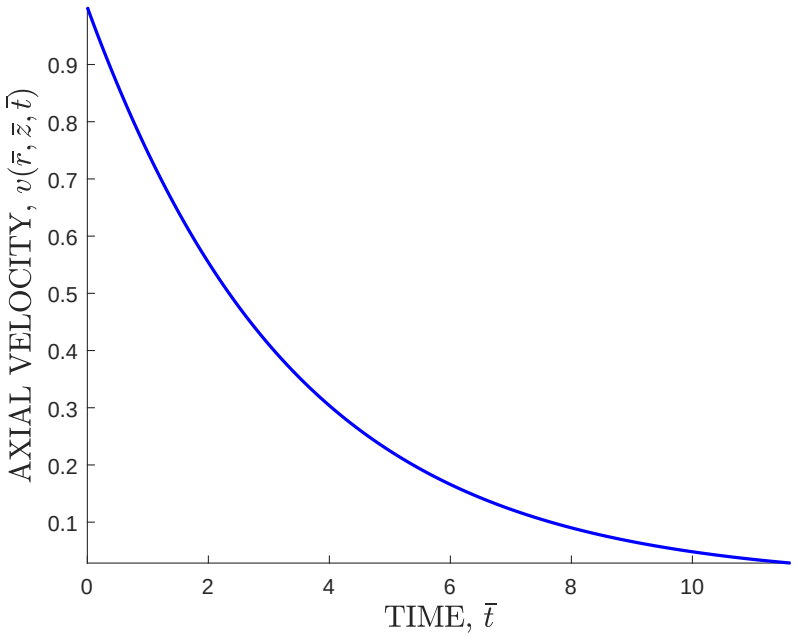

Figure 4.7: Temporal Evolution of the Axial Velocity.

It is observed in Figure 4.7 that the axial velocity profile of waxy crude oil within the pipeline decreases with an increase in time. This is attributed to the gradual accumulation of wax crystals on the pipe walls, which constricts the flow path and reduces the effective cross-sectional area of the pipeline. This constriction effectively reduces the overall flow velocity, contributing to the decrease in axial velocity. Over time, detached wax particles may settle towards the bottom of the pipeline, further reducing the effective flow area and hindering fluid movement. Additionally, the presence of wax deposit can create a temperature gradient along the pipeline. As wax crystals accumulate, they absorb heat from the flowing crude oil, causing a temperature decrease near the wall. This temperature gradient affects the wax precipitation kinetics, potentially accelerating the deposition process and exacerbating the velocity reduction.

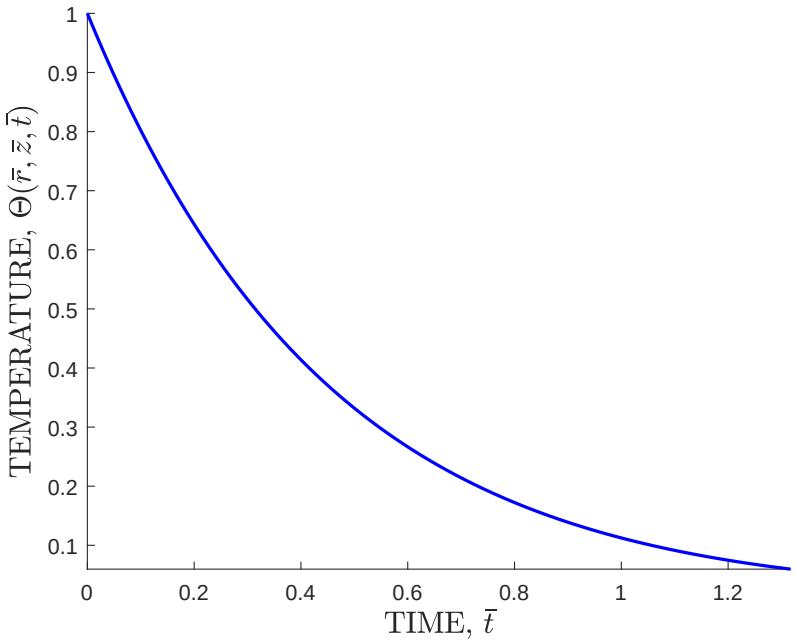

Figure 4.8: Temporal Evolution of the Temperature.

It is observed in Figure 4.8 that the temperature profile of waxy crude oil within the pipeline decreases with an increase in time. This behavior is attributed to the interplay between the heat transfer process and wax deposition. As waxy crude oil flows through the pipeline, it loses heat to the cooler surroundings through the pipeline walls. This heat loss is proportional to the temperature difference between the crude oil and the environment, causing the crude oil to gradually cool down. Furthermore, as wax crystals deposit on the pipeline walls, they release latent heat of fusion, further cooling the waxy crude oil. This exothermic process contributes to the overall decrease in temperature over time.

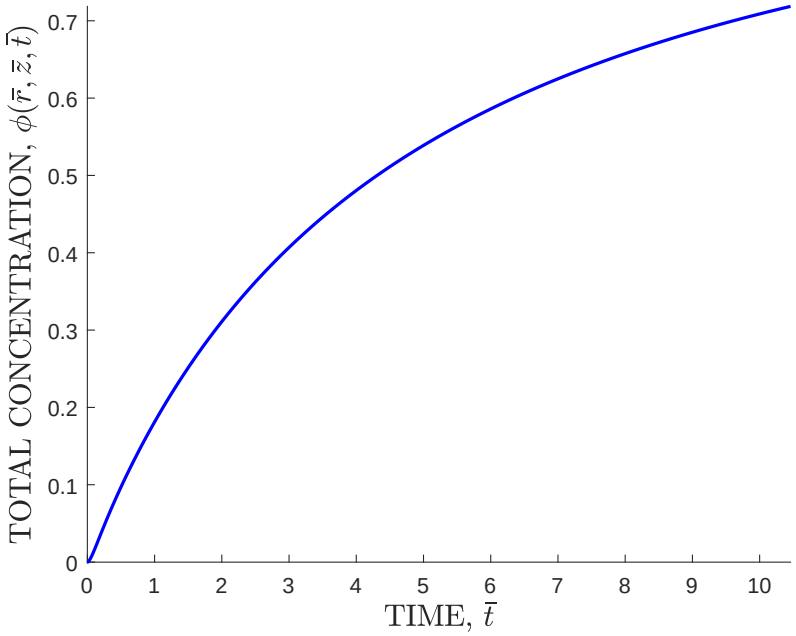

Figure 4.9: Temporal Evolution of the Total Concentration of Wax Molecules.

It is observed in Figure 4.9 that the concentration profile of wax molecules in waxy crude oil within the pipeline increases steadily with an increase in time. This increase is attributed to the ongoing precipitation of wax crystals as the oil temperature decreases. As the temperature falls below the wax appearance temperature (WAT), the solubility of wax molecules in the oil diminishes, causing them to precipitate out of solution and form wax crystals. These newly formed wax crystals then disperse throughout the oil, leading to a gradual increase in the overall concentration of wax molecules.

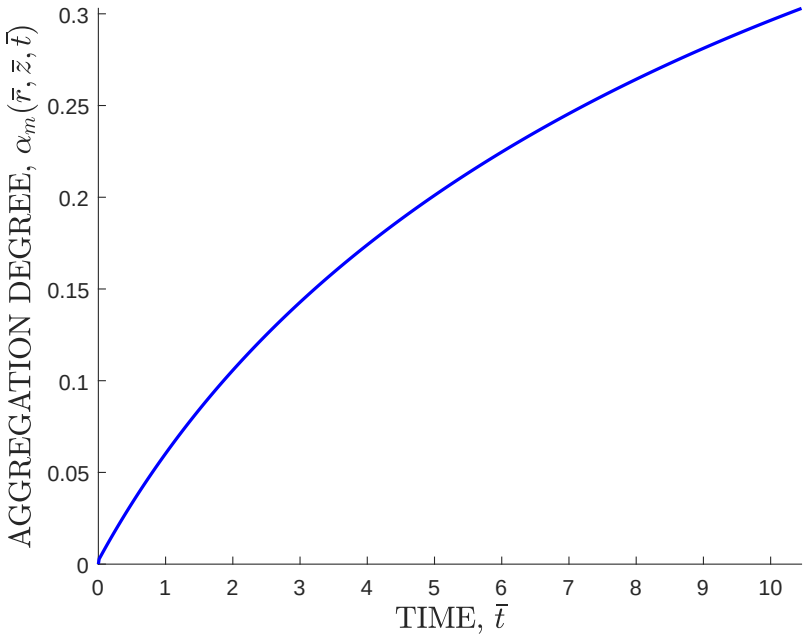

Figure 4.10: Temporal Evolution of the Aggregation Kinetics of Wax.

It is observed in Figure 4.10 that the aggregation degree profile of wax crystals within the waxy crude oil pipeline increases steadily with time. This is because as the crude oil temperature decreases, wax molecules in the oil phase start to form small clusters, known as wax crystals. This process of wax crystal formation, called nucleation, is continuous and occurs throughout the pipeline. Once wax crystals are formed, they continue to grow by attaching to other wax molecules in the oil phase. This growth process is continuous and contributes to the increase in aggregation degree over time.

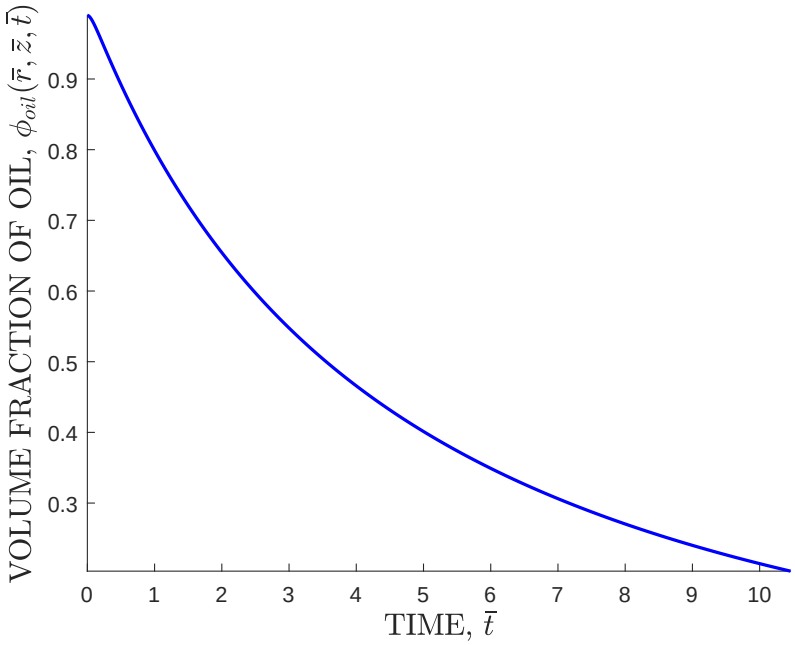

Figure 4.11: Temporal Evolution of the Oil Volume Fraction.

It is observed in Figure 4.11 that the oil volume fraction profile for waxy crude oil within the pipeline decreases steadily with an increase in time. This reduction is attributed to the progressive accumulation of wax crystals on the pipe walls. As wax crystals precipitate and grow, they occupy a larger volume, effectively displacing the oil and gradually reducing the overall oil volume fraction. This displacement of oil is particularly pronounced near the pipe walls, where the wax crystals preferentially accumulate due to the lower temperatures and enhanced shear rates. The reduction in oil volume fraction can have several implications for the flow behavior of waxy crude oil. For example, it can lead to the formation of unstable oil-wax interfaces. These unstable interfaces can become sites for further wax precipitation and deposition, further contributing to the potential blockage of the pipeline.

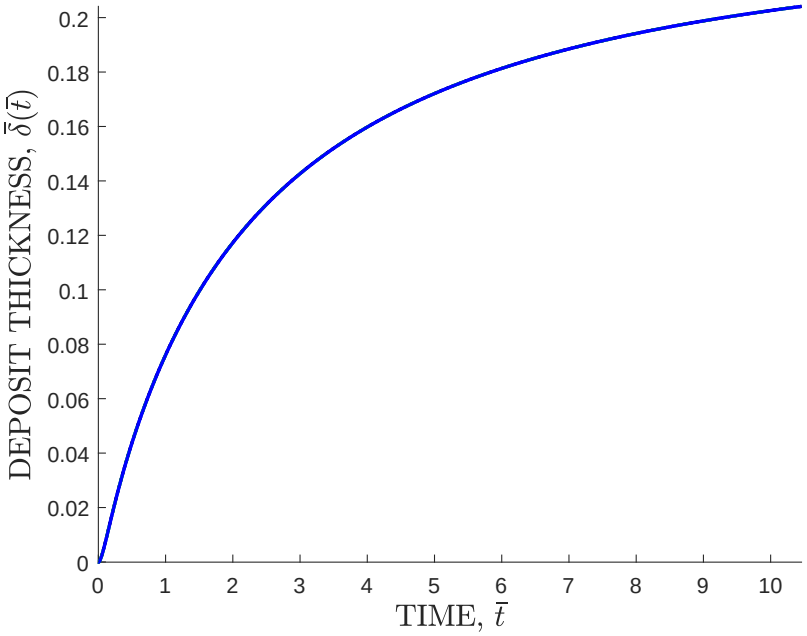

Figure 4.12: Temporal Evolution of the Wax Deposit Thickness.

It is observed in Figure 4.12 that the wax deposition thickness profile for waxy crude oil within the pipeline increases initially and then plateaus, reaching a steady-state. This behavior is attributed to the interplay between wax deposition and removal processes. Initially, as the waxy crude oil flows through the pipeline and its temperature falls below the wax appearance temperature (WAT), wax molecules precipitate from the solution and form wax crystals. These crystals accumulate on the pipe walls, leading to a gradual increase in the wax deposit thickness. The wax deposition rate is initially high due to the substantial concentration gradient between the bulk oil and the pipe wall, creating a favorable environment for crystal nucleation and growth. However, as the wax deposit thickness increases, the wax deposit acts as an insulator, impeding heat transfer from the bulk oil to the pipe wall. This reduced heat transfer slows down the wax precipitation kinetics, causing the deposition rate to decline over time. Eventually, a steady-state is reached when the deposition rate is balanced by the removal rate, resulting in a stable wax deposit thickness profile.

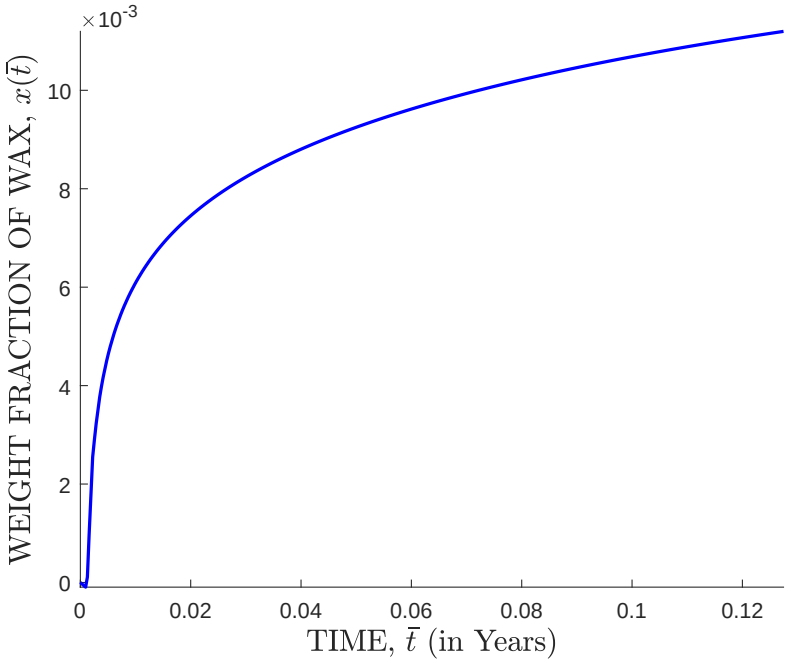

Figure 4.13: Temporal Evolution of the Weight Fraction of Wax in the Gel Layer.

It is observed in Figure 4.13 that the weight fraction of wax crystals in the gel layer for the flow of waxy crude oil within the pipeline increases with an increase in time and then reaches a steady-state. This behavior is attributed to the interplay between wax deposition and gelation processes. Initially, as waxy crude oil flows through the pipeline, wax crystals precipitate and accumulate on the pipe walls, forming a gel layer. This gel layer gradually increases in weight fraction as more wax crystals deposit and integrate into the gel structure. However, as the weight fraction of wax crystals in the gel layer increases, the growing gel layer enhances the viscosity of the oil near the pipe walls, hence weakening the shear forces that can disrupt the gel structures. This reduced shear force decelerates the gelation process and impedes the further incorporation of wax crystals into the gel layer. Eventually, a steady-state is attained when the rate of wax deposition and gelation is balanced by the reduced rate of crystal incorporation and gel growth, resulting in a stable weight fraction of wax crystals in the gel layer.

4.3 Effects of Varying Flow Parameters on the Flow Variables

This section presents the results of a parametric study aimed at investigating the effects of various flow parameters on the flow variables. The flow variables in this study are the

radial velocity, axial velocity, temperature, species concentration, aggregation degree and volume fraction of oil. The following two-dimensional graphs are the results obtained by varying the various flow parameters, one at a time.

4.3.1 Effects of Varying Reynolds Number

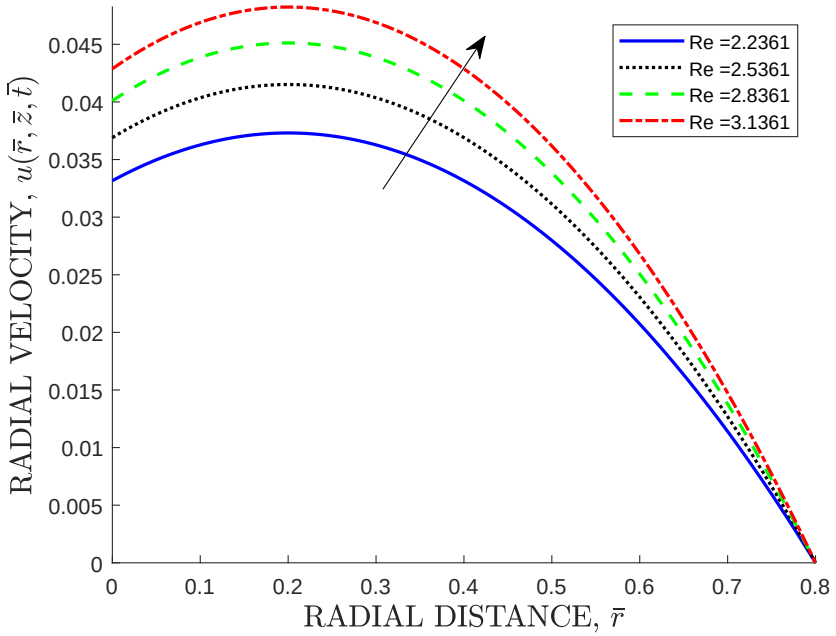

Figure 4.14: Effects of Varying Re **on the Radial Velocity Profiles**.

It is observed from Figure 4.14 that an increase in Reynolds number leads to an increase in the radial velocity profiles of waxy crude oil in the pipeline under laminar flow conditions. The Reynolds number represents the ratio of inertial forces to viscous forces acting on a fluid element. The observed trend can be attributed to the enhanced shear stress acting on the fluid. As the Reynolds number increases, the shear stress, which represents the frictional force between adjacent fluid layers, becomes strong enough to induce mixing between the layers. This mixing, known as shear dispersion, facilitates the distribution of wax particles more evenly across the pipe radius. The increased shear stress enables the waxy molecules to overcome the cohesive forces that tend to aggregate them, allowing them to slide past each other more easily. Consequently, the tendency of wax particles to deposit on the pipe walls decreases, and the radial velocity profiles become more uniform across the radial direction.

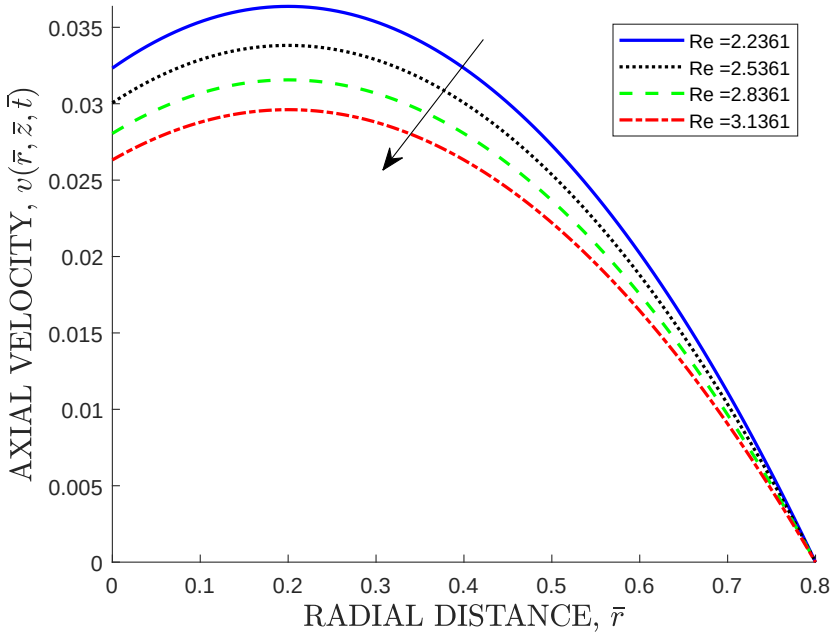

Figure 4.15: Effects of Varying Re **on the Axial Velocity Profiles**.

It is observed from Figure 4.15 that an increase in Reynolds number results in a decrease in the axial velocity profiles of waxy crude oil in the pipeline under laminar flow conditions. This trend can be attributed to the enhanced drag force acting on the fluid. As the Reynolds number increases, the drag force, which opposes the movement of fluid particles, also intensifies. The increased drag force causes the fluid particles to decelerate in the axial direction, leading to a reduction in the average axial velocity. Additionally, with an increase in Reynolds number, the axial velocity profile becomes more non-uniform. The slower-moving fluid particles near the oil-gel interface exert a retarding effect on the faster-moving fluid particles at the pipe centerline, contributing to the decline in average axial velocity.

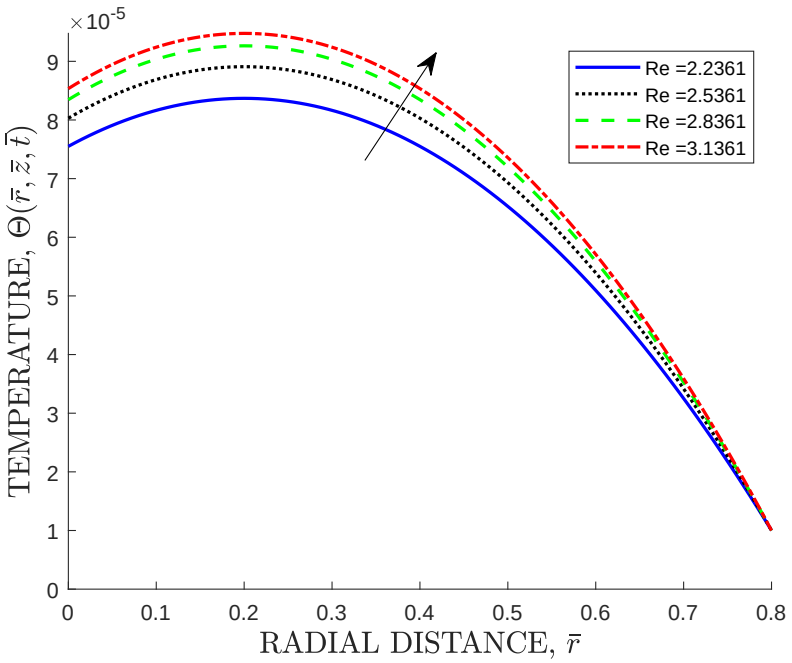

Figure 4.16: Effects of Varying Re **on the Temperature Profiles**.

It is observed from Figure 4.16 that an increase in Reynolds number leads to an increase in the temperature profiles of waxy crude oil in the pipeline under laminar flow conditions. As the Reynolds number increases, the shear stress, which represents the frictional force between adjacent fluid layers, also intensifies. This increased shear stress causes the waxy crude oil molecules to rub against each other with greater force, generating heat due to internal friction. The generated heat is then transferred to the surrounding fluid, resulting in an overall increase in temperature. Furthermore, with an increase in Reynolds number, the thickness of the thermal boundary layer, which is a thin layer of fluid adjacent to the oil-deposit interface where temperature gradients are significant, decreases. This reduction in boundary layer thickness can be attributed to the increased shear stress, which disrupts the stagnant layer of fluid near the pipe wall and promotes more efficient heat transfer. The thinner boundary layer allows heat to dissipate more effectively from the oil-deposit interface into the bulk fluid, contributing to the overall increase in temperature profiles.

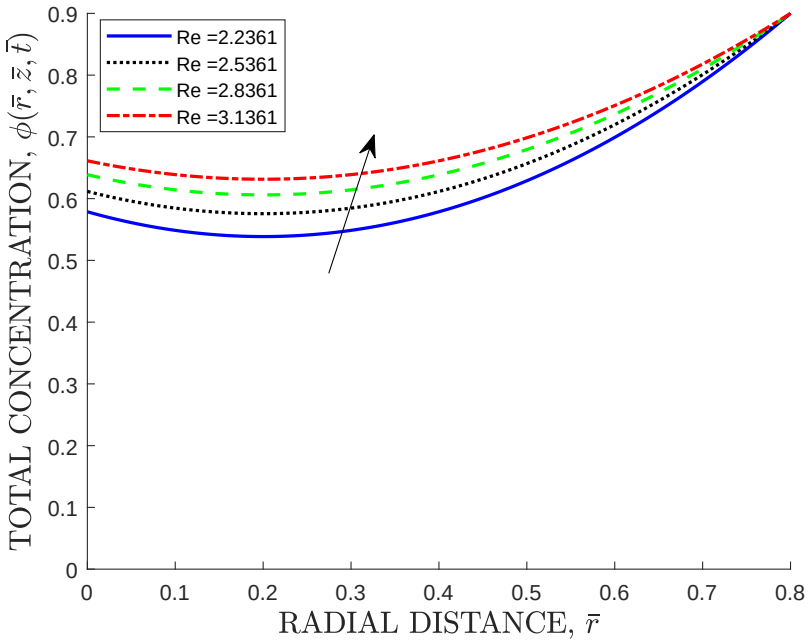

Figure 4.17: Effects of Varying Re **on the Concentration Profiles**.

It is observed from Figure 4.17 that an increase in Reynolds number leads to an increase in the total concentration profiles of wax in crude oil pipelines under laminar flow conditions. This trend arises because higher Reynolds numbers signify stronger fluid motion driven by inertial forces relative to viscous forces. As the Reynolds number increases, the waxy crude oil encounters greater fluid movement in the radial direction, promoting mixing within the pipeline. This increased flow facilitates the distribution and dispersion of waxy components more evenly throughout the fluid, resulting in higher total concentration profiles. In essence, the enhanced fluid motion counteracts the tendency of waxy components to settle or adhere to the oil-gel interface, leading to a more uniform distribution of waxy crude oil within the pipeline.

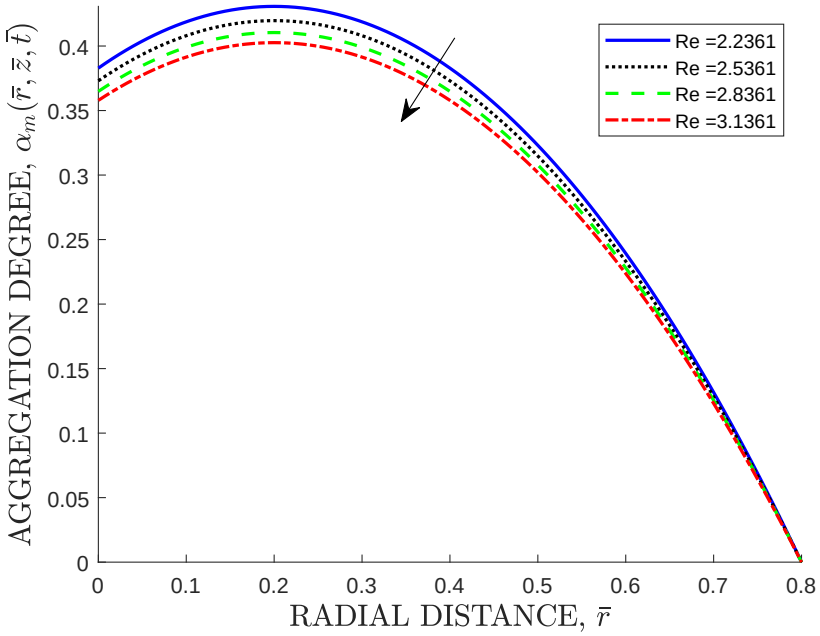

Figure 4.18: Effects of Varying Re **on the Aggregation Degree Profiles**.

It is observed from Figure 4.18 that an increase in Reynolds number leads to a decrease in the aggregation degree profiles of wax crystals in crude oil pipelines under laminar flow conditions. This trend is attributed to the stronger fluid motion driven by inertial forces relative to viscous forces at higher Reynolds numbers. When the Reynolds number increases, the fluid's enhanced radial velocity and turbulence promote better mixing and dispersion of waxy components. This vigorous flow hinders the waxy particles from sticking together or forming aggregates, resulting in lower aggregation degree profiles. Essentially, the enhanced fluid motion disrupts the tendency of waxy components to clump or adhere to each other, thereby reducing aggregation within the pipeline.

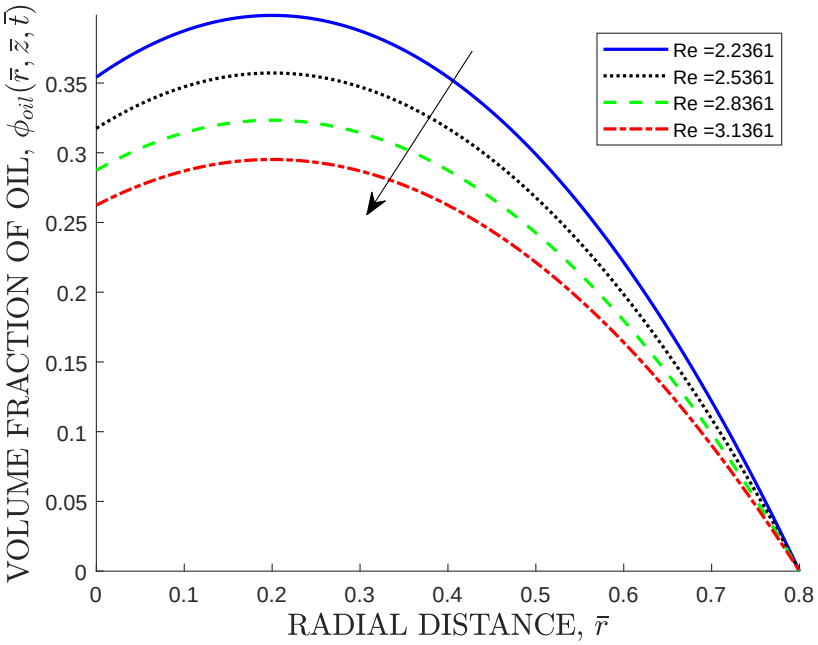

Figure 4.19: Effects of Varying Re **on the Volume Fraction of Oil Profiles**.

It is observed from Figure 4.19 that an increase in Reynolds number leads to a decrease in the volume fraction occupied by crude oil in the pipeline under laminar flow conditions. As the Reynolds number increases, shear stress between fluid layers also increases. This increased shear stress causes the waxy crude oil molecules to deform and flow more readily, promoting the dispersion of wax crystals within the fluid. The increased shear stress breaks up the agglomerates of wax crystals, causing them to become more uniformly dispersed within the fluid, resulting in an overall increase in wax concentration. This increase in wax concentration leads to a reduction in the volume fraction of crude oil. Moreover, the increased shear stress also minimizes wax deposition on the oil-gel interface. As the waxy crystals are more effectively dispersed, they are less prone to precipitation and adhesion to the pipe wall, reducing the accumulation of wax deposits. This reduced deposition enables more wax crystals to remain in suspension within the bulk fluid, further contributing to the reduction in the volume fraction of crude oil. This phenomenon bears practical implications for the efficient transport and processing of crude oil in pipelines, as it directly impacts the quality and composition of the transported fluid.

4.3.2 Effects of Varying Mass Grashof Number

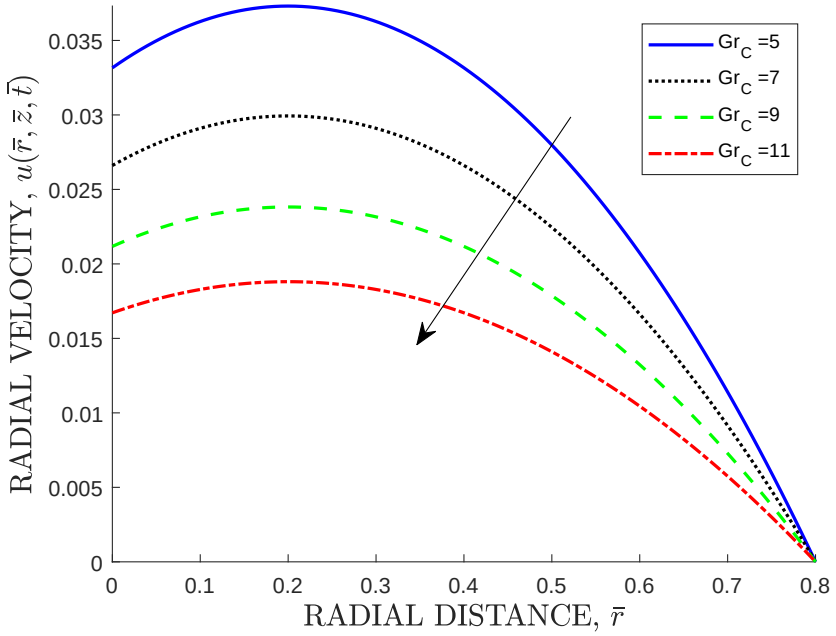

Figure 4.20: Effects of Varying $\mathrm{Gr_C}$ on the Radial Velocity Profiles.

It is observed from Figure 4.20 that an increase in the mass Grashof number leads to a decrease in the radial velocity profiles of waxy crude oil in the pipeline. Mass Grashof number indicates the ratio of the buoyancy forces acting on the wax crystals to the viscous hydrodynamic forces. The observed trend arises from the enhanced buoyancy forces acting on the wax crystals associated with higher mass Grashof number. This increased buoyancy forces cause the wax crystals to rise towards the oil-gel interface, forming a layer of wax-enriched fluid with higher viscosity compared to the surrounding bulk oil, leading to a reduction in its flow rate. Therefore, the velocity boundary layers adjacent to the oil-gel interface thicken. The thickened boundary layer impedes radial fluid motion, consequently reducing the radial velocities across the pipe's cross-sectional area.

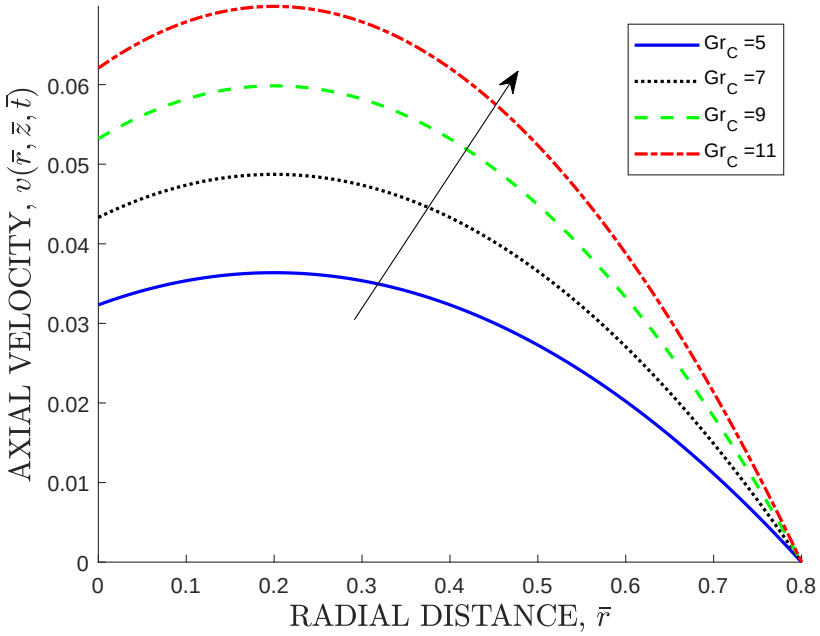

Figure 4.21: Effects of Varying $\mathrm{Gr_C}$ on the Axial Velocity Profiles.

It is observed from Figure 4.21 that an increase in the mass Grashof number leads to an increase in the axial velocity profiles of waxy crude oil in the pipeline. As the mass Grashof number increases, the species buoyancy forces become more dominant relative to viscous hydrodynamic forces. Consequently, the buoyancy of the waxy crude oil increases, making it more likely to move upward within the pipeline. The upward movement of waxy crude oil induces a flow of oil in the axial direction of the pipeline. This axial flow thins the hydrodynamic boundary layer, the layer of oil adjacent to the pipe wall that is slowed down due to friction. The thinned hydrodynamic boundary layer facilitates the unrestricted flow of waxy crude oil in the axial direction, resulting in an increase in the axial velocity profile.

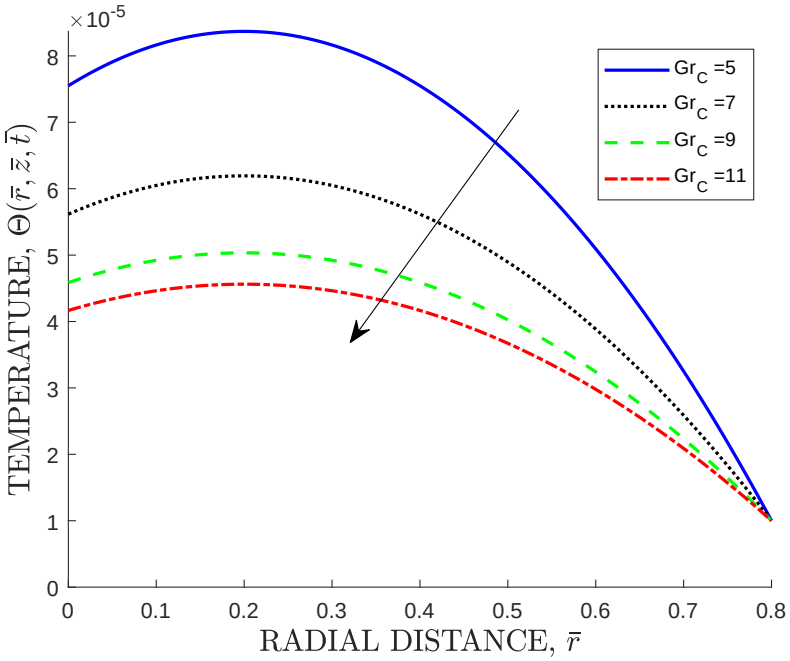

Figure 4.22: Effects of Varying $\mathrm{Gr_C}$ on the Temperature Profiles.

It is observed from Figure 4.22 that an increase in the mass Grashof number leads to a decrease in the temperature profiles of waxy crude oil in the pipeline. With increasing mass Grashof number, buoyant forces acting on the fluid become more dominant than viscous forces. This means that the warmer, less dense oil at the pipe centerline rises more readily, while the cooler, denser oil near the oil-gel interface sinks more readily. This circulation of oil promotes a more uniform distribution of heat throughout the pipe, consequently leading to a reduced overall temperature profile.

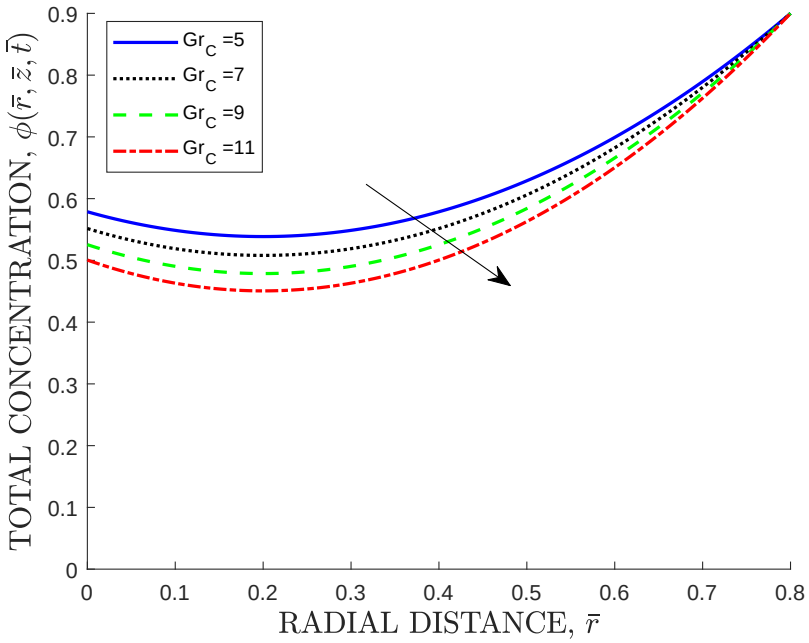

Figure 4.23: Effects of Varying $\mathrm{Gr_C}$ on the Concentration Profiles.

It is observed from Figure 4.23 that an increase in the mass Grashof number leads to a decrease in the total concentration profiles of wax molecules in the crude oil pipeline. The observed trend arises from the increased dominance of species buoyancy forces over viscous hydrodynamic forces. With increasing mass Grashof number, buoyant forces propel wax molecules away from the oil-gel interface and towards the bulk of the fluid. The enhanced natural convection currents within the oil promote a more comprehensive mixing of wax molecules across the pipeline's cross-section. Consequently, the concentration of wax molecules near the pipe centerline diminishes, resulting in a decline in the overall concentration profile.

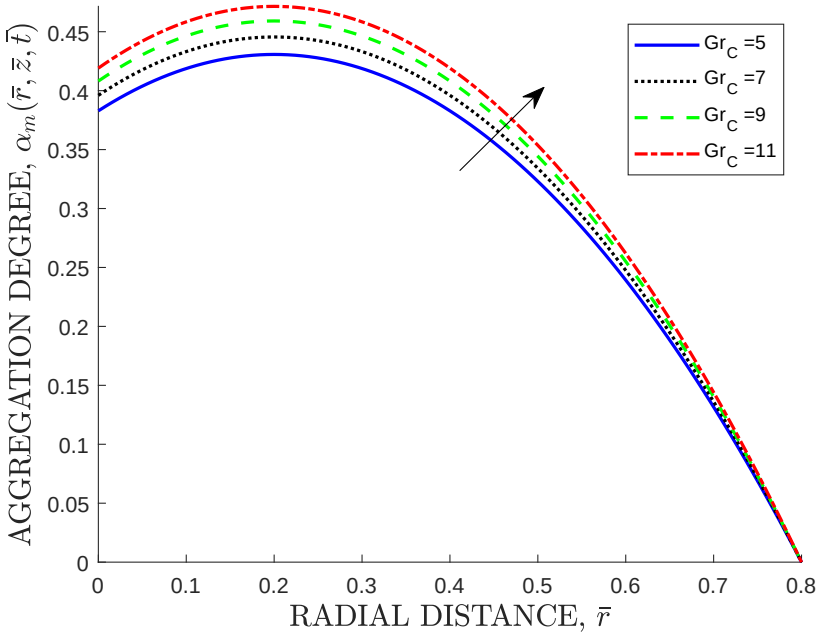

Figure 4.24: Effects of Varying $\mathrm{Gr_C}$ on the Aggregation Degree Profiles.

It is observed from Figure 4.24 that an increase in the mass Grashof number leads to an increase in the aggregation degree profiles of wax crystals on the pipe wall in crude pipelines. This is because as the mass Grashof number increases, the buoyancy forces acting on the fluid also intensify. These intensified buoyancy forces drive a more vigorous convective flow, which promotes mixing and shear stress within the fluid. This increased turbulence in the flow creates eddies and vortices that promote the dispersion and collision of wax crystals, increasing the likelihood of their aggregation. Aggregation occurs when wax crystals collide and adhere to each other, forming larger clusters. These larger clusters are more likely to deposit on the pipe wall due to their increased inertia and reduced ability to remain suspended in the flow.

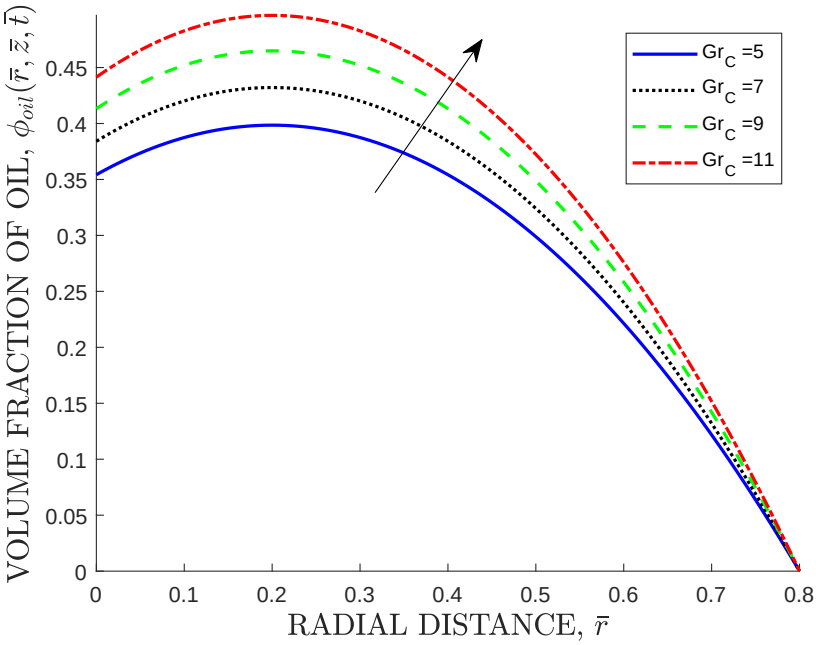

Figure 4.25: Effects of Varying $\mathrm{Gr_C}$ on the Volume Fraction of Oil Profiles.

It is observed from Figure 4.25 that an increase in the mass Grashof number causes an increase in the volume fraction occupied by crude oil in the pipeline. The observed trend is because as the mass Grashof number increases, the buoyancy forces acting on the wax crystals become stronger, causing them to disperse more effectively within the crude oil. This dispersion reduces the tendency of wax crystals to accumulate and form deposits on the pipe wall, thereby increasing the volume fraction of crude oil flowing through the pipeline.

4.3.3 Effects of Varying Eckert Number

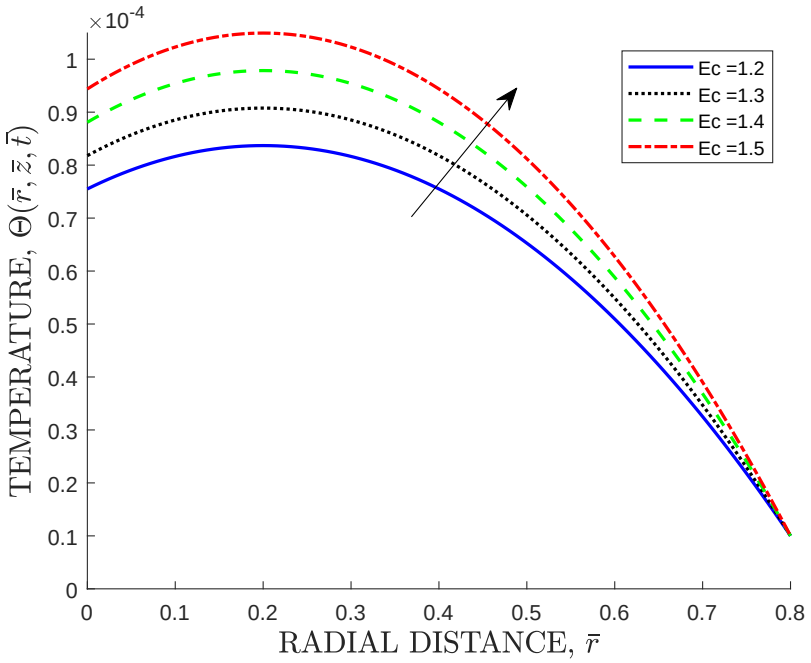

Figure 4.26: Effects of Varying Ec **on the Temperature Profiles**.

It is observed from Figure 4.26 that an increase in the Eckert number leads to an increase in the temperature profiles of waxy crude oil within the pipeline. This phenomenon is attributed to the enhanced viscous heating effect. The Eckert number represents the ratio of viscous dissipation to thermal conduction. As the Eckert number increases, the viscous shear stresses acting on the oil also increase. This increased shear stress generates more heat through viscous dissipation, which in turn increases the oil temperature. The increased temperature enhances Brownian motion of the wax crystals, causing them to collide more frequently and break down into smaller particles. These smaller particles are less prone to deposition and contribute to a more uniform temperature distribution across the pipeline.

4.3.4 Effects of Varying Weber Number

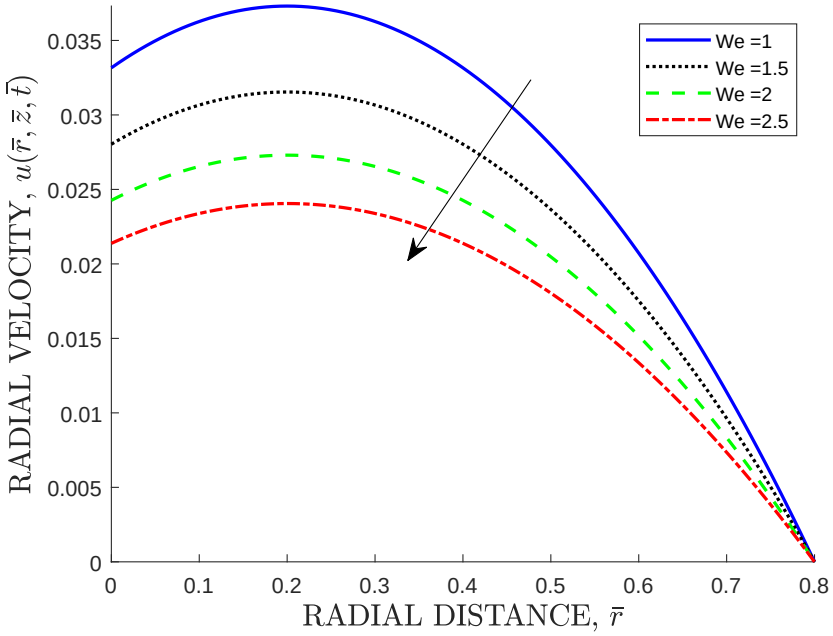

Figure 4.27: Effects of Varying We **on the Radial Velocity Profiles**.

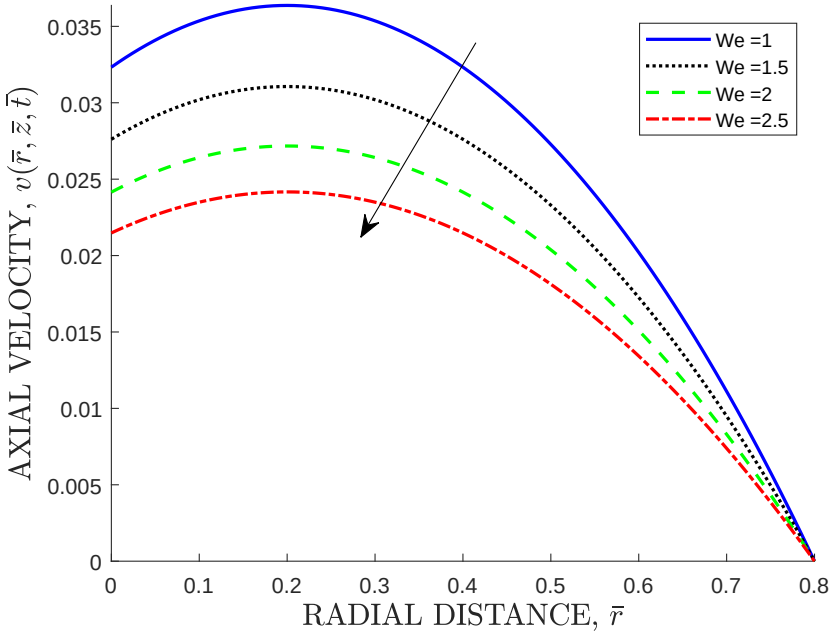

Figure 4.28: Effects of Varying We **on the Axial Velocity Profiles**.

It is observed from Figure 4.27 and Figure 4.28 that an increase in the Weber number causes a decrease in both radial and axial velocity profiles of waxy crude oil within the pipeline. The Weber number represents the ratio of inertial forces to surface tension forces within the fluid. With an increase in the Weber number, inertial forces, which are responsible for dispersing fluid particles, become relatively more dominant in comparison to surface tension forces, which act to stick fluid particles together. Consequently, the fluid's resistance to deformation or breakup due to surface tension weakens as inertial forces take precedence. This weakening leads to a decrease in the fluid's capacity to sustain radial and axial velocities, resulting in a decrease in the velocity profiles.

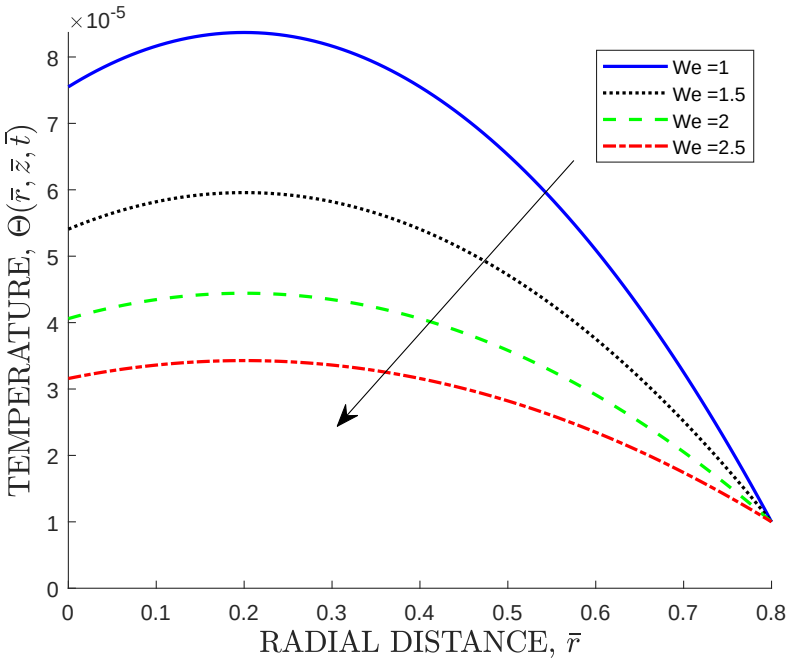

Figure 4.29: Effects of Varying We **on the Temperature Profiles**.

It is observed from Figure 4.29 that an increase in the Weber number leads to a decrease in the temperature profiles of waxy crude oil within the pipeline. This decrease is attributed to the enhanced mixing and heat transfer between the oil and the surrounding environment. With an increase in the Weber number, inertial forces, which are responsible for fluid mixing and turbulence, become relatively more dominant compared to surface tension forces, which tend to dampen mixing. This increased dominance of inertial forces leads to enhanced turbulence and mixing within the oil, promoting heat transfer from the oil's core to its outer regions. Consequently, the temperature at the pipeline's centerline, which represents the core of the flow, decreases. The increased turbulence also results in the formation of a thinner thermal boundary layer near the pipe

wall. The thermal boundary layer is a region of the fluid where temperature gradients are significant. A thinner boundary layer indicates more efficient heat transfer between the oil and the surrounding environment, further contributing to the decrease in temperature of the bulk oil.

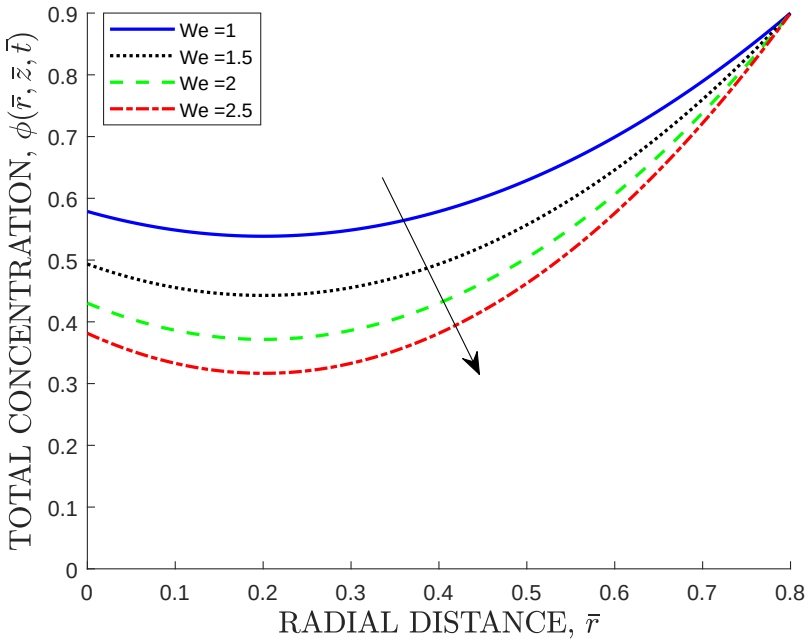

Figure 4.30: Effects of Varying We **on the Concentration Profiles**.

It is observed from Figure 4.30 that an increase in Weber number causes a decrease in the total concentration profiles of waxy crude oil within the pipeline. The observed trend is attributed to enhanced mixing and shear-induced wax dispersion. With an increase in the Weber number, inertial forces, which are responsible for fluid mixing and turbulence, become relatively more dominant compared to surface tension forces, which tend to promote wax particle aggregation and deposition. The increased turbulence promotes the mixing of the oil phases, distributing waxy particles more uniformly throughout the pipeline cross-section. This reduces the concentration of wax particles in the near-wall region, where deposition is most likely to occur.

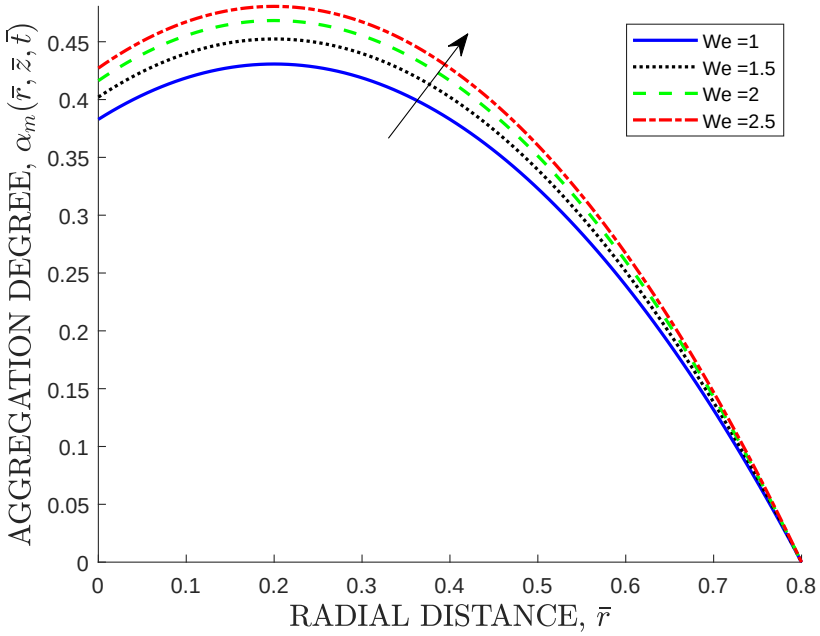

Figure 4.31: Effects of Varying We **on the Aggregation Degree Profiles**.

It is observed from Figure 4.31 that an increase in the Weber number causes an increase in the aggregation degree profiles of wax crystals within crude oil pipeline. This increase is attributed to the weakening of surface tension forces relative to inertial forces as the Weber number increases. This weakening allows wax crystals to overcome surface tension and collide with each other more frequently. Consequently, wax crystals are more likely to aggregate or stick together and form larger clusters, leading to higher aggregation degree profiles near the oil-gel interface.

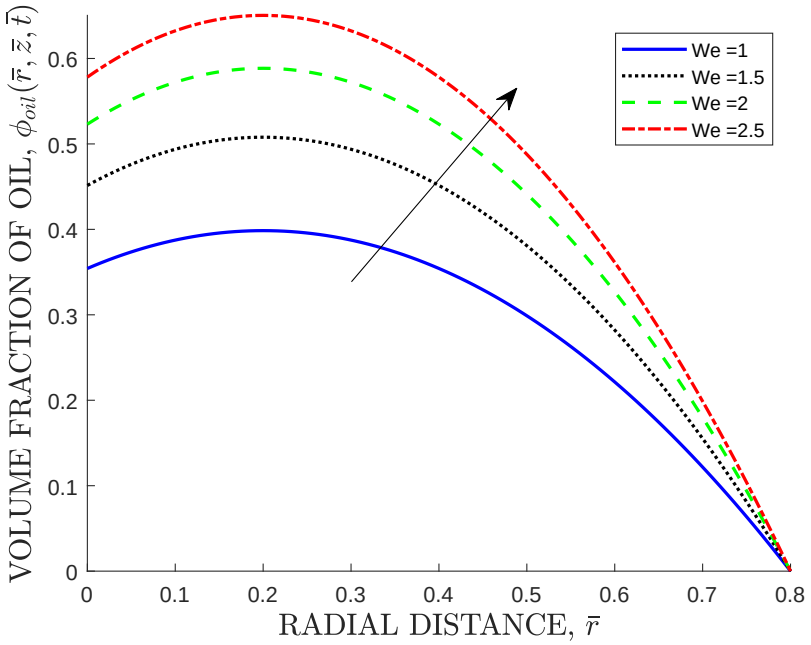

Figure 4.32: Effects of Varying We **on the Volume Fraction of Oil**.

It is evident from Figure 4.32 that an increase in the Weber number causes an increase in the volume fraction occupied by crude oil within the pipeline. The observed trend is because higher Weber numbers represent stronger inertial forces relative to surface tension forces. As a result, the fluid is less constrained by surface tension and has a greater tendency to flow as a continuous, bulk fluid rather than forming stable droplets. This leads to a higher volume fraction occupied by crude oil within the pipeline because the fluid particles are less likely to adhere to the walls and has higher tendency of occupying a larger portion of the pipeline's internal volume.

4.4 Skin-Friction Coefficient and Rates of Heat and Mass Transfer

The quantities of practical interest in this study are the skin-friction coefficient and the rates of heat and mass transfer. The parameters Re, $\mathrm{Gr_T}$, $\mathrm{Gr_C}$, Ec, Sc, and We are varied on the local skin-friction coefficient ($C_f\mathrm{Re}$), local Nusselt number (Nu_z) and local Sherwood number (Sh_z) and their numerical values are presented in Table 4.1.

Table 4.1: Skin-friction Coefficient and Rates of Heat and Mass Transfer for Various Values of the Parameters Re**,** $\mathrm{Gr_T}$**,** $\mathrm{Gr_C}$**,** Ec**,** Sc**, and** We

Re	$\mathrm{Gr_T}$	$\mathrm{Gr_C}$	Ec	Sc	We	$C_f\mathrm{Re}$	Nu_z	Sh_z
2.24	5	5	1.2	1.5	1.0	0.1230	1.9907	1.3916
3.24	5	5	1.2	1.5	1.0	0.1874	1.9912	1.3206
4.24	5	5	1.2	1.5	1.0	0.2926	1.9911	1.2494
2.24	10	5	1.2	1.5	1.0	0.1246	1.9907	1.3926
2.24	15	5	1.2	1.5	1.0	0.1262	1.9907	1.3935
2.24	20	5	1.2	1.5	1.0	0.1277	1.9907	1.3944
2.24	5	10	1.2	1.5	1.0	0.2038	1.9915	1.4182
2.24	5	15	1.2	1.5	1.0	0.2793	1.9921	1.4438
2.24	5	20	1.2	1.5	1.0	0.3495	1.9925	1.4683
2.24	5	5	2.7	1.5	1.0	0.1233	1.9890	1.3922
2.24	5	5	4.2	1.5	1.0	0.1236	1.9874	1.3928
2.24	5	5	5.7	1.5	1.0	0.1238	1.9857	1.3933
2.24	5	5	1.2	3.0	1.0	0.1098	1.9906	1.4851
2.24	5	5	1.2	4.5	1.0	0.1055	1.9905	1.5162
2.24	5	5	1.2	6.0	1.0	0.1033	1.9905	1.5318
2.24	5	5	1.2	1.5	1.5	0.1113	1.9919	1.5007
2.24	5	5	1.2	1.5	2.0	0.1047	1.9925	1.5614
2.24	5	5	1.2	1.5	2.5	0.1004	1.9929	1.6002

From the table, the following observations are noted:

i) An increase in the Reynolds number (Re) increases the skin friction coefficient but leads to a decrease in the Nusselt number and Sherwood number. This phenomenon is a consequence of the relationship between wall shear stress and the velocity gradient. As Re rises, the velocity profile increases, resulting in higher wall shear stress and, consequently, an elevated skin friction coefficient. Additionally, the increase in Re causes the thermal boundary layer to thicken, leading to a decreased Nusselt number. The Sherwood number, on the other hand, diminishes because higher Reynolds numbers cause a thickening of the concentration boundary layer, reducing the rate of species transport within it.

ii) An increase in the thermal Grashof number ($\mathrm{Gr_T}$) increases the skin friction coefficient and Sherwood number, but has no effect on the Nusselt number. The rise in the skin friction coefficient is attributed to the thermal Grashof number causing an increase in velocity, which subsequently thins the velocity boundary layer. Conversely, the elevation in the Sherwood number is a consequence of the thermal Grashof number leading to a reduction in the thickness of the concentration boundary layer, thereby increasing the rate of species transport

within this layer. The Nusselt number, however, remains unaffected.

iii) An increase in the mass Grashof number ($\mathrm{Gr_C}$) results in an increase in the skin friction coefficient, Nusselt number, and Sherwood number. This observed pattern is because the higher values of the mass Grashof number lead to the thinning of the velocity, thermal, and concentration boundary layers. This, in turn, results in a higher rate of transportation within these boundary layers, accounting for the increased values of the skin friction coefficient, Nusselt number, and Sherwood number.

iv) An increase in the Eckert number (Ec) causes an increase in the skin friction coefficient and Sherwood number but decreases the Nusselt number. This pattern arises from the fact that higher values of the Eckert number result in an increased fluid velocity, subsequently leading to higher wall shear stress. As the Eckert number rises, it also contributes to the thickening of the thermal boundary layer, which reduces the heat transfer rate at the pipeline wall, consequently lowering the Nusselt number. However, this thickening of the thermal boundary layer enhances the rate of species transport, leading to an increase in the Sherwood number.

v) An increase in the Schmidt number (Sc) causes a decrease in the skin friction coefficient and Nusselt number but increases the Sherwood number. This phenomenon is attributed to the influence of the Schmidt number on fluid behavior. As Sc increases, it decelerates the axial velocity of fluid particles, causing the velocity boundary layer to thicken, which in turn reduces the motion of fluid particles and leads to a decrease in the skin friction coefficient. Additionally, the thermal boundary layer thickness increases with higher Sc, resulting in reduced heat transfer at the pipeline wall and a lower Nusselt number. In contrast, the concentration boundary layer thickness decreases with increasing Sc, leading to an enhanced rate of species transportation and an increase in the Sherwood number.

vi) An increase in the Weber number (We) decreases the skin friction coefficient but it increases the Nusselt number and Sherwood number. This trend can be attributed to the influence of the Weber number on the behavior of the fluid. An increase in We results in the deceleration of fluid particle velocities, leading to the thickening of the velocity boundary layer, which subsequently reduces particle motion and causes a decrease in the skin friction coefficient. Moreover, an increase in We causes the thermal boundary layer thickness to decrease, resulting in a higher rate of heat transfer. The Sherwood number experiences an increase because higher values of the Weber number lead to a reduction in concentration boundary layer thickness, enhancing the rate of species transport.

4.5 Deposit Growth and Aging

The data about deposit thickness and weight fraction of wax in the deposit extracted from the computer simulations are also plotted against time, while varying the various flow parameters. Moreover, the values of the deposit growth and aging rates are presented in Table 4.2.

4.5.1 Effects of Flow Parameters on Deposit Thickness

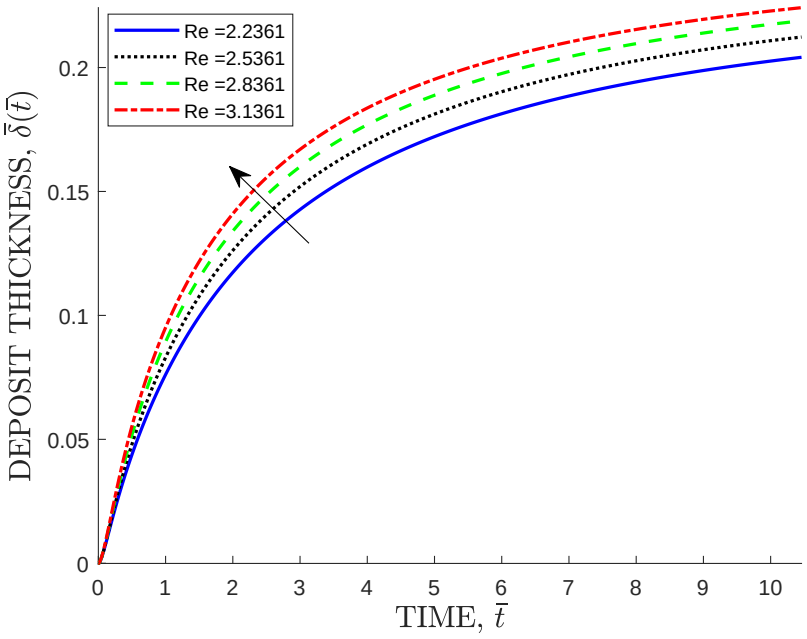

Figure 4.33: Effects of Varying Re **on the Deposit Thickness**.

It is observed in Figure 4.33 that an increase in the Reynolds number causes an increase in the wax deposit thickness for flow of waxy crude oil in a pipeline within the laminar flow regime. Increasing the Reynolds number implies that the inertial forces become more dominant than the viscous forces. This observed trend is attributed to the increase in shear stress at the oil-gel interface as the Reynolds number increases. This shear stress enhances the rate of diffusion of wax molecules from the bulk of the oil to the oil-gel interface. This enhancement occurs because the shear stress causes the wax molecules to move faster from the bulk of the crude oil to the oil-gel interface, which then leads to their precipitation and deposition on the pipe inner wall, consequently increasing the deposit thickness.

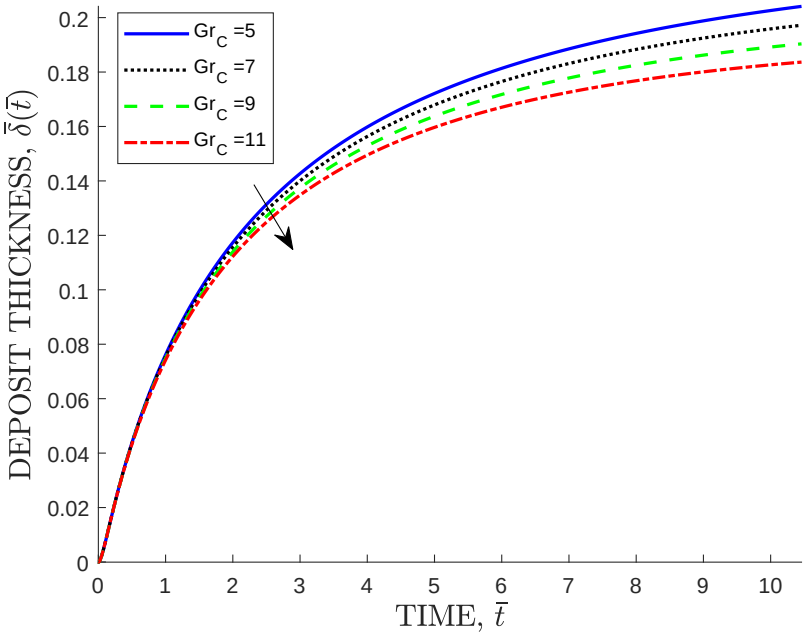

Figure 4.34: Effects of Varying $\mathrm{Gr_C}$ on the Deposit Thickness.

It is observed in Figure 4.34 that an increase in the mass Grashof number causes a decrease in the thickness of wax deposit profiles for flow of waxy crude oil in a pipeline. An increase in the mass Grashof number signifies that buoyancy forces, which arise from density differences due to temperature variations, become more dominant than viscous forces, which govern the flow behavior in laminar conditions in the pipeline. The enhanced buoyancy forces lead to a more buoyant flow pattern, disrupting the diffusion of wax molecules from the bulk oil towards the pipe wall. This diffusion process is crucial for wax deposition to occur. The increased turbulence caused by buoyancy forces can re-entrain wax molecules that have already deposited on the pipe wall, preventing them from forming a thick deposit layer. The dominant buoyancy forces promote a stratified flow pattern, where the oil with the highest wax concentration is located closer to the pipe wall. This reduces the concentration gradient driving wax diffusion, further hindering deposition. The combined effects of disrupted diffusion, wax re-entrainment, and stratified flow lead to a decrease in the rate of wax deposition, resulting in thinner deposit profiles.

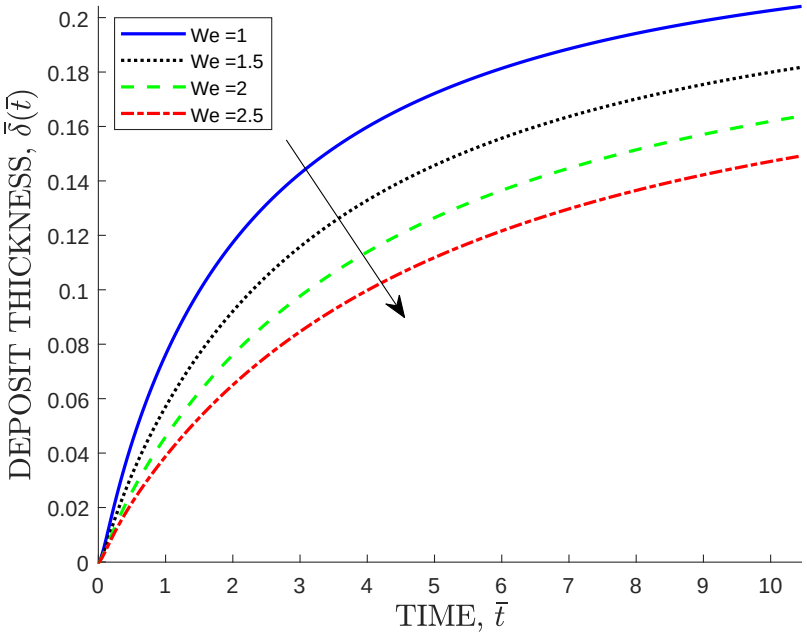

Figure 4.35: Effects of Varying We **on the Deposit Thickness**.

It is observed in Figure 4.35 that an increase in the Weber number causes a decrease in the thickness of wax deposit profiles for flow of waxy crude oil in a pipeline. Increasing the Weber number implies that inertial forces, which represent the flow stresses, become more dominant than surface tension forces, which represent the cohesive forces between wax crystals. Thus, the observed trend is attributed to the interplay between flow stresses and wax deposition processes. As the Weber number increases, the flow stresses near the pipe wall intensify, leading to a more dispersed distribution of wax crystals throughout the flow cross-section. This dispersion diminishes the concentration gradient between the bulk oil and the pipe wall, making it more challenging for wax crystals to adhere to the pipe surface. Furthermore, the elevated flow stresses can act to remove wax crystals that have already deposited on the pipe walls. This mechanical removal process contributes to limiting the overall thickness of the wax deposit.

4.5.2 Effects of Flow Parameters on Weight Fraction of Wax in the Deposit

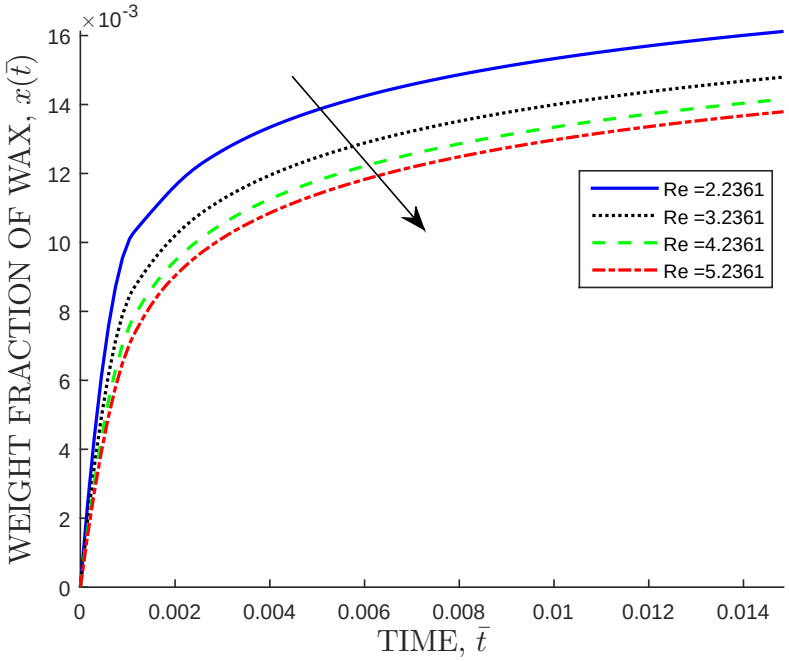

Figure 4.36: Effects of Varying Re on the Weight Fraction of Wax in Oil.

It is observed from Figure 4.36 that an increase in Reynolds number results in a decrease in the weight fraction of wax in the deposited layer. The observed trend is because the exposure of the deposited layer to a range of temperatures and shear stress triggers physical and chemical processes on the wax deposit, which alters its molecular structure and properties. The thermal gradient across the deposit may result in an internal mass flux which yields a continuous increase in the wax content of the deposited layer. Thus it leads to the hardening of the deposit as time elapses, a process called aging of the deposit.

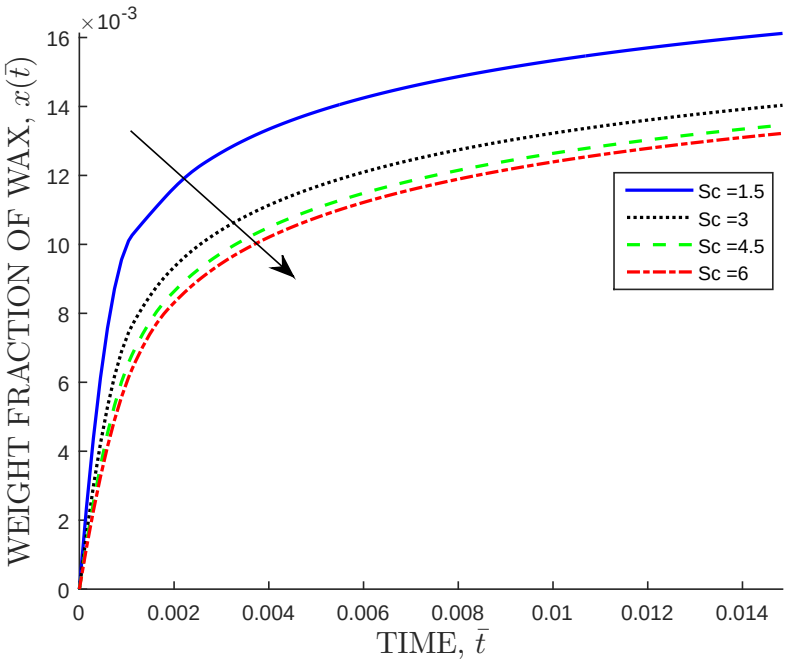

Figure 4.37: Effects of Varying Sc on the Weight Fraction of Wax in Oil.

It is observed from Figure 4.37 that an increase in Schmidt number results in a decrease in the weight fraction of wax in the deposited layer. The observed trend is because the Schmidt number decreases the deposit thickness. Hence, the thinner deposit layer increases the temperature gradient in the deposited layer, which increases the diffusion flux in the deposited layer. Thus it leads to the continuous diffusion of wax molecules into the deposited layer, increasing the wax content in the deposited layer.

4.5.3 Rates of Deposit Growth and Aging

Table 4.2: Rates of Deposit Growth and Aging for Various Values of the Parameters Re**,** $\mathrm{Gr_T}$**,** $\mathrm{Gr_C}$**,** Ec**,** Sc**, and** We

Re	$\mathrm{Gr_T}$	$\mathrm{Gr_C}$	Ec	Sc	We	Growth Rate	aging Rate
2.24	5	5	1.2	1.5	1.0	2.067×10^{-5}	4.990×10^{-4}
3.24	5	5	1.2	1.5	1.0	1.190×10^{-5}	3.174×10^{-4}
4.24	5	5	1.2	1.5	1.0	8.139×10^{-6}	2.245×10^{-4}
2.24	10	5	1.2	1.5	1.0	2.067×10^{-5}	4.997×10^{-4}
2.24	15	5	1.2	1.5	1.0	2.067×10^{-5}	5.005×10^{-4}
2.24	20	5	1.2	1.5	1.0	2.068×10^{-5}	5.012×10^{-4}
2.24	5	10	1.2	1.5	1.0	2.069×10^{-5}	5.221×10^{-4}
2.24	5	15	1.2	1.5	1.0	2.070×10^{-5}	5.467×10^{-4}
2.24	5	20	1.2	1.5	1.0	2.071×10^{-5}	5.727×10^{-4}
2.24	5	5	2.7	1.5	1.0	2.065×10^{-5}	4.990×10^{-4}
2.24	5	5	4.2	1.5	1.0	2.064×10^{-5}	4.991×10^{-4}
2.24	5	5	5.7	1.5	1.0	2.062×10^{-5}	4.991×10^{-4}
2.24	5	5	1.2	3.0	1.0	7.572×10^{-6}	2.962×10^{-4}
2.24	5	5	1.2	4.5	1.0	4.443×10^{-6}	2.114×10^{-4}
2.24	5	5	1.2	6.0	1.0	3.108×10^{-6}	1.650×10^{-4}
2.24	5	5	1.2	1.5	1.5	2.085×10^{-5}	5.960×10^{-4}
2.24	5	5	1.2	1.5	2.0	2.097×10^{-5}	6.707×10^{-4}
2.24	5	5	1.2	1.5	2.5	2.105×10^{-5}	7.300×10^{-4}

It is observed from Table 4.2 that both the Reynolds number and Schmidt number significantly affect the wax deposit growth and aging rates. As the wax flow progresses, the deposit growth and aging rates decrease due to an increase in the interfacial temperature (because the oil-deposit interface moves away from the pipeline wall) and to the onset of deposit removal.

4.5.4 Prediction of Wax Deposit Thickness and Weight Fraction of Wax in the Gel Layer

This study proposes simplified prediction models for the deposit thickness and weight fraction of wax in the gel layer using the Lagrange interpolation technique. Applying the MATLAB® Basic Fitting toolkit to Figures 4.12 and 4.13, we obtain the following polynomials:

$$\begin{aligned}\delta(t) = &-\left(1.529\times10^{-6}\right)t^6+\left(5.746\times10^{-5}\right)t^5-\left(8.772\times10^{-4}\right)t^4\\ &+\left(7.095\times10^{-3}\right)t^3-\left(3.388\times10^{-2}\right)t^2+\left(1.054\times10^{-1}\right)t \qquad (4.1)\end{aligned}$$

and

$$x(t) = -\left(1.9 \times 10^{6}\right) t^{4} + \left(6.6 \times 10^{4}\right) t^{3} - \left(8.3 \times 10^{2}\right) t^{2} + 4.6t \tag{4.2}$$

Equation (4.1) is used to estimate the deposit thickness, while equation (4.2) is used to estimate the weight fraction of wax in the gel layer at any time t.

The deposit growth and aging rates are obtained by differentiating equations (4.1) and (4.2) with respect to time t, respectively. Accurate predictions of the rates of wax deposit growth and aging in the crude oil pipeline will lead to an optimal pigging frequency, informing geochemists and mechanical engineers on the appropriate time to carry out the pigging operations. This will ensure continuous transport of waxy crude oil with minimal downtime, thus minimizing production losses and capital investments.

4.6 Validation of the Results

The results of this study are validated against experimental data from Magnini & Matar (2019). The authors conducted a fundamental study of wax deposition in crude oil flows in a pipeline via interface-resolved numerical simulations. The wax deposit thickness profile is compared in both studies, as shown in Figures 4.38(a) and 4.38(b). It is observed that the deposit thickness profiles follow a similar trend as time increases.

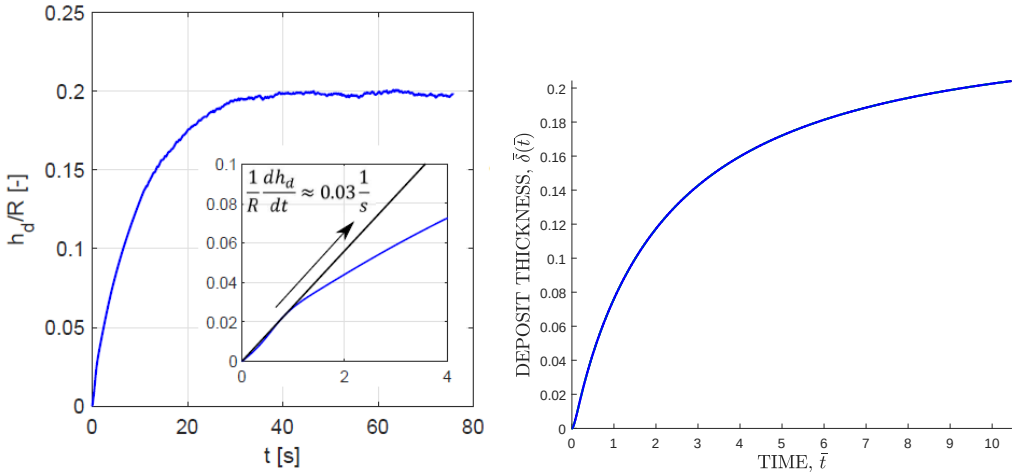

(a) Average Thickness of the Wax Deposit (Magnini & Matar, 2019)

(b) Deposit Thickness (Present Study)

Figure 4.38: Graphs of Deposit Thickness in Magnini & Matar (2019) and in the Present Study.

The observed trends in deposit thickness mean that our model successfully captures the key aspects of wax deposition in pipeline flows. While there might be slight quantitative differences between the profiles in Figures 4.38(b) and 4.38(a), the qualitative agreement over time validates the applicability of our model to real-world scenarios.

Further validation of the the results from this study is achieved by comparing the time evolution of temperature against experimental data from Ying *et al.* (2019), who conducted a phase-change heat transfer analysis of a shutdown overhead pipeline. The fluid temperature profile is compared in both studies, as shown in 4.39(a) and 4.39(b). It is observed that the temperature profiles exhibit a similar trend as time progresses.

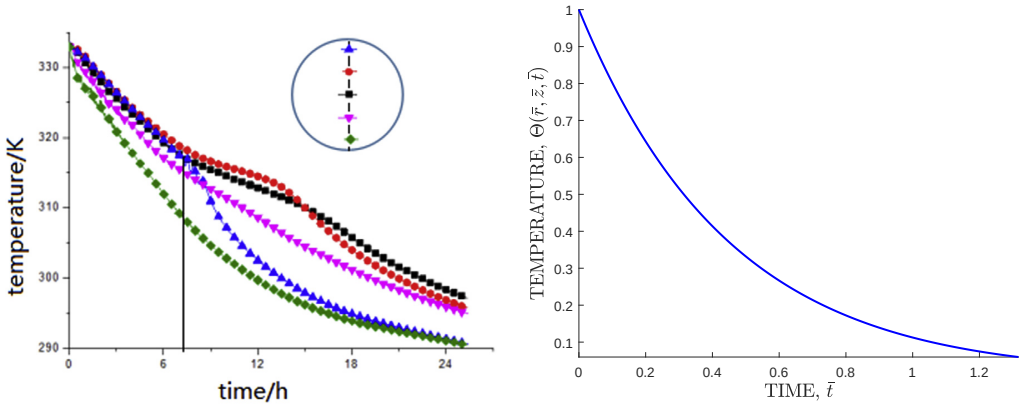

(a) Temperature drop curves at some typical positions in the pipe (Ying *et al.*, 2019)

(b) Temporal evolution of the fluid temperature (Present study)

Figure 4.39: Graphs of Temperature Profile in Ying *et al.* (2019) and in the Present Study.

The observed trends in temperature profile mean that our model accurately predicts the transient thermal behavior of the fluid during pipeline cool-down. While there might be deviations in the absolute temperature values between Figures 4.39(b) and 4.39(a), the qualitative agreement in the cooling trend strengthens the model's credibility for real-world pipeline operations.

The validations presented in Figure 4.38 and Figure 4.39 demonstrate the model's ability to accurately predict wax deposition under various flow conditions. The next chapter presents the conclusions drawn from this study and recommendations of the research findings to the consumers and future researchers.

CHAPTER FIVE

CONCLUSIONS AND RECOMMENDATIONS

The conclusions and recommendations based on the study of wax deposition from multiphase flow in field-scale crude oil pipeline transport systems; are presented in this chapter.

5.1 Conclusions

A mathematical model has been developed to predict wax deposition and aging in field-scale crude oil pipeline transport systems, utilizing the VOF and PSP approaches. In this model, waxy crude oil and the wax deposit are treated as two immiscible phases separated by a smooth interface. The wax concentration is modeled by considering a practical fluid model, which accounts for two forms of wax: dissolved wax and crystallized wax (or precipitated wax). Molecular diffusion and shear dispersion are considered as the primary deposition mechanisms. The model involves the numerical solution of coupled mass, momentum, energy, and species transport equations, along with equations for wax aggregation degree, conservation of volume fraction, deposit growth, and aging in the presence of water-in-oil emulsions.

The profiles of the flow variables are determined through computer simulations. The study investigates the impact of various flow parameters, such as Reynolds number, Grashof number, Eckert number, Schmidt number, and Weber number, on the flow variables, as well as the skin-friction coefficient and the rates of heat and mass transfer. Additionally, the study calculates and predicts the rates of wax deposition on the inner wall of crude oil pipelines and the rate of aging of the gel layer. From this research, the following conclusions have been drawn:

1. The deposit thickness steadily increases during the initial phases of wax deposition. Afterward, it reaches a steady-state value of 0.2 and maintains that value over time.
2. The weight fraction of wax in the gel layer steadily increases during the initial phases of wax deposition. Afterward, it reaches a steady-state value of 0.012 and maintains

that value over time.

3. The deposit thickness increases by at most 2.5% with increasing Reynolds number from 2.2361 to 3.1361. However, it decreases by at most 2.0% with increasing mass Grashof number from 5 to 11. Additionally, it decreases by at most 7.0% with increasing Weber number from 1.0 to 2.5.

4. The weight fraction of wax in the gel layer decreases by at most 0.3% with increasing Reynolds number from 2.2361 to 3.1361, and by at most 0.25% with increasing mass Grashof number from 1.5 to 6.0.

5. The aggregation of wax crystals in the pipeline decreases by at most 2.5% with increasing Reynolds number from 2.2361 to 3.1361. However, it increases by at most 3.4% with increasing mass Grashof number from 5 to 11. Additionally, it increases by at most 4.8% with increasing Weber number from 1.0 to 2.5.

6. The total concentration of waxy components in the pipeline increases by at most 10.0% with increasing Reynolds number from 2.2361 to 3.1361. However, it decreases by at most 8.0% with increasing mass Grashof number from 5 to 11. Additionally, it decreases by at most 20% with increasing Weber number from 1.0 to 2.5.

7. The fraction of the volume occupied by waxy crude oil in the pipeline decreases by up to 10.0% with increasing Reynolds number from 2.2361 to 3.1361. However, it increases by up to 9.0% with increasing mass Grashof number from 5 to 11, and by up to 25% with increasing Weber number from 1.0 to 2.5.

8. The temperature of waxy crude oil in the pipeline increases by at most 0.001% with increasing Reynolds number from 2.2361 to 3.1361, and by at most 0.002% with increasing Eckert number from 1.2 to 1.5. However, it decreases by at most 0.0034% with increasing mass Grashof number from 5 to 11. Additionally, it decreases by at most 1.3% with increasing Weber number from 1.0 to 2.5.

9. The radial velocity of waxy crude oil in the pipeline increases by at most 1.0% with increasing Reynolds number from 2.2361 to 3.1361. However, it decreases by at most 1.8% with increasing mass Grashof number from 5 to 11. Additionally, it decreases by at most 1.3% with increasing Weber number from 1.0 to 2.5.

10. The axial/streamwse velocity of waxy crude oil in the pipeline decreases by at most 0.7% with increasing Reynolds number from 2.2361 to 3.1361, and by at most 1.2% with increasing Weber number from 1.0 to 2.5. However, it increases by at most 3.0% with increasing mass Grashof number from 5 to 11.

11. Skin friction coefficient increases from 0.1230 to 0.4022 with increasing Reynolds number from 2.2361 to 5.2361, and from 0.1230 to 0.1277 with increasing mass Grashof number from 5 to 20. It also increases from 0.1230 to 0.1334 with increasing Weber number from 1.0 to 2.5.

12. The Nusselt number increases from 1.9907 to 4.9834 with increasing Reynolds number from 2.2361 to 5.2361 and from 1.9907 to 2.0225 with increasing mass Grashof number from 5 to 20. It also increases from 1.9907 to 2.0434 with increasing Weber number from 1.0 to 2.5.

13. The Sherwood number increases from 1.3916 to 7.2234 with increasing mass Grashof number from 5 to 20, and from 1.3916 to 1.6002 with increasing Weber number from 1.0 to 2.5.

14. The proposed simplified wax deposition models, given by equations (4.1) and (4.2), can be used to predict the deposit growth and aging at any time, respectively, in field-scale waxy crude oil pipeline transport systems.

Hence, varying values of the flow parameters in this study can be used to control the flow variables, such as velocity, wax concentration, wax aggregation degree, and oil volume fraction, quite effectively in waxy crude oil transportation pipelines. Moreover, this study asserts that the flow parameters have a substantial effect on engineering parameters of concern, such as the coefficient of skin friction and the rates of heat and mass transfer at the pipeline wall.

The study results have been validated versus experimental wax deposition data available from the literature. The insight gained via the numerical simulations has been utilized to develop a prediction method to estimate the rates of wax deposition and aging.

5.2 Recommendations

This study is a significant contribution to the studies on unsteady multiphase flows in pipelines in the presence of water-in-oil emulsions. To reduce the deposition of wax in the pipeline, the following are the recommendations made from this study to the policymakers and future researchers.

5.2.1 Recommendations to the Policymakers

Policymakers are all the people responsible for formulating or amending policies. They often have the influence and opportunity to use research findings to alter or develop policies, working hand-in-hand with the researchers. From the research findings, the following recommendations are made to the *designers* of crude oil pipelines when developing equipment or systems in the petroleum industry; used to transport petroleum products:

1. Industry standards for pipeline design and operation should be established, requiring the use of multiphase flow models and wax deposition prediction tools to optimize flow parameters and minimize deposition risks. This research demonstrates the efficacy of utilizing multiphase flow models and wax deposition prediction tools. We recommend incorporating their use into standardized pipeline design and operation protocols to ensure preventative measures are implemented across the industry.
2. Appropriate insulation should be used to prevent heat loss through conduction. This will ensure that the temperature of the waxy crude oil is maintained above the wax-appearance temperature (WAT), hence preventing precipitation and deposition of wax in the pipeline.

Furthermore, the main *users* of this study are the pipeline operators, mechanical engineers, and geochemists. Thus, it is recommended to the consumers of the research findings that:

1. The proposed wax deposition model should be adopted to determine the thickness of wax deposits in the crude oil pipeline. This will help achieve optimal pigging frequency, which in turn will inform policy decisions on the appropriate time to carry out pigging operations. This will further ensure continuous transport of waxy crude oil with very minimal production-downtime, thus minimizing losses in production and capital investment.
2. Pipeline operators should find a balance between inlet velocity, pressure, and flow parameters to maximize discharge and minimize deposition while considering the impact on downstream equipment performance and energy consumption.
3. Utilize data on rates of heat and mass transfer, as well as friction between crude oil and the pipe to determine the material and modifications for pipe walls that

conserve energy and prevent/control deposition and corrosion. This will ensure that the temperature of the waxy crude oil is maintained above the WAT, hence preventing precipitation and deposition of wax.

Finally, the following are the recommendations to the governments (both national and international) and the non-governmental organizations (NGOs):

1. Mandate pipeline operators to publicly report annual economic losses due to wax deposition shutdowns, cleaning, and reduced flow rates. This data can inform policy decisions regarding industry-wide cost burdens and potential savings through preventative measures. Requiring public reporting of the pipeline losses would highlight the economic impact and incentivize investment in mitigation strategies.
2. Allocate funding for research and development of environmentally friendly wax control technologies, such as biodegradable pour point depressants or bio-inspired surface modifications. This study calls for environmentally friendly alternatives to traditional wax control methods. We urge policymakers to invest in research and development of such technologies to minimize environmental impact while ensuring pipeline efficiency.

5.2.2 Recommendations for Future Research Studies

The knowledge gathered from this study can motivate the researchers in this field to study this work with interest. Based on the assumptions of this study, it is recommended that future researchers who aim to extend this work should:

1. Study non-axisymmetric flow of waxy crude oil with particle slip at the solid-liquid boundary.
2. Study oil-water-gas three-phase flow in waxy crude oil pipeline transport systems.
3. Study the effect of flow geometry on wax deposition process, considering curved pipes.
4. Optimize flow parameters in the model equations utilizing real-world pipeline operation data and least-squares curve fitting techniques to achieve desired results in field-scale crude oil pipeline transport systems.

5. Investigate the effects of wax inhibitors, corrosion, and other solid materials such as sediments on wax deposition in turbulent flow regimes.

REFERENCES

Ahmadi Nadooshan, A. & Shirani, E. (2008). Interface pressure model for surface tension force for vof-based methods in interfacial flows. *Engineering Applications of Computational Fluid Mechanics*, ***2***(4), 496--513.

Al-Ahmad, M., Al-Fariss, T., & Obaid-ur Rehman, S. (1990). Solubility studies on a paraffin wax in base oils. *Fuel*, ***69***(3), 293--296.

Azevedo, L. & Teixeira, A. (2003). A critical review of the modeling of wax deposition mechanisms. *Petroleum Science and Technology*, ***21***(3-4), 393--408.

Banki, R., Hoteit, H., & Firoozabadi, A. (2008). Mathematical formulation and numerical modeling of wax deposition in pipelines from enthalpy--porosity approach and irreversible thermodynamics. *International Journal of Heat and Mass Transfer*, ***51***(13-14), 3387--3398.

Bergman, T. L., Lavine, A., Incropera, F. P., & Dewitt, D. P. (2017). *Fundamentals of heat and mass transfer*. John Wiley & Sons New York.

Brackbill, J. U., Kothe, D. B., & Zemach, C. (1992). A continuum method for modeling surface tension. *Journal of computational physics*, ***100***(2), 335--354.

Cengel, Y. A. & Cimbala, J. M. (2010). *Fluid Mechanics: Fundamentals and Applications*. Tata McGraw-Hill Education.

Cragoe, C. S. (1929). *Thermal Properties of Petroleum Products: November 9, 1929*. Number 97. US Government Printing Office.

Currie, I. G. (2016). *Fundamental mechanics of fluids*. CRC press.

Cussler, E., Hughes, S. E., Ward III, W. J., & Aris, R. (1988). Barrier membranes. *Journal of membrane science*, ***38***(2), 161--174.

Fasano, A., Fusi, L., & Correra, S. (2004). Mathematical models for waxy crude oils. *Meccanica*, ***39***(5), 441--482.

Fatkhullina, Y., Musin, A., Kovaleva, L., & Akhatov, I. S. (2015). Mathematical modeling of a water-in-oil emulsion droplet behavior under the microwave impact. In *Journal of Physics: Conference Series*, volume 574, (pp. 012110). IOP Publishing.

Fusi, L. (2003). On the stationary flow of a waxy crude oil with deposition mechanisms. *Nonlinear Analysis: Theory, Methods & Applications*, ***53***(3-4), 507--526.

Goqo, S. P., Mondal, S., Sibanda, P., & Motsa, S. S. (2019). Efficient multi-domain bivariate spectral collocation solution for mhd laminar natural convection flow from a vertical permeable flat plate with uniform surface temperature and thermal radiation. *International Journal of Computational Methods*, ***16***(06), 1840029.

Gupta, A. & Sircar, A. (2017). Wax deposition modelling and comparison with field data for some indian oil fields. *STM. J.*, ***4***, 1--15.

Huang, Z. (2011). Application of the fundamentals of heat and mass transfer to the investigation of wax deposition in subsea pipelines.

Huang, Z., Lee, H. S., Senra, M., & Scott Fogler, H. (2011). A fundamental model of wax deposition in subsea oil pipelines. *AIChE Journal*, ***57***(11), 2955--2964.

Ibrahim, W. (2020). Spectral quasilinearization method for solution of convective heating condition. *Engineering Transactions*, ***68***(1), 69--87.

Jiang, H., Liu, X., Zhao, H., Liu, Y., Ma, C., & Li, X. (2020). Numerical study for removing wax deposition by thermal washing for the waxy crude oil gathering pipeline. *Science Progress*, ***103***(3), 0036850420958529.

Johnston, H. & Liu, J.-G. (2004). Accurate, stable and efficient navier--stokes solvers based on explicit treatment of the pressure term. *Journal of Computational Physics*, ***199***(1), 221--259.

Kok, M. V., Saracoglu, O., *et al.* (2000). Mathematical modelling of wax deposition in crude oil pipeline systems. In *SPE Asia Pacific Oil and Gas Conference and Exhibition*. Society of Petroleum Engineers.

Leal, L. G. (2007). *Advanced transport phenomena: fluid mechanics and convective transport processes*, volume 7. Cambridge University Press.

Magagula, V. M., Motsa, S. S., & Sibanda, P. (2020). On the bivariate spectral quasilinearization method for nonlinear boundary layer partial differential equations. In *Applications of Heat, Mass and Fluid Boundary Layers* (pp. 177--190). Elsevier.

Magagula, V. M., Motsa, S. S., Sibanda, P., & Dlamini, P. G. (2016). On a bivariate spectral relaxation method for unsteady magneto-hydrodynamic flow in porous media. *SpringerPlus*, ***5***(1), 455.

Magnini, M. & Matar, O. K. (2019). Fundamental study of wax deposition in crude oil flows in a pipeline via interface-resolved numerical simulations. *Industrial & Engineering Chemistry Research*, ***58***(47), 21797--21816.

Motsa, S., Magagula, V., Sibanda, P., *et al.* (2014). A bivariate chebyshev spectral collocation quasilinearization method for nonlinear evolution parabolic equations. *The Scientific World Journal*, ***2014***.

Moukalled, F., Mangani, L., Darwish, M., *et al.* (2016). *The finite volume method in computational fluid dynamics*, volume 113. Springer.

Mouketou, F. N. & Kolesnikov, A. (2019). Modelling and simulation of multiphase flow applicable to processes in oil and gas industry. *Chemical Product and Process Modeling*, ***14***(1).

Nazar, A. S., Dabir, B., & Islam, M. (2005). Experimental and mathematical modeling of wax deposition and propagation in pipes transporting crude oil. *Energy sources*, ***27***(1-2), 185--207.

Ochieng, F. O. (2018). *Hydromagnetic Jeffery-Hamel Unsteady Flow of a Dissipative Non-Newtonian Fluid with Nonlinear Viscosity*. PhD thesis, JKUAT-PAUSTI.

Ochieng, F. O., Kinyanjui, M. N., & Kimathi, M. E. (2018). Hydromagnetic jeffery-hamel unsteady flow of a dissipative non-newtonian fluid with nonlinear viscosity and skin friction. *Global Journal of Pure and Applied Mathematics*, ***14***(8), 1101--1119.

Ogbuanu, K. & Roy, R. V. (2022). Numerical computation of the effective thermal conductivity of two-phase composite materials by digital image analysis. *International Journal of Heat and Mass Transfer*, ***197***, 123377.

Orszag, S. A., Israeli, M., & Deville, M. O. (1986). Boundary conditions for incompressible flows. *Journal of Scientific Computing*, ***1***(1), 75--111.

Ramirez-Jaramillo, E., Lira-Galeana, C., & Manero, O. (2004). Modeling wax deposition in pipelines. *Petroleum science and technology*, ***22***(7-8), 821--861.

Safaei, M. R., Jahanbin, A., Kianifar, A., Gharehkhani, S., Kherbeet, A. S., Goodarzi, M., & Dahari, M. (2016). Mathematical modeling for nanofluids simulation: a review of the latest works. *Modeling and simulation in engineering sciences*.

Salih, A. (2011). Conservation equations of fluid dynamics. *Department of Aerospace Engineering Indian Institute of Space Science and Technology, Thiruvananthapuram*.

Salih, A. (2013). Streamfunction-vorticity formulation. *Department of Aerospace Engineering Indian Institute of Space Science and Technology, Thiruvananthapuram-Mach*.

Samuel, F. & Motsa, S. (2019). Solving hyperbolic partial differential equations using a highly accurate multidomain bivariate spectral collocation method. *Wave Motion*, ***88***, 57--72.

Shi, B., Hong, J., Wang, Z., Chang, Z., & Li, F. (2023). Treatment of paraffin deposition behavior in gas-condensate wells with chemical inhibitors. *Journal of Petroleum Exploration and Production Technology*, 1--19.

Singh, P., Venkatesan, R., Fogler, H. S., & Nagarajan, N. (2000). Formation and aging of incipient thin film wax-oil gels. *AIChE Journal*, ***46***(5), 1059--1074.

Skjæraasen, O., Oschmann, H.-J., Paso, K., & Sjöblom, J. (2014). Accurate assessment of pipeline restart behavior at subsea conditions for a highly waxy crude oil employing advanced computational pressure wave modeling. *Industrial & Engineering Chemistry Research*, ***54***(16), 4429--4440.

Stubsjøen, M. (2013). Analytical and numerical modeling of paraffin wax in pipelines. Master's thesis, Institutt for petroleumsteknologi og anvendt geofysikk.

Sun, D., Zhu, Z., Hu, Z., & Wu, M. (2020). Experimental and theoretical study on wax deposition and the application on a heat insulated crude oil pipeline in northeast china. *Oil & Gas Science and Technology--Revue d'IFP Energies nouvelles*, ***75***, 3.

Trefethen, L. N. (2000). *Spectral methods in MATLAB*. Philadelphia: SIAM.

Waheed, S. E. & Megahed, A. M. (2022). Melting heat transfer effects on flow of a micropolar fluid with heat generation (absorption) in slip flow regime. *Applied Mathematics & Information Sciences*, ***16***(1), 35--44.

Wu, J., Yu, S.-T., & Jiang, B.-N. (1998). Simulation of two-fluid flows by the least-squares finite element method using a continuum surface tension model. *International journal for numerical methods in engineering*, ***42***(4), 583--600.

Yang, H., Vanka, S. P., & Thomas, B. G. (2019). Mathematical modeling of multiphase flow in steel continuous casting. *ISIJ International*, ***59***(6), 956--972.

Ying, X., Xin, N., Qinglin, C., Zhonghua, D., Xiaoyan, L., Yang, L., & Cong, L. (2019). Phase-change heat transfer analysis of shutdown overhead pipeline. *Case Studies in Thermal Engineering*, 100399.

Zhang, L., Qu, S., Wang, C., & Guan, B. (2018). Prediction temperature field and wax deposition based on heat--fluid coupling method. *Journal of Petroleum Exploration and Production Technology*, 1--6.

Zheng, S., Fogler, H. S., & Haji-Akbari, A. (2017). A fundamental wax deposition model for water-in-oil dispersed flows in subsea pipelines. *AIChE Journal*, ***63***(9), 4201--4213.

Zheng, S., Saidoun, M., Palermo, T., Mateen, K., & Fogler, H. S. (2017). Wax deposition modeling with considerations of non-newtonian characteristics: Application on field-scale pipeline. *Energy & Fuels*, ***31***(5), 5011--5023.

APPENDICES

Appendix I: Publications

Part of this work has been published in high-impact-factor journals. The articles are as follows:

1. Ochieng, F. O., Kinyanjui, M. N., Abonyo, J. O., & Kiogora, P. R. (2022). Mathematical Modeling of Wax Deposition in Field-Scale Crude Oil Pipeline Systems. Hindawi: *Journal of Applied Mathematics*, Volume 2022, Article ID 2845221, 13 pages. DOI: 10.1155/2022/2845221

2. Ochieng, F. O., Kinyanjui, M. N., Kiogora, P. R., & Abonyo, J. O. (2023). Numerical Study of Wax Deposition from Multiphase Flow in Oil Pipelines with Heat and Mass Transfer. Hindawi: *Mathematical Problems in Engineering*, Volume 2023, Article ID 1173505, 18 pages. DOI: 10.1155/2023/1173505

3. Ochieng, F. O., Kinyanjui, M. N., Kiogora, P. R., & Abonyo, J. O. (2024). Predicting Wax Deposition in Oil Pipelines: A Computational Model Incorporating Heat and Mass Transfer Effects. Springer: *International Journal of Applied and Computational Mathematics*, Volume 10, Issue 1, Pages 1-34. DOI: 10.1007/s40819-023-01666-5

Appendix II: Pseudo-Single Phase Approach

Using the Pseudo-Single Phase (PSP) approach presented in detail in (Zheng *et al.*, 2017), the water-in-oil emulsion is treated as a single pseudo-fluid whose physical properties are calculated by averaging the corresponding physical properties of oil, water and gel as follows:

1. Volume-based averaging method:

$$\rho_{\text{mix}} = \phi_{\text{oil}}\rho_{\text{oil}} + \phi_{\text{water}}\rho_{\text{water}} + \phi_{\text{gel}}\rho_{\text{gel}}$$

2. Weight-based averaging method:

$$(Cp)_{\text{mix}} = \frac{\phi_{\text{oil}}\rho_{\text{oil}}\,(Cp)_{\text{oil}} + \phi_{\text{water}}\rho_{\text{water}}\,(Cp)_{\text{water}} + \phi_{\text{gel}}\rho_{\text{gel}}\,(Cp)_{\text{gel}}}{\rho_{\text{mix}}}$$

3. Maxwell–Garnett correlation:

$$k_{\text{mix}} = \frac{(k_{\text{water}} + k_{\text{gel}}) + 2k_{\text{oil}} + 2\phi_{\text{water}}\,(k_{\text{water}} - k_{\text{oil}}) + 2\phi_{\text{gel}}\,(k_{\text{gel}} - k_{\text{oil}})}{(k_{\text{water}} + k_{\text{gel}}) + 2k_{\text{oil}} - \phi_{\text{water}}\,(k_{\text{water}} - k_{\text{oil}}) - \phi_{\text{gel}}\,(k_{\text{gel}} - k_{\text{oil}})}k_{\text{oil}}$$

Appendix III: Standard Vector Operations in Cylindrical Coordinates

The following standard vector operations presented in (Leal, 2007) are used in this study to convert the governing equations to cylindrical coordinates.

$$\text{Gradient operator:} \quad \vec{\nabla}\psi = \frac{\partial \psi}{\partial r}\hat{\mathbf{r}} + \frac{1}{r}\frac{\partial \psi}{\partial \theta}\hat{\mathbf{\Theta}} + \frac{\partial \psi}{\partial z}\hat{\mathbf{k}},$$

$$\text{Divergence operator:} \quad \vec{\nabla}\cdot\vec{A} = \frac{1}{r}\frac{\partial}{\partial r}\left(rA_r\right) + \frac{1}{r}\frac{\partial A_\theta}{\partial \theta} + \frac{\partial A_z}{\partial z},$$

$$\text{Laplace operator:} \quad \nabla^2\psi = \vec{\nabla}\cdot\left(\vec{\nabla}\psi\right) = \frac{1}{r}\frac{\partial}{\partial r}\left(r\frac{\partial \psi}{\partial r}\right) + \frac{1}{r^2}\frac{\partial^2 \psi}{\partial \theta^2} + \frac{\partial^2 \psi}{\partial z^2}.$$

$$\text{Curl operator:} \quad \vec{\nabla}\times\vec{A} = \frac{1}{r}\begin{vmatrix} \hat{\mathbf{r}} & r\hat{\theta} & \hat{\mathbf{k}} \\ \dfrac{\partial}{\partial r} & \dfrac{\partial}{\partial \theta} & \dfrac{\partial}{\partial z} \\ A_r & rA_\theta & A_z \end{vmatrix}$$

Appendix IV: Derivation of Michigan Model for Deposit Aging

Assuming that the thickness ($\delta(t)$) of the gel layer is uniform, the effective radius of the pipeline is given as

$$R_{\text{eff}}(t) = R - \delta(t) \tag{5.1}$$

The mass balance relationship of the molecular diffusion process is given in (Sun *et al.*, 2020) as:

$$\frac{d}{dt}\left(\rho_{\text{gel}}\pi\left[R^2 - R_{\text{eff}}^2(t)\right]x\right) = 2\pi R_{\text{eff}} k_{\text{m}}\left[C - C_{\text{d}}(T_{\text{int}})\right]. \tag{5.2}$$

The term $k_{\text{m}}\left[C - C_{\text{d}}(T_{\text{int}})\right]$ represents the wax molecule pair flow of crude oil to the oil-gel interface. The weight fraction (x) of solid wax in the gel layer is defined in (Ramirez-Jaramillo *et al.*, 2004) as:

$$x = \frac{\text{mass of wax in the gel layer}}{\text{mass of wax in the gel layer } + \text{ mass of oil trapped in the gel layer}} \tag{5.3}$$

The effective radius R_{eff} and weight fraction (x) are both functions of operation time t. Thus, expanding the derivatives involved in equation (5.2), we get

$$\rho_{\text{gel}}\pi\left[R^2 - R_{\text{eff}}^2(t)\right]\frac{dx}{dt} - 2\rho_{\text{gel}}\pi R_{\text{eff}} x\frac{dR_{\text{eff}}}{dt} = 2\pi R_{\text{eff}} k_{\text{m}}\left[C - C_{\text{d}}(T_{\text{int}})\right]. \tag{5.4}$$

Dividing equation (5.4) by $2\rho_{\text{gel}}\pi R_{\text{eff}}$ yields

$$\frac{\left[R^2 - R_{\text{eff}}^2(t)\right]}{2R_{\text{eff}}}\frac{dx}{dt} - x\frac{dR_{\text{eff}}}{dt} = \frac{k_{\text{m}}\left[C - C_{\text{d}}(T_{\text{int}})\right]}{\rho_{\text{gel}}}. \tag{5.5}$$

Eliminating R_{eff} between equations (5.1) and (5.5) yields

$$\frac{\delta\left(2R - \delta\right)}{2\left(R - \delta\right)}\frac{dx}{dt} + x\frac{d\delta}{dt} = \frac{k_{\text{m}}\left[C - C_{\text{d}}(T_{\text{int}})\right]}{\rho_{\text{gel}}}. \tag{5.6}$$

Due to the existence of the temperature gradient between the oil-gel interface and the inner wall of the pipeline, a concentration gradient of wax molecules exists inside the gel layer. Therefore, some wax molecules continue to diffuse from the oil-gel interface into the gel layer, leading to a gradual increase in the wax content inside the gel layer. The increase in the weight fraction of wax in the gel layer with time is called *deposit aging* (or hardening of the gel layer). According to mass balance, the process of formation of the gel layer can

be expressed mathematically as (Sun *et al.*, 2020):

$$-2\rho_{\text{gel}}\pi x R_{\text{eff}}\frac{dR_{\text{eff}}}{dt} = 2\pi R_{\text{eff}}k_{\text{m}}\left[C - C_{\text{d}}(T_{\text{int}})\right] - 2\pi R_{\text{eff}}\left(-D_{\text{e}}\frac{\partial C_{\text{d}}}{\partial r}\bigg|_{r=R_{\text{eff}}}\right). \quad (5.7)$$

The effective diffusivity (D_{e}) of wax inside the gel layer is calculated by the Cussler correlation given in (Cussler *et al.*, 1988; Gupta & Sircar, 2017) as:

$$D_{\text{e}} = \frac{D_{\text{d}}}{1 + \alpha_{\text{avg}}^2\left(\frac{x^2}{1-x}\right)} = f(x)D_{\text{d}}. \quad (5.8)$$

The function $f(x)$ is the coefficient describing diffusion in a porous network (i.e., the gel layer) and is given as:

$$f(x) = \frac{1-x}{\alpha_{\text{avg}}^2 x^2 - x + 1}, \quad (5.9)$$

where α_{avg} denotes the average aspect ratio of the wax crystals (or the wax crystal shape factor) and can be obtained by observing the wax crystal form of the gel layer. It is given in (Sun *et al.*, 2020) as:

$$\alpha_{\text{avg}} = -0.323\ln Q + 1.684. \quad (5.10)$$

where Q is the volumetric flow rate of the mixture fluid. Substituting equation (5.8) into equation (5.7) yields

$$-2\rho_{\text{gel}}\pi x R_{\text{eff}}\frac{dR_{\text{eff}}}{dt} = 2\pi R_{\text{eff}}k_{\text{m}}\left[C - C_{\text{d}}(T_{\text{int}})\right] + 2\pi R_{\text{eff}}f(x)D_{\text{d}}\left(\frac{\partial C_{\text{d}}}{\partial r}\right)_{r=R_{\text{eff}}}. \quad (5.11)$$

Dividing equation (5.11) by $2\pi R_{\text{eff}}\rho_{\text{gel}}$ yields

$$-x\frac{dR_{\text{eff}}}{dt} = \frac{k_{\text{m}}\left[C - C_{\text{d}}(T_{\text{int}})\right]}{\rho_{\text{gel}}} + \frac{f(x)}{\rho_{\text{gel}}}D_{\text{d}}\left(\frac{\partial C_{\text{d}}}{\partial r}\right)_{r=R_{\text{eff}}}. \quad (5.12)$$

Eliminating R_{eff} between equations (5.1) and (5.12) yields

$$x\frac{d\delta}{dt} = \frac{k_{\text{m}}\left[C - C_{\text{d}}(T_{\text{int}})\right]}{\rho_{\text{gel}}} + \frac{f(x)}{\rho_{\text{gel}}}D_{\text{d}}\left(\frac{\partial C_{\text{d}}}{\partial r}\right)_{r=R_{\text{eff}}}. \quad (5.13)$$

Using chain rule of differentiation for derivatives involving C_{d}, equation (5.13) becomes:

$$x\frac{d\delta}{dt} = \frac{k_{\text{m}}\left[C - C_{\text{d}}(T_{\text{int}})\right]}{\rho_{\text{gel}}} + \frac{f(x)}{\rho_{\text{gel}}}D_{\text{d}}\left(\frac{dC_{\text{d}}}{dT}\frac{\partial T}{\partial r}\right)_{r=R_{\text{eff}}}. \quad (5.14)$$

Eliminating $\frac{d\delta}{dt}$ between equations (5.6) and (5.14) and making $\frac{dx}{dt}$ the subject yields

$$\frac{dx}{dt} = -\frac{2\left(R-\delta\right)}{\delta\left(2R-\delta\right)}\frac{f(x)}{\rho_{\text{gel}}}D_{\text{d}}\left(\frac{dC_{\text{d}}}{dT}\frac{\partial T}{\partial r}\right)_{r=R_{\text{eff}}}. \tag{5.15}$$

Equation (5.15) is the Michigan model presented in (Gupta & Sircar, 2017) as the specific equation governing the aging of the gel layer for water-oil two-phase flow in crude oil transportation pipeline.

Appendix V: Computer Simulations

This section presents the MATLAB® code for the bivariate Chebyshev spectral collocation method presented in subsection 3.11.2 for the spatial discretization coupled with Adams-Bashforth and Crank-Nicolson time discretization. The Chebyshev differentiation matrix is computed by the M-file `cheb.m`, which is taken from Trefethen (2000) with permission.

Listing 5.1: `FDM_Spectral_Collocation_PhD_Oketch.m`

```
function FDM_Spectral_Collocation_PhD_Oketch()
clear; % Erases all the variables in the computer memory to create more space
clc; % Clears the command window
clf; % Clears the figure handles
%-------------------------------------------------------------------------
% INPUT
%-------------------------------------------------------------------------
M = 19; % No. of collocation points in r̂
N = 15; % No. of collocation points in ẑ
Tfinal = 2000; % No. of time steps
nProfiles = 4; % No. of profiles in each figure
increment = 1; % Common difference for the varied parameter
tolerance = 1e-6; % Prescribed error tolerance
%%
%-------------------------------------------------------------------------
% Grid setup
%-------------------------------------------------------------------------
lambda = 1-0.20; beta0 = 1e-5; beta1 = 0.90; % beta0->0, beta1->1
r0 = 0; rend = lambda; dr = (rend-r0)/M;
z0 = 0; zend = 10; dz = (zend-z0)/N;
dt = (1e-3)*(1/2)*(dr^2+dz^2); % stability condition
%%
%-------------------------------------------------------------------------
% Declaration and Initialization
%-------------------------------------------------------------------------
nDependentVars = 6; % No. of dependent variables in the numerical schemes
color = {'b-','k:','g--','r-.','m','c'}; % Colours of the profiles
legendMatrix = {'null'}; % Stores the legends of each profile
solMatrix = zeros(nDependentVars*(M+1),(N+1),nProfiles); % matrix to store the solutions
rIndex = floor(0.78*(M+1)); % At the effective pipeline radius i.e., at r = R_eff
zIndex = floor(0.50*(N+1)); % At the center of computational domain
%%
%-------------------------------------------------------------------------
% Flow parameters
%-------------------------------------------------------------------------
Ec = 1.2; % Eckert number
Grt = 5; % Thermal Grashof num1ber
Grc = Grt; % Mass Grashof number
Da = 1e+4; % Darcy number
Pr = 6.9; % Prandtl number
Re = sqrt(Grt); % Reynolds number
Pe = Re*Pr; % Peclet number
Ri = Grt/(Re^2);% Richardson number, [for mixed convection, Ri=1]
Sc = 1.5; % Schmidt number
St = 1.5; % Stanton number
We = 1.0; % Weber number
alpha = pi/12; % Angle of inclination of the pipeline to the horizontal
%%
%-------------------------------------------------------------------------
% Physical Properties
%-------------------------------------------------------------------------
oAPI = 18; % API gravity of waxy crude oil
Cwall = 910; % Concentration of wax at the pipeline wall, [kg/m^3]
Cinf = 905; % Equillibrium concentration of wax in crude oil, [kg/m^3]
R = 0.25; % Inner Radius of the pipeline, [m]
Dp = 4.8e-3; % Shear dispersion coefficient, [m]
d_bar = 1e-2; % Diameter of water droplet, [m]
Q = 1; % Volumetric flow rate of crude oil
alpha_avg = -0.323*log(Q) + 1.684; % Average aspect ratio of wax crystals
phiWater = 0.01; % Volume fraction of water
phiOIL = 0.8; % PLACE HOLDER - Remove it
phiGel = 1 - (phiOIL + phiWater); % Volume fraction of gel layer
rhoOil = 950; rhoWater = 997.1; rhoGel = 900; % Density of oil, water, and gel layer,
    [kg/m^3]
muOil = 0.5; muWater = 8.9e-4; muGel = 0.82;
```

```
betaTOil = 0.9; betaTWater = 256.32e-6; betaTGel = 1.2;
betaCOil = 0.9; betaCWater = 1; betaCGel = 1.2;
CpOil = 2300; CpWater = 4179.6; CpGel = 2900;
kOil = 0.1; kWater = 0.608; kGel = 0.25;
%-------------------------------------------------------------------
% Thermophysical Properties
%-------------------------------------------------------------------
rho_f = (1-phiWater)*rhoOil + phiWater*rhoWater;
rho_mix = (1-phiGel)*rho_f + phiGel*rhoGel;
mu_f = (1-phiWater)*muOil + phiWater*muWater;
mu_mix = (1-phiGel)*mu_f + phiGel*muGel;
betaT_f = (1-phiWater)*betaTOil + phiWater*betaTWater;
betaT_mix = (1-phiGel)*betaT_f + phiGel*betaTGel;
betaC_f = (1-phiWater)*betaCOil + phiWater*betaCWater;
betaC_mix = (1-phiGel)*betaC_f + phiGel*betaCGel;
Cp_f = ((1-phiWater)*(rhoOil*CpOil) + phiWater*(rhoWater*CpWater))/rho_f;
Cp_mix = ((1-phiGel)*(rho_f*Cp_f) + phiGel*(rhoGel*CpGel))/rho_mix;
k_f =
    ((kWater+2*kOil+2*phiWater*(kWater-kOil))/(kWater+2*kOil-phiWater*(kWater-kOil)))*kOil;
k_mix = ((kGel+2*k_f+2*phiGel*(kGel-k_f))/(kGel+2*k_f-phiGel*(kGel-k_f)))*k_f;
%%
%-------------------------------------------------------------------
% Constants (DON'T change)
%-------------------------------------------------------------------
phi0 = (Cinf - rhoGel)/(Cwall - Cinf);
phi1 = (Cwall - Cinf)/rhoGel;
lambda1 = rho_f/rho_mix;
lambda2 = (mu_mix/mu_f)*lambda1;
lambda3 = betaT_mix/betaT_f;
lambda4 = betaC_mix/betaC_f;
lambda5 = (k_mix/k_f)*lambda1*(Cp_f/Cp_mix);
lambda6 = lambda1*(Cp_f/Cp_mix);
lambda7 = (mu_mix/mu_f)*lambda6;
ep = Dp/R;                          % Shear dispersion parameter.
MWoil = 6084/(oAPI - 5.9);  % Molecular weight of waxy crude oil
Sf = (0.0077.*MWoil - 1.737); c1 = 0.981; c2 = 0.0677; c3 = - 0.0208; % Constants
epsilon = 1e-5; % Small parameter to avoid division by zero
%%
%-------------------------------------------------------------------
% Chebyshev Differentiation Matrices and Collocation Points
%-------------------------------------------------------------------
[D_cheb,r_hat] = cheb(M);
[d_cheb,z_hat] = cheb(N);
%%%%%%%%%%%%%%%%%%%%%%%%%%%%%%%%%%%%%%%%%%%%%%%%%%%%%%%%%%%%%%%%%%%
% D_cheb:      Standard first -order Chebyshev differentiation matrix
%                of size (M + 1) x (M + 1)
% d_cheb:      Standard first -order Chebyshev differentiation matrix
%                of size (N + 1) x (N + 1)
% r_hat:       Collocation points, r_hat in [-1, 1]
% z_hat:       Collocation points, z_hat in [-1, 1]
%%%%%%%%%%%%%%%%%%%%%%%%%%%%%%%%%%%%%%%%%%%%%%%%%%%%%%%%%%%%%%%%%%%
r0 = r0 + epsilon; % to avoid division by zero
r = ((rend-r0)/2)*r_hat + (rend+r0)/2;       % Linear transformation for r
z = ((zend-z0)/2)*z_hat + (zend+z0)/2;       % Linear transformation for z
I = eye(M+1);                       % Identity matrix
D = (2/(rend-r0))*D_cheb;   % Scaling the differentiation matrix D_cheb
d = (2/(zend-z0))*d_cheb;   % Scaling the differentiation matrix d_cheb
D2 = D^2; d2 = d^2;                 % Secod-order Chebyshev differentiation matrices
%-------------------------------------------------------------------
% Initial conditions (at t = 0)
%-------------------------------------------------------------------
[Ukm,Vkm,Tkm,Ckm,alphaMkm,Pkm] = deal(zeros(M+1,N+1));
[phiOILkm] = ones(M+1,N+1) - phiWater;
[DELTAkm,Xkm] = deal(0.1*ones(1,1));
%-------------------------------------------------------------------
% Start the computations
%-------------------------------------------------------------------
tic % Start timing
for p = 1: nProfiles
    t = 0;
    for k = 1: Tfinal       % Time-stepping by AB and CN formula
        %-----------------------------------------------------------
        % Initialize the coefficient matrix and the right-hand side vector
        %-----------------------------------------------------------
        [A1,A2,A3,A4,A5,A6,A7] = deal(cell(N+1,N+1)); % create cell arrays
        [R1k,R2k,R3k,R4k,R5k,R6k,R7k] = deal(zeros(M+1,N+1));
        [R8k,R9k] = deal(zeros(1,N+1));
        for j=1:N+1
            %-------------------------------------------------------
```

```
% Construct the matrix of coefficints
%-----------------------------------------
% r-momentum Eq.
a0kj = - dt*lambda2/Re;  a1kj = - (dt*lambda2/Re).*(1./r);
a2kj = 1 + (dt*lambda2/Re).*(1./(r.^2)) + dt*lambda2/(2*Re*Da);
a3kj = - dt*lambda2/(2*Re);
A1j = diag(a0kj)*D2 + diag(a1kj)*D + diag(a2kj)*I;   % Square matrix of size (M+1)
A1{j,j} = A1j + a3kj.*(d2(j,j)*I);                   % diagonal cells
% z-momentum Eq.
b0kj = - dt*lambda2/(2*Re);  b1kj = - (dt*lambda2/(2*Re)).*(1./r);
b2kj = 1 + dt*lambda2/(2*Re*Da); b3kj = - dt*lambda2/Re;
A2j = diag(b0kj)*D2 + diag(b1kj)*D + diag(b2kj)*I;   % Square matrix of size (M+1)
A2{j,j} = A2j + b3kj.*(d2(j,j)*I);                   % diagonal cells
% Energy Eq.
d0kj = - dt*lambda5/(2*Pe);  d1kj = - (dt*lambda5/(2*Pe)).*(1./r);
d2kj = 1 + St*dt*lambda6/(2*d_bar); d3kj = - dt*lambda5/(2*Pe);
A4j = diag(d0kj)*D2 + diag(d1kj)*D + diag(d2kj)*I;   % Square matrix of size (M+1)
A4{j,j} = A4j + d3kj.*(d2(j,j)*I);                   % diagonal cells
% Species concentration Eq.
A5j = I;  A5{j,j} = A5j;                  % diagonal cells
% Precipitation kinetics Eq.
A6j = I;  A6{j,j} = A6j;                  % diagonal cells
% Oil volume fraction Eq.
A7j = I;  A7{j,j} = A7j;                  % diagonal cells
%
for n = 1:N+1
    if (n ~= j) % non-diagonal cells
        A1{j,n} = a3kj.*(d2(j,n).*I);  % r-momentum Eq.
        A2{j,n} = b3kj.*(d2(j,n).*I);  % z-momentum Eq.
        A4{j,n} = d3kj.*(d2(j,n).*I);  % Energy Eq.
        A5{j,n} = zeros(M+1); % Species concentration Eq.
        A6{j,n} = zeros(M+1); % Precipitation kinetics Eq.
        A7{j,n} = zeros(M+1); % Oil volume fraction Eq.
    end
end
%-----------------------------------------------------------
% Construct the right-hand side vector
%-----------------------------------------------------------
[SUMZ1Ukm,SUMZ1Vkm,SUMZ1Pkm,SUMZ1Tkm,SUMZ1Ckm,SUMZ1alphaMkm,SUMZ1phiOILkm,...
    SUMZ2Ukm,SUMZ2Vkm,SUMZ2Tkm,SUMZ2phiOILkm] = deal(zeros(size(r)));
for n=1:N+1
    SUMZ1Ukm = SUMZ1Ukm + d(j,n).*Ukm(:,n);
    SUMZ1Vkm = SUMZ1Vkm + d(j,n).*Vkm(:,n);
    SUMZ1Pkm = SUMZ1Pkm + d(j,n).*Pkm(:,n);
    SUMZ1Tkm = SUMZ1Tkm + d(j,n).*Tkm(:,n);
    SUMZ1Ckm = SUMZ1Ckm + d(j,n).*Ckm(:,n);
    SUMZ1alphaMkm = SUMZ1alphaMkm + d(j,n).*alphaMkm(:,n);
    SUMZ1phiOILkm = SUMZ1phiOILkm + d(j,n).*phiOILkm(:,n);
    SUMZ2Ukm = SUMZ2Ukm + d2(j,n).*Ukm(:,n);
    SUMZ2Vkm = SUMZ2Vkm + d2(j,n).*Vkm(:,n);
    SUMZ2Tkm = SUMZ2Tkm + d2(j,n).*Tkm(:,n);
    SUMZ2phiOILkm = SUMZ2phiOILkm + d2(j,n).*phiOILkm(:,n);
end
for n=1:N+1
    RKkm(:,n) = -(((D*phiOILkm(:,n)).^2 + SUMZ1phiOILkm.^2).^(-3/2))...
        .*(((D*phiOILkm(:,n)).^2).*(((1./r).*(D*phiOILkm(:,n))+SUMZ2phiOILkm))...
        -2*(D*phiOILkm(:,n)).*(SUMZ1phiOILkm.*(D*SUMZ1phiOILkm))...
        + (SUMZ1phiOILkm.^2).*(D2*phiOILkm(:,n) + (1./r).*(D*phiOILkm(:,n))));
    Cdkm(:,n) = (1/Sf)*((c1+c2*Tkm(:,n))./(1+c3*Tkm(:,n)));  % Solubility of wax
        in crude oil
    Cd1km(:,n) = (1/Sf)*((c2-c1*c3)./(1+c3*Tkm(:,n)).^2);    % First derivative of
        Cd wrt Theta
    Cd2km(:,n) = (1/Sf)*(-2*c3*(c2-c1*c3)./(1+c3*Tkm(:,n)).^3); % Second
        derivative of Cd wrt Theta
    K1km(:,n) = c1*Tkm(:,n)+c2; K2km(:,n) = (c3*Tkm(:,n)).^2;   % Positive
        functions of temperature
    fXkm = (1-Xkm)./(alpha_avg^2*Xkm.^2-Xkm+1); % Coefficient describing
        diffusion in the gel layer
end
for n=1:N+1
    % Euler's forward scheme
    Uk(:,n) = Ukm(:,n) + dt*(...
        - Ukm(:,n).*(D*Ukm(:,n)) - Vkm(:,n).*SUMZ1Ukm - D*Pkm(:,n)...
        + (lambda2/Re)*(2*(D2*Ukm(:,n))+SUMZ2Ukm +D*SUMZ1Vkm
            +(2./r).*(D*Ukm(:,n))...
        - (2./(r.^2)).*Ukm(:,n)) - (lambda2/(Re*Da))*Ukm(:,n)...
        + (lambda3*Grt/(Re^2))*cos(alpha)*Tkm(:,n) ...
        + (lambda4*Grc/(Re^2))*cos(alpha)*Ckm(:,n) ...
        + (lambda1/We)*RKkm(:,n).*(D*phiOILkm(:,n))...
        );
```

```
        Vk(:,n) = Vkm(:,n) + dt *(...
            - Ukm(:,n).*(D*Vkm(:,n)) - Vkm(:,n).*SUMZ1Vkm - SUMZ1Pkm...
            + (lambda2/Re)*(D2*Vkm(:,n) + 2*SUMZ2Vkm +
                D*SUMZ1Ukm+(1./r).*SUMZ1Ukm...
            - (1./r).*(D*Vkm(:,n))) - (lambda2/(Re*Da))*Vkm(:,n) ...
            + (lambda3*Grt/(Re^2))*sin(alpha)*Tkm(:,n) ...
            + (lambda4*Grc/(Re^2))*sin(alpha)*Ckm(:,n) ...
            + (lambda1/We)*RKkm(:,n).*SUMZ1phiOILkm...
            );
        Pk(:,n) = Pkm(:,n);
        Tk(:,n) = Tkm(:,n) + dt *(...
            - Ukm(:,n).*(D*Tkm(:,n)) - Vkm(:,n).*SUMZ1Tkm...
            + (lambda5/Pe)*(D2*Tkm(:,n)+(1./r).*(D*Tkm(:,n))+SUMZ2Tkm)...
            + (lambda7*Ec/Re)*(2*((D*Ukm(:,n)).^2)+ 2*((Ukm(:,n)./r).^2) +
                2*(SUMZ1Vkm.^2)...
            + (D*Vkm(:,n) + SUMZ1Ukm).^2) - St*lambda6/(d_bar)*Tkm(:,n)...
            );
        Ck(:,n) = Ckm(:,n) + dt *(...
            - Ukm(:,n).*(D*Ckm(:,n)) - Vkm(:,n).*SUMZ1Ckm...
            +
                ep*((1-alphaMkm(:,n)).*((Ckm(:,n)-Cdkm(:,n)).*(D2*Vkm(:,n)+(1./r).*(D*Vkm(:,n)))) ...
            + ((1-alphaMkm(:,n)).*(D*Ckm(:,n)-Cd1km(:,n).*(D*Tkm(:,n)))...
            - (Ckm(:,n)-Cdkm(:,n)).*(D*alphaMkm(:,n))).*(D*Vkm(:,n))) ...
            +
                (1/(Re*Sc))*(Cd1km(:,n).*(D2*Tkm(:,n)+(1./r).*(D*Tkm(:,n))+SUMZ2Tkm)...
            + Cd2km(:,n).*((D2*Tkm(:,n)).^2 + (SUMZ1Tkm).^2))...
            );
        alphaMk(:,n) = alphaMkm(:,n) + dt *(...
            - Ukm(:,n).*(D*alphaMkm(:,n)) - Vkm(:,n).*SUMZ1alphaMkm...
            + (1-alphaMkm(:,n)).*K1km(:,n)...
            - (Re/lambda2)*alphaMkm(:,n).*(D*Vkm(:,n)).^2.*K2km(:,n)...
            );
        phiOILk(:,n) = phiOILkm(:,n) + dt *(...
            - Ukm(:,n).*(D*phiOILkm(:,n)) - Vkm(:,n).*SUMZ1phiOILkm...
            );
        TempGradkm(:,n) = D*Tkm(:,n); VelGradkm(:,n) = D*Vkm(:,n);
        DELTAk = DELTAkm + dt*(...
            phi1*((1-fXkm)./Xkm).*((1/(Re*Sc))*Cd1km(rIndex,n).*TempGradkm(rIndex,n))...
            );
        Xk = Xkm + dt *(...
            phi1*fXkm*(2*(1-DELTAkm)./(DELTAkm*(2-DELTAkm)))....
            *((1/(Re*Sc))*Cd1km(rIndex,n).*TempGradkm(rIndex,n)...
            +
                ep*(1-alphaMkm(rIndex,n))*(Ckm(rIndex,n)-Cdkm(rIndex,n)).*VelGradkm(rIndex,n))...
            );
    end
    [SUMZ1Uk,SUMZ1Vk,SUMZ1Pk,SUMZ1Tk,SUMZ1Ck,SUMZ1alphaMk,SUMZ1phiOILk,SUMZ2Uk,...
        SUMZ2Vk,SUMZ2Tk,SUMZ1RKk,SUMZ2Pk,SUMZ2phiOILk] = deal(zeros(size(r)));
    for n=1:N+1
        SUMZ1Uk = SUMZ1Uk + d(j,n).*Uk(:,n);
        SUMZ1Vk = SUMZ1Vk + d(j,n).*Vk(:,n);
        SUMZ1Pk = SUMZ1Pk + d(j,n).*Pk(:,n);
        SUMZ1Tk = SUMZ1Tk + d(j,n).*Tk(:,n);
        SUMZ1Ck = SUMZ1Ck + d(j,n).*Ck(:,n);
        SUMZ1alphaMk = SUMZ1alphaMk + d(j,n).*alphaMk(:,n);
        SUMZ1phiOILk = SUMZ1phiOILk + d(j,j).*phiOILk(:,j);
        % SUMZ1RKk = SUMZ1RKk + d(j,n).*RKk(:,n);
        SUMZ2Uk = SUMZ2Uk + d2(j,n).*Uk(:,n);
        SUMZ2Vk = SUMZ2Vk + d2(j,n).*Vk(:,n);
        SUMZ2Pk = SUMZ2Pk + d2(j,n).*Pk(:,n);
        SUMZ2Tk = SUMZ2Tk + d2(j,n).*Tk(:,n);
        SUMZ2phiOILk = SUMZ2phiOILk + d2(j,j).*phiOILk(:,j);
    end
    %-------------------------------------------------------------
    % Right-hand side
    %-------------------------------------------------------------
    RKk(:,j) = -(((D*phiOILk(:,j)).^2 +
        SUMZ1phiOILk.^2).^(-3/2)).*(((D*phiOILk(:,j)).^2) .*...
        (((1./r).*(D*phiOILk(:,j))+SUMZ2phiOILk))...
        -2*(D*phiOILk(:,j)).*(SUMZ1phiOILk.*(D*SUMZ1phiOILk))...
        + (SUMZ1phiOILk.^2).*(D2*phiOILk(:,j) + (1./r).*(D*phiOILk(:,j))));
    Cdk(:,j) = (1/Sf)*((c1+c2*Tk(:,j))./(1+c3*Tk(:,j)));  % Solubility of wax in crude
        oil
    Cd1k(:,j) = (1/Sf)*((c2-c1*c3)./(1+c3*Tk(:,j)).^2);   % First derivative of Cd wrt
        Theta
    Cd2k(:,j) = (1/Sf)*(-2*c3*(c2-c1*c3)./(1+c3*Tk(:,j)).^3);   % Second derivative of
        Cd wrt Theta
    K1k(:,j) = c1*Tk(:,j).^4+c2; K2k(:,j) = (c3*Tk(:,j)).^2;     % Positive functions
        of temperature
```

```
fXk = (1-Xk)./(alpha_avg^2*Xk.^2-Xk+1); % Coefficient describing diffusion in the gel layer
% r-momentum Eq.
R1k(:,j) = Uk(:,j) + dt *(...
    -((3/2)*Uk(:,j).*(D*Uk(:,j))-(1/2)*Ukm(:,j).*(D*Ukm(:,j))) ...
    - ((3/2)*Vk(:,j).*SUMZ1Uk - (1/2)*Vkm(:,j).*SUMZ1Ukm) - D*Pk(:,j)...
    + (lambda2/Re)*(D2*Uk(:,j)+(1/2)*SUMZ2Uk+D*SUMZ1Vk+(1./r).*(D*Uk(:,j))...
    - (1./(r.^2)).*Uk(:,j)) - (lambda2/(2*Re*Da))*Uk(:,j) ...
    + (lambda3*Grt/(Re^2))*cos(alpha)*Tk(:,j)+
        (lambda4*Grc/(Re^2))*cos(alpha)*Ck(:,j) ...
    +
        (lambda1/We)*((3/2)*RKk(:,j).*(D*phiOILk(:,j))-(1/2)*RKkm(:,j).*(D*phiOILkm(:,j))) ...
    );
% z-momentum Eq.
R2k(:,j) = Vk(:,j) + dt *(...
    - ((3/2)*Uk(:,j).*(D*Vk(:,j))-(1/2)*Ukm(:,j).*(D*Vkm(:,j))) ...
    - ((3/2)*Vk(:,j).*SUMZ1Vk - (1/2)*Vkm(:,j).*SUMZ1Vkm) - SUMZ1Pk...
    + (lambda2/Re)*((1/2)*D2*Vk(:,j)+SUMZ2Vk+D*SUMZ1Uk+(1./r).*SUMZ1Uk...
    - (1./(2*r)).*(D*Vk(:,j))) - (lambda2/(2*Re*Da))*Vk(:,j) ...
    + (lambda3*Grt/(Re^2))*sin(alpha)*Tk(:,j)+
        (lambda4*Grc/(Re^2))*sin(alpha)*Ck(:,j) ...
    +
        (lambda1/We)*((3/2)*RKk(:,j).*SUMZ1phiOILk-(1/2)*RKkm(:,j).*SUMZ1phiOILkm)...
    );
% Energy Eq.
R4k(:,j) = Tk(:,j) + dt *(...
    - ((3/2)*Uk(:,j).*(D*Tk(:,j))-(1/2)*Ukm(:,j).*(D*Tkm(:,j))) ...
    - ((3/2)*Vk(:,j).*SUMZ1Tk - (1/2)*Vkm(:,j).*SUMZ1Tkm)...
    + (lambda5/(2*Pe))*(D2*Tk(:,j)+(1./r).*(D*Tk(:,j))+SUMZ2Tk)
        -St*lambda6/(2*d_bar)*Tk(:,j)...
    + (lambda7*Ec/Re)*(2*((3/2)*(D*Uk(:,j)).^2-(1/2)*(D*Ukm(:,j)).^2) ...
    + 2*((3/2)*(Uk(:,j)./r).^2-(1/2)*(Ukm(:,j)./r).^2) + 2*((3/2)*(SUMZ1Vk).^2....
    - (1/2)*(SUMZ1Vkm).^2) + (3/2)*(D*Vk(:,j)+SUMZ1Uk).^2 -
        (1/2)*(D*Vkm(:,j)+SUMZ1Ukm).^2)...
    );
% Species concentration Eq.
R5k(:,j) = Ck(:,j) + dt *(...
    - ((3/2)*Uk(:,j).*(D*Ck(:,j))-(1/2)*Ukm(:,j).*(D*Ckm(:,j))) ...
    - ((3/2)*Vk(:,j).*SUMZ1Ck - (1/2)*Vkm(:,j).*SUMZ1Ckm)...
    +
        ep*((3/2)*(1-alphaMk(:,j))).*((Ck(:,j)-Cdk(:,j)).*(D2*Vk(:,j)+(1./r).*(D*Vk(:,j)))) ...
    -
        (1/2)*(1-alphaMkm(:,j)).*((Ckm(:,j)-Cdkm(:,j)).*(D2*Vkm(:,j)+(1./r).*(D*Vkm(:,j)))) ...
    + (3/2)*((1-alphaMk(:,j)).*(D*Ck(:,j)-Cd1k(:,j).*(D*Tk(:,j))) ...
    - (Ck(:,j)-Cdk(:,j)).*(D*alphaMk(:,j))).*(D*Vk(:,j)) ...
    - (1/2)*((1-alphaMkm(:,j)).*(D*Ckm(:,j)-Cd1km(:,j).*(D*Tkm(:,j))) ...
    - (Ckm(:,j)-Cdkm(:,j)).*(D*alphaMkm(:,j))).*(D*Vkm(:,j))) ...
    + (1/(Re*Sc))*(3/2)*(Cd1k(:,j).*(D2*Tk(:,j)+(1./r).*(D*Tk(:,j))+SUMZ2Tk)...
    + Cd2k(:,j).*((D2*Tk(:,j)).^2 + (SUMZ1Tk).^2))...
    -
        (1/(Re*Sc))*(1/2)*(Cd1km(:,j).*(D2*Tkm(:,j)+(1./r).*(D*Tkm(:,j))+SUMZ2Tkm)...
    + Cd2km(:,j).*((D2*Tkm(:,j)).^2 + (SUMZ1Tkm).^2))...
    );
% Precipitation kinetics Eq.
R6k(:,j) = alphaMk(:,j) + dt *(...
    - ((3/2)*Uk(:,j).*(D*alphaMk(:,j)) - (1/2)*Ukm(:,j).*(D*alphaMkm(:,j))) ...
    - ((3/2)*Vk(:,j).*SUMZ1alphaMk - (1/2)*Vkm(:,j).*SUMZ1alphaMkm)...
    + (1-alphaMk(:,j)).*K1k(:,j) ...
    - (Re/lambda2)*((3/2)*(alphaMk(:,j).*(D*Vk(:,j)).^2).*K2k(:,j) ...
    - (1/2)*(alphaMkm(:,j).*(D*Vkm(:,j)).^2).*K2km(:,j)) ...
    );
% Oil volume fraction Eq.
R7k(:,j) = phiOILk(:,j) + dt *(...
    -((3/2)*Uk(:,j).*(D*phiOILk(:,j)) - (1/2)*Ukm(:,j).*(D*phiOILkm(:,j))) ...
    -((3/2)*Vk(:,j).*SUMZ1phiOILk - (1/2)*Vkm(:,j).*SUMZ1phiOILkm)...
    );
% Deposit growth rate Eq.
TempGradk(:,j) = D*Tk(:,j); VelGradk(:,j) = D*Vk(:,j);
R8k(j) = DELTAk + dt*(...
    - (phi1/(2*Re*Sc))*(3*((1-fXk)./Xk).*Cd1k(rIndex,j).*TempGradk(rIndex,j) ...
    -((1-fXkm)./Xkm).*Cd1km(rIndex,j).*TempGradkm(rIndex,j))...
    );
% Deposit aging rate Eq.
R9k(j) = Xk + dt *(...
    (3/2)*phi1*fXk*(2*(1-DELTAk)./(DELTAk*(2-DELTAk)))....
    *((1/(Re*Sc))*Cd1k(rIndex,j).*TempGradk(rIndex,j) ...
    +
        ep*(1-alphaMk(rIndex,j))*(Ck(rIndex,j)-Cdk(rIndex,j)).*VelGradk(rIndex,j)) ...
```

```
        - (1/2)*phi1*fXkm*(2*(1-DELTAkm)./(DELTAkm*(2-DELTAkm)))....
        *((1/( Re*Sc))*Cd1km(rIndex,j).*TempGradkm(rIndex,j)...
        +
            ep*(1-alphaMkm(rIndex,j))*(Ckm(rIndex,j)-Cdkm(rIndex,j)).*VelGradkm(rIndex,j)) ...
        );
    %-----------------------------------------------------------
    % Impose the boundary conditions
    %-----------------------------------------------------------
    %----: BCs at r = r0 and r = rend  :----------
    for n = 1:N+1
        % zero the first row of each cell
        A1{j,n}(1,:) = 0;   A2{j,n}(1,:) = 0;
        A4{j,n}(1,:) = 0;   A5{j,n}(1,:) = 0;   A6{j,n}(1,:) = 0;
        A7{j,n}(1,:) = 0;   A8{j,n}(1,:) = 0;   A9{j,n}(1,:) = 0;
        % zero the last row of each cell
        A1{j,n}(end,:) = 0; A2{j,n}(end,:) = 0;
        A4{j,n}(end,:) = 0; A5{j,n}(end,:) = 0; A6{j,n}(end,:) = 0;
        A7{j,n}(end,:) = 0; A8{j,n}(end,:) = 0; A9{j,n}(end,:) = 0;
    end
    %----: At r = r0 (pipeline centerline ) :----------
    A1{j,j}(end,:) = D(end,:); R1k(end,j) = 0;   % BC: u'(r_0,z,t)
    A2{j,j}(end,:) = D(end,:); R2k(end,j) = 0;   % BC: v'(r_0,z,t)
    A4{j,j}(end,:) = D(end,:); R4k(end,j) = 0;   % BC: Θ'(r_0,z,t)
    A5{j,j}(end,:) = D(end,:); R5k(end,j) = 0;   % BC: φ'(r_0,z,t)
    A6{j,j}(end,:) = D(end,:); R6k(end,j) = 0;   % BC: α_m'(r_0,z,t)
    %----: At r = rend (pipeline wall) :----------
    A1{j,j}(1,:) = I(1,:); R1k(1,j) = 0;         % BC: u(r_end,z,t)
    A2{j,j}(1,:) = I(1,:); R2k(1,j) = 0;         % BC: v(r_end,z,t)
    A4{j,j}(1,:) = I(1,:); R4k(1,j) = 1;         % BC: Θ(r_end,z,t)
    A5{j,j}(1,:) = I(1,:); R5k(1,j) = 1;         % BC: φ(r_end,z,t)
    A6{j,j}(1,:) = I(1,:); R6k(1,j) = 1;         % BC: α_m(r_end,z,t)
    %
    %----------: BCs at z = 0 (pipeline inlet) :------
    A1{end,j} = zeros(M+1); A1{end,end} = I;
    R1k(:,end) = zeros(size(r));                 % BC: u(r,z_0,t)
    A2{end,j} = zeros(M+1); A2{end,end} = I;
    R2k(:,end) = ones(size(r));                  % BC: v(r,z_0,t)
    A4{end,j} = zeros(M+1); A4{end,end} = I;
    R4k(:,end) = zeros(size(r));                 % BC: Θ(r,z_0,t)
    A5{end,j} = zeros(M+1); A5{end,end} = I;
    R5k(:,end) = zeros(size(r));                 % BC: φ(r,z_0,t)
    A6{end,j} = zeros(M+1); A6{end,end} = I;
    R6k(:,end) = zeros(size(r));                 % BC: α_m(r,z_0,t)
    A7{end,j} = zeros(M+1); A7{end,end} = I;
    R7k(:,end) = ones(size(r)) - phiWater;       % BC: φ_oil(r,z_0,t)
end
%-----------------------------------------------------------
% Merge the cell arrays to form bigger matrices
%-----------------------------------------------------------
A1 = cell2mat(A1); A2 = cell2mat(A2);
A4 = cell2mat(A4); A5 = cell2mat(A5); A6 = cell2mat(A6);
A7 = cell2mat(A7);
%-----------------------------------------------------------
% Reshape the right-hand side vectors to form column vectors
%-----------------------------------------------------------
R1 = reshape(R1k,(M+1)*(N+1),1); R2 = reshape(R2k,(M+1)*(N+1),1);
R4 = reshape(R4k,(M+1)*(N+1),1); R5 = reshape(R5k,(M+1)*(N+1),1);
R6 = reshape(R6k,(M+1)*(N+1),1); R7 = reshape(R7k,(M+1)*(N+1),1);
R8 = reshape(R8k,(N+1),1); R9 = reshape(R9k,(N+1),1);
%-----------------------------------------------------------
% Solve the matrix equations
%-----------------------------------------------------------
U = A1\R1; % u^{n+1}
V = A2\R2; % v^{n+1}
T = A4\R4; % Θ^{n+1}
C = A5\R5; % φ^{n+1}
alphaM = A6\R6;  % α_m^{n+1}
phiOIL = A7\R7;  % φ_oil^{n+1}
Delta = R8(zIndex);  % δ^{n+1}
X = R9(zIndex);     % x^{n+1}
error = norm([U;V;T;C] - [Uk(:);Vk(:);Tk(:);Ck(:)], Inf);   % =
    max(max(abs(Ukp1-Uk)));
%-----------------------------------------------------------
% Solve the PPE (pressure Poisson Eq.)
%-----------------------------------------------------------
%{-
c0kj = 1;   c1kj = 1./r;  c2kj = 1;
```

```
            A3j = diag(c0kj)*D2 + diag(c1kj)*D;              % Square matrix of size (M+1)
            A3{j,j} = A3j + c2kj.*(d2(j,j)*I);               % insert diagonal cells
            RK(:,j) = -((D*phiOIL(:,j)).^2 +
                  SUMZ1phiOIL.^2).^(-3/2).*(((D*phiOIL(:,j)).^2) .*...
                        (((1./r).*(D*phiOIL(:,j))+SUMZ2phiOIL))...
                        -2*(D*phiOIL(:,j)).*(SUMZ1phiOIL.*(D*SUMZ1phiOIL))...
                        + (SUMZ1phiOIL.^2).*(D2*phiOIL(:,j) + (1./r).*(D*phiOIL(:,j))));
            R3k(:,j) = - (2./(r.^2)).*(U(:,j).^2) ...
                  - 2*(SUMZ1Ukm.*(D*V(:,j)))...
                  + (lambda1/We)*(RK(:,j).*(D2*phiOIL(:,j)+(1./r).*(D*phiOIL(:,j)) ...
                  + SUMZ2phiOIL) + (D*RK(:,j).*(D*phiOIL(:,j))+d(j,j)*RK(:,j).*SUMZ1phiOIL))...
                  +
                        (lambda3*Grt/(Re^2))*(cos(alpha)*(D*T(:,j)+(1./r).*T(:,j))+sin(alpha)*SUMZ1T)...
                  +
                        (lambda4*Grc/(Re^2))*(cos(alpha)*(D*C(:,j)+(1./r).*C(:,j))+sin(alpha)*SUMZ1C);
      %}
      %-----------------------------------------------------------
      % Reshape the results onto 2D grid and update the previous solutions
      %-----------------------------------------------------------
      Ukm = reshape(Uk,M+1,N+1); Uk = reshape(U,M+1,N+1);
      Vkm = reshape(Vk,M+1,N+1); Vk = reshape(V,M+1,N+1);
      Pkm = reshape(Pk,M+1,N+1); Pk = reshape(P,M+1,N+1);
      Tkm = reshape(Tk,M+1,N+1); Tk = reshape(T,M+1,N+1);
      Ckm = reshape(Ck,M+1,N+1); Ck = reshape(C,M+1,N+1);
      alphaMkm = reshape(alphaMk,M+1,N+1); alphaMk = reshape(alphaM,M+1,N+1);
      phiOILkm = reshape(phiOILk,M+1,N+1); phiOILk = reshape(phiOIL,M+1,N+1);
      DELTAkm = reshape(DELTAk,1,1); DELTAk = reshape(Delta,1,1);
      Xkm = reshape(Xk,1,1); Xk = reshape(X,1,1);
      %-----------------------------------------------------------
      % Check whether a steady-state solution has been reached
      %-----------------------------------------------------------
      if (error < tolerance)
            fprintf('Steady-state solution has been reached\n')
            break;
      else
            t = t + dt;   % Update time
      end
end
%-----------------------------------------------------------
% The approximate solutions
%-----------------------------------------------------------
baru = Uk;   % Radial velocity
barv = Vk;   % Axial velocity
Theta = Tk;  % Temperature
phi = Ck;    % Total wax concentration
Am = alphaMk;          % Aggregaion degree of wax
phiOil = phiOILk;      % Volume fraction of oil
delta = DELTAk;        % Deposit thickness
x = Xk;                % weight fraction of wax in gel layer
DdeltaDt = 0;          % Deposit growth rate
DxDt = 0;              % Deposit aging rate
Cd = Cdk;                        % Concentration of dissolved wax crystals
Cnon = (1-Am).*(phi-Cd);         % Concentration of non-aggregated wax crystals
Ca = phi - Cd - Cnon;            % Concentration of aggregated wax crystals
Cp = Ca + Cnon;                  % Concentration of precipitated wax crystals
C = Cd(:,:,tIndex) + Cp;         % Total wax concentration
Cfr = Cfr(:,:,tIndex);   % Skin-friction coefficient along r-direction
Cfz = Cfz(:,:,tIndex);   % Skin-friction coefficient along z-direction
Nu = Nu(:,:,tIndex);     % local Nusselt number (rate of heat transfer)
Sh = Sh(:,:,tIndex);     % local Sherwood number (rate of mass transfer)
%-----------------------------------------------------------
% Store the soluions for plotting purpose
%-----------------------------------------------------------
solMatrix(:,:,p) = [baru;barv;Theta;phi;Am;phiOil];
Dsol(:,p) = delta;
Xsol(:,p) = x;
%-----------------------------------------------------------
% Vary the flow parameters
%-----------------------------------------------------------
% => Change the variedParameter and its name (3 instances) <=
variedParameter = Re; % Change the varied parameter <<<------
variedParameterName = 'Re'; % Change the varied parameter <<<
legendMatrix = [legendMatrix , strcat(variedParameterName, ' = ' ,...
      num2str(variedParameter))];
fprintf([variedParameterName '=%.2f: CfRe = %.4f, Nu = %.4f, Sh = %.4f\n' ],...
      variedParameter,CfRe,Nu,Sh) % Print skin-friction coefficient, Nusselt and Sherwood
      numbers
fprintf('\t\t Deposit growth rate = %e, Deposit aging rate = %e\n' ,...
      DdeltaDt,DxDt) % Print deposit growth rate
variedParameter = variedParameter + increment; % update the varied parameter
```

```
    Re = variedParameter; % Change the varied parameter <<<------
end % Stop the computations
fprintf('-----------------------------------\n')
fprintf('Time elapsed, t = %.6f (units)\n',t)
%%
%-------------------------------------------------------------
% Plotting Section
%-------------------------------------------------------------
%---3D Plots:
profile3D = {'$\bar{u}(\bar{r},\bar{z},\bar{t})$',...
    '$\bar{v}(\bar{r},\bar{z},\bar{t})$',...
    '$\Theta(\bar{r},\bar{z},\bar{t})$',...
    '$\phi(\bar{r},\bar{z},\bar{t})$',...
    '$\alpha_m(\bar{r},\bar{z},\bar{t})$',...
    '$\phi_{oil}(\bar{r},\bar{z},\bar{t})$'};
for flowVariable = 1:nDependentVars
    % Specify the range of rows of the flow variable in the solMatrix
    rowsfV = (1:M+1)+(flowVariable-1)*(M+1);
    % Plot the approximate solutions
    figure(flowVariable)
    sp = spapi({3,4},{r(:),z(1:nz)},solMatrix(rowsfV,1:nz,nProfiles)); % Spline interpolation (bivariate)
    fnplt(sp), colorbar; % Plot and show data->color mapping
    xlabel('$\bar{r}$','FontSize',14,'InterPreter','LaTeX');
    ylabel('$\bar{z}$','FontSize',14,'InterPreter','LaTeX');
    zlabel(profile3D{flowVariable},'FontSize',14,'InterPreter','LaTeX');
end
%--2D Plots
profile2D = {'RADIAL VELOCITY, $\bar{u}(\bar{r},\bar{z},\bar{t})$',...
    'AXIAL VELOCITY, $\bar{v}(\bar{r},\bar{z},\bar{t})$',...
    'TEMPERATURE, $\Theta(\bar{r},\bar{z},\bar{t})$',...
    'TOTAL CONCENTRATION, $\phi(\bar{r},\bar{z},\bar{t})$',...
    'AGGREGATION DEGREE, $\alpha_m(\bar{r},\bar{z},\bar{t})$',...
    'VOLUME FRACTION OF OIL, $\phi_{oil}(\bar{r},\bar{z},\bar{t})$',...
    'DEPOSIT THICKNESS, $\bar{\delta}(\bar{t})$',...
    'WEIGHT FRACTION OF WAX, $x(\bar{t})$'};
zIndex = floor(0.4*(N+1)); % Specify the index for z
for flowVariable = 1:nDependentVars
    % Specify the range of rows of the flow variable in the solMatrix matrix
    rowsfV = (1:M+1)+(flowVariable-1)*(M+1);
    % Plot the approximate solutions
    figure(flowVariable+nDependentVars)
    hold on
    for p=1:nProfiles
        sp = spapi(3,r,solMatrix(rowsfV,zIndex,p)); % Spline interpolation
        fnplt(sp,1.5,color{p})%,set(gca,'Fontsize',10)
    end
    hold off
    axis([0 Inf 0 Inf]);
    xlabel('RADIAL DISTANCE, $\bar{r}$','FontSize',14,'InterPreter','LaTeX');
    ylabel(profile2D{flowVariable},'FontSize',14,'InterPreter','LaTeX');
    legend(legendMatrix{:,2:nProfiles+1});
    %
    % Magnify very close profiles
    errorNorm = norm(solMatrix(rowsfV,zIndex,nProfiles) ...
        - solMatrix(rowsfV,zIndex,1),Inf); % compute norm infinity
    if errorNorm < 0.03 && nProfiles >1
        % zoomIn(r,solMatrix,rowsfV,nProfiles,color) % Zoom In (+) the profiles
    end
end
figure(13)
hold on
for p=1:nProfiles
    sp = spapi(3,t,Dsol(:,p)); % Spline interpolation
    fnplt(sp,1.5,color{p})%,set(gca,'Fontsize',10)
end
hold off
axis tight
xlabel('TIME, $\bar{t}$','FontSize',14,'InterPreter','LaTeX')
ylabel(profile2D{7},'FontSize',14,'InterPreter','LaTeX')
legend(legendMatrix{:,2:nProfiles+1});
%
figure(14)
hold on
for p=1:nProfiles
    sp = spapi(3,t,Xsol(:,p)); % Spline interpolation
    fnplt(sp,1.5,color{p})%,set(gca,'Fontsize',10)
end
```

```
hold off
axis tight
xlabel('TIME, $\bar{t}$','FontSize',14,'InterPreter','LaTeX')
ylabel(profile2D{8},'FontSize',14,'InterPreter','LaTeX')
legend(legendMatrix{:,2:nProfiles+1});
fprintf('\nCPU time = %.6f seconds\n\n',toc) % Display CPU time elapsed
```

Listing 5.2: `cheb.m`

```
% CHEB compute D = differentiation matrix, x = Chebyshev grid
function [D,x] = cheb(N)
if N==0, D=0; x=1; return, end
x = cos(pi*(0:N)/N)';
c = [2; ones(N-1,1); 2].*(-1).^(0:N)';
X = repmat(x,1,N+1);
dX = X-X';
D = (c*(1./c)')./(dX+(eye(N+1)));          % off-diagonal entries
D = D - diag(sum(D'));                      % diagonal entries
```